STUDIES OF THERMAL AND MECHANICAL PROPERTIES OF NANO-TITANIUM DIOXIDE DOPED PVA NANOCOMPOSITES

Ph.D. Thesis

Vandana Kaler
ID: 2014RMT9530

DEPARTMENT OF METALLURGICAL AND MATERIALS ENGINEERING
MALAVIYA NATIONAL INSTITUTE OF TECHNOLOGY JAIPUR

July 2019

STUDIES OF THERMAL AND MECHANICAL PROPERTIES OF NANO-TITANIUM DIOXIDE DOPED PVA NANOCOMPOSITES

A THESIS

Submitted in
fulfillment of the requirements for the degree of

Doctor of Philosophy

by

Vandana Kaler
(2014RMT9530)

Under the Supervision of

Dr. Rajendra Kumar Duchaniya

Prof. Upender Pandel

DEPARTMENT OF METALLURGICAL AND MATERIALS ENGINEERING

MALAVIYA NATIONAL INSTITUTE OF TECHNOLOGY JAIPUR

July 2019

Dedication

To Lord Almighty, for enabling me to pursue my doctorate.

To my supervisors, Dr. Rajendra Kumar Duchaniya & Prof. Upender Pandel for guiding me.

To my parents, Mr. Ramniwas Kaler & Mrs. Bhagawati for their unconditional love and support.

To my daughter, Ms. Mandana for her cuteness & lovely smiles.

To my husband, Mr. Manjeet Singh Bhambu for his unfaltering faith and patience. I am grateful to him for supporting me. Without his support this thesis would have been tough to complete.

To my inlaws, Mr. Vijaypal Singh Bhambu, Mrs. Chandra, Mrs. Deepa Singh & Ms. Nistha for encouraging me to pursue my doctorate.

To my brother Mr. Pankaj Kaler and sister Mrs. Prerana Kaler for their support when I needed.

Declaration

I, **Vandana Kaler** declare that this thesis titled, **"Studies of Thermal and Mechanical Properties of Nano-Titanium Dioxide Doped PVA Nanocomposites"** and the work presented in it, are my own. I confirm that:

- The work was done wholly or mainly while in candidature for a research degree at this university.
- Where any part of this thesis has previously been submitted for a degree or any other qualification at this university or any other institution, this has been clearly stated.
- Where I have consulted the published work of others, this is always clearly attributed.
- Where I have quoted from the work of others, the source is always given. With the exception of such quotations, this thesis is entirely my own work.
- I have acknowledged all main sources of help.
- Where the thesis is based on work done by myself, jointly with others, I have made clear exactly what was done by others and what I have contributed myself.

Date: **Vandana Kaler**

Place: ID: 2014RMT9530

Certificate

This is to certify that the thesis entitled **"Studies of Thermal and Mechanical Properties of Nano-Titanium Dioxide Doped PVA Nanocomposites"** being submitted by **Vandana Kaler (2014RMT9530)** is a bonafide original research work carried out under my supervision and guidance in fulfillment of the requirement for the award of the degree of Doctor of Philosophy in the **Department of Metallurgical and Materials Engineering,** Malaviya National Institute of Technology Jaipur, India. The content of this thesis is original and has not been submitted to any other University or Institute for the award of any other degree.

Dr. Upender Pandel
Professor
(Co-Supervisor)

Dr. Rajendra Kumar Duchaniya
Associate Professor
(Supervisor)

Department of Metallurgical and Materials Engineering
Malaviya National Institute of Technology Jaipur

Place: Jaipur
Date:

Acknowledgement

Firstly, I would like to express my sincere gratitude and indebtedness to my supervisor, Dr. Rajendra Kumar Duchaniya, Associate Professor, Department of Metallurgical and Materials Engineering, MNIT Jaipur for his guidance, all the useful discussions and brainstorming sessions, especially during the difficult conceptual development stage. He has constantly forced me to remain focused on achieving my goal. His deep insights helped me at various stages of my research including writing of this thesis. I owe him much gratitude.

I am also grateful to my co-supervisor, Dr. Upender Pandel, Professor, Department of Metallurgical and Materials Engineering, MNIT Jaipur, for his invaluable suggestions and words of encouragement during this research work.

Besides my supervisors, I wish to express my sincere gratitude to Dr. V. K. Sharma, Professor, Head of Department of Metallurgical and Materials Engineering, Prof. A. K. Bhargava (Ex-HOD), and Prof. Upender Pandel (Ex-HOD), Department of Metallurgical and Materials Engineering for their kind support in utilizing departmental facilities.

My sincere thanks also goes to Dr. Rajendra Kumar Duchaniya, Convener, Departmental Post Graduate Committee, and Dr. S. K. Gupta (Ex-Convener) for providing their valuable academic and administrative support required for academic requirements.

I am thankful to DREC members, Dr. Vijay N. N., Assistant Professor, and Dr. S. K. Gupta, Associate Professor, and all the faculty members of the Department of Metallurgical and Materials Engineering, MNIT Jaipur for their valuable suggestions and technical inputs during this research work.

I would like to thank all team members of our research group Dr. Shrikant Verma, Dr. Vibha Uttam, Ms. Premlata, Mr. Vijay Kumar Pandey, Mr. Sunil Kumar Jatav, and Mr. Nikunj Patel. The group has been a source of friendship as well as good advice and collaboration.

I would also like to thank Mr. Ankit Goyal, Mr. Ravindra Singh, Ms. Nitika Kundan, Mrs. Varsha Goyal and all the Research Scholars of the Department for their help in my work whenever I needed.

I would like to acknowledge our technical and administrative staff of the Department Mr. Lalchand Kumawat, Mr. Vidyasagar, Mr. R. M. Vairagi, Mr. Nathu Singh, Mr. Mahesh, Mr. Lalaram, Mr. Jagdeesh, Ms. Sunita and Mr. Kishan for their assistance in academic requirements at various stages of the work.

I wish to express my sincere gratitude to Dr. M. K. Totlani for his advice and valuable inputs. He is a great inspiration.

I am also thankful to the staff of Material Research Centre, MNIT Jaipur for helping in characterization of samples and their interpretation. Also, I am grateful to Banasthali Vidyapith for providing characterization facilities.

I owe a special thanks to my family, my parents, my brother and sister who supported me and helped me throughout my life and during this study. I dedicate this work to you all. Words are not enough to explain my feeling for my parents. They have provided me with the opportunity to be where I am today.

I am grateful to my daughter Mandana who is pride and joy of my life. I love you more than anything and I appreciate all your patience and support during mumma's Ph.D. studies.

I would like to express my heartfelt gratitude to my husband, Manjeet for being so understanding. I thank God for enlightening my life with your presence.

In the end, I am grateful to all the persons who helped me directly or indirectly to complete this thesis.

(**VANDANA KALER**)

Abstract

The addition of inorganic nanomaterials into polymer-matrix have been practiced recently to improve optical, electrical, magnetic, thermal, and mechanical properties of polymer-matrix nanocomposites. Nanocomposites are different from conventional composite materials as they have reinforcing phase in nano range. Thus, area of interaface is very high in case of nanocomposites than composites. The degree of interaction between matrix phase and reinforced phase significantly affect the overall properties of nanocomposite. Thus, materials with desired properties for specific application can be fabricated by choosing appropriate inorganic filler material.

Here, polyvinyl alcohol is chosen as matrix phase and TiO_2 nanoparticles are chosen as dispersed phase. Polyvinyl alcohol has low cost, film forming ability, easy processing, light weight, and biodegradability etc. Whereas TiO_2 nanoparticles have excellent chemical, optical, electrical, thermal properties, and non-toxicity. By addition of TiO_2 nanoparticles within PVA matrix improved optical, thermal, and mechanical properties of TiO_2/PVA nanocomposites.

The objective of this research work was to synthesize TiO_2 nanoparticles and TiO_2/PVA nanocomposites. TiO_2 nanoparticles were synthesized by sol-gel method and characterized to study absorbance, band gap, chemical bond vibrations, phase, and surface morphology. TiO_2/PVA nanocomposites with different weight percent of TiO_2 nanoparticles were synthesized using solvent casting technique. The prepared TiO_2/PVA nanocomposites were designated from samples S1 to S30. The effect of concentration of TiO_2 nanoparticles on absorption studies, bond stretching and bond vibrations, and lattice strain of TiO_2/PVA nanocomposites was studied. Also, thermal behaviour of TiO_2/PVA nanocomposites in compare to pure PVA and effect of different weight percent of PVA and TiO_2 nanoparticles on thermal properties like glass transition temperature, themal degradation etc. were investigated. The viscoelastic behaviour of TiO_2/PVA nanocomposites in compare to pure PVA and effect of different weight percent of PVA and TiO_2 nanoparticles on glass transition temperature and damping was also evaluated.

The results of this research work showed that TiO_2 nanoparticles were in anatase phase and blue shift of 0.3 eV in band gap was observed due to quantum confinement effect. The blue shift in absorbance spectra of TiO_2/PVA nanocomposites with increasing concentration of TiO_2 nanoparticles was observed which indicated reduction in aggregation of TiO_2 nanoparticles. Formation of Ti-O-O bond between TiO_2 nanoparticles and PVA was seen by fourier transform infrared spectroscopy. The lattice strain (ε) and dislocation density were increasing with increasing weight percent of TiO_2 nanoparticles whereas, decrement in crystallite size was observed with increasing TiO_2 content for TiO_2/PVA nanocomposites. Presence of Ti, O, and C atoms and homogenous dispersion of TiO_2 nanoparticles within TiO_2/PVA nanocomposites was observed by scanning electron microscopy micrographs with energy dispersive x-ray analysis and mapping analysis. Differential scanning calorimetry results showed increase in glass transition temperature Tg for all TiO_2/PVA nanocomposites in compare with pure PVA. Maximum thermal degradation of TiO_2/PVA nanocomposites occured in second degradation stage and it was reduced with increased doping of TiO_2 nanoparticles as seen by thermal gravimetric analysis results. Also, increase in glass transition temperature Tg of TiO_2/PVA nanocomposites was observed with increasing weight percent of TiO_2 nanoparticles by dynamic mechanical analysis. Dynamic mechanical analysis results also showed shifting from viscous to more elastic behaviour was seen with increasing content of TiO_2 nanoparticles.

Thus, this study showed homogenous incorporation of TiO_2 nanoparticles within PVA matrix which improved overall optical, thermal and mechanical properties of prepared TiO_2/PVA nanocomposites. The improvement in thermal and mechanical properties of TiO_2/PVA nanocomposites is important for end use applications in solar cells, gas sensing, gas purification, and fuel cells etc.

Keywords: TiO_2 nanoparticles, nanocomposites, solvent casting technique, viscoelastic behaviour and glass transition temperature.

Contents

List of Figures

List of Tables

Abbreviations

GA	:	Gluteraldehyde
GO	:	Graphene Oxide
MC	:	Methyl Cellulose
MWNT	:	Multiwalled Carbon Nano Tube
PVA	:	Polyvinyl Alcohol
TTIP	:	Titanium Tetra Isopropoxide
UV-Vis	:	Ultraviolet Visible
FTIR	:	Fourier Transform Infrared
XRD	:	X-ray Diffraction
SEM	:	Scanning Electron Microscopy
DSC	:	Differential Scanning Calorimetry
TGA	:	Thermal Gravimetric Analysis
DMA	:	Dynamic Mechanical Analysis

Chapter 1
INTRODUCTION

1.1 Background

In nature, organic and inorganic components are found combined, at nanolevel and smart materials having outstanding properties and functions such as mechanics, degree of compactness, absorbency, colour, hydrophilicity, etc. are constructed. Some examples of naturally found nanocomposites having combination of organic and inorganic components are crustacean carapaces, mollusc shells, bone and tissues. Initially, in 1998, Oriakhi, published a research paper entitled "Nano sandwiches". In this paper, they wrote, "Nature is a master chemist with incredible talent". Thus, nature has inspired researchers to combine organic and inorganic materials at molecular level in order to obtain remarkable properties.

Nanocomposites are different from conventional composite materials as they have reinforcing phase in nano range. Thus, area of interaface is very high in case of nanocomposites than composites. As mentioned in literature, degree of interaction between matrix phase and reinforced phase significantly affect the overall properties of nanocomposite.

Previously properties of PVA based nanocomposites have been improved by addition of SiO_2, CdS, ZnO, Fe_2O_3, Au, Ag and modified TiO_2 nanoparticles. The research have been focused on optical, and electrical properties mainly. Research on thermal behaviour of PVA based nanocomposites is limited whereas studies on viscoelastic behaviour have not been explored.

In this research work, TiO_2/PVA nanocomposites are prepared by addition of TiO_2 nanoparticles into PVA matrix.

Polyvinyl alcohol alcohol was used due to its low cost, film forming ability, easy processing etc. The thermal and mechanical stabilities of PVA matrix were improved via homogenously dispersing TiO_2 nanoparticles. Nanoparticles were used because of their specific properties of nano size. Nanoparticles have very high

surface to volume ratio which results in markedly change in their properties from bulk.

Titanium dioxide nanoparticles were used as reinforcement material because of their excellent chemical, optical, electrical, thermal properties, and non-toxicity.

The prepared TiO_2/PVA nanocomposites have applications in solar cells, fuel cells, gas separation, air purification, photocatalysis, optical sensing, and water pollution etc. These applications requires thermally and mechanically stable TiO_2/PVA nanocomposites as mentioned in literature. Also, processings to fabricate desired end product demands thermally and mechanically stable TiO_2/PVA nanocomposites.

As mentioned in literature, PVA based nanocomposites have been synthesized previously by addition of SiO_2, CdS, ZnO, Fe_2O_3, and modified TiO_2 nanoparticles as inorganic component to improve their properties. Study on thermal behaviour of TiO_2/PVA nanocomposites is limited and viscoelastic behaviour of TiO_2/PVA nanocomposites is not studied yet.

1.2 Objectives

On the basis of research gap found in literature review, the primary purpose of this research work was to prepare TiO_2/PVA nanocomposites with improved thermal and mechanical properties by solvent casting technique. The improved thermal and mechanical properties of TiO_2/PVA nanocomposites are important for applications in solar cells, gas sensing, air and water purification, and optical sensors. The fabrication of final products and their uses for above mentioned applications requires thermal and mechanical stability of TiO_2/PVA nanocomposites.

To achieve above mentioned primary objectives, the following specific objectives were carried out:

i Synthesis and characterization of TiO_2 nanoparticles.

ii Synthesis of pure PVA films and TiO_2/PVA nanocomposites with different weight percent of PVA and TiO_2 nanoparticles.

iii Effect of absorption studies, bond stretching and bond vibrations, and lattice strain on properties of TiO_2/PVA nanocomposites.

iv Effect of dispersion of TiO_2 nanoparticles on properties of TiO_2/PVA nanocomposites.

v To evaluate thermal behaviour of TiO_2/PVA nanocomposites in compare to pure PVA and effect of different weight percent of PVA and TiO_2 nanoparticles on thermal properties like glass transition temperature, themal degradation etc.

vi To evaluate viscoelastic behaviour of TiO_2/PVA nanocomposites in compare to pure PVA and effect of different weight percent of PVA and TiO_2 nanoparticles on glass transition temperature and damping.

1.3 Thesis Outline

The research work in detail of this thesis is provided in nine chapters. The schematic presentation of thesis outline is given in Figure 1.1 (a) and (b).

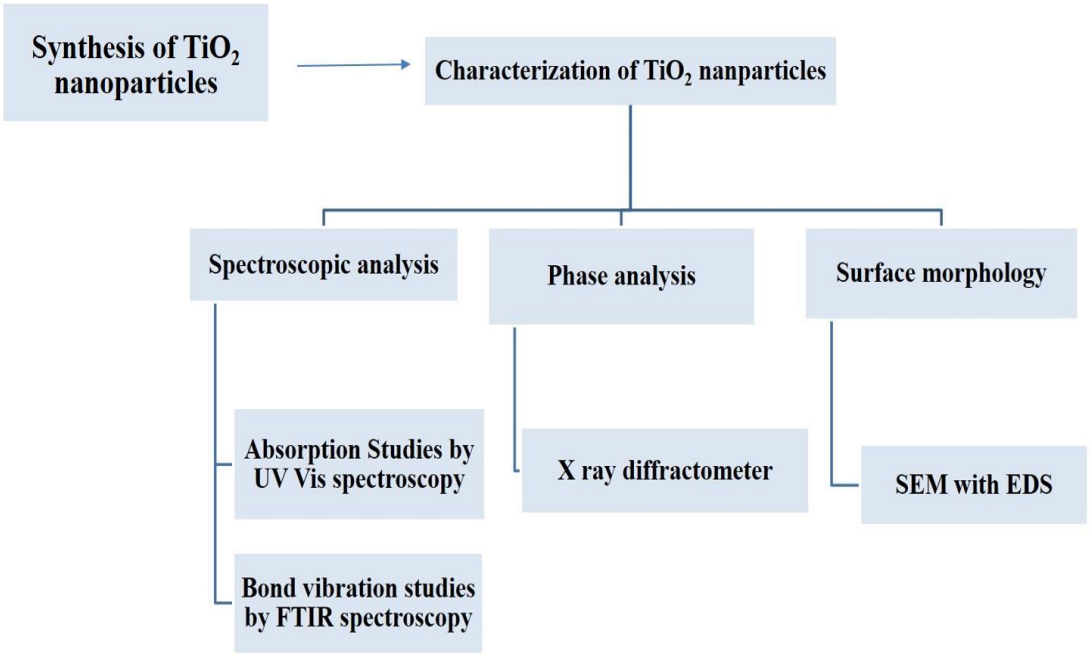

(a)

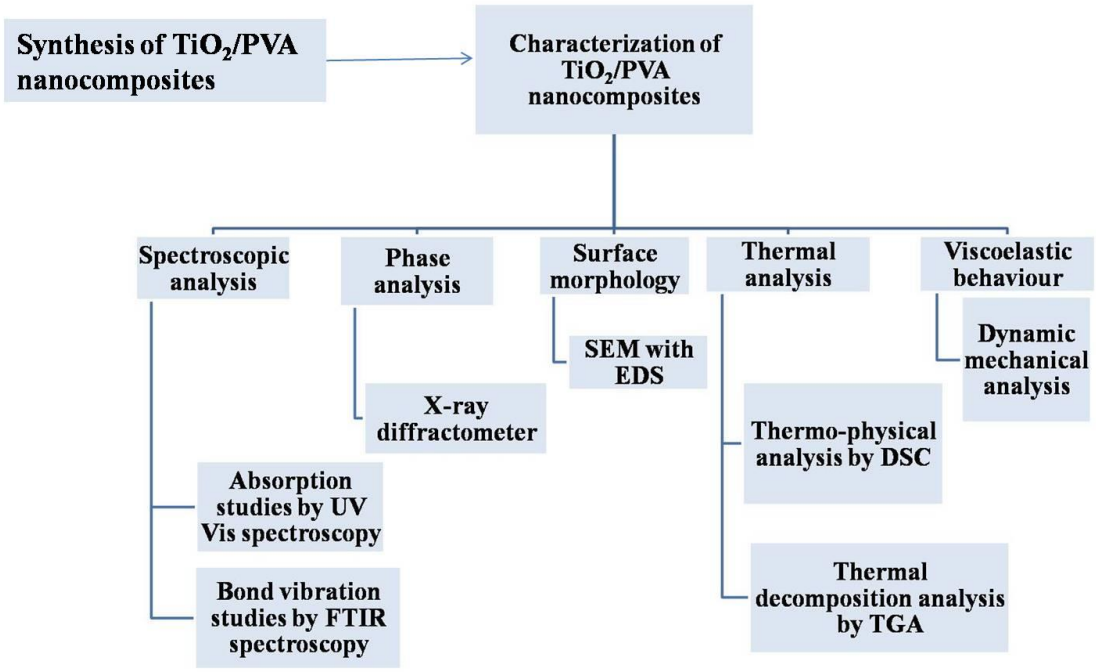

(b)

Figure 1.1: Schematic presentation of outline of thesis (a) Synthesis and characterization of TiO_2 nanoparticles (b) Synthesis and characterization of TiO_2/PVA nanocomposites

Chapter 1 consists of background of this research work, objectives of this research, and outline of thesis. Chapter 2 presents literature review, research gap, and objectives of research work. Optimization of parameters to synthesize TiO_2/PVA nanocomposites are given in chapter 3. Synthesis and characterization of TiO_2 nanoparticles is discussed in chapter 4. Experimental procedure with characterization details is given in chapter 5. Results and discussion of characterization are given in chapter 6, chapter 7, and chapter 8. The research work of this thesis is concluded in chapter 9 with suggestions for future work.

Chapter 1 includes background of this research work with objectives of this research work and outline of the thesis.

Chapter 2 provides review of literature related to nanocomposites, their types, and synthesis methods. Previous studies of TiO_2/PVA nanocomposites are reviewed. Research gap between previous studies and this research work is mentioned. Objectives of this research work are defined on the basis of research gap.

Chapter 3 presents optimization of important parameters for synthesis of TiO_2/PVA nanocomposites. Selection of suitable parameters for preparation of PVA solution, dispersion of TiO_2 nanoparticles, and mixing of PVA solution into dispersion of TiO_2 nanoparticles is given along with their optimization.

Chapter 4 presents synthesis, characterization, and results and discussion related with TiO_2 nanoparticles.

Chapter 5 describes experimental procedure followed to accomplish this research work. Principle of sonication, solvent casting technique, raw materials, composition of TiO_2/PVA nanocomposites, and parameters of characterization studies are specified.

Chapter 6 presents results and discussions of prepared TiO_2/PVA nanocomposites regarding spectroscopic analysis, phase analysis, and morphological analysis.

Chapter 7 consists of results and discussions of prepared TiO_2/PVA nanocomposites regarding thermal properties. Results of thermo-physical analysis and thermal degradation behaviour of TiO_2/PVA nanocomposites are discussed in detail.

Chapter 8 presents results and discussions regarding viscoelastic behaviour of prepared TiO_2/PVA nanocomposites and

Chapter 9 concludes research work of this thesis with suggestions for future work.

This research work of this thesis was carried out according to the objectives and thesis outline as discussed in this chapter. The review of literature is given in next chapter.

Chapter 2
LITERATURE REVIEW

This chapter consists of review of literature related to nanocomposites, their types, and synthesis methods. Thermal and mechanical studies of polymer-matrix nanocomposites are also included. Based on the literature review, research gap is identified and objectives of this research work are established.

2.1 Nanocomposites

Nanocomposites are solid materials which consist of multiple phases and one of these phases must have dimensions in the range of 1-100 nanometres [1-7]. These phases can be categorized as: (i) matrix phase and (ii) reinforced phase [5-7]. Matrix phase is primary phase which is continuous throughout the nanocomposite. Ductility of matrix phase is very high whereas hardness is less. Matrix phase holds reinforced phase by interacting with it. Reinforced phase is secondary phase and it is dispersed in matrix phase discontinuously. These multiple phases may be solid arrangement of bulk matrix and nano-dimensional phase and they differ in properties due to differences in structure and chemistry.

The optical, electrical, thermal, and mechanical properties of nanocomposites are different from their component materials, still the specific features of both phases of nanocomposites are preserved [6-7]. The difference between nanocomposites and conventional composite materials is due to very high surface to volume ratio of the reinforcing phase within nanocomposites. Thus, area of interface between matrix phase and reinforced phase in nanocomposites is much higher than in composites. Two points are important for improving the properties of composites, first one is, by increasing interaction between reinforced material and matrix material and second is, by uniform dispersion of filler material into the matrix [7]. Conventional composite materials have filler materials in the size range of micrometers whereas nanocomposite materials have filler material of nanoscale i.e. 1-100 nm. Generally polymer coils have diameter of 50 nm approximately, thus if nanofillers will be used, there will be increase in molecular interaction between

polymer and filler material. This interaction will result in noval properties which are not present in conventional composites.

Main advantages of nanocomposites over conventional composites are as [7]:

i The properties of nanocomposites can be improved by incorporation of small amount of nanofillers where composites require higher amount of microparticles to improve their properties.

ii Nanocomposites are lighter in weight than conventional composites because nanocomposites have very small amount of nanofillers.

iii Nanofillers enhances physical and chemical properties of nanocomposites to a much greater extent than conventional composites due to size dependence of these properties.

Hence, nanocomposites have better properties than conventional composites and they can replace composites. Different types of nanocomposites are discussed in next section.

2.2 Types of Nanocomposites

The classification of nanocomposites can be done on the basis of nature of matrix material or nature of reinforced material. Here, nanocomposites are categorized into three types on the basis of nature of matrix material used.

2.2.1 Nanocomposites with ceramic as matrix material

Nanocomposites having ceramic as matrix material are a new class of engineering materials. They have extensive range of applications in industrial sector because of their outstanding electrical and mechanical properties. Conventional ceramic materials like alumina, aluminium nitride, and silicon nitride fracture easily under thermal or thermo-mechanical loads due to cracks initiated by small defects. Nanoparticles are incorporated into them to improve crack resistance of these materials.

In these materials, matrix material and reinforcement material, both are from ceramic class of materials. Some common examples of ceramic matrix nanocomposites are C/C, C/SiC, Al_2O_3/SiO_2, SiC/SiC, Al_2O_3/Al_2O_3, Al_2O_3/TiO_2 and Al_2O_3/SiC [8-

15]. Also, ceramic matrix nanocomposites with carbon nanotubes as reinforced phase include Al_2O_3/CNT, $MgAl_2O_4$/ CNT and MgO/CNT.

Generally, ceramic matrix nanocomposites are synthesized by traditional powder method, polymer precursor method, sintering, electrophoresis, and spray pyrolysis. Wet chemical methods for synthesis of ceramic matrix nanocomposites are sol-gel process, colloidal and precipitation method and template synthesis [16-26].

2.2.2 Nanocomposites with metal as matrix material

Nanocomposites with metal as matrix material have ductile metal or alloy as matrix material and nanoparticles are reinforced as filler material. These nanocomposites are made up of metal or alloy matrix reinforced with nanoparticles. They show entirely different physical, chemical and mechanical properties with compare to matrix material. The nanoparticles are usually used to improve mechanical properties like wear resistance, and damping [27]. Mechanical properties are improved at nano scale because interaction of particles with dislocations becomes significant.

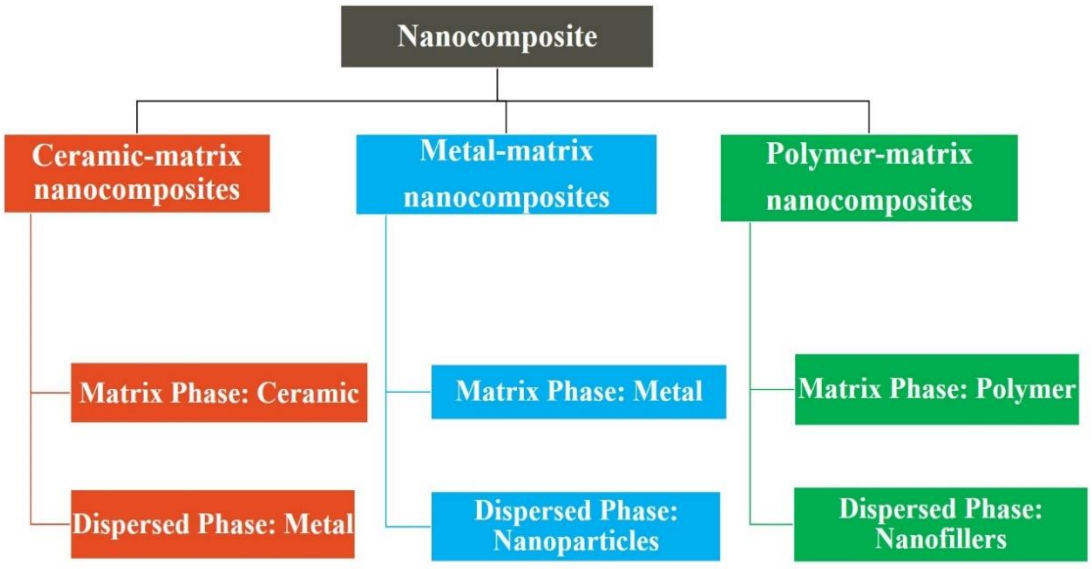

Figure 2.1: Classification of nanocomposites

The nanoparticles behave as a barrier in movement of dislocations and thus mechanical properties are improved. These materials can work in wide range of temperatures, resistant to moisture, absorbance and radiation damage [28-34].

Metal matrix nanocomposites may have matrix material as aluminium, magnesium, or titanium whereas reinforcement material like alumina and silicon carbide [27]. Some examples of nanocomposites with metal as matrix material are Fe-Cr/Al_2O_3, Ni/Al_2O_3, Fe/MgO, Al/CNT and Mg/CNT.

The common methods for synthesis of metal matrix nanocomposites can be divided into three parts: solid, liquid, and vapour methods [28-34]. Two common solid methods are powder blending and consolidation, and foil diffusion bonding. Liquid methods are electroplating, stir casting, pressure infiltration, squeeze casting, spray deposition, and reactive processing. Main vapour technique is physical vapour deposition. Also there are some chemical procedures like colloidal and sol-gel methods [26].

2.2.3 Nanocomposites with polymer as matrix material

Nanocomposites with polymer as matrix material have nano-fillers as reinforcement material. One-dimensional (nanotubes and nanofibers), two-dimensional (layered nanomaterials such as nano-clays) or three-dimensional (spherical nanoparticles) nano-additives can be used. The selection of filler material depends on the applications of nanocomposites e.g. carbon fibres are broadly used as filler material in aerospace industry. Polymer nanocomposites have exceptional mechanical properties for example high elastic stiffness and strength can be achieved with a small concentration of nanofillers. They also show excellent optical, electrical, magnetic, mechanical, and flame retardancy properties [8, 35].

The interaction between polymer matrix and fillers is due to weak intermolecular forces, or chemical bonding. If the filler material is dispersed at molecular level and chemical bonding between filler material and matrix material is formed, then notable improvements in the all properties of the nanocomposite can be attained.

Important properties of polymers are lightweight, high strength, easy handling, corrosion resistance, ductility and low cost but they have relatively poor mechanical, thermal and electrical properties compared to ceramics and metals. Other poor properties of polymers are gas barrier, heat resistant and fire performance. Density of polymers is lesser than ceramic and metal materials and they have lower coordination number. Backbone of polymers is made up of carbon and hydrogen, which are lightweight atoms. Thus, these nanocomposites are suitable for applications such as automobile, defense, aerospace and electronics makes them suitable for structural components in lightweight [36].

The properties of polymer nanocomposites are mainly affected by nanoscale phenomenon. The addition of nanoparticles with high surface area, high surface energy and often with anisotropic geometry in the polymer matrix decreases the interparticle distance and increases polymer matrix interaction strength. Thus, polymer nanocomposites with entirely new set of properties are prepared [37].

Some examples of polymer-matrix nanocomposites are PANI/TiO_2, PVA/GO, PVA/Ag, PANI/TiO_2, PANI/Graphene etc.

Polymer-matrix nanocomposites have been fabricated by intercalation, melt mixing, in situ polymerization, sol-gel method, and direct mixing.

Apart from the properties of individual components, properties of nanocomposites also depends on the following parameters [38-40]:

i Fabrication method of nanocomposite
ii Types of additives and their orientations
iii Mixing of matrix phase and dispersed phase
iv Type of interaction at the matrix interface
v Characteristics of nanoparticle

The homogenous dispersion of nanoparticles into matrix phase is important to achieve enriched properties of nanocomposites. Lacking this, there will be agglomeration of particles which will act as defects and limits the property enhancement of nanocomposite.

The other significant parameter is the nature of interface between matrix and filler material which affects the nanocomposite property enhancement. the existence of phase border between matrix and filler material and the development of interface layer between the two. The properties, composition and microstructure at the interface vary across the interface region and are different from both matrix and filler. If the interface region has good bond between matrix and filler material the overall properties of the nanocomposite will be much profound. Most of the interphase properties depend on the bound surface and therefore the nanocomposite properties can be tailored by optimizing the interfacial bond between the nanofiller and polymer matrix. The interaction between the interconnecting phases depends on the ratio of surface energy of filler and matrix. Nanosized particles have high surface area and the total surface area of a nanoparticle determines the extent of interface phenomenon contributing to the properties of nanocomposites [21-22].

Among above three types of nanocomposites, polymer-matrix type nanocomposites will be discussed in this study.

2.3 Polymer-matrix Nanocomposites

The major component of polymer-matrix nanocomposites is polymer. Four types of polymers are used to fabricate polymer-matrix nanocomposites [9]:

i Thermoplastics
ii Thermosets
iii Elastomers
iv Natural and Biodegradable polymers

The polymer matrix material to synthesize polymer matrix nanocomposites is chosen by their mechanical, electrical, magnetic, optical, biocompatibility, chemical stability and functionalization for a specific application. Thermoset based nanocomposites have been used in many applications, but recently thermoplastic-based nanocomposites have been investigated both in industry and academia. The properties of polymers mainly depend on the structure of polymer, chemical composition, surface morphology and processing parameters.

Thermosets and thermoplastics behave in different manner upon heating due to difference in their structure [40-41]. Polyvinyl alcohol (PVA) is chosen as matrix material in this research work and it is thermoplastic polymer.

Polymer matrix nanocomposites are fabricated by chemical and mechanical processes. Important fabrication methods of polymer nanocomposites are discussed below (Fig.2.2):

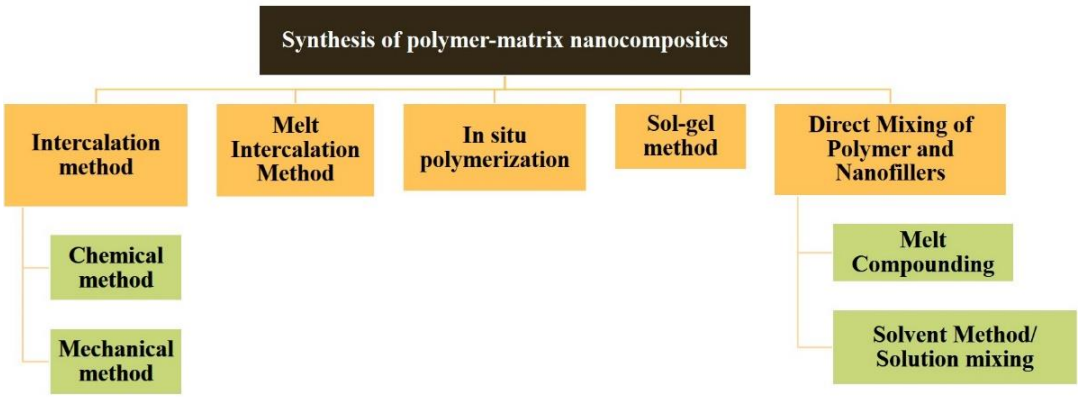

Figure 2.2: Different synthesis approach for polymer-matrix nanocomposites

a. Intercalation method

This method lies in top down approach. Nanoplatelets like filler materials are dispersed into the polymer matrix in this method. It is familiar that bulk characteristics such as rigidity, shrinkage and flammability of polymer matrices are improved by incorporation of nano-clays. The surface of nanoplatelets is modified in order to homogeneously disperse plate-like nanofillers in the polymer matrix otherwise nanoplatalates may aggregate. . Intercalated morphology takes place when polymer chains diffuse in between the gap of layered structure. The homogeneous dispersion of nanoplatelets is achieved by two methods [42-44]:

(i) Chemical method

In this method, nanoplatelets are swollen in monomer solution and then polymer is formed in between the intercalated sheets by in-situ polymerization method.

(ii) Mechanical method

In this method, two solutions are prepared. One solution is prepared by swollening nanoplatelets in the solvent and other solution is prepared by dissolving polymer in a co-solvent. Then, these two solutions are mixed together, to get polymer-matrix nanocomposite.

b. Melt intercalation method

The polymers, which are not appropriate for in-situ polymerization and solution intercalation methods, are synthesized by this method. Melt intercalation method is widely used in the industry. In this method, nanoclays are mixed into the polymer matrix at molten temperature. Also, it is well-suited with current industrial processes, like extrusion and injection molding. Melt blending method is similar to melt intercalation method. In this method, a viscous solution is formed by the melting of polymer and nanofillers are added into polymer solution by shearing at high rate along with high temperature diffusion. The final material can be fabricated by compression molding, injection molding or fiber production technique.

c. In situ polymerization

This method involves the swelling of the nanofillers in monomer solution. Monomer solution having the low-molecular weight, easily leaches in between layers triggering swelling [44]. The resultant mixture can be polymerized by various methods such as radiation, heat, initiator diffusion or by organic initiator. Then, the monomer is polymerized between nanolayers to form either exfoliated or intercalated nanocomposites. In-situ template synthesis is similar process to in-situ polymerization. In this method, both polymer matrix and clay layers are dissolved in an aqueous solution and resultant gel is usually refluxed at high temperature. The nucleation and growth of clay layers occur in such a way that polymer chains are trapped inside the clay layers. The only disadvantage of this method is that high temperature synthesis may result in degradation of polymer.

d. Sol-gel method

In this method, sol is formed by colloidal suspension of nanoparticles within monomer solution and gel is formed by polymerization reactions which results in 3D networking between phases [44]. Then hydrolysis reaction occurs and 3D network

between nanoparticle and polymer extends all over the liquid. Here, the polymer works as a nucleating agent and stimulates the growth of layered crystals. Thus, the polymer is seeped between layers and nanocomposite is synthesized.

e. Direct mixing of polymer and nanofillers

In this method, aggregated nanofillers are breakeddown at first and then mixing of polymer with nanoparticle occurs. It is divided into two types on the basis of ways of mixing as [44-45]:

The other way involves mixing of polymer and nanofillers in solution employing solvents, generally called solvent method/solution mixing [35].

(i) Melt Compounding

This method involves addition of nanofillers to the polymer above the glass transition temperature of the polymer. Homogenous and uniform dispersion of nanofillers into polymer matrix is achieved by breaking down agglomerated nanoparticles by applying shear stress [44-45].

(ii) Solvent Method/Solution mixing

In this method, two solutions are prepared. First solution is prepared by dispersing nanoparticles in the solvent by sonication and second solution is prepared by dissolving polymer in a co-solvent. The shear stresses induced in the polymer matrix are lowered in solution mixing than compare to melt compounding. [45].

After synthesis of the polymer-matrix nanocomposites by any of the above mentioned methods, they are processed to get desired shape. The processing can be accomplished by injection molding, calendaring, casting, compression molding, blow molding, rotational molding, extrusion molding, thermoforming, etc [35].

2.4 TiO_2/PVA Nanocomposites

TiO_2/PVA nanocomposites lies in the category of polymer-matrix nanocomposites. The introduction to polymer-matrix nanocomposites with their synthesis techniques is given above. TiO_2/PVA nanocomposites have poly vinyl alcohol (PVA) as matrix material whereas TiO_2 nanoparticles are used as filler material. The specific properties of TiO_2/PVA nanocomposites to be used in

photocatalysis, sensing, and charge carrier in battries etc. are due to properties of its constituents i.e. individual properties of TiO_2 and PVA. All materials have structure property correlation, so structure, properties, and applications of TiO_2 nanoparticles and PVA are described below.

2.4.1 PVA as matrix material

Polyvinyl alcohol is a water-soluble artificial polymer which was discovered in 1924 by Herrman and Haehnel. They mixed an alkali solution with a solution of polyvinyl acetal (PVAc) and got an opaque solution. As PVAc is not able to crystallize whereas PVA crystallizes easily. The structure of PVAc was changed by mixing it with alkali which lead to formation of PVA [46].

PVA is not synthesized by its monomer because monomer vinyl alcohol is less stable in compare to its tautomer acetaldehyde. The tautomeric form of vinyl alcohol is shown in scheme 2.1. Vinyl alcohol is less stable than acetaldehyde at room temperature by 42.7 KJ/mol [47]. PVA is usually synthesized by polymerization of vinyl acetate into polyvinyl acetate and then polyvinyl acetate is converted into polyvinyl alcohol by base-catalysed transesterification with ethanol [47-48]. Synthesis of PVA from polyvinyl acetate is presented by chemical reaction in scheme 2.2.

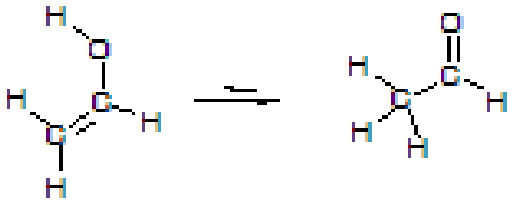

Scheme 2.1: Tautomeric form of vinyl alcohol

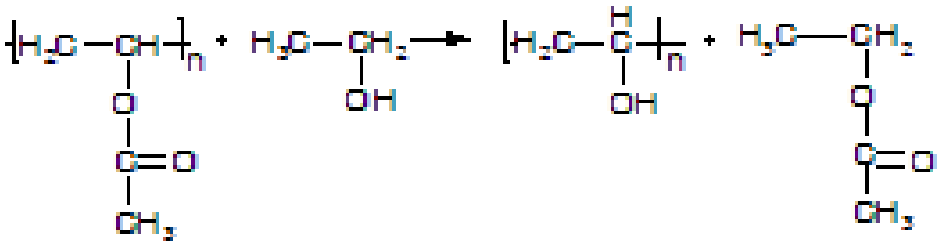

Scheme 2.2: Synthesis of polyvinyl alcohol

2.4.1.1 Structure of polyvinyl alcohol

The chemical structure of polyvinyl alcohol is made up of repeat units of monomer [–CH_2-CH(OH)-]. It is atactic polymer because OH groups are not present at fix positions. It is composed mainly of 1,3-diol linkages, but 1,2-diols linkages may also present in few percentage. PVA is semi-crystalline polymer [47-48]. It contains both crystalline and amorphous regions. Crystallinity in PVA is due to intermolecular and intramolecular hydrogen bonding as shown in Figure 2.3.

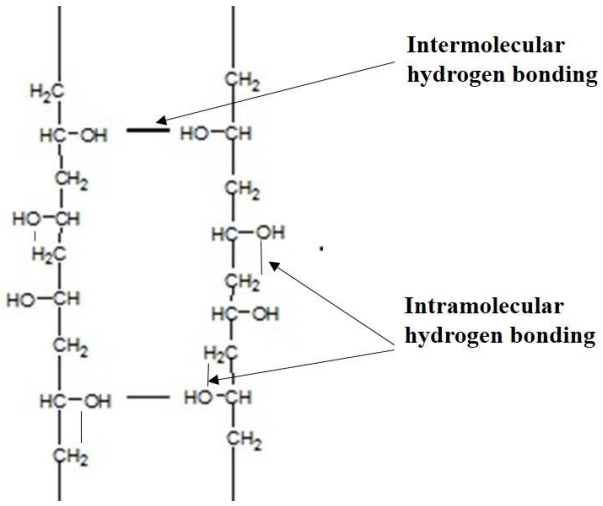

Figure 2.3: Structure of polyvinyl alcohol

2.4.1.2 Properties of polyvinyl alcohol

The degree of hydrolysis of PVA plays main role on its physical and chemical properties. For example, the tensile strength of 99% hydrolyzed PVA is 67-110 MPa whereas for 89% hydrolyzed PVA it is 24-79 MPa [46]. Also, Shalaby et al. (1991) found that the water solubility of PVA is strongly depreciated as the hydrolysis degree is below 30 mol %. The mechanical properties of PVA are also affected by its molecular weight. Some special characteristics of PVA are as follows [48-70]:

i Film forming ability

ii High hydrophilicity

iii Easy processability, and biocompatibility

iv Reasonable chemical resistance

v Nontoxicity

vi Thermal stability: There is no significant change between 40℃ to 160℃.

vii Good tensile strength, high flexibility, more hardness and gas and aroma barrier physical characteristics.

Due to above mentioned physical and chemical characteristics of PVA, it was chosen as matrix material in this study.

2.4.1.3 Applications of polyvinyl alcohol

Based upon physical and chemical properties of PVA, it is widely used in industrial, academic, commercial, medical, and food sectors. Also, it has been used to produce many end products, like lacquers, resins, surgical threads, and food packaging materials that are often in touch with food. Main applications of PVA are as [48-70]:

i To strengthen textile yarn and papers
ii Coating agent for food supplements
iii Coating of medicinal tablets
iv PVA fiber, as reinforcement in concrete
v As a form release because materials like epoxy do not stick to it

2.4.2 TiO_2 nanoparticles as reinforcement

Three polymorphs of TiO_2 are found in nature: anatase, brookite and rutile. Rutile is most stable phase as bulk TiO_2; though, solution based phase preparation methods for TiO_2 usually favour the anatase structure [71-76]. The stability of particular phase of TiO_2 depends upon surface energy and precursor chemistry. It has been seen that at very small particle dimensions (i.e. <30 nm), the surface energy of anatase phase of TiO_2 is lower than those of rutile and brookite. [77-80]. Anatase TiO_2 belongs to the indirect bandgap class of semiconductors whereas rutile TiO_2 belongs to the indirect bandgap class. Photocatalytic activity of anatase TiO_2 is better than than the other phases due to its wide-band gap (3.2 eV).

2.4.2.1 Structure of TiO_2 nanoparticles

In anatase, rutile, and brookite phases of TiO_2, TiO_6 octahedra is formed by co-ordination between titanium ($Ti^{4+)}$ atoms and six oxygen (O^{2-}) atoms [81]. The difference in these phases is only in the arrangement of these TiO_6 octahedra. In the anatase and rutile forms, tetragonal crystal structure is formed by corner sharing and

edges sharing, respectively. Whereas, in brookite form, both edges and corners are shared to give an orthorhombic structure [82]. The crystal structure of these three phases is shown in Figure 2.4.

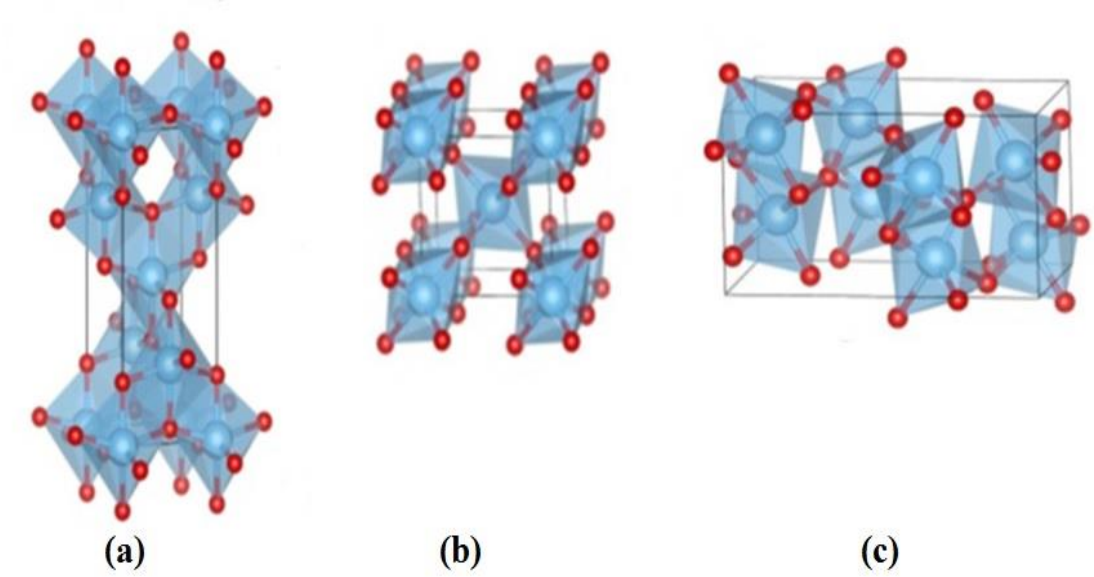

Figure 2.4: Crystal structures of TiO_2 polymorphs (a) anatase (b) rutile (c) brookite [82]

2.4.2.2 Properties of TiO_2 nanoparticles

The important properties of TiO_2 nanoparticles are as [71-82]:

i Anatase TiO_2 shows better photocatalytic activity Properties of TiO_2

ii Oxide semiconductor

iii Good chemical stability

iv High refractive index

v Hydrophilicity

vi UV absorbance

vii Nontoxicity

viii Excellent transparency for the visible light.

2.4.2.3 Synthesis of TiO_2 nanoparticles

Surface morphology of TiO_2 nanoparticles may be like nanotubes [83], nanowires [84], nanorods [85], and mesoporous structures [86] on the basis of the synthesis method. Different synthesis methods have been developed to synthesize TiO_2 nanoparticles in desired shape and structure like hydrothermal approach [87], solvothermal approach [88], sol-gel approach [89], direct oxidation approach [90], chemical vapor deposition (CVD) [91], electrodeposition [92], sonochemical method [93], and microwave method [94] have been used for the preparation of TiO_2 nanostructured.

Among above mentioned methods, synthesis of anatase TiO_2 nanoparticles with high crystallinity have been reported by sol-gel method [95-96].

In sol-gel process, a colloidal suspension which is known as sol, is formed via hydrolysis and polymerization reactions of the precursors. Precursors are usually inorganic metal salts or metal organic compounds such as metal alkoxides. Liquid sol is changes into gel phase by polymerization and loss of solvent. The gel is converted into dense ceramic by further drying and heating. Thus, highly porous and low density material is obtained, known as aerogel. Ceramic powders are formed from this aerogel by precipitation, or spray pyrolysis techniques. Under proper conditions, nanomaterials can be obtained [89].

To synthesize TiO_2 nanoparticles by sol gel method, hydrolysis of a titanium precursor i.e. titanium (IV) alkoxide is followed by condensation. Hydrolysis step is acid catalysed. Formation of Ti-O-Ti chains is favored with lower water concentrations, slow hydrolysis rates, and availability of titanium alkoxide in excess in the reaction mixture. Polymeric skeleton is formed by closed packing of Ti-O-Ti chains [89, 97].

R. Vijayalakshmi et al. compared properties of TiO_2 nanoparticles prepared by sol-gel method and hydrothermal method. They found that TiO_2 nanoparticles prepared via sol-gel method were more crystalline and smaller than prepared by hydrothermal method.

2.4.2.4 Applications of TiO_2 nanoparticles

The important applications of TiO_2 nanoparticles are as [71-82]:

i In water and air pollution treatments due to photocatalytic activity.

ii Proposed for solar cells and laser diodes for its high refractive index (2.38 for 600 nm wavelength), and chemical stability.

iii In industrial and consumer goods including paints, coatings, adhesives, paper and paperboard, plastics and rubber, printing inks, coated fabrics and textiles.

iv In catalyst systems, ceramics, floor coverings, roofing materials, cosmetics and pharmaceuticals, food colorants and in automotive products.

2.5 Properties of PVA Based Nanocomposites

Polyvinyl alcohol based nanocomposites have PVA as matrix material and nanomaterials as reinforcement. The properties of PVA like toughness, strength, modulus, heat and scratch resistance, dimensional stability, thermal, and electrical conductivity are improved by addition of nanomaterials [98]. Some common nanofillers which have been extensively used to improve properties of PVA are metal nanoparticles like Ag, Cu, Au, Co, and metal oxides like ZnO, Fe_2O_3, CuO, and TiO_2, and carbon based material like graphenes [99-100].

Nanocomposites have properties of both of its constituents and enhancement in properties is achieved by interaction between filler material and PVA. Spectroscopic, structural, thermal and mechanical properties of PVA based nanocomposites are described below.

2.5.1 Structural properties

The properties of materials are dependent on their structure. Hence, it is important to study the structure of materials in order to understand their properties. This section covers effect of reinforcement material on phase analysis and surface morphology of PVA based nanocomposites.

In 2007, Chun-Chen Yang [101] prepared PVA/TiO_2 composite polymer membrane via a solution casting technique. The ratios of PVA and TiO_2 were taken as 1:1–20 wt%, respectively. They used glutaraldehyde (GA) as a cross-linker for the nanocomposite polymer membrane and crystallinity of nanocomposites was examined. It was observed by XRD analysis (Fig. 2.5) that the amorphousness of the nanocomposite membranes increased with both the addition of TiO_2 ceramic fillers and treatment of the PVA polymer by the cross-linking reaction of GA.

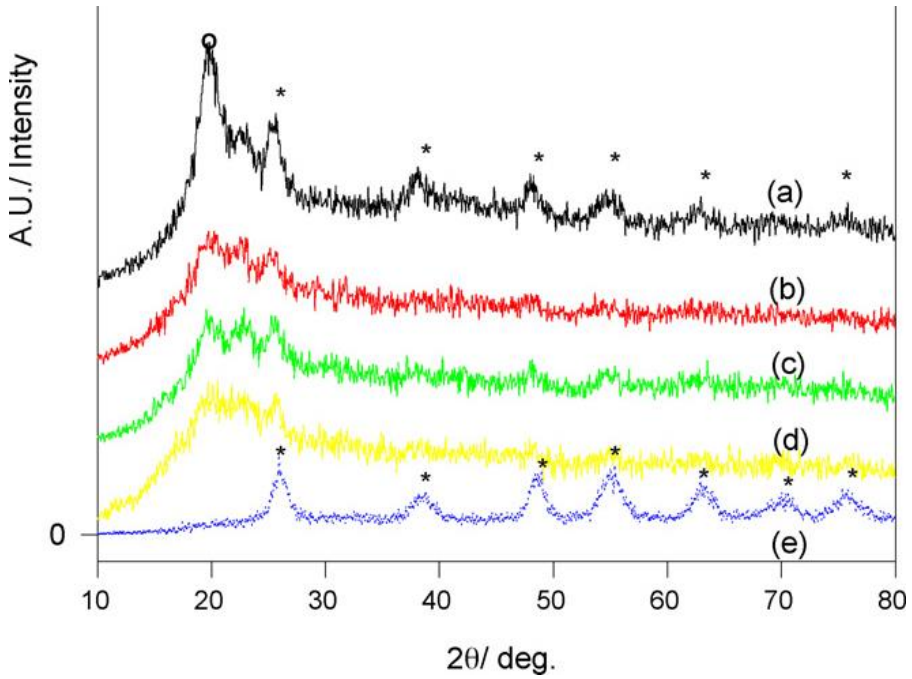

Figure 2.5: XRD graphs of (a) 10 wt% PVA/TiO_2 nanocomposite without crosslink, (b) 10 wt% PVA/TiO_2 nanocomposite crosslinked by GA for 6 hour, (c) 10 wt% PVA/TiO_2 nanocomposite crosslinked by GA for 12 hour, (d) 10 wt% PVA/TiO_2 nanocomposite crosslinked by GA for 48 hour, and (e) nano-TiO_2 [101]

Chun-Chen Yang found that the surface morphology of the GA crosslinked PVA/TiO_2 nanocomposite polymer membrane showed many different sizes of PVA and TiO_2 aggregates or lumps that were randomly distributed on the top surface. It was found that the dimension of these TiO_2 embedded in PVA lumps was about 1–20 μm. This indicated that the nano-TiO_2 particles were not dispersed well within the PVA polymer matrix, as shown in Fig. 2.6(b).

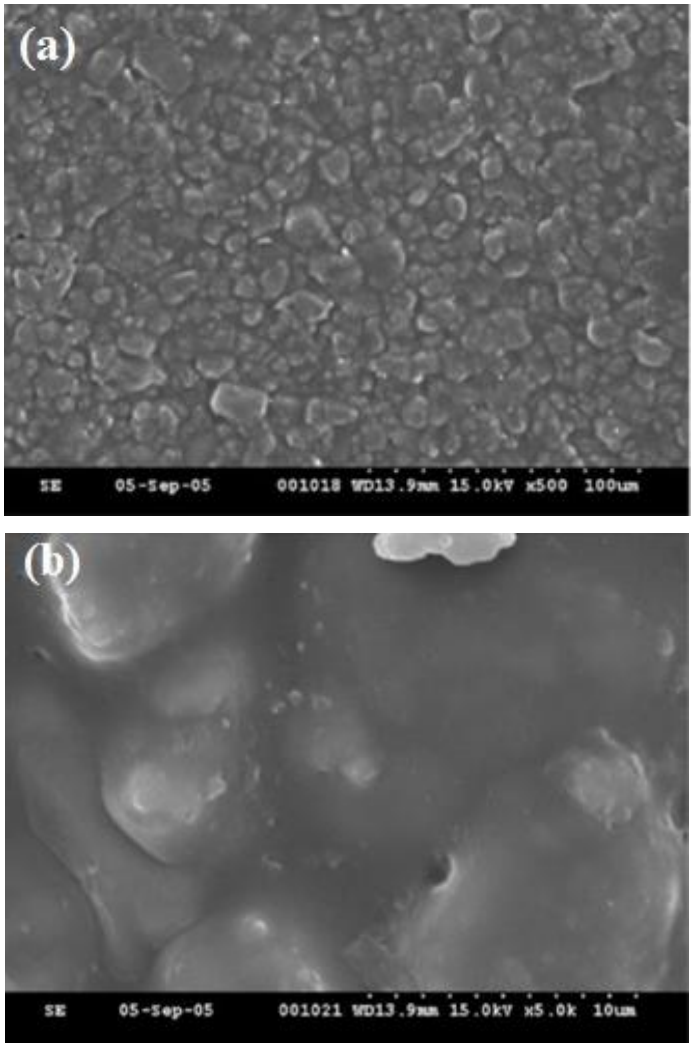

Figure 2.6: SEM images of GA crosslinked PVA/TiO_2 (20 wt%) nanocomposite at two magnifications (a) 500x and (b) 5kx [101]

In 2010, Jeongwoo Lee et al. [102] coated TiO_2 particles with polyvinyl alcohol (PVA) using a simple method of coacervation. In this method, conventional polymerization step was not required. The suspension of PVA-coated TiO_2 particles was then microencapsulated by the coacervation of gelatin and gum Arabic. The TEM images of TiO_2 and TiO_2 particles with PVA-coating are shown in Fig. 2.7 (a) and (b). The average size of TiO_2 particles was measured as 180 nm and these particles were forming clusters by aggregation. The morphology of PVA coated TiO_2 nanoparticles (Fig. 2.7 (b)) indicated that TiO_2 nanoparticles are coated by PVA. The magnified microphotograph shows the PVA layer was formed around TiO_2 particles and the average thickness of the PVA layer was measured as 1.07 nm.

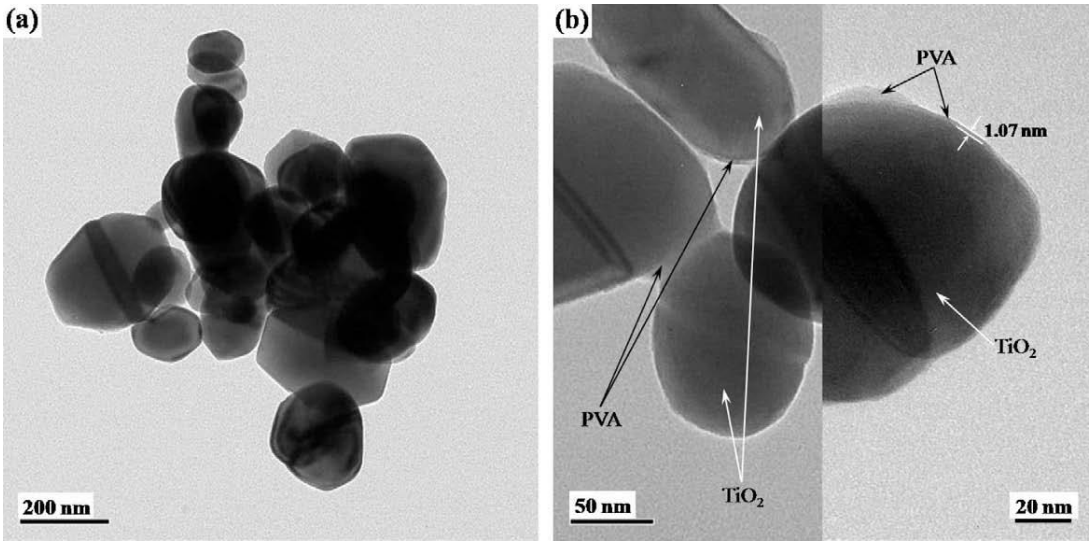

Figure 2.7: TEM micrographs showing (a) TiO_2 and (b) PVA-coated TiO_2 nanoparticles [102]

In 2011, Shadpour Mallakpoura et al. [103] prepared polyvinyl alcohol/titanium dioxide nanocomposites by different TiO_2 loading under ultrasonic irradiation process for applications in coating against UV radiation. They modified surface of TiO_2 nanoparticles by coupling with aminopropyl triethoxy silane. Then, PVA/TiO_2 films were synthesized via solution casting method. XRD patterns of (a) pure PVA, (b) surface modified TiO_2 nanoparticles and (c) PVA/TiO_2 (10 wt%) nanocomposite are shown in Fig. 2.8. They observed that crystallinity of PVA matrix is reduced by the addition of modified TiO_2 nanofillers. They explained this reduction in crystallinity is due to covalent bond formation between modified TiO_2 and PVA chain.

Shadpour Mallakpoura et al. also studied surface morphology of PVA and PVA/TiO_2 nanocomposite with 10 wt% TiO_2 nanoparticles as shown in Fig. 2.9 (c, d, e, f). They observed that TiO_2 nanoparticles were homogenously dispersed in the PVA matrix. They also mentioned that during the fabrication of PVA/TiO_2 nanocomposites, the morphology of PVA was altered and both PVA beads and TiO_2 were well distributed throughout the matrix. They concluded from SEM images that the modified TiO_2 nanofiller had excellent adhesion and strong interfacial bonding with PVA beads.

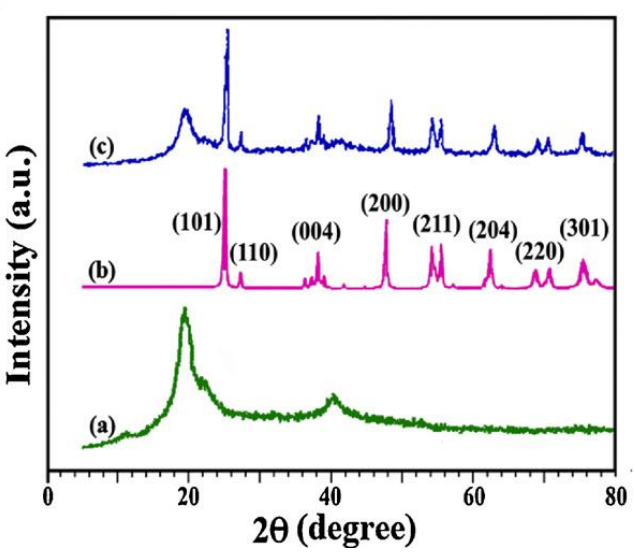

Figure 2.8: XRD graphs of (a) PVA, and (b) modified TiO_2 nanoparticles and (c) PVA/TiO_2 nanocomposite with 10 wt% TiO_2 [103]

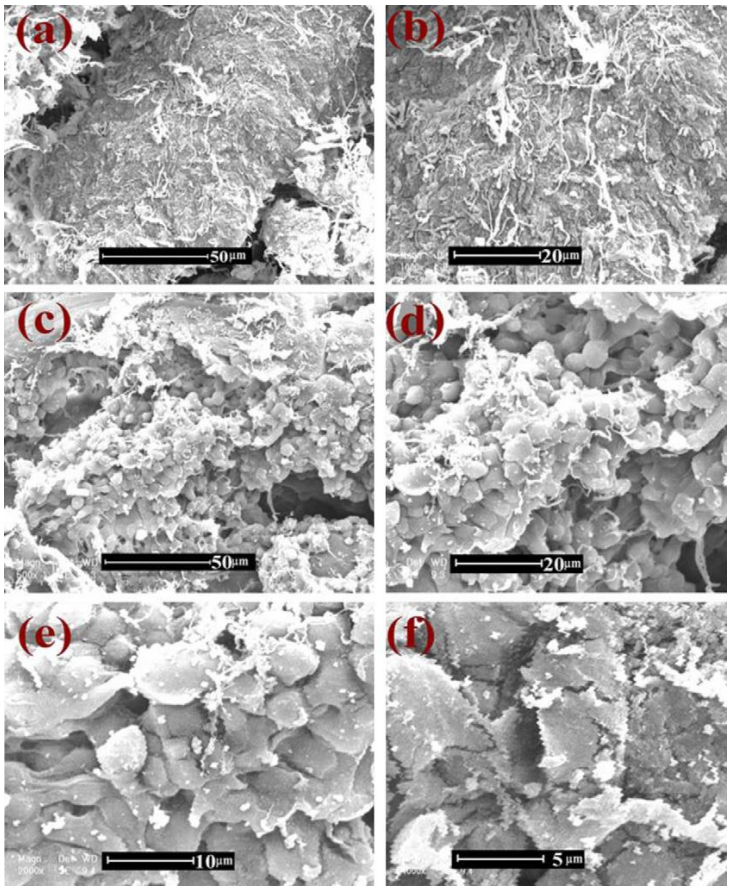

Figure 2.9: SEM images of (a) PVA with 50 μm scale, (b) PVA with 20 μm scale, (c) 10 wt% PVA/TiO_2 nanocomposite with 50 μm scale, (d) 10 wt% PVA/TiO_2 nanocomposite with 20 μm scale pure PVA, (e) 10 wt% PVA/TiO_2 nanocomposite with 10 μm scale, and (f) 5 wt% PVA/TiO_2 nanocomposite with 10 μm scale [103]

In 2012, Archana Maurya et al. [104] prepared PVA/TiO_2 nanocomposites at low temperature by sol–gel method. They used rutile phase of TiO_2 nanoparticles as filler material within PVA.

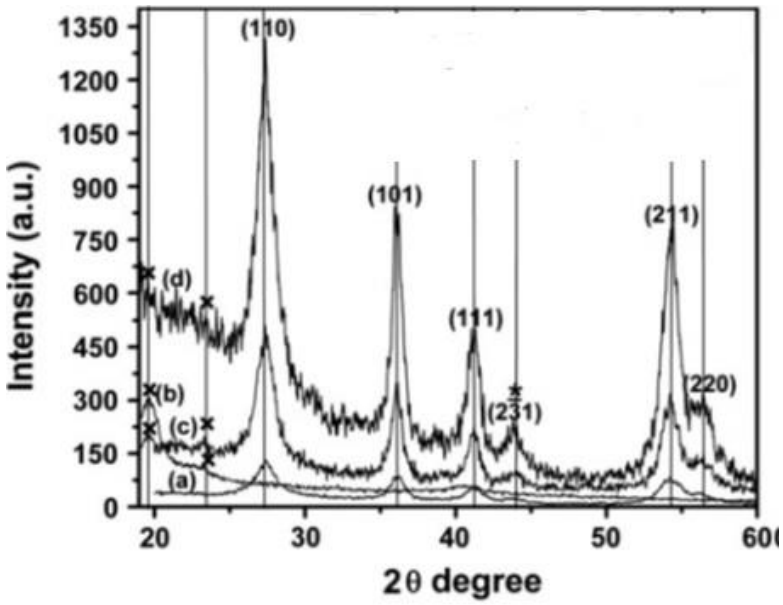

Figure 2.10: XRD graphs of (a) TiO_2, (b) PVA, (c) PVA/TiO_2 nanocomposites with 2 wt% PVA, and (d) PVA/TiO_2 nanocomposites with 4 wt% PVA [104]

Powder XRD patterns of: (a) pure TiO_2, (b) pure PVA, (c) PVA/TiO_2 nanocomposite with 2 wt% PVA, and (d) PVA/TiO_2 nanocomposite with 4 wt% PVA are shown in Fig. 2.10. They marked planes reflections (hkl) corresponding to the rutile phase of TiO_2 nanoparticles in the diffraction pattern. Additional phases present in diffractogram due to PVA and TiO were marked with cross and asterisk, respectively. They observed that TiO_2 nanoparticles were elongated along a- and b-direction but contracted along c-direction. They also observed that the rutile TiO_2 nanoparticles present in nanocomposite had an increased crystallinity in compare to pure TiO_2 nanoparticles.

Archana Maurya et al. performed TEM experiment to get thorough information about the microstructure and morphology of nanocomposites. The morphology of the pure TiO_2 and PVA/TiO_2 nanocomposite with 2 wt% PVA are shown by TEM image in Fig. 2.11 (a) and (b), respectively. They observed from these images that nanorods and prismlike structures were formed which were dense and unevenally

oriented throughout the nanocomposite. They found that nanocomposites were highly crystalline by XRD graph. The outer diameter and longest length of nanorods were found as 4 nm and 36 nm for the pure rutile TiO_2 nanoparticles. Though, for PVA/TiO_2 nanocomposite outer diameter and longest rod length were found as 20 nm and 96 nm. They concluded from these observations that addition of PVA in TiO_2 increases the rod width and length.

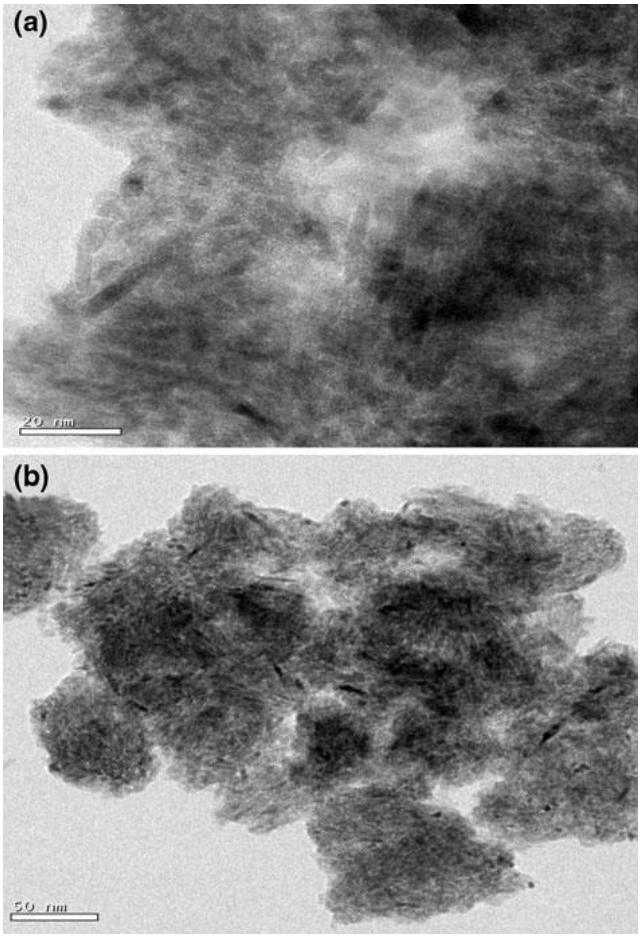

Figure 2.11: TEM micrograph of (a) TiO_2 and (b) PVA/TiO_2 nanocomposite with 2 wt% of PVA [104]

In 2013, Shadpour Mallakpour et al. [105] prepared PVA/TiO_2 nanocomposites with different TiO_2 loadings by using ultrasound irradiation in continuation to their previous research. They prepared these nanocomposites to be used as electrolyte additive in methanol fuel cells. To improve dispersion of TiO_2 nanoparticles and to increase possible interactions between nanoparticles and PVA, γ-aminopropyltriethoxy silane was used to modify the surface of TiO_2 nanoparticles. They observed

reduction in crystallinity of PVA matrix by addition of TiO_2 nanofillers as shown in Fig. 2.12. They concluded from XRD data that modified TiO_2 were connected to PVA chain via covalent bond which increased molecular interaction between the two components in the nanocomposite.

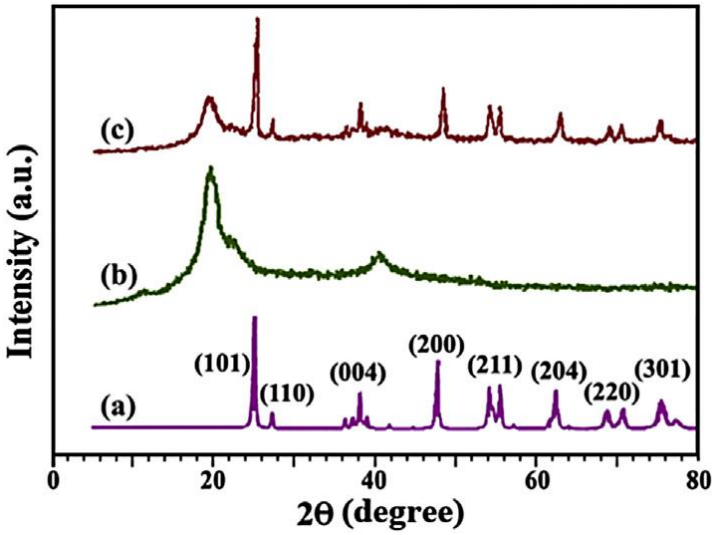

Figure 2.12: XRD graphs of (a) surface modified TiO_2 nanocrystals, (b) PVA and (c) 10 wt% PVA/TiO_2 nanocomposite [105]

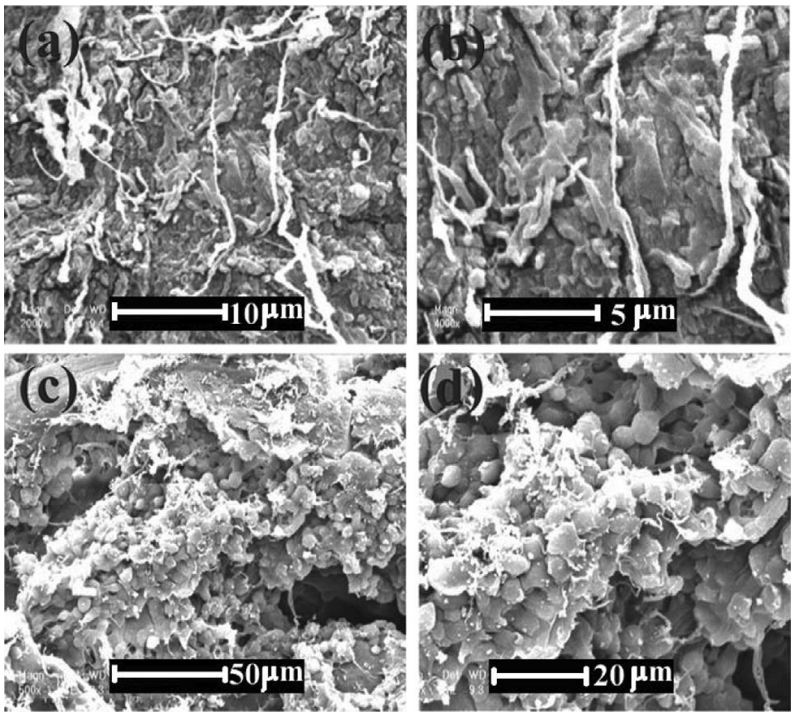

Figure 2.13: SEM micrographs of (a) PVA with 10 μm scale, (b) PVA with 5 μm scale, (c) 10 wt% PVA/TiO_2 nanocomposite with 50 μm scale and (d) 10 wt% PVA/TiO2 nanocomposite with 20 μm scale [105]

Shadpour Mallakpour et al. also conducted SEM and TEM analysis so that the microstructures and the surface morphology of PVA/TiO_2 nanocomposites can be examined with distribution of nanofiller within the nanocomposite. The SEM micrographs of PVA matrix (a, b) and PVA/TiO_2 10 wt% (c, d, e, f) nanocomposite with different magnifications are shown in Fig. 2.13. They observed from SEM images that PVA beads and TiO_2 were well distributed throughout the matrix. They concluded that the modified TiO_2 nanofiller had excellent adhesion and strong interfacial bonding with PVA beads. Fig. 2.14 shows TEM images of PVA/TiO_2 10 wt% nanocomposite at different magnifications. From these TEM results they inferred that the surface modification of nanoparticles prevented their aggregation and good dispersion of TiO_2 nanoparticles within PVA was achieved.

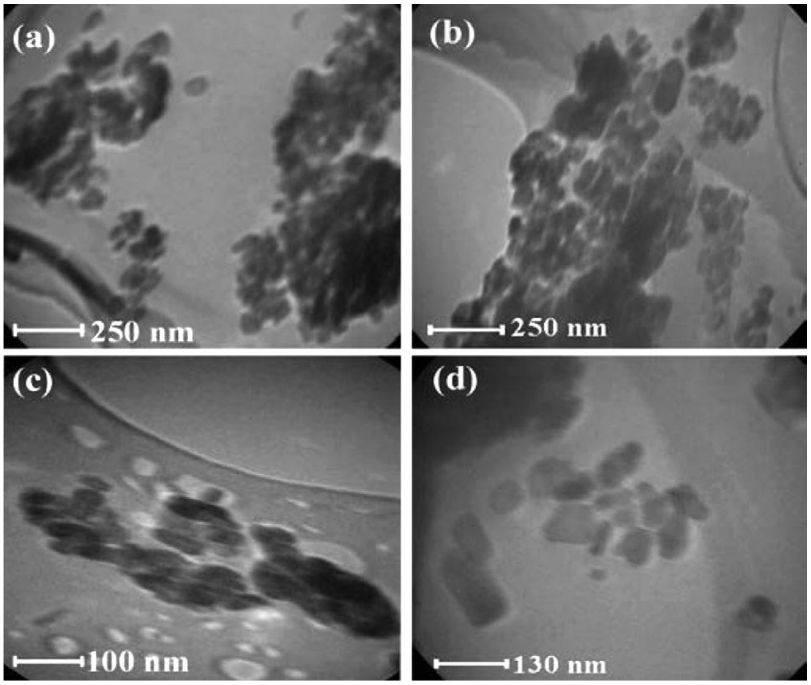

Figure 2.14: TEM micrographs of 10 wt% PVA/TiO_2 nanocomposite with (a) 250 nm scale, (b) 250 nm scale, (c) 100 nm scale, and (d) 130 nm scale [105]

In 2015, A. F. Mansour et al. [106] prepared PVA/ZnO nanocomposites by solution casting method with different concentrations (0, 0.15, 0.5, 1, 2, 2.5, and 3 wt %) of ZnO nanoparticles. The XRD graphs of ZnO/ PVA nanocomposites are shown in Fig. 2.15. The slight change in position of peaks was seen with increasing ZnO content in ZnO/ PVA nanocomposites. They concluded that shifting of peaks was due to change in lattice constants of the two phases but the obtained lattice

parameters nearly had the same values (a= 0.322 nm ± 0.001) and (c= 0.516 nm ± 0.001) to the standard values matched with JCPDS card no. 36-1451. It indicated that ZnO nanoparticles retained their structure even after formation of nanocomposite films which is due to absence of interaction between polyvinyl alcohol and zinc oxide in forming nanocomposites.

In 2018, Abu Hannifa Abdullah et al. [107] fabricated PVA/Graphene nanocomposite by simple solution method. XRD diffractogram of PVA/Graphene nanocomposite with different graphene content is shown in Fig. 2.16. They concluded that the XRD of the PVA/Graphene nanocomposite is showing the exfoliation of graphene in the nanocomposite at molecular level which resulted in decreased crystallinity of PVA and thus influencing the properties of the nanocomposites. The reason behind the alteration in crystallinity of the PVA/Graphene nanocomposite was molecule restriction of PVA chains caused by graphene.

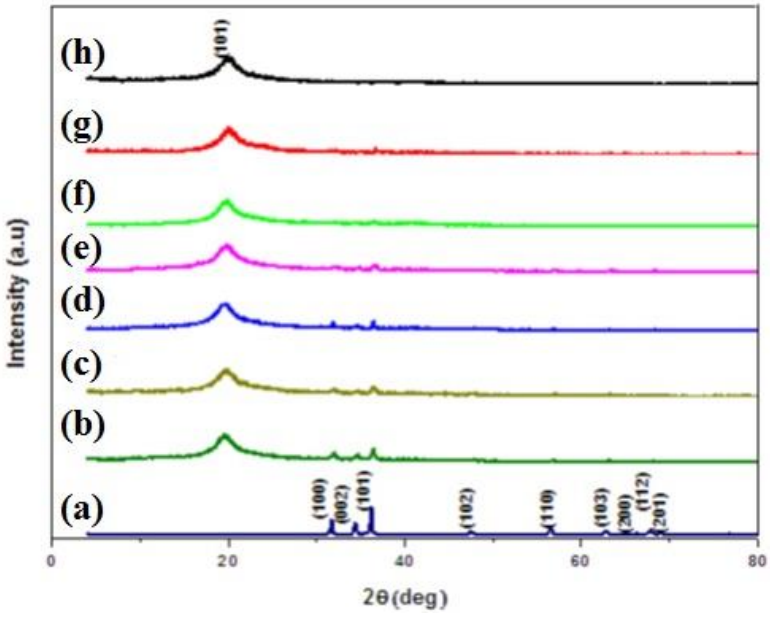

Figure 2.15: XRD graphs of (a) ZnO, (b) 3 wt% ZnO/PVA nanocomposites, (c) 2.5 wt% ZnO/PVA nanocomposites, (d) 2 wt% ZnO/PVA nanocomposites, (e) 1 wt% ZnO/PVA nanocomposites, (f) 0.5 wt% ZnO/PVA nanocomposites, (g) 0.15 wt% ZnO/PVA nanocomposites, and (h) PVA [106]

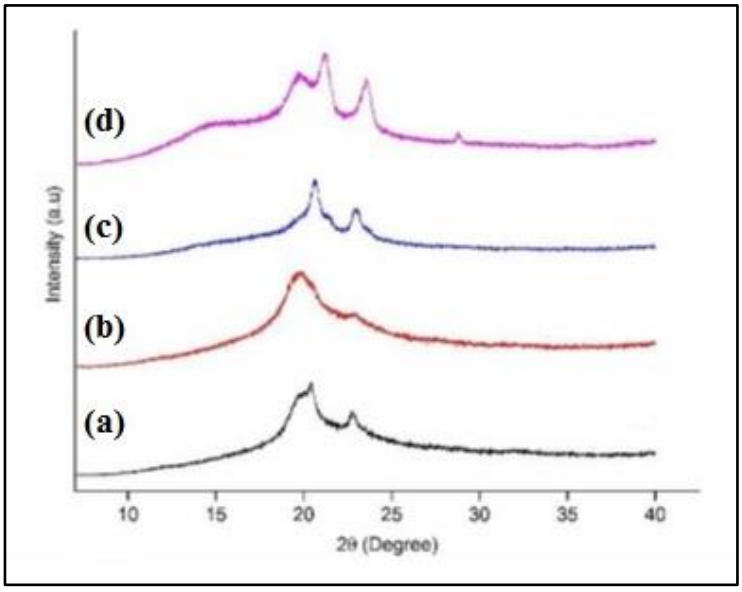

Figure 2.16: XRD graphs of (a) PVA, (b) PVA/Graphene nanocomposites with 0.01 wt% graphene, (c) PVA/Graphene nanocomposites with 0.05 wt% graphene, and (d) PVA/Graphene nanocomposites with 0.1 wt% graphene [107]

Above studies show the structures of PVA based nanocomposites having glutaraldehyde linked PVA, and nanofillers like rutile TiO_2 nanoparticles, modified anatase TiO_2 nanoparticles by aminopropyltriethoxy silane coupling, ZnO nanoparticles and graphene. The addition of nanomaterials results into decreased crystallinity of PVA whereas overall crystallinity of PVA based nanocomposite was improved. The homogenous dispersion of nanofillers within PVA was observed by SEM and TEM images.

2.5.2 Spectroscopic properties

The spectroscopic properties of PVA based nanocomposites are important because interaction between PVA matrix and reinforcement material is identified by these techniques. For this purpose UV-Vis absorption studies and fourier transform infrared studies of PVA based nanocomposites are discussed here.

In 2006, B. Karthikeyan et al. [108] synthesized Ag/PVA nanocomposite, Au/PVA nanocomposite, and Au-Ag/PVA nanocomposite by in-situ synthesis method. The absorption studies of these nanocomposites are shown in Fig. 2.17.

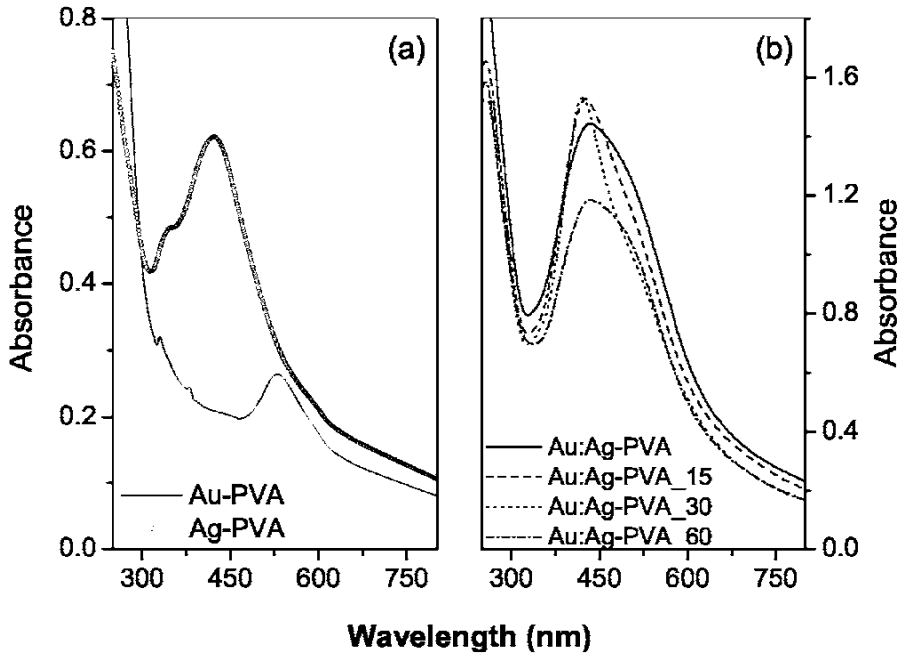

Figure 2.17: Absorption spectra of (a) Au/PVA and Ag/PVA nanocomposites, and (b) as-synthesized and annealed Au:Ag/PVA nanocomposites for 15, 30, and 60 minutes [108]

The absorbance for Ag-PVA and Au-PVA nanocomposites was observed at 410 and 530 nm, respectively. Whereas as prepared Au:Ag-PVA nanocomposites showed broad absorbance. It was due to bimetallic behaviour. After annealing for 15 and 30 minutes, the peak at 410 nm was growing but after annealing for 60 minutes, broad peak reappears for Au:Ag-PVA nanocomposites. They explained that moderate annealing resulted into reduced Ag ions and a core shell structure having Au at centre with covering of Ag. Annealing for 60 minutes destroyed the outer covering of core shell structure.

In 2010, Jeongwoo Lee et al. [102] coated TiO_2 particles with polyvinyl alcohol (PVA) using a simple method of coacervation. In this method, conventional polymerization step was not required. The suspension of PVA-coated TiO_2 particles was then microencapsulated by the coacervation of gelatin and gum Arabic. The FTIR spectra of PVA, TiO_2 nanoparticles with PVA coating, and pure TiO_2 is shown in Fig. 2.18. They confirmed existence of PVA on the surface of TiO_2 nanoparticles by FTIR spectra. For TiO_2 nanoparticles with PVA coating, Ti-O stretching peak appeared along with specific peaks of PVA. Though, the characteristic peaks of PVA were weakened because of very small amount of PVA wrapped on TiO_2 nanoparticles.

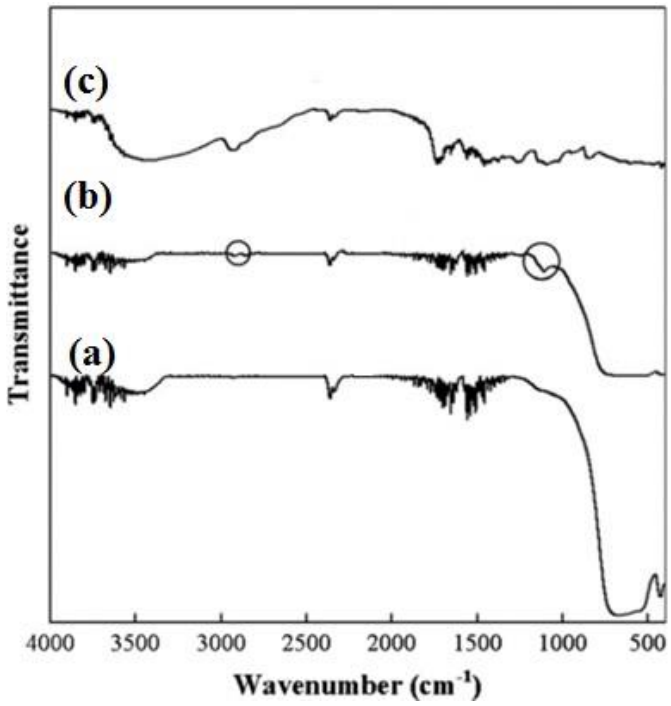

Figure 2.18: FTIR spectra of (a) TiO_2 nanoparticles, (b) TiO_2 nanoparticles with PVA coating, and (c) PVA [102]

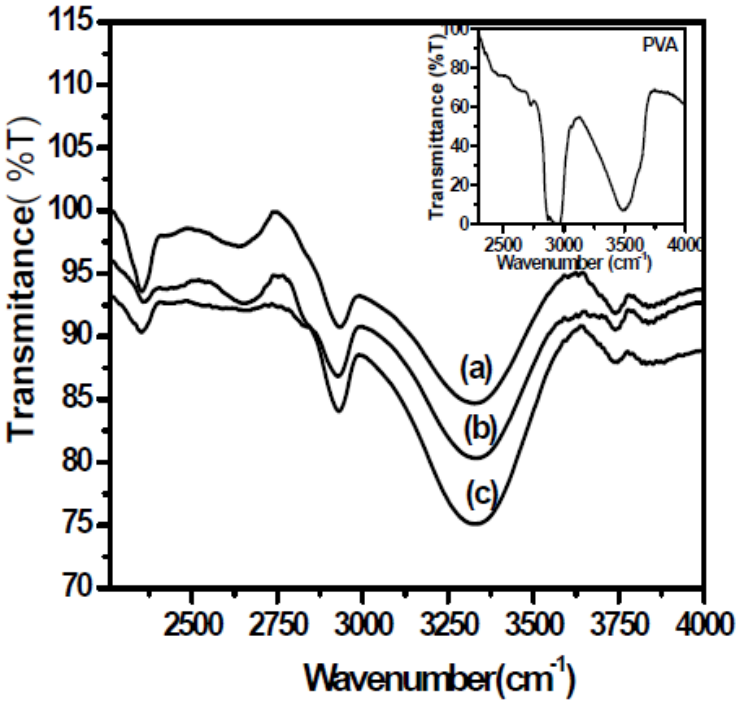

Figure 2.19: FTIR spectra of PVA (inset), (a) PVA/Fe_2O_3 nanocomposites with 4 wt% Fe_2O_3, (b) PVA/Fe_2O_3 nanocomposites with 8 wt% Fe_2O_3, and (c) PVA/Fe_2O_3 nanocomposites with 12 wt% Fe_2O_3 [109]

In 2014, V. S. Upadhayay et al. [109] synthesized PVA/Fe_2O_3 nanocomposite by spin coating method. The FTIR spectra of PVA/Fe_2O_3 nanocomposite is shown in Fig. 2.19. The peaks observed in PVA were shifted to lower wavenumber in PVA/Fe_2O_3 nanocomposite which indicated bonding between PVA and Fe_2O_3.

In 2015, A. F. Mansour et al. [106] prepared PVA/ZnO nanocomposites by solution casting method at different concentrations (0, 0.15, 0.5, 1, 2, 2.5, and 3 wt %) of ZnO nanoparticles. FTIR spectra of PVA, ZnO and ZnO/ PVA nanocomposites are presented in Fig. 2.20. All bands related with PVA and ZnO were present corresponding to their wavenumber. No shifting in band position was observed which indicated that there were no interactions between polyvinyl alcohol and zinc oxide in forming nanocomposites.

A. F. Mansour et al. also studied the absorbance of the nanocomposite films (Fig. 2.21) and observed increase in absorbance with increasing ZnO concentration. This is because of the added ZnO nanoparticles absorb the incident radiation by its free electrons. There is no shift in the absorption edge of PVA and ZnO; indicating no clear interaction between PVA matrix and ZnO nanoparticles.

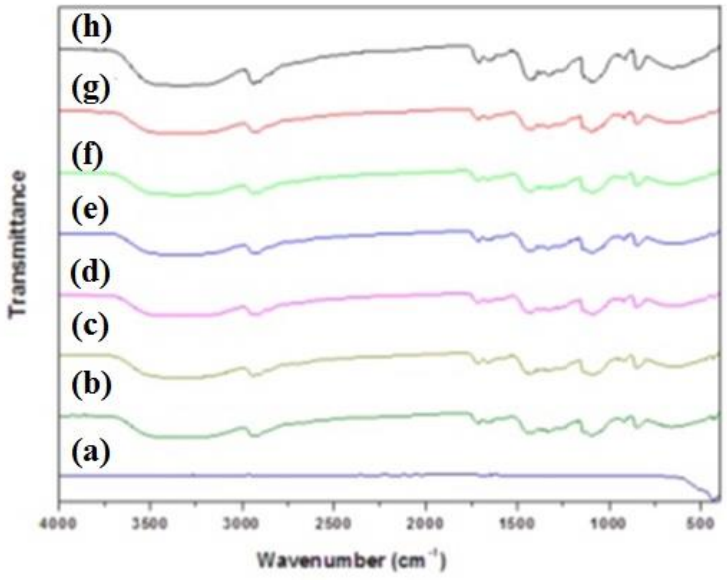

Figure 2.20: FTIR spectra of (a) ZnO, (b) 3 wt% ZnO/PVA nanocomposites, (c) 2.5 wt% ZnO/PVA nanocomposites, (d) 2 wt% ZnO/PVA nanocomposites, (e) 1 wt% ZnO/PVA nanocomposites, (f) 0.5 wt% ZnO/PVA nanocomposites, (g) 0.15 wt% ZnO/PVA nanocomposites, and (h) PVA [106]

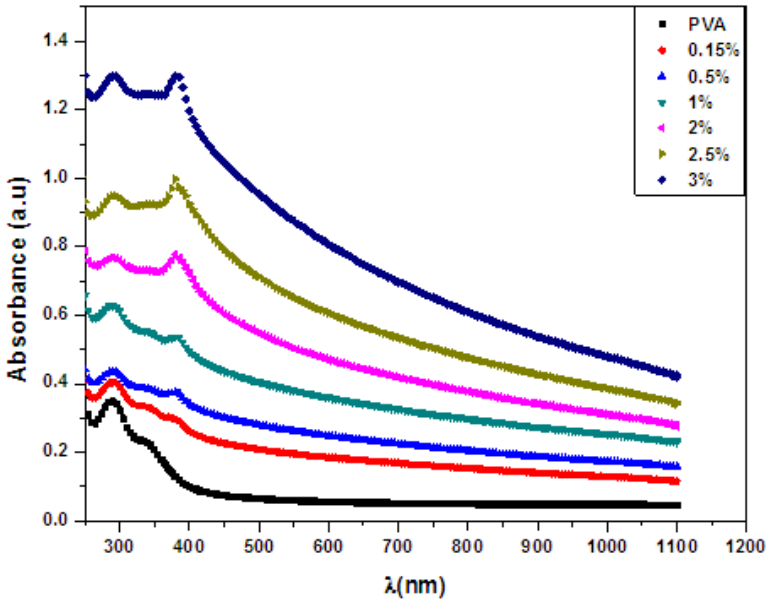

Figure 2.21: UV-Vis absorption spectra of PVA, and ZnO/ PVA films with 3 wt%, 2.5 wt%, 2 wt%, 1 wt%, 0.5 wt%, 0.15 wt% of ZnO [106]

From above studies, the presence of nanofillers within PVA matrix was seen by UV and FTIR spectroscopy. The shifting of peaks of absorption spectra indicates interaction between PVA and nanofillers. The shift in peaks of FTIR spectra confirms bond formation between PVA and nanofillers. In case of ZnO nanoparticles, no interaction between PVA and ZnO was seen whereas interaction between Fe2O3 nanoparticles and PVA was reported.

2.5.3 Thermal properties

Thermal properties of PVA based nanocomposites are important because end products usually requires processing at high temperature. The improvement in thermal stability of PVA by nanoadditives had been investigated by DSC and TGA. Some reported research work regarding thermo-physical analysis and thermogravimetric analysis of PVA based nanocomposites is mentioned here.

In 2005, Zheng Peng et al. [110] prepared PVA/SiO_2 nanocomposite with a unique self-assembled monolayer technique. They studied thermal properties of PVA/SiO_2 nanocomposite by performing DSC analysis as shown in Fig. 2.22. It was observed that addition of the SiO_2 nanoparticles within PVA matrix resulted in substantial increase in glass transition temperature. They inferred from this data that

the SiO_2 nanoparticles are well dispersed in the PVA matrix. The SiO_2 nanoparticles have high relative surface areas and strong adsorptive capacity. Thus, the amorphous molecular chains of PVA became stable and interacted strongly with the SiO_2 nanoparticles. Consequently, the SiO_2 nanoparticles restricted the thermal motion of the PVA molecular segments. The glass transition temperature is the limiting temperature for the applications of plastic polymers, an improvement in Tg is very important for PVA. As for melting point temperature, no clear change was observed between the PVA and PVA/SiO_2 nanocomposite.

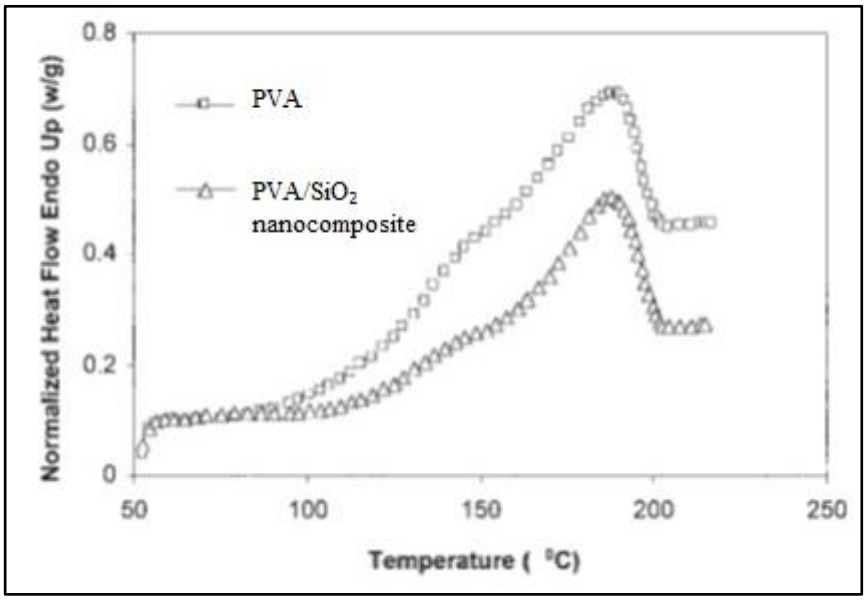

Figure 2.22: Thermograms of PVA and PVA/SiO_2 nanocomposite [110]

In 2007, Hongmei Wang et al. [111] prepared CdS/PVA nanocomposites via in situ synthesis method by chemical reaction of Cd^{+2} dispersed PVA and H_2S. They checked thermal stability of CdS/PVA nanocomposites by TGA curves as shown in Fig. 2.23. It was seen that thermal degradation temperature of CdS/PVA nanocomposite film dropped by 100°C in compare to pure PVA film which is due to decreased interaction between the PVA chains and the degree of crystallization, thus thermal stability of PVA/CdS nanocomposites was lesser than PVA.

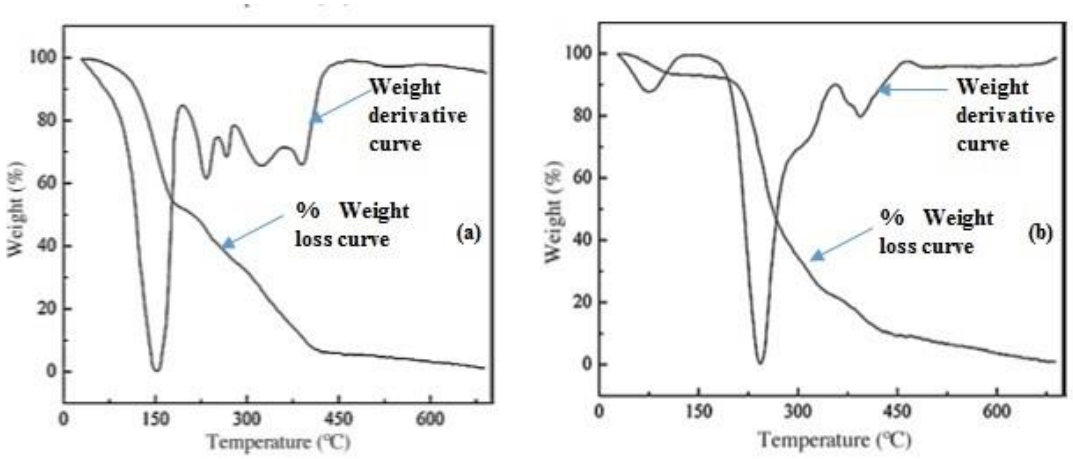

Figure 2.23: TGA curves of (a) CdS/PVA nanocomposites and (b) PVA showing % weight loss and weight derivative curves [111]

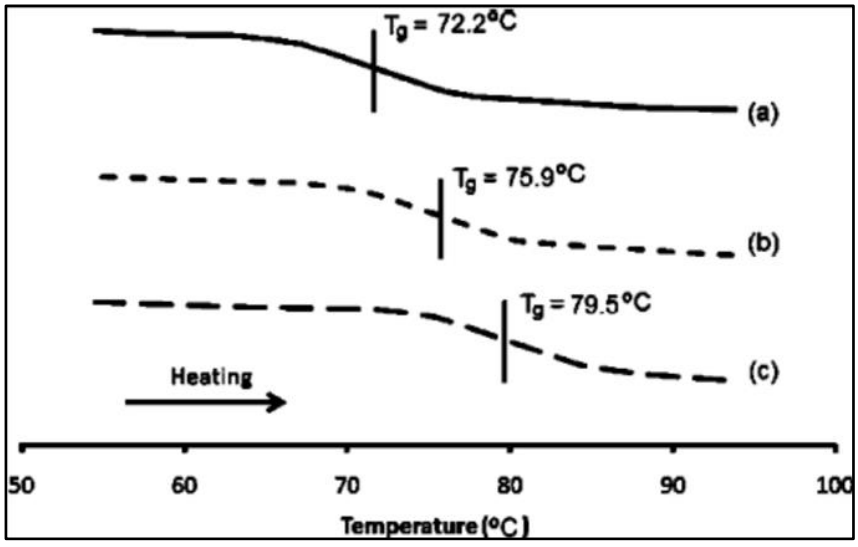

Figure 2.24: Thermogram of (a) PVA, (b) GO/PVA nanocomposite with 1 wt% GO, and (c) GO/PVA nanocomposites with 1.4 wt% GO [112]

In 2012, Henry Kuo Feng Cheng et al. [112] synthesized PVA/GO nanocomposites by integration of PVA-grafted graphene oxide. The PVA-grafted graphene oxide (PVA-g-GO) was used for the strong interfacial adhesion of graphene oxide (GO) to the PVA matrix. The effect of PVA-g-GO on the glass transition temperature of the PVA matrix in the nanocomposites was seen by performing differential scanning calorimetry (DSC) analysis as shown in Fig. 2.24.

In 2013, S. Mallakpour et al. [113] PVA/Al_2O_3 nanocomposites with different compositions by solvent casting method. Thermal stability of PVA/Al_2O_3

nanocomposites was measured by performing TGA as shown in Fig. 2.25. Thermal stability of nanocomposite is enhanced in compare to pure which is result of homogeneous dispersion of Al_2O_3 nanoparticless in PVA matrix. Also, strong hydrogen bonding between O–H groups of PVA and the O–H groups of the Al_2O_3 nanoparticles was observed.

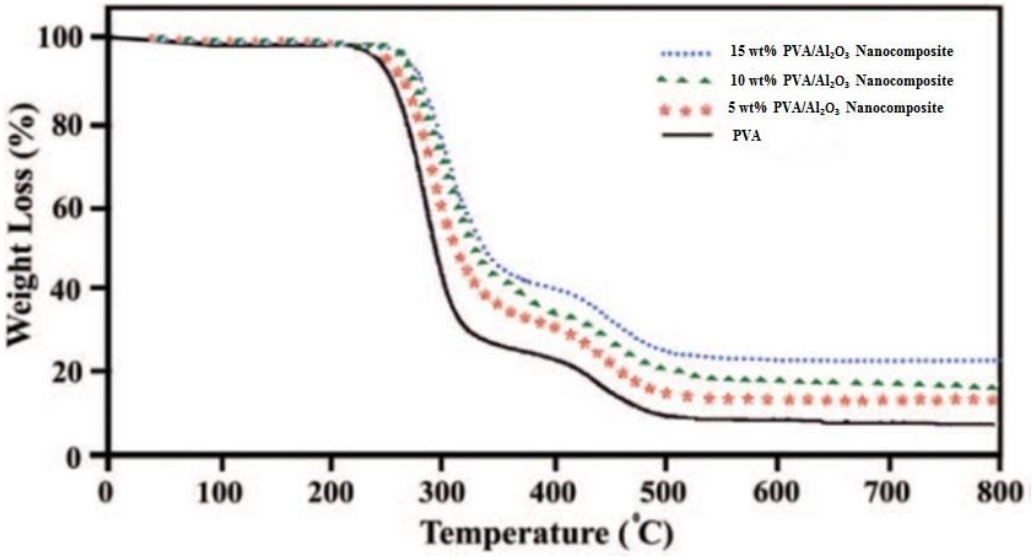

Figure 2.25: TGA curves of PVA and PVA/Al_2O_3 nanocomposite with 5, 10, 15 wt% Al_2O_3 [113]

In 2018, Abu Hannifa Abdullah et al. [107] fabricated PVA/Graphene nanocomposite using simple solution method. They investigated thermal stability of PVA and graphene nanocomposites by TGA thermograms as shown in Fig. 2.26. The thermal stability of PVA and graphene nanocomposites were analysed according to the value of the temperature at 10% weight loss (T10) and 50% weight loss (T50). The increase of T10 in nanocomposite is result of good dispersion of graphene in the polymer matrix which form a barrier labyrinth effect. The stability of the chemical structure of graphene also acted as a physical barrier to the nanocomposite. As, thermal conductivity of graphene is good, so it speeds up the heat transfer and ultimately causes the degradation temperature of nanocomposite to decline further on as showed for T50. The decreasing thermal degradation temperature for PVA is also triggered by the thermal conductivity of graphene in an agglomerated graphene nanocomposite. It causes heat to focus in agglomerated graphene nanocomposite are and thus speeding the thermal degradation process.

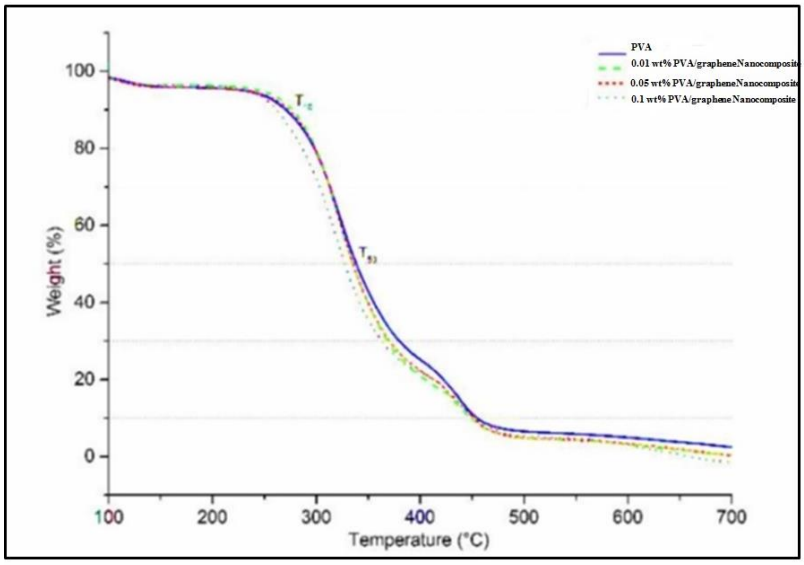

Figure 2.26: TGA curves of PVA and PVA/graphene nanocomposite with 0.01, 0.0.5, and 0.1 wt% graphene [107]

The above mentioned thermal properties of PVA matrix are affected by addition of SiO_2, CdS, PVA-grafted graphene oxide, Al_2O_3 and graphene. The thermal stability of PVA matrix was improved in case of addition of SiO_2, and Al_2O_3 nanoparticles due to interaction between PVA matrix and filler material whereas deprived thermal properties were observed with addition of CdS, PVA-grafted graphene oxide, and graphene. Thus, improvement or deterioration of thermal properties of PVA matrix strongly depends upon the properties of filler material.

2.5.4 Mechanical properties

The mechanical properties of PVA based nanocomposites have been studies for tensile strength mainly. Negligible work has been reported about viscoelastic behaviour of these nanocomposites which is given below.

In 2001, J.-S. Park et al. [114] synthesized blend hydrogels based on polyvinyl alcohol (PVA) and methylcellulose (MC) in an aqueous solution by crosslinking with glutaraldehyde (GA) in the presence of HCl. The determination of the glass transition temperature of blend hydrogels by DMA showed that they exhibit a higher miscibility than the non-crosslinked blends. The temperature dependence of tanδ of PVA/MC blend hydrogels with different MC contents 0-80 wt% is shown in Fig. 2.27. Three relaxation peaks were observed for 20-60 wt% MC content, two for the PVA hydrogel and one for the MC hydrogel. The PVA/MC blend hydrogels with greater than 80 wt% MC content are showing only one relaxation peak which indicates a homogenous and miscible structure.

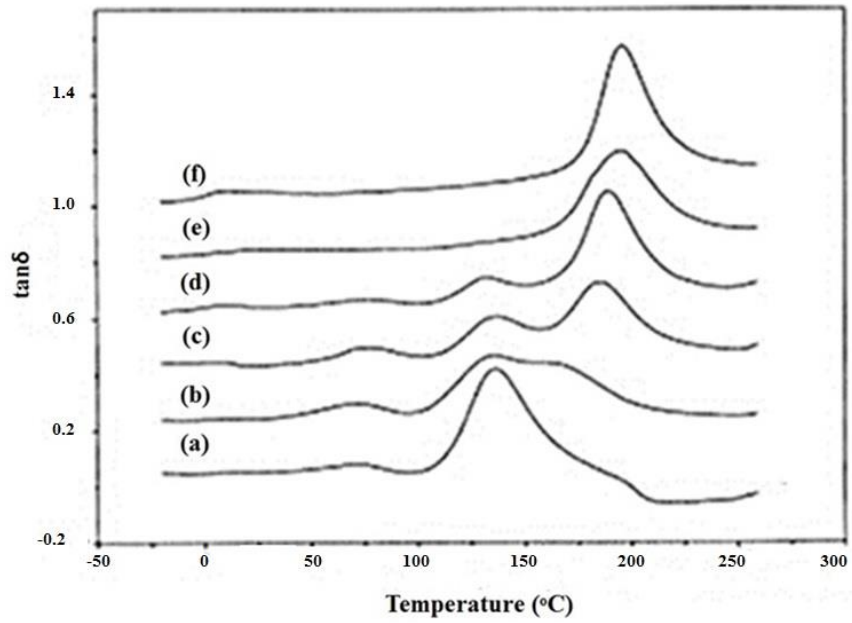

Figure 2.27: The tanδ verses temperature curve of (a) PVA (b) PVA/methylcellulose blend hydrogels with 20 wt% (c) PVA/methylcellulose blend hydrogels with 40 wt% (d) PVA/methylcellulose blend hydrogels with 60 wt% (e) PVA/methylcellulose blend hydrogels with 80 wt% (f) PVA/methylcellulose blend hydrogels with 100 wt% of methylcellulose [114]

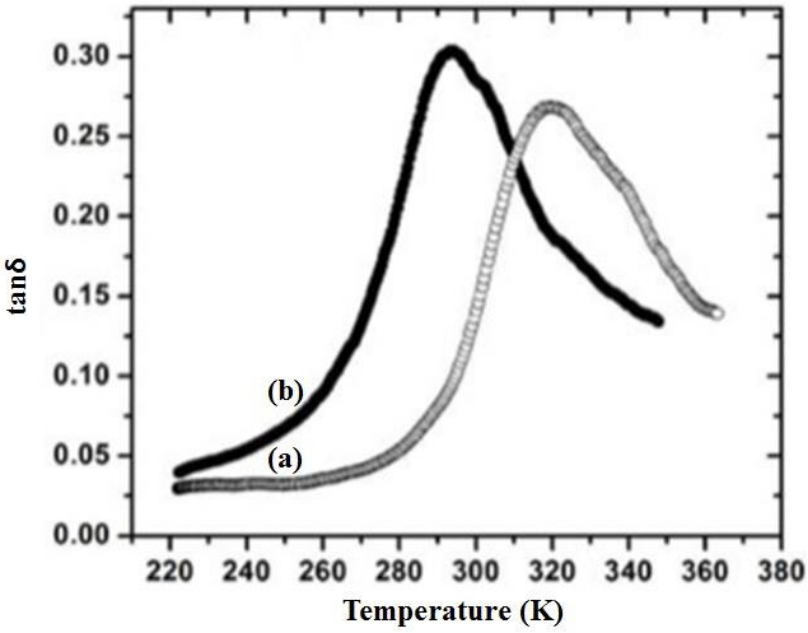

Figure 2.28: The tanδ verses temperature curve of (a) PVA and (b) Graphene/PVA nanocomposite [115]

In 2013, S. Mitra et al. [115] synthesized Graphene/PVA nanocomposite by taking 1 wt% of graphene. The variations in tanδ with respect to temperature were recorded by dynamic mechanical analysis as shown in Fig. 2.28. The glass transition temperature for the Graphene/PVA nanocomposite was found to be lower by 26K than that of pure PVA. It can be explained as reduction of adjacent entanglements of the PVA molecules due to the existence of graphene sheets.

In 2015, S. L. Agrawal et al. [116] prepared MWNTs (multiwall carbon nanotubes) doped PVA: NH_4SCN: DMSO (polyvinyl alcohol-ammonium thiocyanate-dimethyl sulphoxide) dried gel nanocomposite electrolyte arrangement with 2, 4, 6, 8 wt % of MWNTs by solution cast technique. They conducted DMA studies of these nanocomposite electrolytes as shown in Fig. 2.29 and concluded that glass transition temperature is shifting towards lower value with increasing concentration of MWNTs.

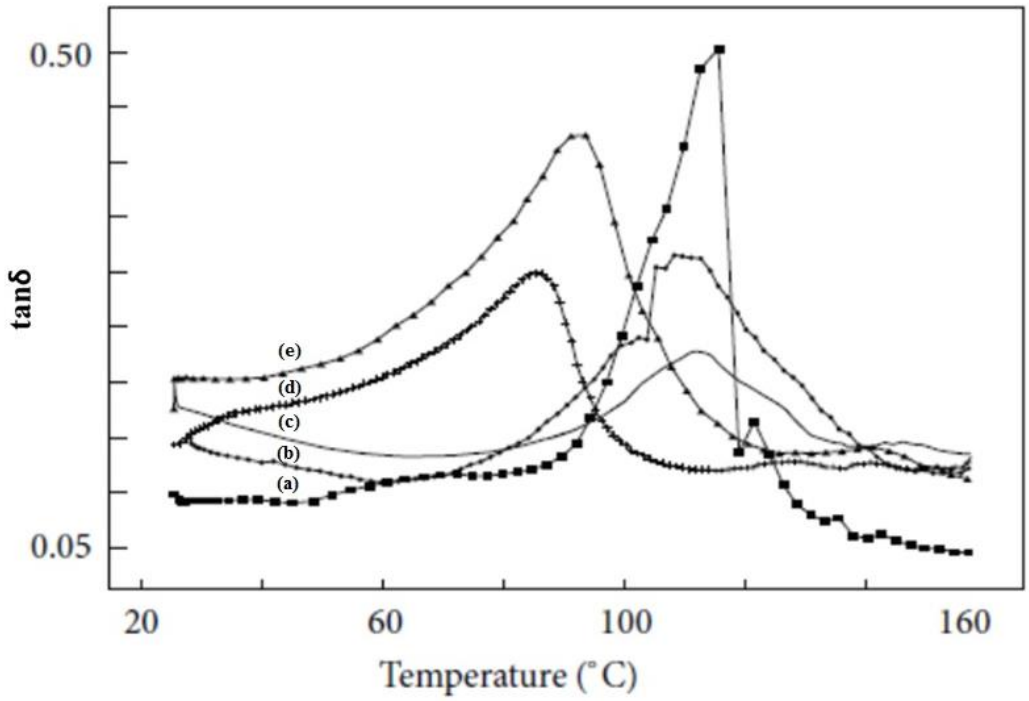

Figure 2.29: The tanδ verses temperature curve of (a) PVA : NH_4SCN : DMSO (b) MWNT/(PVA : NH_4SCN : DMSO) nanocomposite with 2 wt%, (c) MWNT/(PVA : NH_4SCN : DMSO) nanocomposite 4 wt%, (d) MWNT/(PVA : NH_4SCN : DMSO) nanocomposite 6 wt%, and (e) MWNT/(PVA : NH_4SCN : DMSO) nanocomposite 8 wt%, of MWNT [116]

From above studies, it has been seen that addition of nanofillers like MWNTs, methyl cellulose, and graphene into PVA matrix results into improvement in glass transition temperature. The DMA studies of PVA based nanocomposites are limited. That's why it has been chosen to study viscoelastic behaviour of nanocomposite in this study.

The effect of inorganic nanofillers on structural, spectroscopic, thermal and mechanical properties of PVA based nanocomposites are discussed above. Important inferences of these studies are as follows:

From XRD studies, it has been noted that incorporation of: TiO_2 nanoparticles into glutaraldehyde linked PVA, aminopropyl triethoxy silane coupled TiO_2 nanoparticles into PVA, rutile TiO_2 nanoparticles into PVA, and graphene into PVA resulted into reduction in crystallinity of PVA whereas addition of ZnO nanoparticles into PVA did not affect crystallinity. Chun-Chen Yang explained that hydroxyl groups present in PVA reacted with gluteraldehyde to form acetal or semiacetal linkages. Shadpour Mallakpoura et al. explained reduction in crystallinity of PVA as covalent bond formation between aminopropyl triethoxy silane coupled TiO_2 nanoparticles and PVA chain. Archana Maurya et al. reported that crystallinity of rutile TiO_2/PVA nanocomposite increased with increasing PVA. They explained it by interaction between Ti-OH groups on TiO_2 surface and hydroxyl groups on PVA and formation of strong interfacial bond (Ti-O-C). A. F. Mansour et al. explained that there was no interaction between ZnO nanoparticles and PVA, thus crystallinity of PVA was unchanged.

The surface morphology studies of TiO_2 nanoparticles into glutaraldehyde linked PVA, PVA coated TiO_2 nanoparticles, aminopropyl triethoxy silane coupled TiO_2 nanoparticles into PVA, rutile TiO_2 nanoparticles into PVA are discussed. Chun-Chen Yang observed random distribution of gluteraldehyde crosslinked PVA and TiO_2 nanoparticles with presence of aggregates. Whereas Shadpour Mallakpoura et al. found uniform distribution of aminopropyl triethoxy silane coupled TiO_2 nanoparticles into PVA and Archana Maurya et al. observed rodlike and prismlike structures of rutile TiO_2. Jeongwoo Lee et al. also observed aggregates of PVA coated TiO_2.

The FTIR studies of PVA coated TiO_2, Fe_2O_3/PVA nanocomposites, and ZnO/PVA nanocomposites discussed above confirmed presence of respective filler materials into PVA. The shifting and weakening of intensity of PVA peaks was observed for PVA coated TiO_2, and Fe_2O_3/PVA nanocomposites which indicated interaction between PVA and respective filler material. Whereas FTIR spectra of ZnO/PVA nanocomposites showed all the peaks of ZnO and PVA at their position without any chamge. Thus Zno did not interact with PVA.

Absorption studies of Au/PVA, Ag/PVA, Au:Ag/PVA, and ZnO/PVA nanocomposites is discussed. It was seen that presence of two metals (Au and Ag) in PVA showed bimetallic behaviour whereas presence of ZnO did not affect absorption edge because it did not interact with PVA.

Thermophysical analysis of PVA/SiO_2 nanocomposites, and PVA/GO nanocomposites is discussed by DSC thermograms. Both nanocomposites showed increase in glass transition temperature with addition of filler material which is due to interaction between PVA and filler material.

Thermal degradation behaviour of CdS/PVA nanocomposites, Al_2O_3/PVA nanocomposites, and PVA/graphene nanocomposites is discussed by TGA curves. Thermal stability of PVA was improved with addition of CdS and Al_2O_3 as filler due to good ineration of these filler materials with PVA. Whereas thermal degradation temperature of PVA in PVA/graphene nanocomposites was improved at 10 wt% loss but it declined at 50 wt% loss. The reason for decreasing thermal degradation temperature of PVA at 50 wt% loss is good conductivity of graphene which speeds up heat transfer.

The viscoelastic behaviour of PVA/methylcellulose blend hydrogels, PVA/graphene nanocomposites, and PVA:NH_4SCN:DMSO is discussed by tanδ versus temperature curves which shows dynamic glass transition temperature. The value of dynamic glass transition temperature was decreased for PVA with graphene and NH_4SCN:DMSO fillers whereas it was increased for methylcellulose filler.

All above mentioned studies are showing that properties of filler material have significant impact on absorption, bond vibration, phase, surface morphology, thermal and viscoelastic behaviour of PVA. These properties of PVA are altered or unchanged according to interaction between PVA and filler material. As, TiO_2 nanoparticles have good electrical, thermal, and mechanical properties, so incorporation of TiO_2 nanoparticles into PVA matrix improve these properties of PVA by interacting with PVA. From above studies it is noted that thermal studies of anatase TiO_2 doped PVA nanocomposites are limited and viscoelastic behaviour of these nanocomposites has not studied yet.

2.6 Applications

PVA based nanocomposites are investigated now a days due to their wide appliations in biomedical engineering, environmental sector, industries, and academia.

Optical fibers coated with PVA based nanocomposites are significant because of their high sensitivity, corrosion resistance, electromagnetic interference resistant, easy fabrication etc. [117].

Polymer based metal oxide nanocomposites have been succefully designed for their applications in photovoltaics/solar cells, fuel cells, and batteries [118-124].

PVA is widely used polymer to prepare membranes due to its low cost, hydrophilicity, good flexibility, and film forming properties [125]. The properties of these membranes are needed to improve, so addition of inorganic nanofillers into PVA have been topic of research these days. In this research work, TiO_2 nanoparticles are added into PVA to improve properties of PVA.

The applications of TiO_2 doped PVA membranes are mainly in air separation, natural gas purification, and hydrogen recovery [126].

Other applications of TiO_2 doped PVA nanocomposites are in water purification, degradation of organic pollutants, and photocatalysis [127-129]. Schematic presentation of applications of TiO_2 doped PVA nanocomposites is shown in Fig. 2.30.

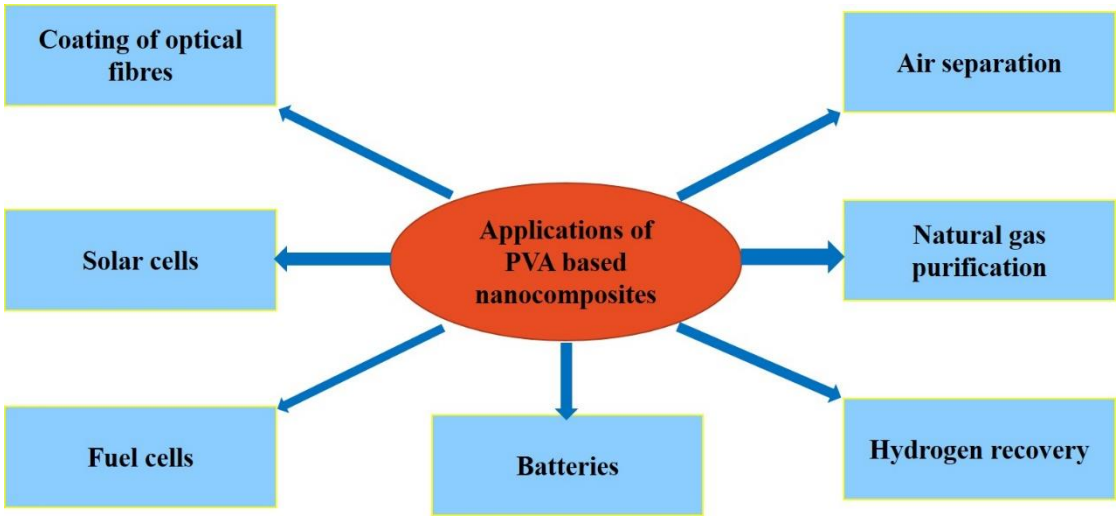

Figure 2.30: Applications of TiO_2 doped PVA nanocomposites

2.7 Identification of Research Gap

After reviewing the available literature, the research gap between literature work and this research work was decided as:

i In previous studies, TiO_2/PVA nanocomposites have been explored mainly for their optical properties. The work on thermal behaviour of TiO_2/PVA nanocomposites is limited.

ii Viscoelastic behaviour of TiO_2/PVA nanocomposites has not been explored yet to the best of researcher's knowledge. So, it was decided to study viscoelastic behaviour of TiO_2/PVA nanocomposites.

iii The concentration of PVA and TiO_2 nanoparticles affects properties of TiO_2/PVA nanocomposites. So, effect of varying concentration of PVA and TiO_2 nanoparticles on spectroscopic study, phase analysis, surface morphology analysis, thermal and mechanical behaviour was chosen for further study.

2.8 Objectives of This Research Work

The primary objectives of this research work are to prepare TiO_2/PVA nanocomposites with different variations of TiO_2 nanoparticles and PVA. Also, to study the properties of TiO_2/PVA nanocomposites. Various characterization techniques such as UV-Vis spectroscopy, FTIR spectroscopy, x-ray diffraction analysis, FESEM with EDS and mapping, differential scanning calorimetry, thermal

gravimetric analysis, and dynamic mechanical analysis were performed for prepared TiO_2/PVA nanocomposites to conduct this research work.

The work presented in this thesis therefore includes following studies of TiO_2/PVA nanocomposites.

i To prepare anatase TiO_2 nanoparticles and confirmation by UV-Vis spectroscopy, fourier transform infrared spectroscopy, x-ray diffraction, and scanning electron microscopy.

ii To develop PVA film and nano-TiO_2 doped PVA nanocomposite films with different weight percent of TiO_2 nanoparticles.

iii To study the effect of different weight percent of TiO_2 nanoparticles and PVA on absorption studies of TiO_2/PVA nanocomposites.

iv To study the effect of different weight percent of TiO_2 nanoparticles and PVA on bond stretching and bond vibrations of TiO_2/PVA nanocomposites.

v To study the effect of different weight percent of TiO_2 nanoparticles and PVA on lattice strain, dislocation density, and crystallite size of TiO_2/PVA nanocomposites.

vi To study the effect of different weight percent of TiO_2 nanoparticles and PVA on surface morphology and dispersion of TiO_2 nanoparticles within PVA.

vii To study the effect of different weight percent of TiO_2 nanoparticles and PVA on thermos-physical analysis and thermal degradation of TiO_2/PVA nanocomposites.

viii To study the effect of different weight percent of TiO_2 nanoparticles and PVA on viscoelastic behaviour of TiO_2/PVA nanocomposites.

On the basis of literature review, research gap was identified and objectives of this research work were formulated at first. Optimization of parameters is required for appropriate synthesis of TiO_2/PVA nanocomposites. So, in the next chapter, optimization of parameters for synthesis of TiO_2/PVA nanocomposites are discussed.

Chapter 3

OPTIMIZATION OF PARAMETERS

TiO_2/PVA nanocomposites lies in the category of polymer-matrix nanocomposites. Polymer-matrix nanocomposites can be synthesized by intercalation method, in-situ polymerization method, sol-gel method, and direct mixing of polymer with nanofillers which are discussed in this research work. Among these methods solvent casting method was most suitable for synthesis of TiO_2/PVA nanocomposites. This method depends on various parameters i.e. solubility of polymer in solvent, dispersion of nanoparticles etc. Some of these parameters are discussed in this chapter.

Optimization of these parameters is very important to proper synthesis of TiO_2/PVA nanocomposites.

3.1 Important Parameters for Synthesis of TiO_2/PVA Nanocomposites

Polymer-matrix nanocomposites are synthesized by intercalation method, in-situ polymerization method, sol gel method, and direct mixing of polymer with nanofillers [130-140].

Intercalation method generally includes the dispersion of nanoplatelets into the polymer matrix. Homogeneous dispersion of the nanoplatelets can be achieved by two methods: Chemical method and Physical method. Chemical method involves in-situ polymerization method in which nanoplatelets are swollen into monomer solution and then polymerization reaction takes place between the intercalated sheets. Whereas in mechanical method the polymer is dissolved in a co-solvent and simultaneously nanoplatelets are swollen in the solvent and then both solutions are mixed with each other, the polymer chains in the solution intercalate into the layers of nanoplatelets and displaces the solvent [141-143].

In situ polymerization method involves the swelling of the nanofillers in monomer solution, then monomer is polymerized between interlayers. Polymerization takes place to form either exfoliated or intercalated nanocomposites [143].

In sol-gel route, solid nanoparticles are dispersed in the monomer solution which forms a colloidal suspension of solid nanoparticles i.e. sol. After that

polymerization reactions occur which are followed by hydrolysis procedure. They form interconnecting network between phases i.e. gel. The 3D network of polymer and nanoparticles extends throughout the liquid. Here, the polymer works as a nucleating agent and stimulates the growth of layered crystals. As the crystals grow, the polymer is soaked between layers and thus nanocomposite is synthesized [143].

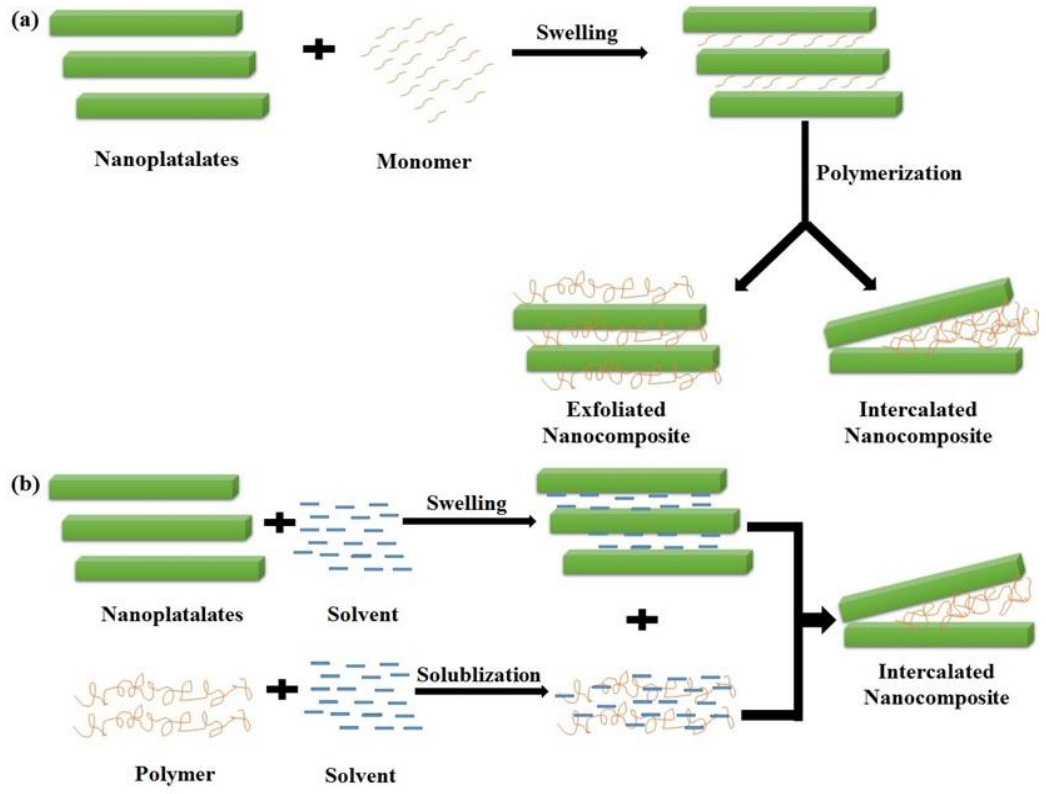

Figure 3.1: Schematic diagram of intercalation method to synthesize polymer-matrix nanocomposites (a) Chemical method, and (b) Physical method

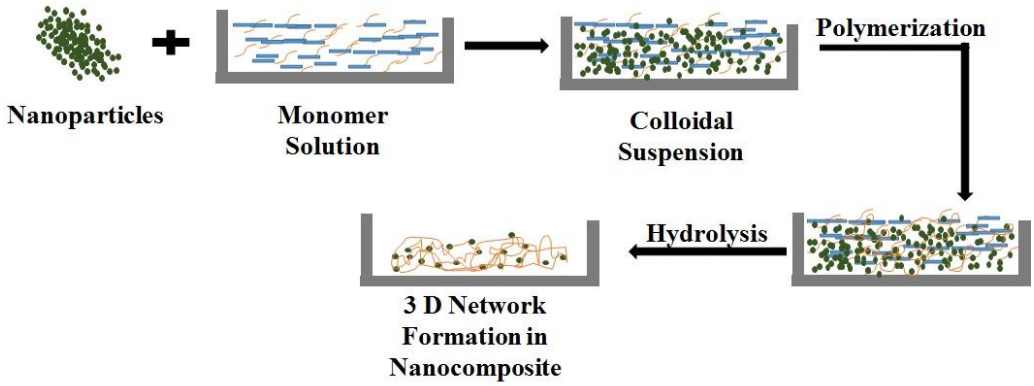

Figure 3.2: Schematic diagram of sol-gel method to synthesize polymer-matrix nanocomposites

Schematic diagrams of intercalation and sol-gel method are shown in Figure 3.1 and Figure 3.2, respectively.

In direct mixing of a polymer matrix and nanofillers, aggregated nanofillers are breaked down during mixing process. There are two ways of mixing the polymer and nanofillers: melt compounding method and solvent method/solution mixing. In first method, polymer is mixed with nanofillers above the glass transition temperature of the polymer, in the absence of any solvents. The second method is solvent method/solution mixing which involves mixing of polymer and nanofillers in solution employing solvents [141-143]. Schematic presentation of melt compounding method and solvent method/solution mixing are shown in Figure 3.3.

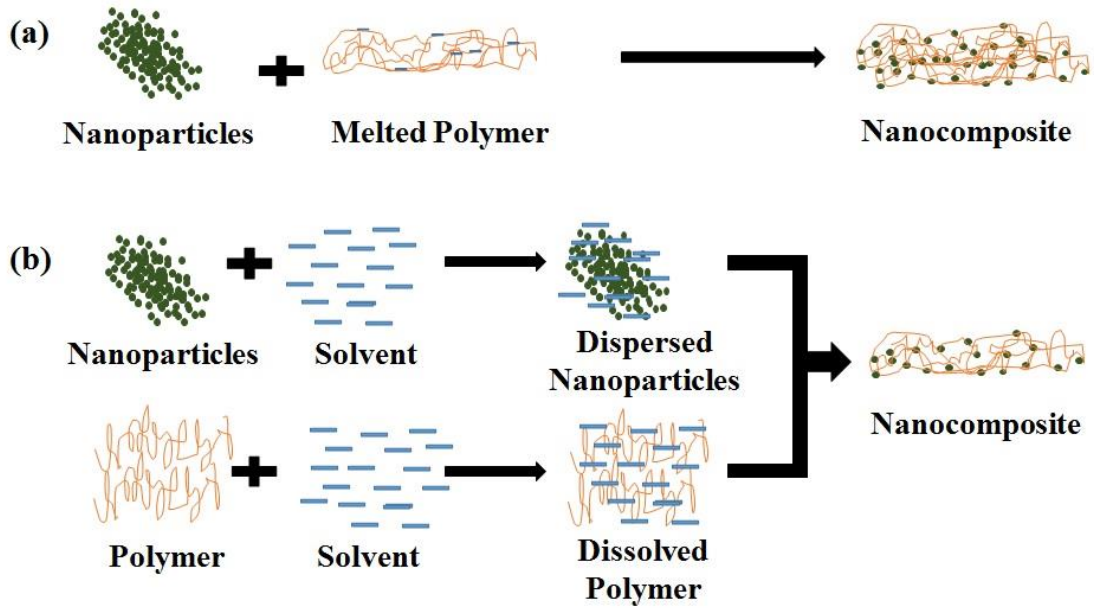

Figure 3.3: Schematic diagram of Direct-mixing method to synthesize polymer-matrix nanocomposites (a) melt compounding method, (b) solvent method

Intercalation method is suitable for nanocomposite synthesis where nanoplatelets are used as filler material. In-situ polymerization method requires high temperature which may degrade polymer. Also, except direct mixing of a polymer matrix and nanofillers, all other methods require a monomer solution of polymer.

In case of PVA, availability of monomer solution was not possible. PVA is not synthesized by polymerization of the corresponding monomer unit because the

theoretical monomer, vinyl alcohol, is less stable than its tautomer and it rearranges into acetaldehyde as shown in scheme 3.1 (discussed in section 2.4.1) [144-146].

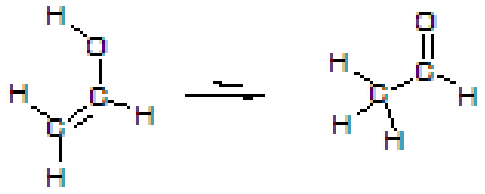

Scheme 3.1: Tautomerization reaction of vinyl alcohol

Hence, PVA is prepared by first polymerizing vinyl acetate, and the resulting polyvinyl acetate is converted to the PVA. Other precursor polymers like formate, chloroacetate groups are also used sometimes used instead of acetate. The formation of polyvinyl alcohol from polyesters is usually facilitated by base-catalysed transesterification with ethanol as:

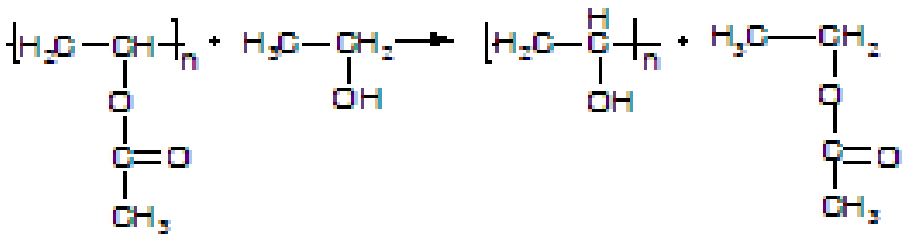

Scheme 3.2: Synthesis of polyvinyl alcohol from vinyl acetate

Thus, among above explained methods, the most suitable method for synthesis of TiO_2/PVA nanocomposites is direct mixing of a polymer matrix and nanofillers. This method is commonly known as solvent casting method. This method involves predispersion of the nanofillers in a solution of the polymer, followed by evaporation of the solvent from the nanofiller-polymer solution, which generally results in homogenous dispersion of nanofillers in the polymer matrix [147-158]. Other benefits of using solvent casting method can be summarized as [159]:

i Nanocomposites are synthesized at low temperature.

ii It is very simple to add nanofillers into polymer matrix by this method.

iii Homogeneous distribution of nanoparticles into polymer matrix is possible.

iv Isotropic orientation regarding thermal, mechanical, and optical properties can be achieved by this method.

The solvent casting method was used in this study to synthesize TiO_2/PVA nanocomposites. Schematic presentation of this method is shown in Figure 3.1. A solution of polymer i.e. solution A, and a dispersion of nanoparticles i.e. solution B is prepared first. Then solution B is added dropwise to solution A with stirring. Resultant solution is then casted on a petriplate. Solvent is allowed to evaporate at room temperature and nanocomposite is obtained.

Important parameters for synthesis of TiO_2/PVA nanocomposites are divided in three subheadings as: parameters for synthesis of PVA solution, parameters for dispersion of TiO_2 nanoparticles, and parameters for mixing of PVA solution and dispersion of TiO_2 nanoparticles. These parameters are discussed as follows:

3.1.1 Parameters for dissolution of PVA in solution

PVA solutions were prepared by taking different weight percent of PVA into distilled water. Prepared solutions were stirred with heating till dissolution of PVA in distilled water and they became transparent.

Stirring affects how rapidly a solute dissolves in a solvent, but it doesn't have any effect on how much solute will dissolve. Whereas temperature affects the amount of solute that dissolves in solution and it increases with increasing temperature of solution.

Stirring simply moves the solvent molecules all over the place, letting them to interact with the solid particles of undissolved solute and carrying the dissolved solute away into the bulk solution.

Without stirring, the concentration of solute will be maximum in the vicinity of solute particles, so dissolution of more solute won't be possible until the dissolved solute particles have been transported away by diffusion.

J. L. Duda et al., and M. L. Huggins, concluded in their research works that the molecular diffusion of a polymer in solution is a complex process. It depends on temperature, concentration, degree of polymerization and its morphology [160-164].

In another studies, Adeyinka Aina et al., R. P. Danner et al., D. Eagland et al., and J. R. Fried et al. found that PVA shows non-ideal solution behaviour which means dissolution time doesn't increase linearly with increasing concentrations of PVA [165-167].

Here, temperature of PVA solution, speed and time of stirring are discussed for optimization.

3.1.1.1 Temperature of PVA solution during stirring

It is well known that PVA is a semi-crystalline polymer. It has ordered structure due to presence of hydroxyl groups. Hence, polymer chains are folded into a regular and thermodynamically stable organisation. It is very difficult to unfold the polymer chains from the ordered state into a disordered state in solution even if the later state is thermodynamically more stable. The unfolding is assisted by heating, so polymer is needed to heat for dissolution. Once dissolved, polymer chains take a random coil orientation till the chain becomes rigid [168].

Table 3.1: Optimization of temperature of PVA solution

S. No.	Weight percent of PVA film (%)	Designation Of PVA	Weight of PVA (gm)	Volume of distilled water (ml)	Temperature (°C)	Observation
1	2.91	P1	1.5	50	70	PVA didn't dissolve in distilled water
2	2.91	P1	1.5	50	80	PVA dissolved
3	2.91	P1	1.5	50	90	Solution became too viscous
4	3.38	P2	1.75	50	70	PVA didn't dissolve in distilled water
5	3.38	P2	1.75	50	80	PVA dissolved
6	3.38	P2	1.75	50	90	Solution became too viscous

Temperature plays crucial role in dissolution of PVA into distilled water. At high temperature, lumps may form; and at very low temperature, dissolution is not possible. So, it is important to optimize temperature of PVA solution during stirring.

Two solutions of PVA (P1 and P2) were taken to optimize the temperature of PVA solution during stirring (see Table 3.1). These samples were continuously stirred at 70°C, 80°C, and 90°C. At 70°C, PVA didn't dissolve in distilled water. Whereas at 90°C, heating rate was too high and solution became too viscous due to evaporation of solvent. PVA was completely dissolved into distilled water at 80°C.

Thus, temperature for dissolution of PVA into distilled water was optimized as 80°C.

3.1.1.2 Speed and time of stirring of PVA solution

Speed and time of stirring affects the overall time of dissolution of solute particles into solution. It has been seen that high speed for more period results into reduction of size of solute particles and vice versa [169].

The effect of the stirring rate on the average grain size was studied by Barclay (1976), and Lewis et al. (1981). They concluded that the particle size is likely to decrease with increasing speed upto a threshold value, after this value size of particles increases [170-171].

Rita Marinho et al. conducted a study about effect of stirring speed on synthesis of poly (vinyl chloride) by suspension polymerization method. They also determined time taken in stabilization of poly (vinyl chloride) particles. The conversion of vinyl chloride into poly (vinyl chloride) was higher at higher stirring speeds. Also, better stability of particles was observed at 900 rpm in compare to 600 rpm [172].

It was seen that, if speed of stirring of PVA solution is kept high in the starting, PVA granules may stick to the wall of glassware due to centrifuging and it will become difficult to dissolve them. Optimization of speed and time during stirring was needed to dissolve PVA into solution without lumps.

Table 3.2: Optimization of speed of stirring for PVA film

S. No.	Weight percent of PVA film (%)	Designation of PVA	Weight of PVA (gm)	Volume of distilled water (ml)	Speed of stirring (rpm)	Observation
1	2.91	P1	1.5	50	High (1500 RPM)	Solute particles were sticking to walls of beaker
2	2.91	P1	1.5	50	Medium (1000 RPM)	Perfect dissolution of PVA was formed
3	2.91	P1	1.5	50	Low (500 RPM)	Solute particles didn't dissolve in distilled water
4	3.38	P2	1.75	50	High (1500 RPM)	Solute particles were sticking to walls of beaker
5	3.38	P2	1.75	50	Medium (1000 RPM)	Perfect dissolution of PVA was formed
6	3.38	P2	1.75	50	Low (500 RPM)	Solute particles didn't dissolve in distilled water

Two samples of PVA (P1 and P2) were taken into distilled water and stirred at 500 RPM, 1000 RPM, and 1500 RPM with continuous heating to optimize speed and time of stirring (see Table 3.2). It can be seen from Table 3.2 that solute particles were sticking to walls of beaker at 1500 RPM, whereas solute particles didn't dissolve in distilled water at 500 RPM. Perfect dissolution of PVA into distilled water was observed at 1000 RPM. Hence, the optimized speed for dissolution of PVA into distilled water was medium (1000 RPM).

To optimize time of stirring, two samples of PVA (P1 and P2) were taken into distilled water. These samples were stirred at 80°C, and 1000 RPM for 1, 2, and 3 hour (see Table 3.3). It can be seen from Table 3.3 that perfect solution of PVA was formed within 2 hours of stirring at 80°C and 1000 RPM. Whereas, solute particles didn't dissolve in distilled water in 1 hour and solution became too viscous in 3 hours due to evaporation of solvent.

Thus, it is concluded that optimized time for dissolution of PVA into distilled water was 2 hours.

Table 3.3: Optimization of time of stirring for PVA film

S. No.	Weight percent of PVA film (%)	Designation of PVA	Weight of PVA (gm)	Volume of distilled water (ml)	Time of stirring (hour)	Observation
1	2.91	P1	1.5	50	1	Solute particles didn't dissolve in distilled water
2	2.91	P1	1.5	50	2	Perfect solution was formed
3	2.91	P1	1.5	50	3	Solution became too viscous
4	3.38	P2	1.75	50	1	Solute particles didn't dissolve in distilled water
5	3.38	P2	1.75	50	2	Perfect solution was formed
6	3.38	P2	1.75	50	3	Solution became too viscous

Schematic presentation of dissolution of PVA into distilled water at optimized temperature, time, and speed is shown in Figure 3.4.

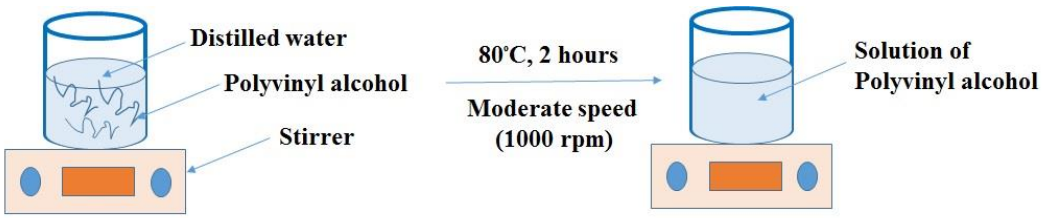

Figure 3.4: Schematic diagram of dissolution of PVA solution at optimized parameters

3.1.2 Parameters for dispersion of TiO_2 nanoparticles in distilled water

This section includes important parameters related with dispersion of TiO_2 nanoparticles. Unique properties of nanoparticles are due to their small size and high surface to volume ratio. Nanoparticles have tendency to agglomerate due to high interfacial area. Agglomeration of nanoparticles increases effective size of

nanoparticles, thus altering their physical properties [173]. The agglomerates are breakdown by applying shear forces via a sonicator [173-175].

The size of dispersed nanoparticles depends upon the conditions of suspension such as solvent type, concentration and volume of suspension solution [176]. In sonication, nucleation and bubbles are created by oscillation of liquid and collapse of solvent, respectively. Formation of bubbles and collapses at the surface of solids is very effective in breaking up aggregated solute particles. In sonication, breaking up of the agglomerates is mainly controlled by power, time and dispersion volume [177]. There are two ways of sonication: bath sonication and probe sonication [178].

J. Jiang et al. showed that probe sonication is better than bath sonication to prepare dispersion of agglomerates of TiO_2 nanoparticles. They used sodium pyrophosphate as stabilizing agent [178]. O. Hayakawa et al. and K. A. Kusters et al. found that deagglomeration is effective in dispersing agglomerated nanoparticles irrespective of the power of sonicator in case of non-oxide samples [176, 179]. Kimitoshi Sato et al. studied about aggregation and dispersion behaviour of TiO_2 nanoparticles in aquous solution by three mechanical dispersion methods: ultrasonication irradiation, milling with 5 mm diameter balls, and milling with 50 μm beads and they found that ultrasonic irradiation method was best among these methods to prepare highly dispersed suspension of nanoparticles [173].

Though sonication breaks up aggregated nanoparticles but nanoparticles have tendency to reaggregate. In order to prepare stable dispersions, only breaking apart agglomerates of nanoparticles is not sufficient [180-181]. The Derjaguin-Landau-Verwey-Overbeek (DLVO) theory explains stability of dispersions of nanoparticle and their tendency to agglomerate [182]. According to this theory, attraction between nanoparticles is due to the van der waals force and each nanoparticle is surrounded by the electrical double layer which is responsible for electrostatic repulsive force. The separation of agglomerated nanoparticles can be achieved by overcoming the weaker attractive forces. For this purpose, stabilization techniques like electrostatic, steric and electrosteric interactions have been

investigated [183-186]. Steric interactions are achieved by coating of either polymer or biomolecules [175].

In previous studies, ploymers like polyethylene glycol, polyacrylamide, polyacrylic acid, and polyethylene (glycol) diacrylate have been used to prepare stable suspension of TiO_2 nanoparticles [186-190].

Also, the nanoparticles are under gravitational force, buoyant force and frictional force in a suspension and balance of these forces keeps them suspended. The sedimentation velocity of nanoparticles can be decreased by [190]:

i Reducing size of nanoparticles

ii Increasing viscosity of base fluid or

iii Minimizing density difference between nanoparticles and the base fluid.

Among the above parameters, reducing the particle size have remarkable effect on decreasing the sedimentation velocity of the nanoparticles and improving the stability of nanofluids. However, the smaller nanoparticles have higher surface energy, so increases the aggregation of nanoparticles. Hence, the key to synthesize stable suspensions of nanoparticles is to use smaller nanoparticles and to prevent the aggregation of the small nanoparticles by proper surface stabilization [190].

From above discussion, it is concluded that TiO_2 nanoparticles can be dispersed in water but after some time TiO_2 nanoparticles settle down in solvent. So, probe sonicator is used to create brownian motion in solution to keep TiO_2 nanoparticles in suspend condition for prolonged time. Schematic diagram of probe sonicator is shown in Figure 3.5.

In this research work, TiO_2 nanoparticles were dispersed into PVA matrix. Here, PVA helps in maintaining stable suspension of TiO_2 nanoparticles by steric repulsion between nanoparticles [175, 181]. As a result of steric repulsion, effective size of nanoparticles is reduced [181].

So, two parameters are important to study in making dispersion of TiO_2 nanoparticles: sonication time, and settling time of TiO_2 nanoparticles after sonication.

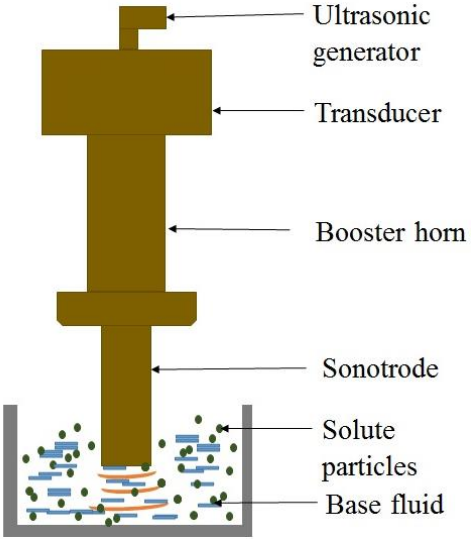

Figure 3.5: Schematic presentation of sonication via probe sonicator

3.1.2.1 Sonication time for dispersion of TiO_2 nanoparticles in distilled water

As discussed in previous section, sonication is required to break agglomerates of TiO_2 nanoparticles but over sonication may accelerate aggregation whereas insufficient sonication cannot disperse nanoparticles. So, it is important to optimize sonication time for preparation of dispersion of TiO_2 nanoparticles.

TiO_2 nanoparticles with 0.5 wt% were sonicated for 1, 2, and 3 hour as shown in table 3.4. In 1 hour, TiO_2 nanoparticles didn't disperse in distilled water whereas in 3 hours, TiO_2 nanoparticles started to reagglomerate. Good dispersion of TiO_2 nanoparticles within distilled water was observed after 2 hours of sonication.

Table 3.4: Optimization of sonication time for dispersion of TiO_2 nanoparticles

S. No.	Weight percent of TiO_2 nanoparticles (%)	Weight of TiO_2 nanoparticles (gm)	Volume of distilled water (ml)	Time of sonication (hour)	Observation
1	0.5	0.25	50	1	TiO_2 nanoparticles didn't disperse in distilled water
2	0.5	0.25	50	2	Good dispersion was formed
3	0.5	0.25	50	3	Reaggregation of TiO_2 nanoparticles was seen

The sonication time for dispersion of TiO_2 nanoparticles was optimized as 2 hours.

3.1.2.2 Settling time of TiO_2 nanoparticles after sonication

Prepared dispersion of TiO_2 nanoparticles is not stable with time. Stabilizing agents are used for preparation of stable suspensions of nanoparticles. In this research work, PVA was used to stabilize dispersion of TiO_2 nanoparticles. PVA solution and dispersion of TiO_2 nanoparticles were prepared simultaneously, so that TiO_2 nanoparticles can be stabilized into PVA matrix before their settling time.

Table 3.5: Settling time of after sonication

S. No.	Weight percent of TiO_2 nanoparticles (%)	Weight of TiO_2 nanoparticles (gm)	Volume of distilled water (ml)	Time (hour)	Observation
1	0.015	0.0078	50	1	No settlement of solute particles
2	0.015	0.0078	50	2	No settlement of solute particles
3	0.015	0.0078	50	3	No settlement of solute particles
4	0.015	0.0078	50	4	No settlement of solute particles
5	0.015	0.0078	50	5	Solute particles started to settle down
6	5	2.63	50	1	No settlement of solute particles
7	5	2.63	50	2	No settlement of solute particles
8	5	2.63	50	3	No settlement of solute particles
9	5	2.63	50	4	No settlement of solute particles
10	5	2.63	50	5	Solute particles started to settle down

In this research work, minimum and maximum weight percent of TiO_2 nanoparticles is taken as 0.015 and 5 wt%, respectively for synthesis of TiO_2/PVA nanocomposites. So, settling time was checked for minimum and maximum concentrations of TiO_2 nanoparticles as shown in Table 3.5.

No settlement of solute particles was observed till 4 hours. After 5 hours of sonication, some solute particles started to settle down.

3.1.3 Parameters for mixing of PVA solution and dispersion of TiO_2 nanoparticles

Already prepared PVA solution and dispersion of TiO_2 nanoparticles are mixed by stirring to get TiO_2/PVA nanocomposites. After sonication, dispersion of TiO_2 nanoparticles is immediately added to PVA solution because TiO_2 nanoparticles will settle down after some time. TiO_2 nanoparticles were added dropwise into PVA solution with continuous stirring at room temperature. Here, two parameters, stirring time and speed are needed to optimize.

3.1.3.1 Speed and time of stirring of TiO_2 nanoparticles/PVA solution

Speed and time of stirring is also important in mixing of solution A and solution B. TiO_2 nanoparticles are dropwise added dropwise into PVA solution with continuous stirring. Stirring speed and stirring time were optimized as shown in Table 3.6 and Table 3.7, respectively.

TiO_2/PVA nanocomposites with 0.5 wt% of TiO_2 nanoparticles and 2.91 wt% of PVA were mixed together at three stirring speeds: 500, 1000, and 1500 rpm.

Table 3.6: Optimization of speed of stirring for TiO_2 nanoparticles/PVA solution

S. No.	Weight percent of TiO_2 (%)	Weight percent of PVA film (%)	Speed of stirring (rpm)	Observation
1	0.5	2.91	High (1500)	Solution was coming out
2	0.5	2.91	Medium (1000)	Perfect mixing
3	0.5	2.91	Low (500)	Mixing was not possible

It can be seen from Table 3.6 that perfect mixing of dispersion of TiO_2 nanoparticles and PVA solution was achieved at medium speed (1000 rpm) of stirring.

TiO_2/PVA nanocomposites with 0.5 wt% of TiO_2 nanoparticles and 2.91 wt% of PVA were mixed together and stirred for 1, 2, 3, and 4 hours. It was observed that proper mixing of TiO_2 nanoparticles within PVA took 4 hours.

Table 3.7: Optimization of time of stirring for TiO_2 nanoparticles/PVA solution

S. No.	Weight percent of TiO_2 (%)	Weight percent of PVA film (%)	Time of stirring (hour)	Observation
1	0.5	2.91	1	Not mixed
2	0.5	2.91	2	Not mixed
3	0.5	2.91	3	Not mixed
4	0.5	2.91	4	Perfect mixing

From Table 3.7, it can be seen that perfect mixing of dispersion of TiO_2 nanoparticles within PVA solution was observed after 4 hours of stirring.

Important parameters for synthesis of TiO_2/PVA nanocomposites were optimized in this chapter and they can be concluded as follows:

i Optimized temperature, stirring rate and stirring time for dissolution of PVA into distilled water were 80°C, moderate speed (1000 rpm), and 2 hours, respectively.

ii Optimized sonication time for preparation of dispersion of TiO_2 nanoparticles is 2 hours.

iii Time of settling down of dispersed TiO_2 nanoparticles after sonicating for 2 hours was 5 hours.

iv Optimum stirring speed and time for mixing of dispersion of TiO_2 nanoparticles within PVA solution were moderate (1000 rpm) and 4 hours, respectively.

TiO_2/PVA nanocomposites were prepared with consideration of above parameters as described in chapter 5. Synthesis and characterization of TiO_2 nanoparticles is discussed in next chapter.

Chapter 4

SYNTHESIS AND CHARACTERIZATION OF TiO_2 NANOPARTICLES

Titanium dioxide nanoparticles exhibit good electrical, physical and chemical properties. To incorporate these properties into PVA matrix, TiO_2 nanoparticles were added into PVA matrix. As reviewed in literature, highly crystalline and anatase phase TiO_2 nanoparticles are prepared by sol-gel method. Thus, in this research work, sol-gel method was followed to synthesize TiO_2 nanoparticles.

4.1 Sol-gel Method

In this method, inorganic salt or metal alkoxide is used as precursor. First of all precursor is hydrolysed, then partially condensation of precursor is performed. It results in formation of a stable colloidal solution which is known as sol. Sol is suspension of solid particles into liquid medium. The further condensation of sol into a three dimensional network form gel. Two phase are present in gel i.e. liquid is entrapped inside solid particles. The removal of entrapped liquid is performed by different drying processes such as supercritical drying, and evaporation etc [191-192].

In this research work, Titanium tetra isopropoxide (TTIP) was used as precursor and TiO_2 nanoparticles were synthesized by sol-gel method.

4.2 Materials for Synthesis of TiO_2 Nanoparticles

Titanium tetra isopropoxide (TTIP), ethanol, distilled water, Nitric acid (HNO_3)

4.3 Synthesis of TiO_2 Nanoparticles

Titanium dioxide nano powders were prepared following sol–gel process using titanium tetra isopropoxide (TTIP) as precursor as discussed above. 2.5 ml of TTIP was dissolved in ethanol and then mixed with 10 ml of water. The ratio of TTIP to water was kept as 1:4. If the water is taken in lesser amount than it is evaporated before completion of the process whereas excess water delays the overall process. The prepared solution was kept under constant stirring on magnetic stirrer

at low speed for about 2 hour. Nitric acid (HNO_3) was added dropwise to adjust pH value in acidic range. The rate of hydrolysis is affected by the pH value. The gels were dried at 50°C for 1.5 hr. resulting in the increase in the viscosity of the solution indicating the evaporation of water and organic impurities. The yellow crystals of titanium dioxide were obtained at the end of drying process. These crystals were crushed into fine powder using a mortar and pestle. Obtained TiO_2 nanoparticles were characterized.

4.4 Characterization of Prepared TiO_2 Nanoparticles

Prepared TiO_2 nanoparticles were characterized to study absorbance, chemical bonds, phase, and surface morphology. UV-Vis spectroscopy, FTIR spectroscopy, x-ray diffraction, and scanning electron microscopy were performed.

4.4.1 Absorption studies

Absorption spectrum of TiO_2 nanoparticles was obtained by UV-Vis spectroscopy. Absorption studies gives information about electronic transition when TiO_2 nanoparticles are irradiated with ultraviolet and visible region of electromagnetic spectrum. The formation of nanoparticles is confirmed by shifting the absorption spectra to lower wavelength region in compare to bulk.

The UV-Vis spectra of TiO_2 nanoparticles was recorded with LAMBDA 750 (Perkin Elmer) UV-VIS NIR spectrophotometer instrument and wavelength was kept between 200-800 nm.

4.4.2 Bond studies

The chemical bonds present in TiO_2 nanoparticles were identified by FTIR spectroscopy. FTIR spectroscopy for TiO_2 nanoparticles was performed over the frequency region 4000-500 cm^{-1} and spectra were recorded in reflection mode. FTIR Spectrum 2 (Perkin Elmer) instrument was used.

4.4.3 Phase analysis

Phase of synthesized TiO_2 nanoparticles was checked by XRD. X-Ray Diffractometer (Panalytical X Pert Pro) was used to perform XRD of TiO_2 nanoparticles. The diffraction angle (2Θ) was kept between 10^o to 80^o. Cu K(α) target (λ = 0.154 Å) was used. Intensity peaks for different elements with respect to

diffraction angle (2Θ) were observed. These peaks were compared with standard JCPDS file to confirm phase of TiO_2 nanoparticles.

4.4.4 Surface morphology

Surface morphology of TiO_2 nanoparticles was studied by field emission-scanning electron microscope (FE-SEM, Nova Nano FE SEM) and operated at 15-20 kV. Elemental analysis of TiO_2 nanoparticles was done by energy diffraction x-ray analyser (EDX/EDS) detector (Bruker, Germany). Surface morphology study is important to know about agglomeration, and index of size of prepared nanoparticles.

Results and discussions of above characterizations for as prepared TiO_2 nanoparticles are discussed below.

4.5 Results and Discussions of Characterized TiO_2 Nanoparticles

The results obtained from absorbance, chemical bonds, phase, and surface morphology studies are discussed below.

4.5.1 Absorption studies

Absorption spectra of TiO_2 nanoparticles obtained using UV-Vis spectroscopy is shown in Fig. 4.1. It is showing absorption peak of TiO_2 nanoparticle at 245.93 nm. This shows blue shift in absorbance in compare to bulk TiO_2 due to quantum confinement effect induced by reduction in size.

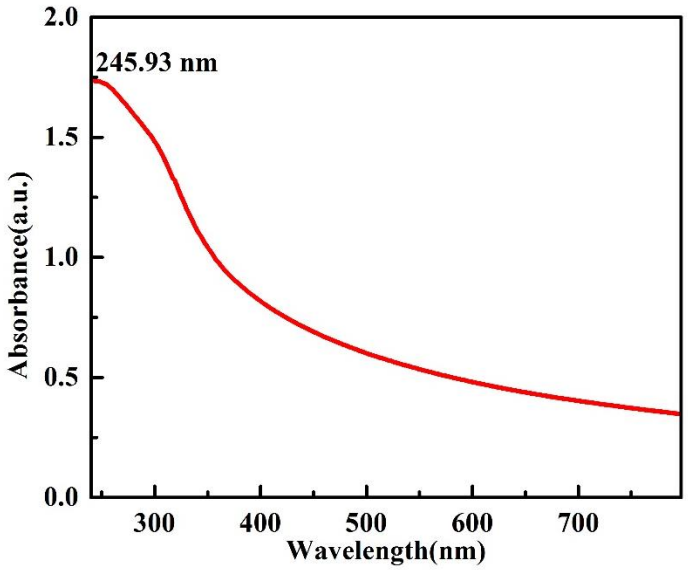

Figure 4.1: Absorption spectrum of TiO_2 nanoparticles

Band gap of prepared TiO_2 nanoparticles was calculated by Tauc's relation. Tauc relation is given as [193]:

$$\alpha h\upsilon = A\,(h\nu - Eg)^{1/2} \qquad \ldots\ldots\ldots\ldots\ 4.1$$

Here,

α = 2.303 log (T/d)

d = thickness of the sample

T = transmission

hυ = photon energy

Equation 4.1 can be rewrite as:

$$(\alpha h\upsilon)^{1/2} = A^2\,(h\upsilon - Eg) \qquad \ldots\ldots\ldots\ldots\ldots 4.2$$

Equation 4.2 was compared with equation of circle and plot between $(\alpha h\upsilon)^{1/2}$ and photon energy was used to calculate band gap of TiO_2 nanoparticles. The value of hυ (photon energy) extrapolated to α=0 gives the band gap of the prepared TiO_2 nanoparticles (Fig. 4.2). The band gap for TiO_2 nanoparticles was obtained as 3.5 eV which shows shifting of 0.3 eV from band gap of bulk TiO_2 (3.2 eV).

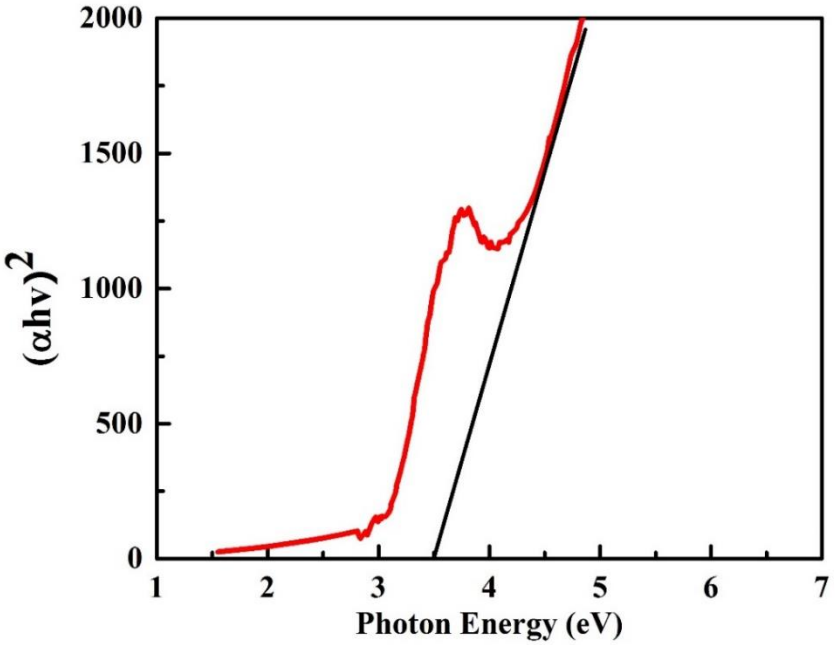

Figure 4.2: Tauc plot of TiO_2 nanoparticles

4.5.2 Bond studies

The FTIR spectrum of prepared TiO_2 nanoparticles recorded in the range of 500 cm^{-1} to 4000 cm^{-1} is shown in Figure 4.3. A peak, appearing at 641 cm^{-1} is due to stretching vibration of Ti-O. The peak at 1388 cm^{-1} and 1631 cm^{-1} corresponds to C-H and NO_3^- ion respectively. The absorption range around 3261cm^{-1} indicates the stretching of hydroxyl (O-H), which is due to bending vibrations of H_2O [191-192].

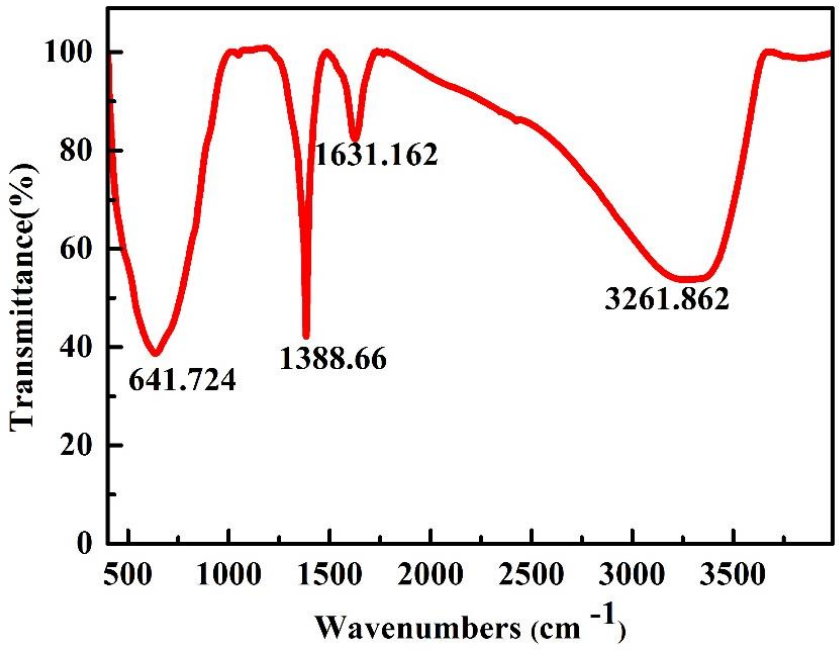

Figure 4.3: FTIR spectrum of of TiO_2 nanoparticles

4.5.3 Phase study

The phase and crystallinity of prepared TiO_2 nanoparticles were analysed by x-ray diffractometer. XRD pattern of prepared TiO_2 nanoparticles is shown in Figure 4.4. XRD pattern shows five peaks at 2θ° = 25.53**,** 37.73, 48.189, 63.00, 69.541 which corresponds to (101), (103), (200), (213), (116) reflection planes, respectively. These reflection planes correspond to the anatase crystalline phase of TiO_2. The XRD pattern was compared with standard JCPDS database and good matching with formation of anatase TiO_2 was seen.

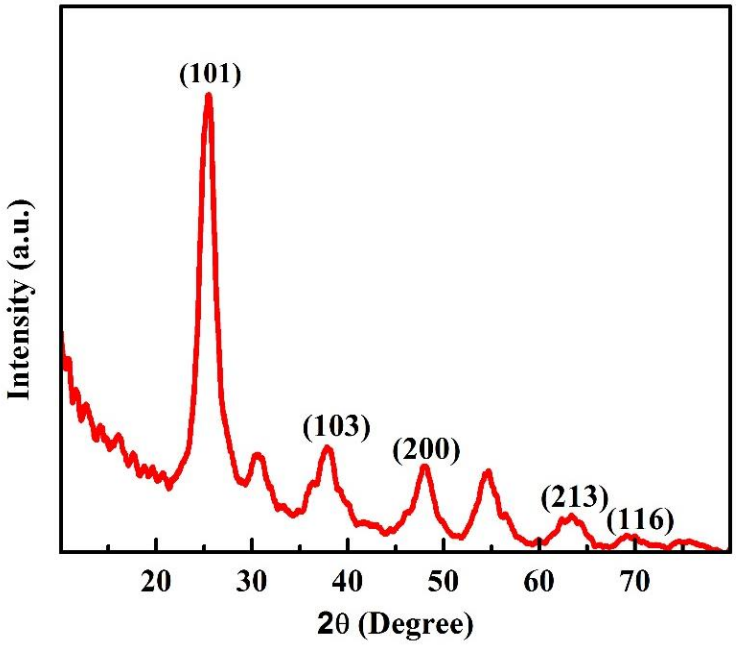

Figure 4.4: XRD diffractogram of TiO_2 nanoparticles

4.5.4 Surface morphology

Surface morphology of TiO_2 nanoparticles and confirmation of elements was performed by SEM. SEM micrographs with EDAX of prepared TiO_2 nanoparticles are shown in Figure 4.5. It can be concluded that prepared TiO_2 nanoparticles were spherical and cluster formation was observed. The EDAX image confirms the presence of Ti and O element in sample.

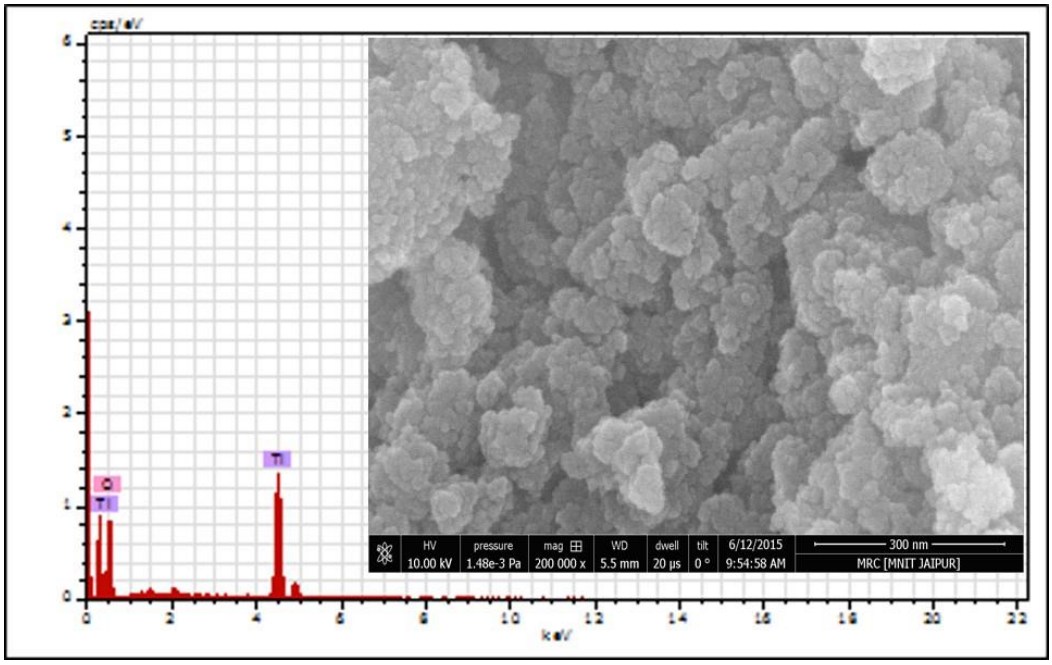

Figure 4.5: SEM image with EDAX of TiO_2 nanoparticles

From above results it can be seen that prepared TiO_2 nanoparticles were in anatase phase, but irregular morphology and cluster formation was observed.

Titanium dioxide nanoparticles prepared by sol- gel method were found to be pristine which was confirmed by EDAX and FTIR. Anatase phase of TiO_2 was confirmed by XRD and SEM analysis confirmed the size of TiO_2 particles in nanometer range. Blue shift of 0.3 eV in band gap of TiO_2 powder was observed due to quantum confinement effect. Wide band gap semiconductor materials have applications in devices which operate at high voltage, high frequency and high temperature.

Chapter 5

EXPERIMENTAL

(Synthesis and Characterization of TiO_2/PVA nanocomposites)

In this chapter, description of raw materials, composition of TiO_2/PVA nanocomposites, principle of sonication, solvent casting technique, and parameters of characterization are discussed. Absorption studies and bond vibration studies were done by UV-Vis spectroscopy and fourier transform infrared spectroscopy, respectively. Phase analysis and surface morphology were studied by x-ray diffraction and scanning electron microscopy. Thermal properties of prepared TiO_2/PVA nanocomposites were studied by differential scanning calorimetry (DSC) and thermal gravimetric analysis (TGA). The glass transition temperature and melting point of prepared nanocomposites were observed by DSC and thermal decomposition behaviour was seen by TGA. The effect of temperature on viscoelastic behaviour of TiO_2/PVA nanocomposites was studied by dynamic mechanical analysis. This chapter is divided into following sections.

5.1 Sonication of TiO_2 Nanoparticles

To prepare TiO_2/PVA nanocomposites by solvent casting method, a dispersion of TiO_2 nanoparticles was desired. For this purpose, probe sonication was used. Probe sonication is better than bath sonication in terms of high intensity and evenly spread.

In sonication, ultrasound energy is (ultrasonic frequencies $>$ 20 kHz) used [194]. It converts an electrical signal into a physical vibration to break substances apart [195]. Basic principle of dispersion of nanoparticles by sonication is described below.

5.1.1 Principle of sonication

During sonication process, high power ultrasound waves propagate into liquid medium which generates alternating high pressure and low pressure cycles by transmitting sound waves in the liquid. Small voids are created during low pressure cycle. When the volume of voids achieve at a threshold value where they can’t

absorb energy, these voids collapses during high pressure cycle of ultrasound waves. This phenomenon is known as cavitation [196]. Cavitation results into, increase in localized temperature and pressure during the collapse i.e. (approx. 5,000 K), and (approx. 2,000 atm), respectively. Also, rapid changes in temperature ($> 10^5$ K/s), and high speed jet streams ($\approx$ 400 Km/hr), are detected during the collapse of voids. This local energy output plays major role in disruptive effect of sonication. Cavitation is responsible for dispersion of nanoparticles in solvent. In Figure 5.1, sonotrode's surface with its cavitational hot spot area is shown.

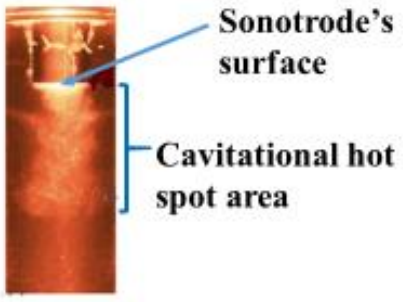

Figure 5.1: Ultrasonic sonotrode transmitting sound waves into liquid [195]

5.1.2 Factors affecting sonication

The intensity of ultra sonication depends on the energy input and the sonotrode's surface area. For a given energy input value, the intensity of ultrasound is inversely proportional to the surface area of the sonotrode [195].

5.1.3 Dispersion of TiO_2 nanoparticles

Nanoparticles may have strong Van der Waals forces due to considerable interfacial contact areas per unit volume. Hence, technique like sonication are required for effective disruption of agglomerates of nanoparticles. Shock waves generated from cavitation are responsible for breakage of nanoparticle agglomerates. Sonication is effective because nanoparticles themselves act as nuclei to start cavitation process [196].

In this research work, TiO_2 nanoparticles were successfully dispersed in distilled water by probe sonication.

5.2 Solvent Casting Technique

In this study, TiO_2/ PVA nanocomposites were prepared by solvent casting technique. Schematic diagram of solvent casting technique is shown in Figure 5.2. Methodology of solvent casting, important parameters, and advantages of this technique are as follows.

5.2.1 Methodology of solvent casting

In solvent casting technique, two solutions are prepared simultaneously. One solution is prepared by dissolving polymer in a suitable solvent; solution 'A', and other solution is prepared by making dispersion of nanoparticles in same solvent; solution 'B'. Then, solution 'B' is added to the solution 'A' and it is casted onto a petriplate. Finally, solvent evaporates from the solution at room temperature and it creates a nanocomposite film consisting nanoparticles within polymer.

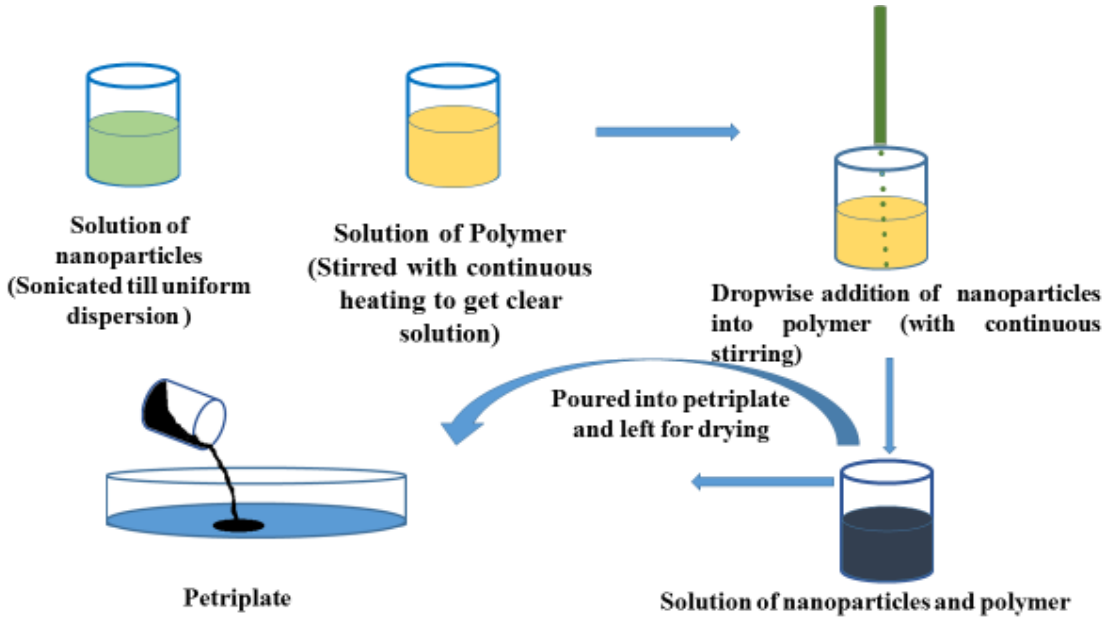

Figure 5.2: Schematic presentation of solvent casting technique

In previous studies, E. G. Ahangar et al., prepared PVA/ZnO nanocomposites by this method [197]. Also, A. Gautam et al. prepared Ag/PVA nanocomposites by this method [198].

Above researchers successfully synthesized polymer-matrix nanocomposites by solvent casting method, hence it was decided to follow the same procedure.

5.2.2 Important parameters for solvent casting method

Solvent casting technique is used to obtain high quality films. The key elements of solvent casting technique include some prerequisites [199]:

i The polymer must be soluble in a volatile solvent or water. To be soluble in water, a polymer should have hydrophilic groups [200].

ii Formation of a stable solution with a sensible minimum solid content and viscosity should be possible.

iii Development of a homogeneous film and release it from the casting support must be possible.

Thin films; prepared by this technology are having uniform thickness distribution, maximum optical purity, and extremely low haze [199].

5.2.3 Advantages of using solvent casting method

Developing process of solvent casting method has following advantages over other traditional methods like intercalation method, in-situ polymerization method etc. [201]:

i Films are processed at low temperatures, which is important for heat sensitive films or applications integrating temperature-sensitive active constituents.

ii Production of high-temperature resistant films is possible from soluble raw materials which can be non-thermoplastic.

iii Incorporation of filler material within polymer is very simple.

iv A free film can be casted

v Wider range of material choices with casting from either aqueous or solvent-based solutions.

Advantages of the prepared film by solvent casting over films produced by other methods include:

i Uniform film thickness, only +/-2% variation is possible.

ii Thickness of film has wide range. It can be controlled by pour volume.

iii Obtained films are gel and pinhole free.

iv Films have excellent flatness and dimensional constancy.

v The film is not stressed during synthesis procedure, hence isotropic orientation (thermal, mechanical and optical) is found.

vi Also, no lubricant is used like typical extrusion process.

Above advantages of solvent casting method over other methods inspired to prepare TiO_2/PVA nanocompositses by this method.

5.3 Materials for Preparation of TiO_2/PVA Nanocomposites

Poly vinyl alcohol, TiO_2 nanoparticles, and distilled water were used to synthesize TiO_2/PVA nanocomposites.

5.3.1 Specifications of PVA: Analysis of PVA is shown in Table 5.1.

Table 5.1: Analysis of Polyvinyl alcohol

S. No.	Parameter	Specification
1	Degree of polymerisation	1700-1800
2	Viscosity	25-32 centipoise
3	Hydrolysis (mole %)	98-99
4	Volatile matter	max 5%
5	Ash	max 0.7%
6	pH (0.2% in water)	5.0-7.0

5.3.2 Specifications of TiO_2 nanoparticles: TiO_2 nanoparticles with average size of 10-25 nm in anatase phase, and 99.5% purity were used (SkySpring Nanomaterials, lnc.).

5.4 Synthesis of PVA Film

Poly vinyl alcohol with 1700-1800 degree of polymerization was used. Two samples of PVA films (2.91 wt% and 3.38 wt%) were prepared by taking 1.5 gm and 1.75 gm of PVA within 50 ml distilled water as shown in Table 5.2. Prepared solutions were stirred at 80^0C until they became transparent. Then, these solutions were poured into petriplate and dried at room temperature to form transparent film of PVA.

Table 5.2: Samples of PVA film

S. No.	Weight of PVA (gm)	Distilled Water (ml)	Weight % of PVA film	Designation of sample
1	1.5	50	2.91	P1
2	1.75	50	3.38	P2

5.5 Synthesis of TiO_2/PVA Nanocomposites

Solutions of TiO_2 were prepared by making dispersion of TiO_2 nanoparticles into distilled water by sonication. Simultaneously solutions of PVA were prepared in distilled water as discussed in subheading 5.4. Prepared TiO_2 solutions were added dropwise to the PVA solution with continuous stirring. After complete mixing of this solution, it was allowed to dry in petri-plate at room temperature to get films. Schematic presentation of this procedure is shown in Fig. 5.3.

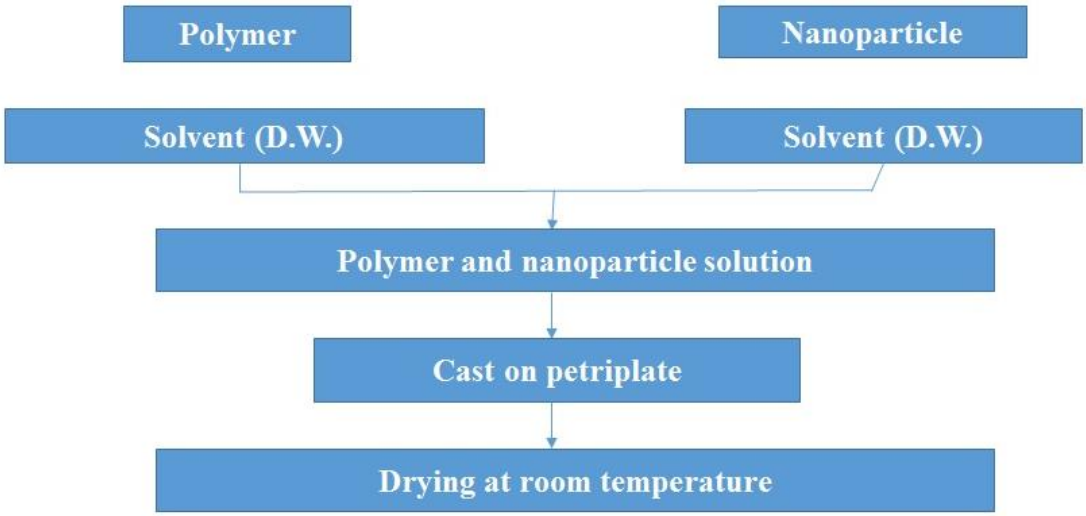

Figure 5.3: Schematic presentation of solvent casting method

Four set of experiments were carried out to prepare TiO_2/PVA nanocomposites with different variations of TiO_2 nanoparticles (see section 5.5.1, 5.5.2, 5.5.3, and 5.5.4). Variations of TiO_2 nanoparticles for dispersion of TiO_2 nanoparticles are shown in Table 5.3 and Table 5.6. Variations of TiO_2/PVA nanocomposites are shown in Table 5.4, Table 5.5, Table 5.7, and Table 5.8. Thirty samples of TiO_2/PVA nanocomposites were prepared by taking fifteen different weight percent of TiO_2 nanoparticles in distilled water with two samples of PVA (2.91 wt% and 3.38 wt%). TiO_2/PVA nanocomposites are given designation from S1 to S30 as shown in Table 5.4, Table 5.5, Table 5.7, and Table 5.8.

5.5.1 Experiment No. 1

In this experiment, five films of TiO_2/PVA nanocomposites were prepared by taking 0.015, 0.031, 0.062, 0.125, and 0.25 wt% of TiO_2 nanoparticles with 2.91 wt% of PVA. Five solutions of TiO_2 nanoparticles with above mentioned different

weight percent were prepared and designated from T1 to T5 as shown in Table 5.3. These solutions were added dropwise into P1 (PVA solution) and obtained TiO_2/PVA nanocomposites were designated from S1 to S5 as shown in Table 5.4.

Table 5.3: Variations of TiO_2 nanoparticles

S. No.	Weight % of TiO_2 nanoparticles	Weight of TiO_2 nanoparticles (gm)	Distilled Water (ml)	Designation of TiO_2 solution
1	0.015	0.0078	50	T1
2	0.031	0.01565	50	T2
3	0.062	0.03125	50	T3
4	0.125	0.0625	50	T4
5	0.25	0.125	50	T5

5.5.2 Experiment No. 2

In this experiment, five films of TiO_2/PVA nanocomposites were prepared by taking 0.015, 0.031, 0.062, 0.125, and 0.25 wt% of TiO_2 nanoparticles with 3.38 wt% of PVA. Five solutions of TiO_2 nanoparticles with above mentioned different weight percent were prepared and designated from T1 to T5 as shown in Table 5.3. These solutions were added dropwise into P2 (PVA solution) and obtained TiO_2/PVA nanocomposites were designated from S6 to S10 as shown in Table 5.5.

Table 5.4: Variations of TiO_2/PVA nanocomposites

S. No.	PVA Solution	TiO_2 Solution	Designation of TiO_2/PVA nanocomposites
1	P1	T1	S1
2	P1	T2	S2
3	P1	T3	S3
4	P1	T4	S4
5	P1	T5	S5

Table 5.5: Variations of TiO_2/PVA nanocomposites

S. No.	PVA Solution	TiO_2 Solution	Designation of TiO_2/PVA nanocomposites
1	P2	T1	S6
2	P2	T2	S7
3	P2	T3	S8
4	P2	T4	S9
5	P2	T5	S10

5.5.3 Experiment No. 3

In this experiment, ten films of TiO_2/PVA nanocomposites were prepared by taking 0.5, 1, 1.5, 2, 2.5, 3, 3.5, 4, 4.5, and 5 wt% of TiO_2 nanoparticles with 2.91 wt% of PVA. Ten solutions of TiO_2 nanoparticles with above mentioned different weight percent were prepared and designated from T6 to T15 as shown in Table 3.6. These solutions were added dropwise into P1 (PVA solution) and obtained TiO_2/PVA nanocomposites were designated from S11 to S20 as shown in Table 5.7.

5.5.4 Experiment No. 4

In this experiment, ten films of TiO_2/PVA nanocomposites were prepared by taking 0.5, 1, 1.5, 2, 2.5, 3, 3.5, 4, 4.5, and 5 wt% of TiO_2 nanoparticles with 3.38 wt% of PVA. Ten solutions of TiO_2 nanoparticles with above mentioned different weight percent were prepared and designated from T6 to T15 as shown in Table 5.6. These solutions were added dropwise into P1 (PVA solution) and obtained TiO_2/PVA nanocomposites were designated from S21 to S30 as shown in Table 5.8.

Table 5.6: Variations of TiO_2 nanoparticles

S. No.	Weight % of TiO_2 nanoparticles	Weight of TiO_2 nanoparticles (gm)	Distilled Water (ml)	Designation of TiO_2 solution
1	0.5	0.25	50	T6
2	1	0.5	50	T7
3	1.5	0.76	50	T8
4	2	1.02	50	T9
5	2.5	1.28	50	T10
6	3	1.54	50	T11
7	3.5	1.81	50	T12
8	4	2.08	50	T13
9	4.5	2.35	50	T14
10	5	2.63	50	T15

Table 5.7: Variations of TiO_2/PVA nanocomposites

S. No.	PVA Solution	TiO_2 Solution	Designation of TiO_2/PVA nanocomposites
1	P1	T6	S11
2	P1	T7	S12
3	P1	T8	S13
4	P1	T9	S14
5	P1	T10	S15
6	P1	T11	S16
7	P1	T12	S17
8	P1	T13	S18
9	P1	T14	S19
10	P1	T15	S20

Table 5.8: Variations of TiO_2/PVA nanocomposites

S. No.	PVA Solution	TiO_2 Solution	Designation of TiO_2/PVA nanocomposites
1	P2	T6	S21
2	P2	T7	S22
3	P2	T8	S23
4	P2	T9	S24
5	P2	T10	S25
6	P2	T11	S26
7	P2	T12	S27
8	P2	T13	S28
9	P2	T14	S29
10	P2	T15	S30

The obtained TiO_2/PVA nanocomposites by above experiments were further characterized as discussed in next section.

5.6 Characterization of TiO_2/PVA Nanocomposites

The obtained PVA film and TiO_2/PVA nanocomposites were characterized to study their spectroscopic, phase study, morphology, thermal and mechanical properties. UV-Vis spectroscopy, FTIR spectroscopy, x-ray diffraction (XRD), scanning electron microscopy (SEM), thermal gravimetric analysis (TGA), differential scanning calorimetry (DSC), and dynamic mechanical analysis (DMA) were carried out.

5.6.1 Spectroscopic analysis

Spectroscopic analysis is performed by interaction of energy with matter. Two spectroscopic techniques; UV-Vis absorption spectroscopy and fourier transform infrared spectroscopy were used in this study. Obtained spectrum from these techniques gives information about atomic and molecular energy levels, and functional groups present in sample.

5.6.1.1 Absorption studies

The absorbance of pure PVA and TiO_2/PVA nanocomposites for ultraviolet and visible region of electromagnetic spectrum was tested by UV-Vis spectroscopy.

Absorption studies are significant in identifying possible electronic transition during irradiation of samples with ultraviolet and visible region of electromagnetic spectrum. The UV-Vis spectra of PVA and TiO_2/PVA nanocomposites was recorded with LAMBDA 750 (Perkin Elmer) UV-VIS NIR spectrophotometer instrument and wavelength was kept between 200-800 nm.

The absorption spectra is result of transition of electrons from lower energy level to higher energy level within a molecule. If a molecule absorbs ultraviolet energy with ν frequency, the value of energy can be given by [202]:

$$E_1 - E_0 = h\nu$$

Where,

E_1 = Energy of excited state

E_0 = Energy of ground state

ν = Frequency of absorbed energy

The molecule absorbs energy when it matches with possible electronic transition within the molecule. A portion of light is absorbed by the molecule and the electrons would be stimulated to the higher energy state orbital. The degree of absorption at different wavelengths is recorded by spectrophotometer.

The UV-Vis spectroscopy was performed for pure PVA (P1 and P2) and TiO_2/PVA nanocomposites (S1, S2, S3, S4, S5, S6, S7, S8, S9, S10, S11, S12, S13, S14, S15, S16, S17, S18, S19, S20, S21, S22, S23, S24, S25, S26, S27, S28, S29, and S30).

5.6.1.2 Bond vibration studies

The bond vibrations of pure PVA and TiO_2/PVA nanocomposites for infrared region of electromagnetic spectrum was tested by fourier transform infrared spectroscopy (FTIR). Generally, molecules absorb light in infra-red region of electromagnetic spectrum and this absorption corresponds to the bond energies of molecule [197]. FTIR study is important in identifying functional groups present in sample by identifying the vibrational motions of molecules. Different amounts of energy are absorbed for different motions among different groups of atoms. This energy is recorded in terms of frequency by FTIR.

FTIR spectroscopy for PVA and TiO_2/PVA nanocomposites was performed over the frequency region 4000-500 cm^{-1} and spectra were recorded in reflection mode. FTIR Spectrum 2 (Perkin Elmer) instrument was used. At first, background emission spectrum of IR source without sample is recorded, then emission spectrum of IR source with sample is recorded. The resultant absorption spectrum is ratio of sample spectrum to the background spectrum which indicates that particular chemical bond is present [197].

In this study, O-H vibration, C-H vibration, C=O stretching, C-O-C vibration, Ti-O vibration, and Ti-O-O vibration were identified by FTIR spectroscopic analysis of prepared TiO_2/PVA nanocomposites.

The FTIR spectroscopy was performed for pure PVA (P1 and P2) and TiO_2/PVA nanocomposites (S1, S2, S3, S4, S5, S6, S7, S8, S9, S10, S11, S12, S13, S14, S15, S16, S17, S18, S19, S20, S21, S22, S23, S24, S25, S26, S27, S28, S29, and S30).

5.6.2 Phase analysis

X-Ray diffractometer (Panalytical X Pert Pro) was used to perform XRD of PVA and TiO_2/PVA nanocomposites. The diffraction angle (2Θ) was kept between 10^o to 80^o. Cu K(α) target (λ = 0.154 Å) was used. Intensity peaks for different elements with respect to diffraction angle (2Θ) were observed. These peaks were compared with standard JCPDS files to confirm phases of elements.

XRD was performed to determine lattice parameters and crystallinity of TiO_2/PVA nanocomposites with respect to pure PVA. The average crystallite size for TiO_2/PVA nanocomposites was determined by Debye-Scherrer equation. It relates the size of crystallites, in a solid to the broadening of a peak in a diffraction pattern. The Scherrer equation can be written as:

$$Dp = \frac{K\lambda}{\beta Cos\Theta} \qquad \text{..... 5.1}$$

where:

Dp is the mean size of the ordered (crystalline) domains, which may be smaller or equal to the grain size;

K is a dimensionless shape factor, with a value close to unity. The shape factor has a typical value of about 0.94, but varies with the actual shape of the crystallite;

λ is the x-ray wavelength (CuKα);

β is the line broadening at half the maximum intensity (FWHM); and

θ is the Bragg angle (in degrees).

Also, the lattice parameters were decided by using the following formula for tetragonal lattice:

$$\frac{1}{d^2} = \frac{h^2+k^2}{a^2} + \frac{l^2}{c^2} \quad \text{..... 5.2}$$

Here,

d = Interplanar Spacing,

h, k, l = Miller Indices,

a, c = Lattice Constant

The XRD studies were performed for pure PVA (P1 and P2) and TiO_2/PVA nanocomposites (S1, S3, S5, S6, S8, S10, S12, S14, S16, S18, S20, S22, S24, S26, S28, and S30).

5.6.3 Surface morphology

Surface morphology of TiO_2/PVA nanocomposites and dispersion of TiO_2 nanoparticles into PVA matrix was studied by Field Emission-Scanning Electron Microscope (FE-SEM, Nova Nano FE SEM) and operated at 15-20 kV. Elemental analysis and dispersion of nanofiller into PVA matrix was done by energy diffraction x-ray analyser (EDX/EDS) detector (Bruker, Germany). PVA and TiO_2/PVA nanocomposites are non-conducting, so gold coating was done by vacuum sputtering prior to SEM imaging.

It is important to study dispersion of TiO_2 nanoparticles into PVA matrix because thermal and mechanical stability of TiO_2/PVA nanocomposites depends upon it. If there is homogenous dispersion, then there will be good thermal and mechanical stability.

The SEM micrographs were recorded for pure PVA (P1 and P2) and TiO_2/PVA nanocomposites (S1, S5, S6, S10, S12, S14, S16, S18, S20, S22, S24, S26, S28, and S30).

5.6.4 Thermal analysis

Thermal analysis of TiO_2/PVA nanocomposites was performed to study glass transition temperature and thermal degradation behaviour. In thermal analysis, sample is subjected to a variable temperature and physical properties are recorded with respect to time. Thermal properties of TiO_2/PVA nanocomposites were studied by differential scanning calorimetry (DSC) and thermal gravimetric analysis (TGA). The calorific phenomenon for TiO_2/PVA nanocomposites were observed by DSC with no detectable weight change; but, the TGA curves gave information about variation in weight.

5.6.4.1 Thermo-physical analysis

Differential scanning calorimetry (DSC) analysis was carried out to study change in glass transition temperature of PVA after doping of TiO_2 nanoparticles. It is important to study glass transition temperature because physical properties and mechanical behaviour of polymer changes significantly after it.

DSC 404 F3 Pegasus (NETZSCH) instrument was used and the heat flow with respect to temperature is recorded in DSC curve. Glass transition region and melting point were observed by this curve. Experimental parameters are shown in Table 5.9.

Thermo-physical analysis studies were performed for pure PVA (P1 and P2) and TiO_2/PVA nanocomposites (S1, S2, S3, S4, S5, S6, S7, S8, S9, S10, S11, S12, S13, S14, S15, S16, S17, S18, S19, S20, S21, S22, S23, S24, S25, S26, S27, S28, S29, and S30).

Table 5.9: Parameters for differential scanning calorimetry

Parameter	Value
Temperature	upto 300°C
Heating Rate	10°C/min.
Atmosphere	Nitrogen
Weight of sample taken	9-12 mg

5.6.4.2 Thermal decomposition behaviour

Thermal decomposition behaviour of TiO_2/PVA nanocomposites was studied by thermal gravimetric analysis (TGA). The change in weight percent of sample over time with respect to temperature is recorded by TGA. It tells about physical and chemical phenomena of material like phase transition, absorption, desorption, chemisorption, thermal decomposition and oxidation-reduction reactions [201]. The STA 6000 (Perkin Elmeris) instrument was used to record weight loss with respect to temperature of prepared PVA and TiO_2/PVA nanocomposites. Experiment parameters are shown in Table 5.10.

TGA analysis were performed for pure PVA (P1 and P2) and TiO_2/PVA nanocomposites (S1, S5, S6, S10, S11, S12, S13, S14, S15, S16, S17, S18, S19, S20, S21, S22, S23, S24, S25, S26, S27, S28, S29, and S30).

Table 5.10: Parameters for thermal gravimetric analysis

Parameter	Value
Temperature	upto 600°C
Heating Rate	20°C/min.
Atmosphere	Nitrogen
Weight of sample taken	9-12 mg

5.6.5 Dynamic mechanical analysis

Viscoelasticity is time dependent inelastic behaviour of materials which means the response to a stimulus is delayed due to loss of energy inside the material. Viscoelastic behaviour usually occurs at different relaxation times in the same material. The response occurring at short relaxation times (less than 1 second) is investigated in dynamic tests, by applying an oscillating stimulus at constant frequency or sweeping through a frequency range. The response occurring at high relaxation times (from 1 second to hours) can be explored by experiments of creep (a load is applied and kept constant, while deformation is followed) or relaxation (the material is strained and kept under constant strain, while the stress is tracked temporally). Viscoelasticity is an intrinsic property of all polymers, but it may also be affected by the flow of liquid through the porous matrix.

Viscoelastic behaviour of TiO_2/PVA nanocomposites with respect to temperature was studied by dynamic mechanical analysis (DMA). This study tells about how good a material is at absorbing energy when load is applied. DMA 8000 (Perkin Elmer) instrument was used to carry out temperature scan in tensile mode. Experimental parameters are shown in Table 5.11. Damping (tanδ) with respect to temperature was recorded. Peak of tanδ indicates energy dissipation which can be measured as glass transition temperature. The tanδ peak occurs when a material changes from more rigid to elastic state and this transformation is due to movement of small molecules and chains of polymer.

The DMA analysis was performed for pure PVA (P1 and P2) and TiO_2/PVA nanocomposites (S1, S2, S3, S4, S5, S6, S7, S8, S9, S10, S11, S12, S13, S14, S15, S16, S17, S18, S19, S20, S21, S22, S23, S24, S25, S26, S27, S28, S29, and S30).

Table 5.11: Parameters for dynamic mechanical analysis

Parameter	**Value**
Temperature	upto 200°C
Heating Rate	3°C/min.
Atmosphere	Nitrogen
Mode	Tensile

The observations seen in this chapter are discussed in chapter 6, chatper 7 and chatper 8. The results and discussions of TiO_2/PVA nanocomposites are divided in three chapters. In sixth chapter, spectroscopic, phase analysis, and surface morphology are discussed. In seventh and eigth chapter, thermal and mechanical behaviour are discussed, respectively.

Chapter 6

RESULTS AND DISCUSSIONS-I

(Spectroscopic analysis, phase analysis, and morphological analysis of TiO_2/PVA nanocomposites)

TiO_2/PVA nanocomposites were prepared by solvent casting method as discussed in previous chapter. Two samples of PVA (P1 and P2) and thirty samples of TiO_2/PVA nanocomposites (S1-S30) were prepared by taking fifteen different weight percent of TiO_2 nanoparticles with two samples of PVA (P1 and P2). Results and discussions of spectroscopic analysis, phase analysis, and morphological analysis of TiO_2/PVA nanocomposites are presented in this chapter.

This chapter is divided into four sections. Absorption studies carried out by UV-Vis are discussed in first section. Second section comprises results and discussions of fourier transform infrared spectroscopy. Third and fourth section includes results of Phase analysis and morphological studies performed by x-ray diffraction and scanning electron microscopy, respectively. In the end, summary of this chapter is enclosed.

6.1 Absorption Studies

This section includes UV-Vis absorption spectra of pure PVA and TiO_2/PVA nanocomposites. The nature of electronic transition in TiO_2/PVA nanocomposites was identified by UV-Vis spectroscopy. Relative energies of orbitals are shown in a bar graph with possible electronic transitions. Explanation of broad absorbance peak of TiO_2/PVA nanocomposites is also given. The shifting of absorbance spectra of TiO_2/PVA nanocomposites to higher wavelength i.e. red shift or lower wavelength i.e. blue shift in compare to pure PVA is demonstrated by making plot between absorbance and sample.

UV-Vis absorption spectra for pure PVA (P1, P2) are shown in Fig. 6.1. Absorbance occurred at 278 nm and 272 nm for P1 and P2 respectively. This absorbance can be assigned to n-π^* electronic transition [202]. P1 and P2 showed absorbance only in narrow region of UV and complete transparency was seen in visible region.

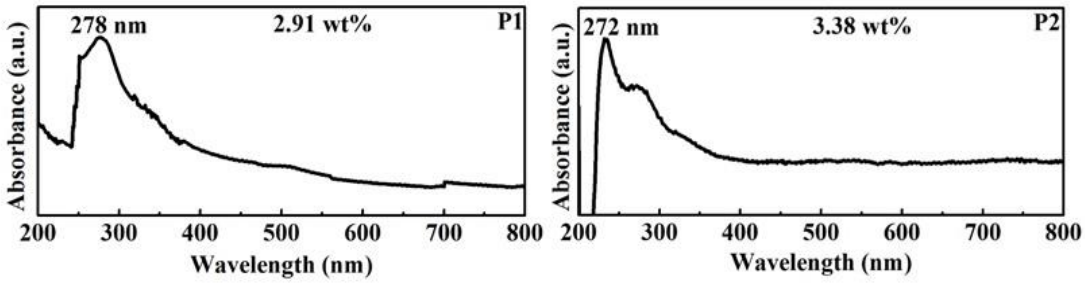

Figure 6.1: UV-Vis spectra of PVA (P1 and P2)

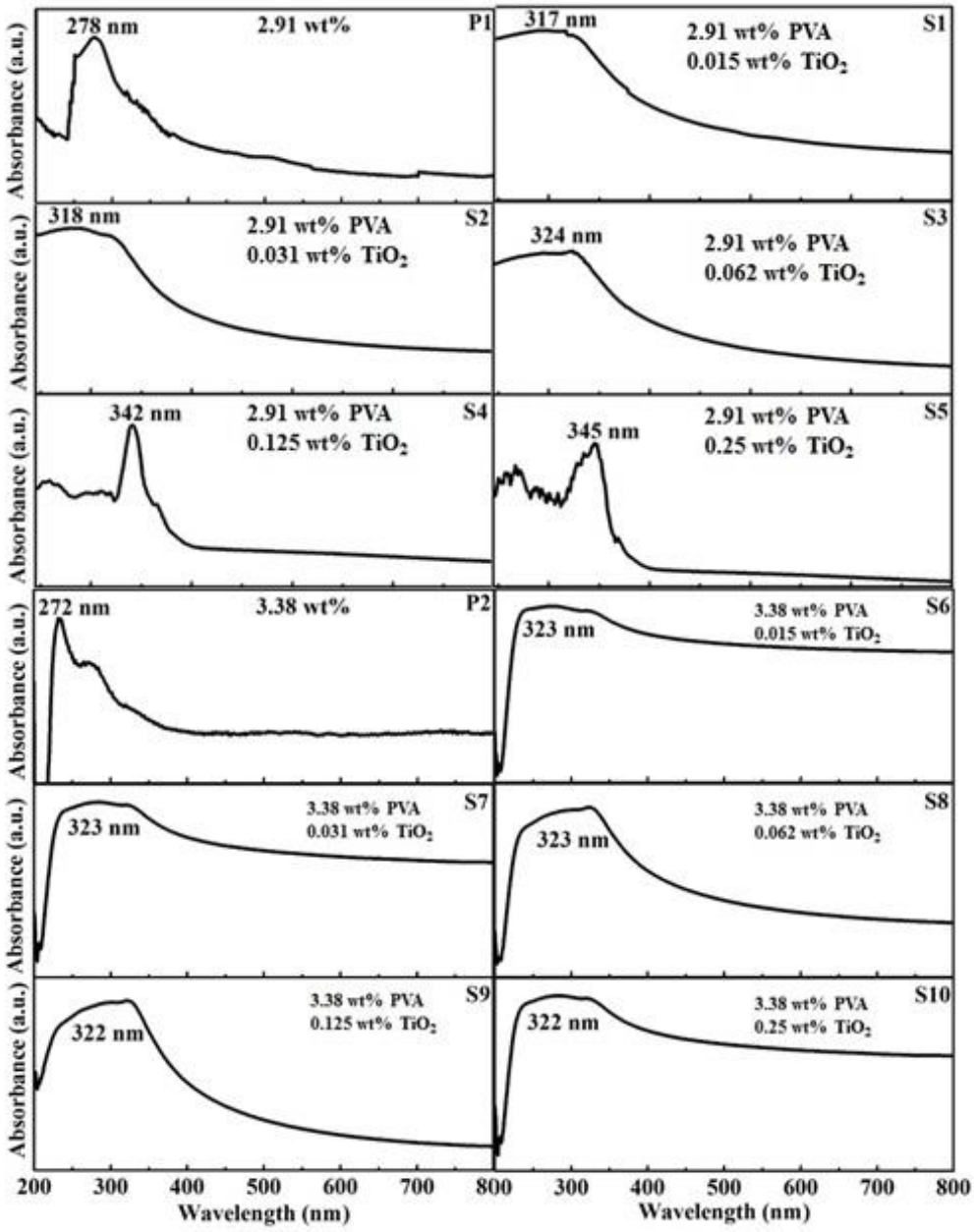

Figure 6.2: UV-Vis spectra of TiO_2/PVA nanocomposites with 2.91 wt% PVA (P1, S1, S2, S3, S4, S5) and 3.38 wt% PVA (P2, S6, S7, S8, S9, S10)

UV-Vis spectra of TiO_2/PVA nanocomposites are shown in Fig. 6.2 (S1, S2, S3, S4, S5, S6, S7, S8, S9, and S10), Fig. 6.3 (S11, S12, S13, S14, S15, S16, S17, S18, S19, and S20), and Fig. 6.4 (S21, S22, S23, S24, S25, S26, S27, S28, S29, and S30). In S1 to S5 and S11 to S20 samples of TiO_2/PVA nanocomposites, different weight percent of TiO_2 nanoparticles are doped in 2.91 wt% of PVA (P1). Whereas, in S6 to S10 and S21 to S30 samples of TiO_2/PVA nanocomposites, different weight percent of TiO_2 nanoparticles are doped in 3.38 wt% of PVA (P2).

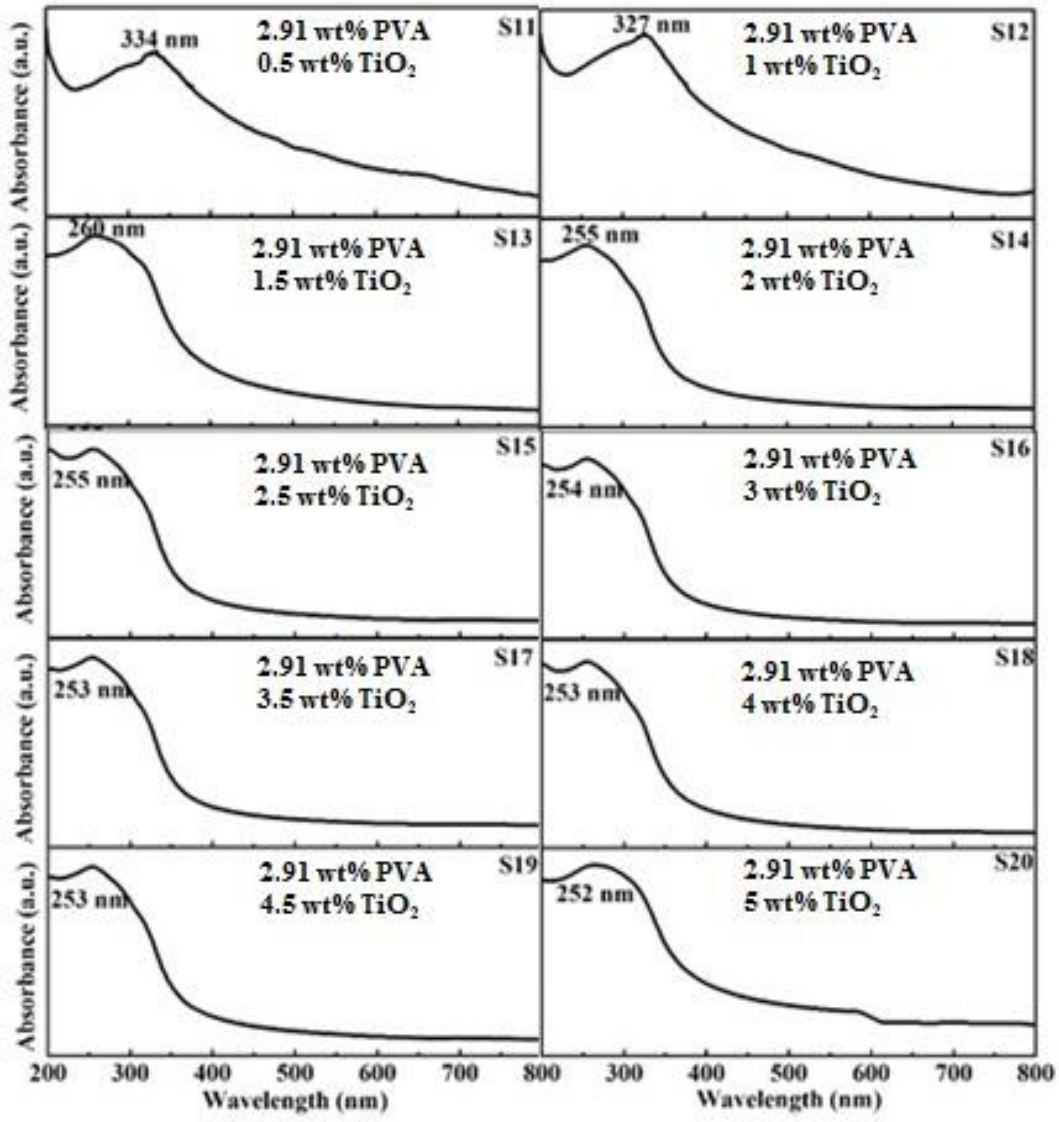

Figure 6.3: UV-Vis spectra of TiO_2/PVA nanocomposites (S11, S12, S13, S14, S15, S16, S17, S18, S19 and S20) with 2.91 wt% PVA

Broad absorbance peak for S1, S2, S3, S4, and S5 was observed at 317 nm, 318 nm, 324 nm, 342 nm, and 345 nm, respectively. Also, this broadened peak was

observed for S6, S7, S8, S9, and S10 at 323 nm, 323 nm, 323 nm, 322, and 322 nm, respectively. Absorbance peak for S11, S12, S13, S14, S15, S16, S17, S18, S19, and S20 was observed at 334 nm, 327 nm, 260 nm, 255 nm, 255 nm, 254 nm, 253 nm, 253 nm, 253 nm, and 252 nm respectively and that for S21, S22, S23, S24, S25, S26, S27, S28, S29, and S30 was observed at 261 nm, 257 nm, 256 nm, 255 nm, 255 nm, 254 nm, 253 nm, 253 nm, 253 nm, and 253 nm, respectively. Absorbance peaks for TiO_2/PVA nanocomposites are observed due to $\pi \rightarrow \pi^*$ electronic transition.

Thus, red shift in absorbance was observed for S1, S2, S3, S4, S5 and blue shift in absorbance was observed for S11, S12, S13, S14, S15, S16, S17, S18, S19, S20 samples of TiO_2/PVA nanocomposites in compare to P1 (2.91 wt% of PVA). Maximum broadened peak was observed for S20 sample (maximum TiO_2 content i.e. 5 wt% with 2.91 wt% of PVA) which was extended in complete UV region.

Also, red shift in absorbance was observed for S6, S7, S8, S9, S10 and blue shift in absorbance was observed for S21, S22, S23, S24, S25, S26, S27, S28, S29, S30 samples of TiO_2/PVA nanocomposites in compare to P2 (3.38 wt% of PVA). Maximum broadened peak was observed for S30 sample (maximum TiO_2 content i.e. 5 wt% with 3.38 wt% of PVA) which was extended in complete UV region.

From above observations, it can be inferred that all TiO_2/PVA nanocomposites are showing absorbance only in UV region and they are completely transparent for visible region. Hence, doping of TiO_2 nanoparticles did not affect absorbance of PVA in visible region. Absorbance spectra of TiO_2/PVA nanocomposites are shifting towards lower wavelength i.e. blue shift, in compare to PVA with increasing wt% of TiO_2 nanoparticles. Also, broadening of absorbance peak is observed for all TiO_2/PVA nanocomposites. Explanation of these broad peaks is given below.

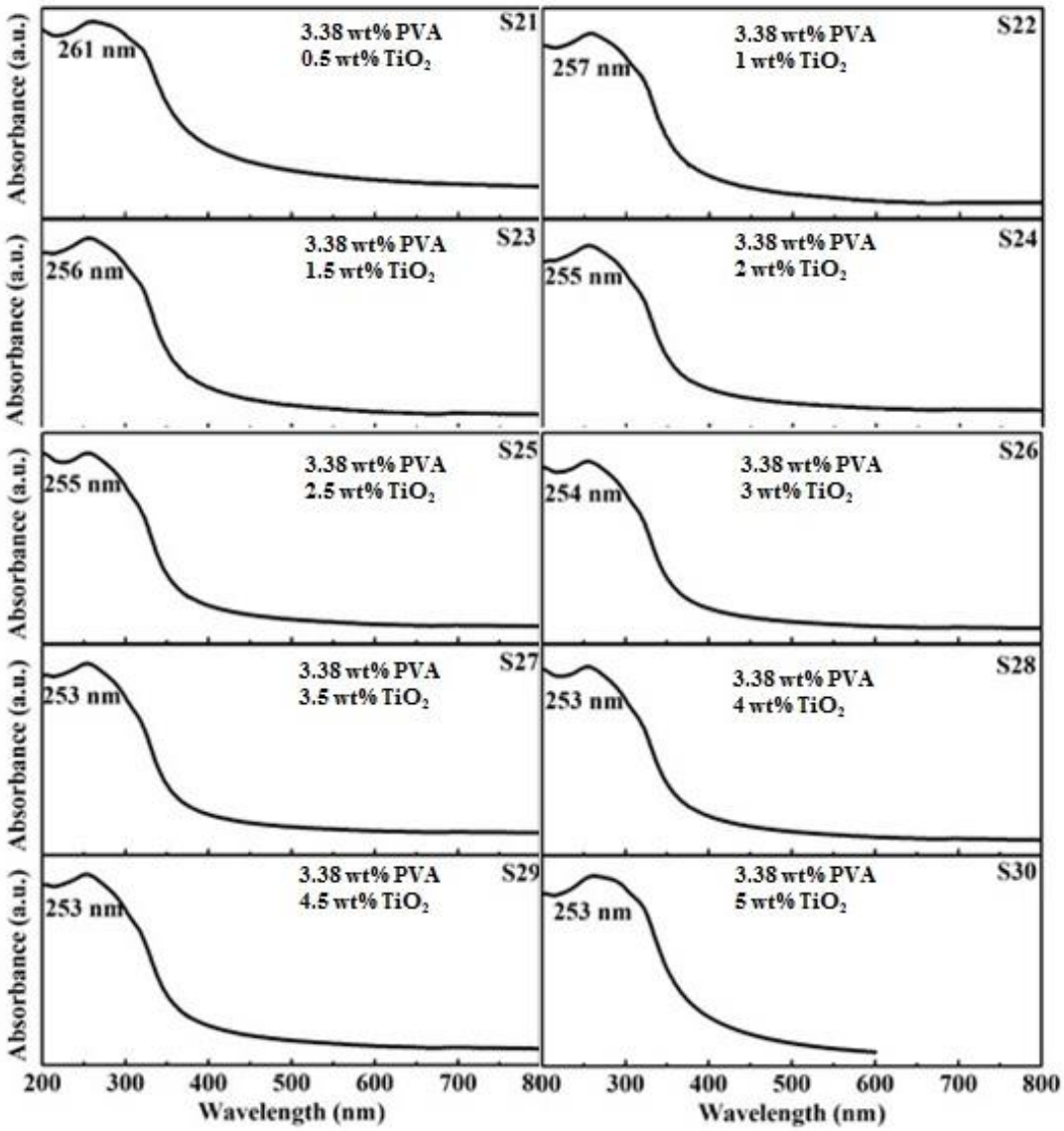

Figure 6.4: UV-Vis spectra of TiO_2/PVA nanocomposites (S21, S22, S23, S24, S25, S26, S27, S28, S29, and S30) with 3.38 wt% PVA

All molecules have internal energy which is sum of the energy of their electrons, the energy of vibrations between their constituent atoms and the energy associated with rotations of the molecule. Simple molecules have widely separated electronic energy levels and mostly only the absorption of high energy photon can cause excitation of electrons from lower energy level to higher energy level in them. But in case of complex molecules such as polymers, and nanocomposites etc. the energy levels are more closely spaced and photons of lower energy (e.g. near ultraviolet and visible light) can cause electronic transition [203].

The vibrational energy states of the various parts of a molecule are much closer together than the electronic energy levels and protons of lower energy are sufficient to carry out vibrational changes. The absorption of photons due to only vibrational changes occurs in the infrared region (see section 6.2) and that for rotational changes occurs in far infrared and microwave region [203].

In UV-Vis spectra, when light passes through sample, energy of light is absorbed to excite electron from a bonding or non-bonding orbital into one of the empty anti-bonding orbitals. Relative energies of these orbitals are shown in Fig. 6.5. Six possible electronic transitions exists (see Fig. 6.5) but only two transitions i.e. ($n \rightarrow \pi^*$) and ($\pi \rightarrow \pi^*$) can be seen in UV-Vis absorption study because they lies in the energy range which is used by UV-Vis spectroscopy [203].

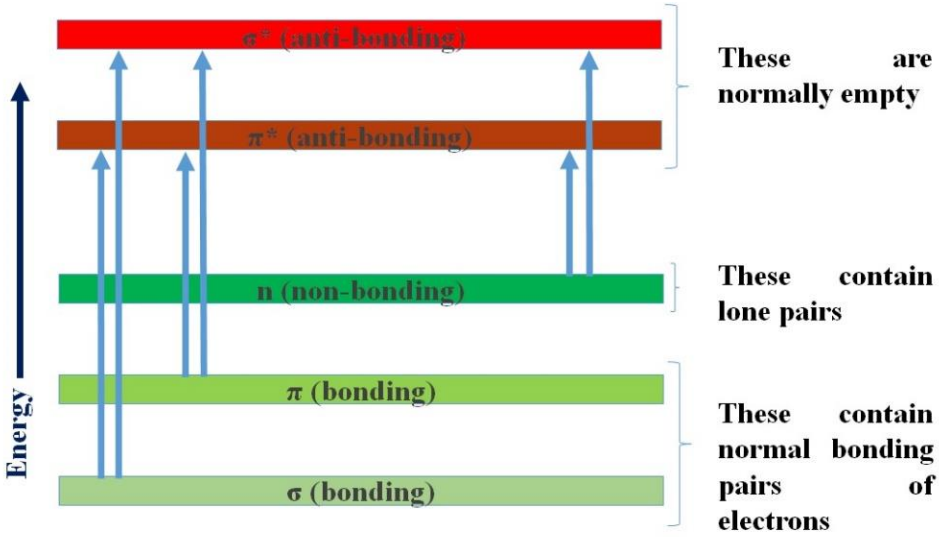

Figure 6.5: Orbitals with their relative energies (diagram isn't intend to be to scale)

From this discussion, it is expected that absorption spectrum of prepared samples should show a few sharp lines and each line should occur at a wavelength which exactly matches the energy required for an electronic transition. But, broad absorption peak is observed for all samples rather than single line peak. An excitation from π bonding orbital to π antibonding orbital is supposed to have a fixed energy and therefore absorb a fixed wavelength. In fact, nanocomposites are absorbing over a range of wavelength proposing a whole range of energy jumps. Reason behind this is that an electronic level transition is usually accompanied by rotations and vibrations in the molecule which results in change in energies of the

orbitals. Thus, the energy gap between them is changing continually as well. As a result, absorption takes place over a range of wavelengths instead of fixed one [204].

In Fig. 6.6, 6.7, 6.8, and 6.9, absorbance peaks of TiO_2/PVA nanocomposites (S1 to S30) are plotted with respect to samples to compare them with absorbance of pure PVA (P1 and P2). Red shift was observed in S1, S2, S3, S4, S5, S6, S7, S8, S9, S10, S11, and S12 samples whereas blue shift was observed in S13, S14, S15, S16, S17, S18, S19, S20, S21, S22, S23, S24, S25, S26, S27, S28, S29, and S30 samples of TiO_2/PVA nanocomposites. It is concluded that at higher concentrations of TiO_2 nanoparticles, blue shift is observed in TiO_2/PVA nanocomposites in compare to PVA. It is well known that as particle size increases UV-Vis spectra is shifted to higher wavelength i.e. red shift and vice-versa. In a previous research, Wolfgang Haiss et al. has reported that red shift was observed for gold nanoparticles after coalescence [204]. Noshir S. Pesika et al. correlated radius of particle with absorption energy for ZnO quantum particles and observed red shift for large particles in compare to small particles.

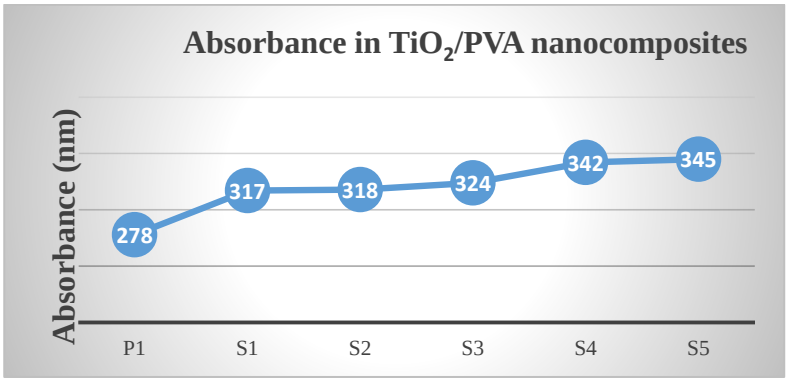

Figure 6.6: Red shift in TiO_2/PVA nanocomposites

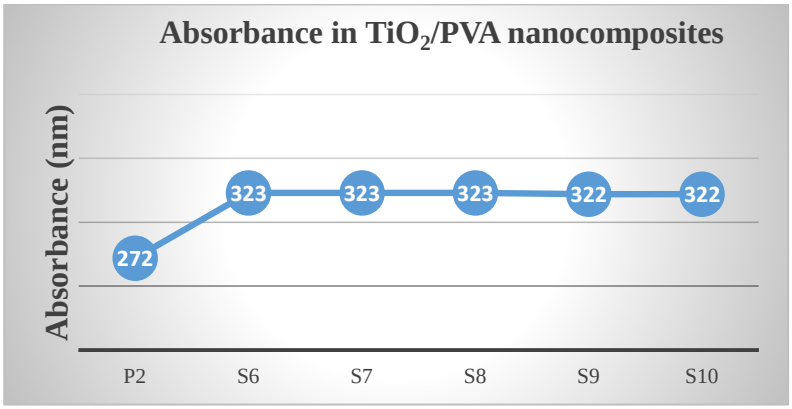

Figure 6.7: Red shift in TiO_2/PVA nanocomposites

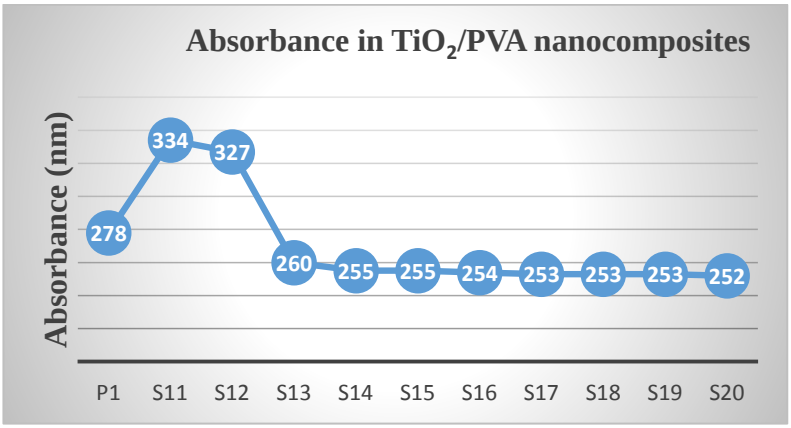

Figure 6.8: Red and blue shift in TiO_2/PVA nanocomposites

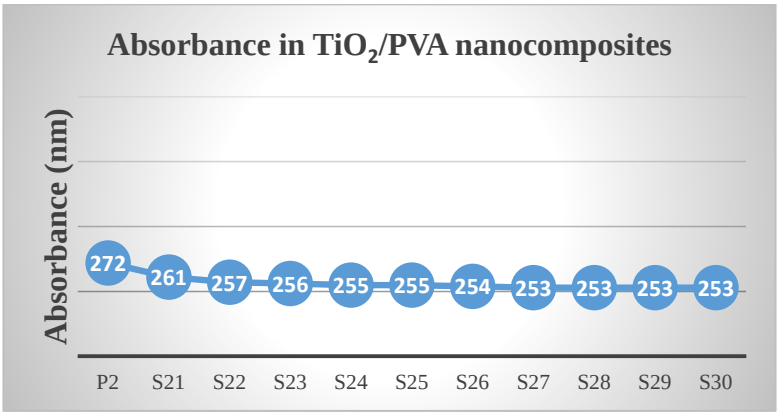

Figure 6.9: Blue shift in TiO_2/PVA nanocomposites

Whereas, in this research work, blue shift at higher concentrations of TiO_2 nanoparticles is observed which indicates aggregation of TiO_2 nanoparticles is prevented by bonding between TiO_2 nanoparticles and PVA. Thus, effective size of TiO_2 nanoparticles remain small.

It can be inferred from UV-Vis spectra of TiO_2/PVA nanocomposites that broad absorbance peak observed in UV region is due to vibrations and rotations associated with $\pi \rightarrow \pi^*$ electronic transition and no separate peak for PVA was seen. The variation in concentrations of PVA did not show any remarkable influence on absorption spectra of TiO_2/PVA nanocomposites. But, absorbance for S21, S22, and S23 samples of TiO_2/PVA nanocomposites was shifted to slightly lower wavelength in compare to S11, S12, and S13 samples of TiO_2/PVA nanocomposites, respectively. It might be due to availability of more hydroxyl groups to interact with TiO_2 nanoparticles. Also, blue shift with increasing concentration of TiO_2

nanoparticles with both P1 (2.91 wt% PVA) and P2 (3.38 wt% PVA) indicates reduction in aggregation of TiO_2 nanoparticles. The reduction in aggregation of TiO_2 nanoparticles will result in smaller crystallite sizes of TiO_2 nanoparticles. The crystallite sizes of TiO_2 nanoparticles were determined using Debye-Scherrer formula from XRD graphs (see section 6.3). The crystallite sizes obtained by XRD results are in agreement with blue shift observed in UV-Vis spectra. The prevention of aggregation of TiO_2 nanoparticles within TiO_2/PVA nanocomposites is due to interaction between TiO_2 nanoparticles and PVA. This interaction occurs due to presence of Ti ions and –OH group of PVA and results in H-bonding between them [205]. The bond formation between TiO_2 nanoparticles and PVA will improve overall thermal and mechanical stability of prepared TiO_2/PVA nanocomposites. The chemical bonds present in TiO_2/PVA nanocomposites were identified by FTIR spectroscopy which are discussed in next section.

6.2 Bond Studies

FTIR was performed to understand the nature of organics present in TiO_2/PVA nanocomposites. As discussed in UV-Vis spectroscopy, the interaction between polymer matrix and TiO_2 nanoparticles depends upon loading and inter-particle distance [206, 207]. This interaction might result in chemical bond formation. The chemical bonds present in TiO_2/PVA nanocomposites were identified by FTIR. Energies absorbed in FTIR are involved in bond vibrations. Bonds, present in molecules, vibrate all the time and they can be kicked into higher state if exactly the right amount of energy is delivered. The energy absorbed in this process is recorded in percent transmittance versus wavenumber spectra. The bands obtained by FTIR spectroscopy corresponding to the wavenumber indicate particular chemical bond.

FTIR spectra of pure PVA and TiO_2/PVA nanocomposites are shown in Fig. 6.10 (P1, S1, S2, S3, S4, and S5), Fig. 6.11 (P2, S6, S7, S8, S9, and S10), Fig. 6.12 (S11, S12, S13, and S14), Fig. 6.13 (S15, S16, S17, and S18), Fig. 6.14 (S19, and S20), Fig. 6.15 (S21, S22, S23, S24, S25) and Fig. 6.16 (S26, S27, S28, S29, and S30).

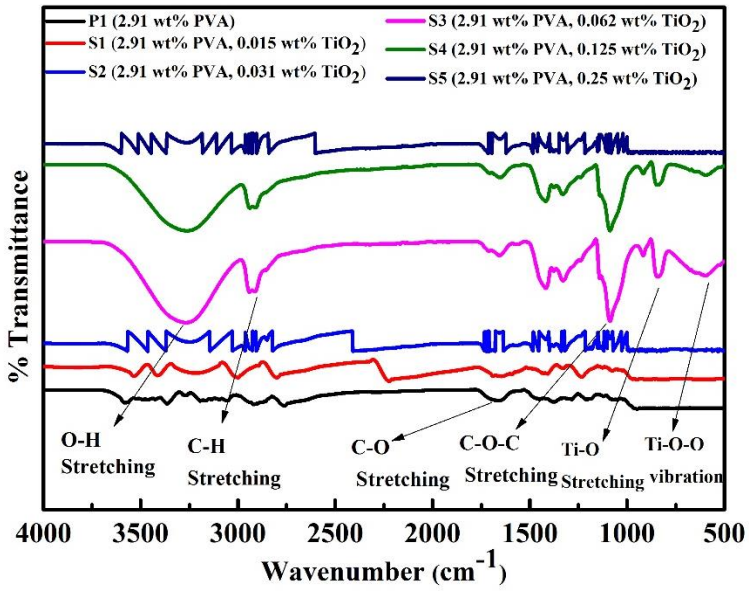

Figure 6.10: FTIR spectra of TiO_2/PVA nanocomposites (P1, S1, S2, S3, S4, and S5) with 2.91 wt% PVA

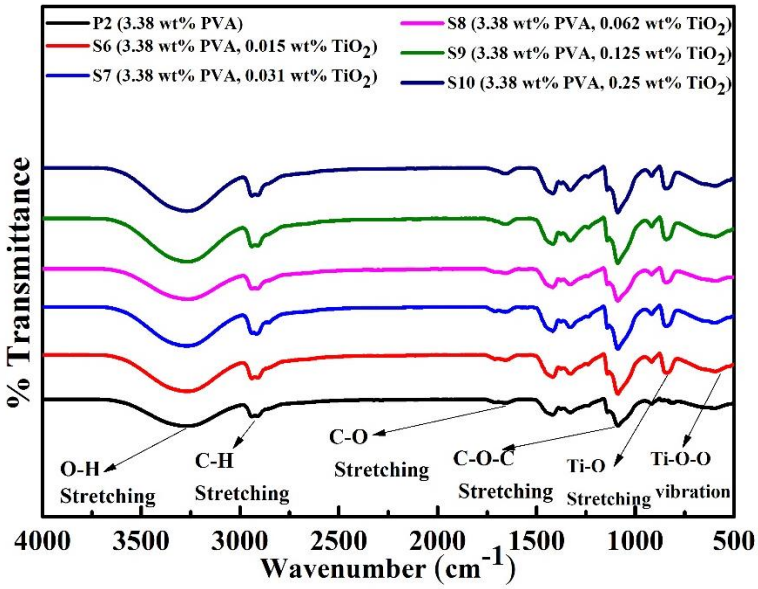

Figure 6.11: FTIR spectra of TiO_2/PVA nanocomposites (P2, S6, S7, S8, S9, and S10) 3.38 wt% PVA

In S1 to S5 and S11 to S20 samples of TiO_2/PVA nanocomposites, different weight percent of TiO_2 nanoparticles are doped in 2.91 wt% of PVA (P1). Whereas, in S6 to S10 and S21 to S30 samples of TiO_2/PVA nanocomposites, different weight percent of TiO_2 nanoparticles are doped in 3.38 wt% of PVA (P2).

The complete assignments for the wavenumbers of different groups and their respective vibrational modes of PVA and TiO_2/PVA nanocomposites are shown in Table 6.1. For pure PVA (P1 and P2), characteristic absorption bands were observed at 3272 cm^{-1}, 2920 cm^{-1}, 1418 cm^{-1}, and 1088 cm^{-1} for O-H stretching, C-H stretching, C=O stretching, and C-O-C vibration respectively [4, 5].

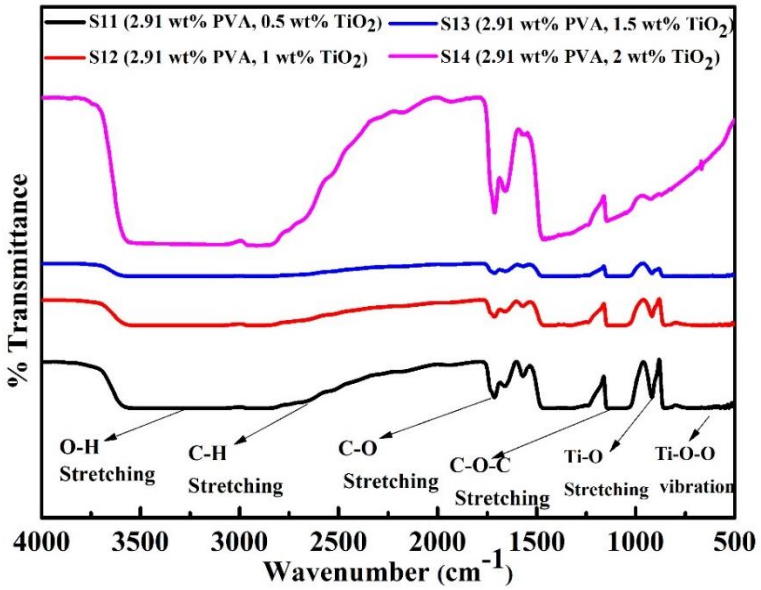

Figure 6.12: FTIR spectra of TiO_2/PVA nanocomposites (S11, S12, S13, and S14) with 2.91 wt% PVA

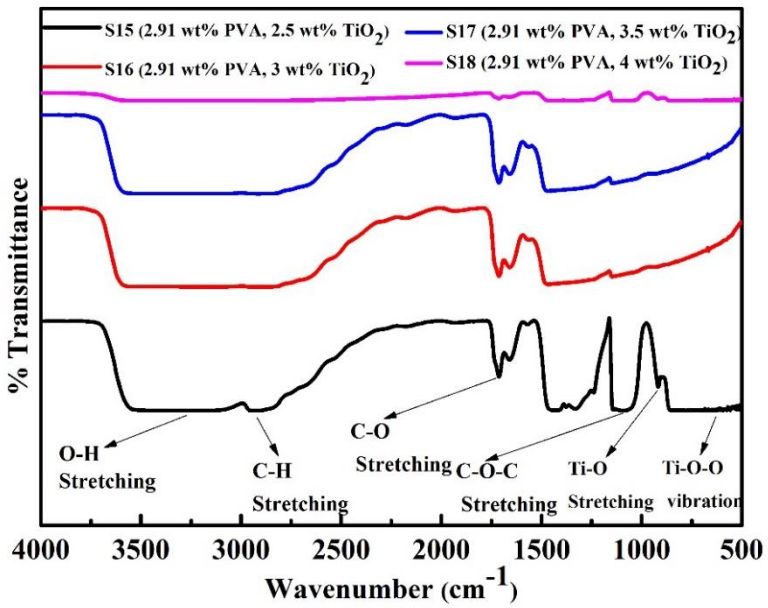

Figure 6.13: FTIR spectra of TiO_2/PVA nanocomposites (S15, S16, S17, and S18) with 2.91 wt% PVA

In all TiO_2/PVA nanocomposites, the bands were observed at 3272 cm^{-1}, 2900 cm^{-1}, 1740 cm^{-1}, 1000-1250 cm^{-1}, 900 cm^{-1}, and 500-850 cm^{-1} for OH stretching, C-H stretching, C=O stretching, C-O-C vibration, Ti-O vibration, and Ti-O-O vibration respectively. The absorption band for O-H stretching was broadened in TiO_2/PVA nanocomposites in compare to PVA and broadening of this band was increasing with increasing weight percent of TiO_2 nanoparticles. Maximum broadening for O-H stretching was observed for S30 sample which has maximum TiO_2 content i.e. 5 wt%.

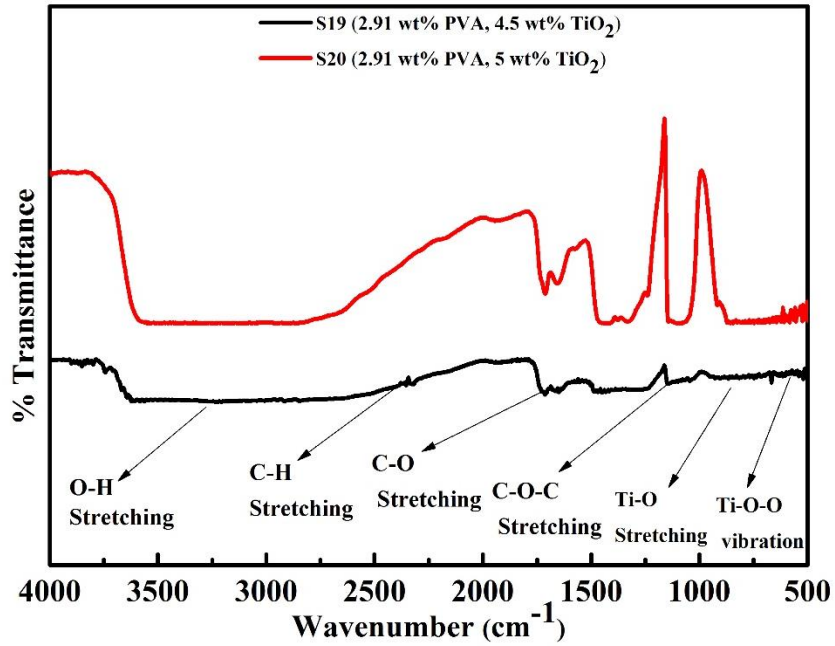

Figure 6.14: FTIR spectra of TiO_2/PVA nanocomposites (S19 and S20) with 2.91 wt% PVA

In addition to this, the band for C-H vibrations is shifted to lower wavenumber in all TiO_2/PVA nanocomposites in compare to PVA.

Also, C=O stretching band is broadened in TiO_2/PVA nanocomposites in compare to that of PVA. It can be observed from the infrared spectra that doping of TiO_2 nanoparticles induced noticeable changes in the wavenumber region 1000-400 cm^{-1}. Broad absorption band observed in TiO_2/PVA nanocomposites at 500-850 cm^{-1} was absent in PVA which is assigned for vibration of Ti-O-O groups [208].

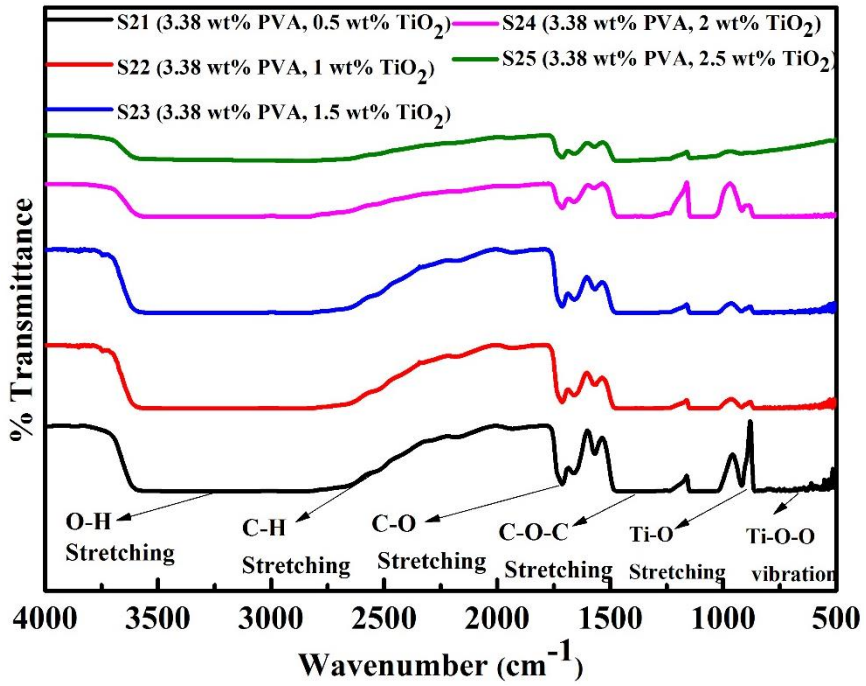

Figure 6.15: FTIR spectra of TiO_2/PVA nanocomposites (S21, S22, S23, S24, and S25) with 3.38 wt% PVA

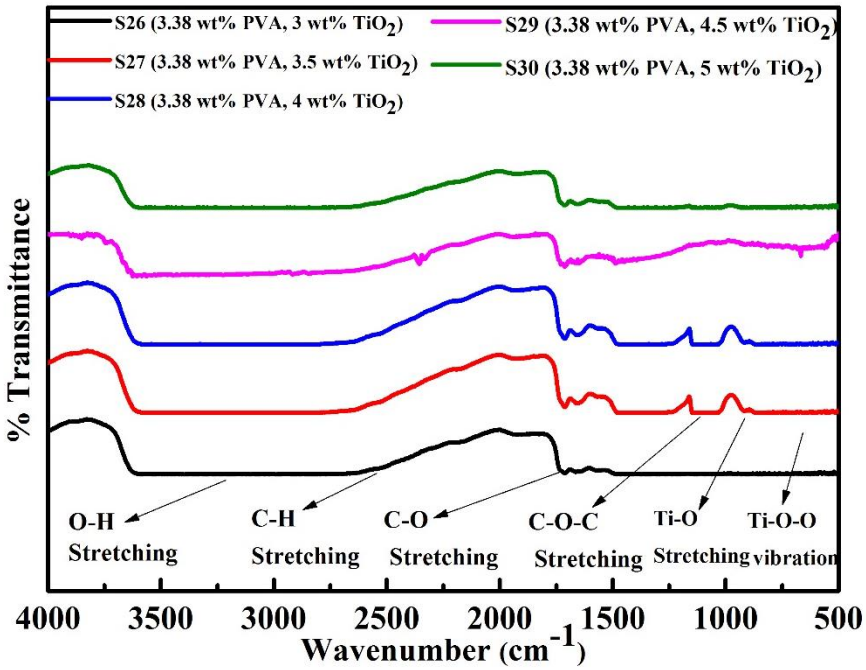

Figure 6.16: FTIR spectra of TiO_2/PVA nanocomposites (S26, S27, S28, S29, and S30) with 3.38 wt% PVA

Maximum broadening of this band was noticed in TiO_2/PVA nanocomposite with 5 wt% loading of TiO_2 nanoparticles (S20 and S30 samples).

Ti-O vibrations correspond to Ti-O-Ti group present in nanocomposite (see Fig. 6.17) and Ti-O-O vibrations corresponds to hydrogen bond formed between TiO_2 and PVA (Fig. 6.18).

Comparison of FTIR spectra of PVA and TiO_2/PVA nanocomposites clearly shows that band for O-H and C-H stretchings are broadened in TiO_2/PVA nanocomposites in compare with PVA and band for C=O stretching is broadened and shifted from 1418 cm^{-1} to 1740 cm^{-1} in TiO_2/PVA nanocomposites in compare to PVA. These broadening and shifting are due to possible hydrogen bond formation between –OH groups on the surface of titania nanocrystals and β-diketone groups from the polymer chain [209]. This bonding is responsible for good dispersion of TiO_2 nanoparticles into PVA matrix. Also, variations of PVA did not affect position of bands in FTIR spectra of TiO_2/PVA nanocomposites.

From above discussions, it is established that OH stretching, CH stretching, CO stretching, and C-O-C vibration, observed in FTIR spectra represents chemical bonds present within PVA and Ti-O vibration corresponds to chemical bond present in TiO_2 nanoparticles. Whereas Ti-O-O vibration were observed due to chemical bond formation between TiO_2 nanoparticles and PVA. The bonding between TiO_2 nanoparticles and PVA prevents aggregation of TiO_2 nanoparticles which results in homogenous dispersion of TiO_2 nanoparticles within PVA matrix. The homogenous dispersion of TiO_2 nanoparticles within PVA matrix was also seen by SEM images of TiO_2/PVA nanocomposites. The homogenous dispersion of TiO_2 nanoparticles within PVA matrix is important in improving thermal and mechanical stability of TiO_2/PVA nanocomposites.

Table 6.1: Characteristic infrared absorption of PVA and TiO_2/PVA nanocomposites

Functional Group	**Wavenumber (cm^{-1})**	**Intensity**
OH stretching	3272	High, and broad peak
CH stretching	2900	Low
CO stretching	1740	Low
C-O-C vibration	1000-1250	High
Ti-O vibration	900	Low and broad peak
Ti-O-O vibration	500-850	Very low and broad peak

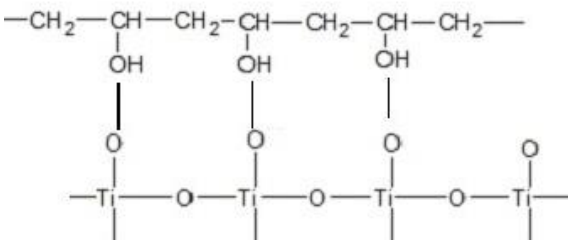

Figure 6.17: Schematic diagram of Ti-O-Ti group present in TiO_2/PVA nanocomposite

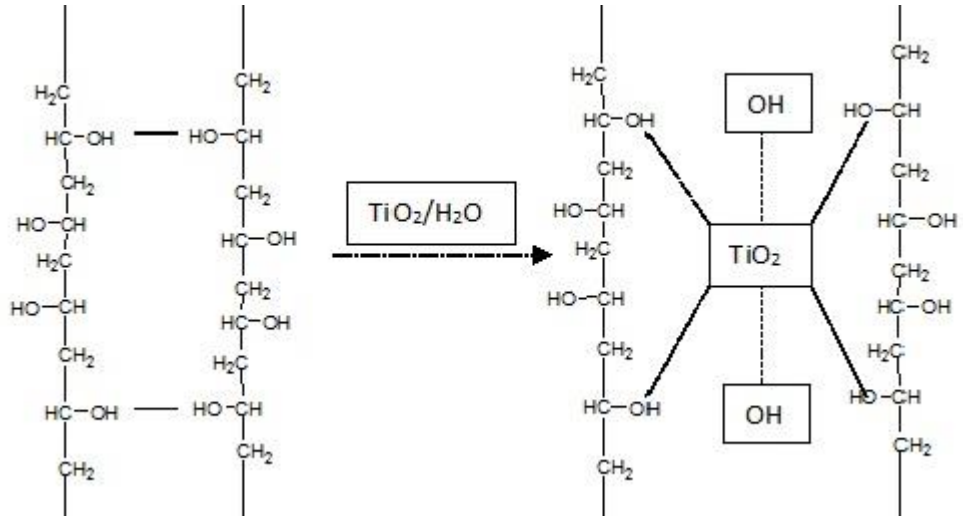

Figure 6.18: Schematic diagram of bonding between TiO_2/PVA nanocomposites

6.3 Phase Analysis

Phase analysis was performed to check crystallinity and phases of TiO_2 nanoparticles and PVA within TiO_2/PVA nanocomposites. Also, changes in lattice parameters of TiO_2 nanoparticles after doping in PVA were determined. The average crystallite size was determined by Debye-Scherrer formula. (equation 5.1) and lattice parameters were decided by using formula for tetragonal lattice (equation 5.2).

In this research work, S1 to S5 and S11 to S20 samples of TiO_2/PVA nanocomposites, were prepared by doping of different weight percent of TiO_2 nanoparticles in 2.91 wt% of PVA (P1). Whereas, S6 to S10 and S21 to S30 samples of TiO_2/PVA nanocomposites, were prepared by doping of different weight percent of TiO_2 nanoparticles in 3.38 wt% of PVA (P2). The XRD was performed for P1, P2, S1, S3, S5, S6, S8, S10, S12, S14, S16, S18, S20, S22, S24, S26, S28, S30 samples of TiO_2/PVA nanocomposites.

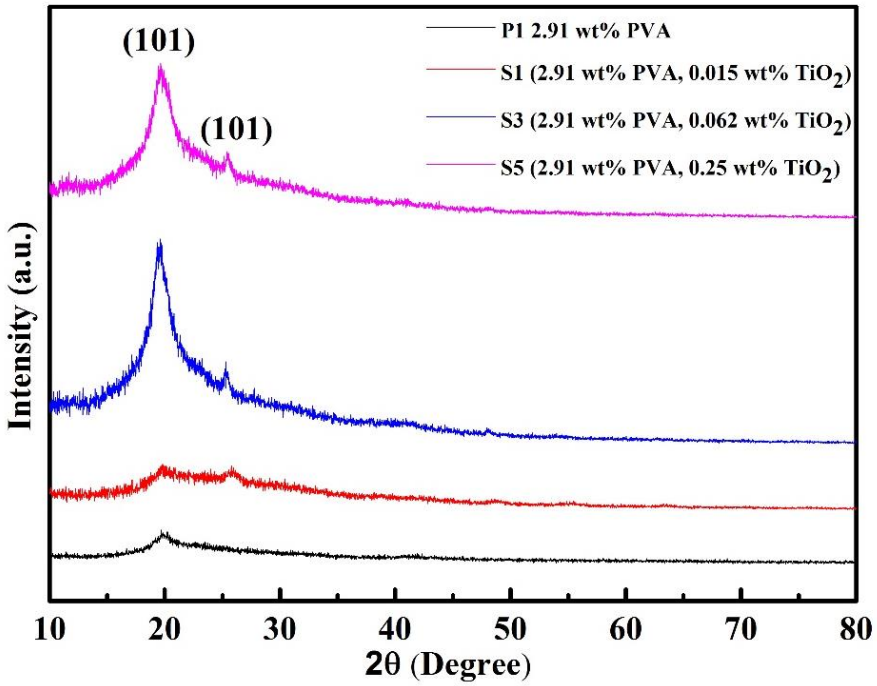

Figure 6.19: X-ray diffractogram of TiO_2/PVA nanocomposites (P1, S1, S3, S5) with 2.91 wt% PVA

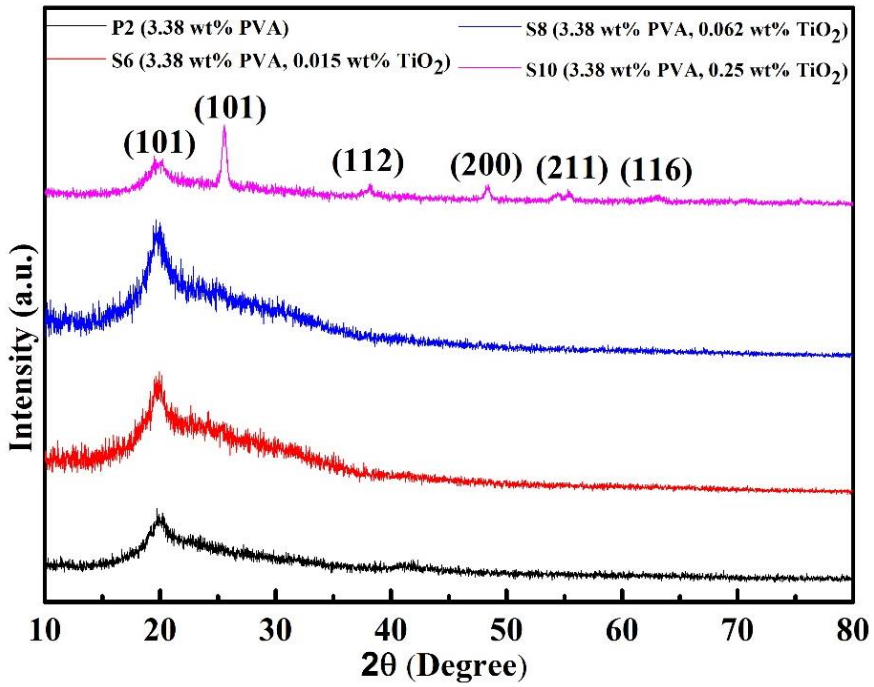

Figure 6.20: X-ray diffractogram of TiO_2/PVA nanocomposites (P2, S6, S8, S10) with 3.38 wt% PVA

The comparison of x-ray diffractograms of pure PVA and TiO_2/PVA nanocomposites for the angle range of $2\theta = 10\text{-}80^{\circ}$ are shown in Fig. 6.19 (P1, S1, S3, S5), Fig. 6.20 (P2, S6, S8, S10), Fig. 6.21(P1, S12, S14, S16, S18, S20), and Fig. 6.22 (P2, S22, S24, S26, S28, S30). The diffraction patterns of pure PVA (P1 and P2) are showing a single broad peak between $2\theta = 20.51^{\circ}$, which corresponds to (101) plane reflection of orthorhombic lattice [205, 210]. This broad peak was perfectly matching with standard data from JCPDS file [00-061-1401]. It indicates semicrystalline nature of PVA which results from intermolecular hydrogen bonding between PVA chains [205, 210-211]. The intensity of this peak is decreasing with increasing weight percent of TiO_2 nanoparticles within TiO_2/PVA nanocomposites which indicates reduction in degree of crystallinity of PVA. It has been reported by Hodge et al. that intensity of XRD peaks decreases as degree of crystallinity decreases [212]. The peak for pure PVA is clearly visible in S1, S3, S5, S6, S8, and S10 samples and it was not identified in S12, S14, S16, S18, S20, S22, S24, S26, S28, and S30 samples. The reason of disappearance of this peak in S12, S14, S16, S18, S20, S22, S24, S26, S28, and S30 samples might be due to interaction between TiO_2 nanoparticles and PVA matrix which resulted in reduction in intermolecular hydrogen bonding between PVA chains [212].

The diffraction patterns of TiO_2/PVA nanocomposites (S10, S12, S14, S16, S18, S20, S22, S24, S26, S28, and S30 samples) are showing diffraction peaks at $2\theta = 25.55^{\circ}$, 38.07°, 48.27°, 54.29°, and 63.17° which were indexed as (101), (112), (200), (211), and (116) plane reflections of anatase TiO_2 after matching with standard data from JCPDS file [00-021-1272].

The diffraction patterns of TiO_2/PVA nanocomposites (S1, S3, S5, S6, and S8) are showing only a single peak at $2\theta = 25.55^{\circ}$ which is indexed as (101) plane reflections of anatase TiO_2 as matched with JCPDS file [00-021-1272]. Also, the diffraction patterns of TiO_2/PVA nanocomposites (S1, S3, S5, S6, and S8) are not showing clearly distinguishable peak for $2\theta = 38.07^{\circ}$, 48.27°, 54.29°, and 63.17°, but a broad peak between $2\theta = 20.51^{\circ}$ is observed, which corresponds to (101) plane reflection of orthorhombic lattice of PVA.

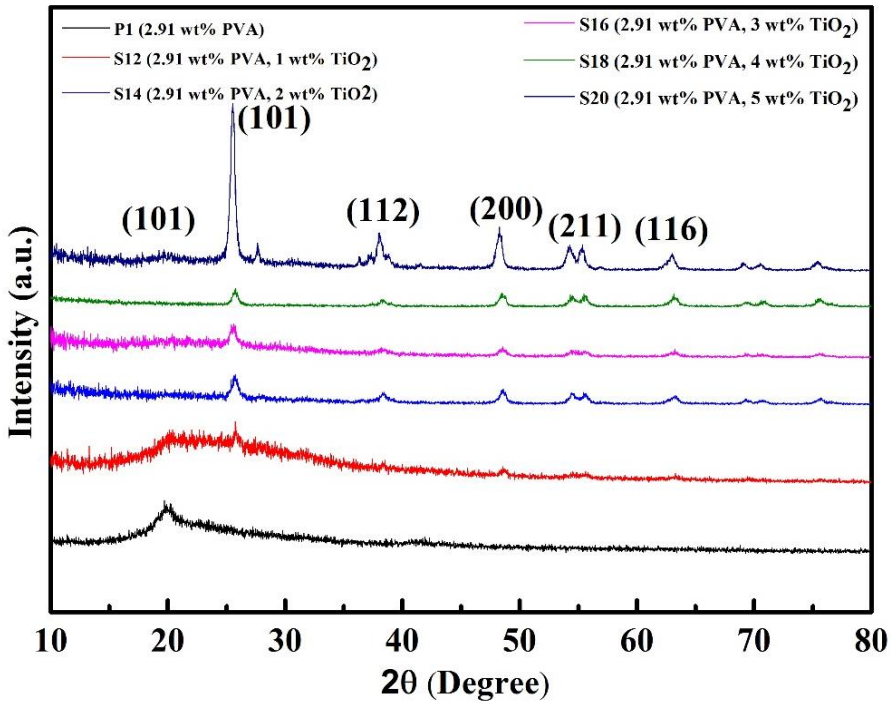

Figure 6.21. X-ray diffractogram of TiO_2/PVA nanocomposites (P1, S12, S14, S16, S18, S20) with 2.91 wt% PVA

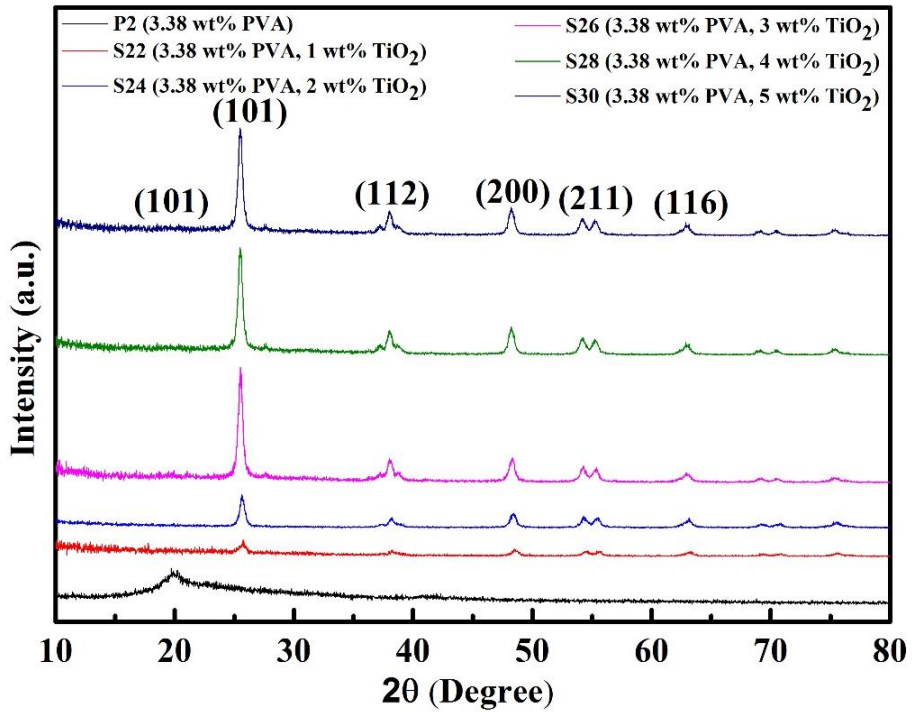

Figure 6.22: X-ray diffractogram of TiO_2/PVA nanocomposites (P2, S22, S24, S26, S28, S30) with 3.38 wt% PVA

Table 6.2: Crystal structure, lattice parameter, and dislocation density

S. No.	Sample	Crystal structure	2θ° and d_{hkl} (Å)	Lattice Parameter (Å)	Unit cell Volume (Å)	Crystallite Size d (nm)	Dislocation Density $1/d^2$ (m^{-2})	Lattice Strain ε
1	S12	Tetragonal	25.61 3.48	a=b=3.78 c=8.91	127.31	27.03	$1.4x10^{15}$	0.006
2	S14	Tetragonal	25.89 3.44	a=b=3.74 c=8.75	136.30	18.03	$3.1x10^{15}$	0.009
3	S16	Tetragonal	25.71 3.47	a=b=3.74 c=9.29	129.94	18.03	$3.1x10^{15}$	0.009
4	S18	Tetragonal	25.74 3.46	a=b=3.74 c=9.1	127.91	18.03	$3.1x10^{15}$	0.009
5	S20	Tetragonal	25.77 3.46	a=b=3.76 c=8.83	124.84	15.46	$4.2x10^{15}$	0.012
6	S22	Tetragonal	25.63 3.48	a=b=3.76 c=9.19	129.92	30.90	$1.0x10^{15}$	0.005
7	S24	Tetragonal	25.55 3.49	a=b=3.76 c=9.37	132.47	24.03	$1.7x10^{15}$	0.007
8	S26	Tetragonal	25.61 3.48	a=b=3.76 c=9.19	129.92	24.03	$1.7x10^{15}$	0.007
9	S28	Tetragonal	25.53 3.49	a=b=3.78 c=9.08	129.74	21.63	$2.1x10^{15}$	0.008
10	S30	Tetragonal	25.77 3.46	a=b=3.76 c=8.83	124.84	21.63	$2.1x10^{15}$	0.008

This broad peak is characteristic for PVA and it was absent in diffraction patterns of TiO_2/PVA nanocomposites (S12, S14, S16, S18, S20, S22, S24, S26, S28, and S30), suggesting dominance of amorphous region in PVA.

At higher weight percent of TiO_2 nanoparticles plane reflections of anatase TiO_2 nanoparticles became more prominent in compare to that of PVA. It is also clear from Fig. 6.19, Fig. 6.20, Fig. 6.21, and Fig. 6.22 that crystallinity of TiO_2/PVA nanocomposites is increased with increasing weight percent of TiO_2 nanoparticles. The reason behind increased crystallinity of TiO_2/PVA nanocomposites is bonding between TiO_2 nanoparticles and PVA which results in ordered structure. The Ti-O-O bond formation between TiO_2 nanoparticles and PVA was confirmed by FTIR.

The crystal structure, interplanar distance (d_{hkl}), lattice constants (a, b, and c), unit cell volume ((abc) for tetragonal lattice), crystallite size (d), dislocation density ($1/d^2$), and lattice strain (ε) were calculated for TiO_2 nanoparticles within TiO_2/PVA nanocomposites (S12, S14, S16, S18, S20, S22, S24, S26, S28, and S30) as shown in Table 6.2. These data were matched with standard data from JCPDS file [00-021-1272] and deviation in lattice parameters and unit cell volume was as follows.

According to JCPDS file [00-021-1272], lattice parameters for anatase TiO_2 are a = b = 3.785 Å and c = 9.514 Å. Thus, in this study, a contraction along a-axis, b-axis, and c-axis is observed along with reduction in unit cell volume for TiO_2/PVA nanocomposites (S12, S14, S16, S18, S20, S22, S24, S26, S28, and S30) (see Table 6.2). Whereas, in a previous study, Archana Maurya et al. observed an elongation along a-axis, and b-axis whereas a contraction towards c-axis for rutile phase of TiO_2 which resulted in overall increase in unit cell volume. But, in this work, reduction in unit cell volume is observed which indicates TiO_2 nanoparticles are entrapped within PVA matrix and steric hindrance of large polymer chains inhibits aggregation of TiO_2 nanoparticles. The other reason is bonding between TiO_2 nanoparticles and PVA.

The trend in variations of lattice strain, dislocation density, and crystallite size is demonstrated by plotting curves of these parameters with respect to samples of TiO_2/PVA nanocomposites.

The effect of different TiO_2 content with 2.91 wt% of PVA on lattice strain is shown in Fig. 6.23, and that with 3.38 wt% of PVA is shown in Fig. 6.24. It can be seen that lattice strain is increasing with increasing weight percent of TiO_2 nanoparticles. The lattice strain was increased by 0.006 for S20, and 0.003 for S30 sample in compare to S12, and S22, respectively. Thus displacements of atoms are higher in TiO_2/PVA nanocomposites with 2.91 wt% of PVA than in 3.38 wt% of PVA.

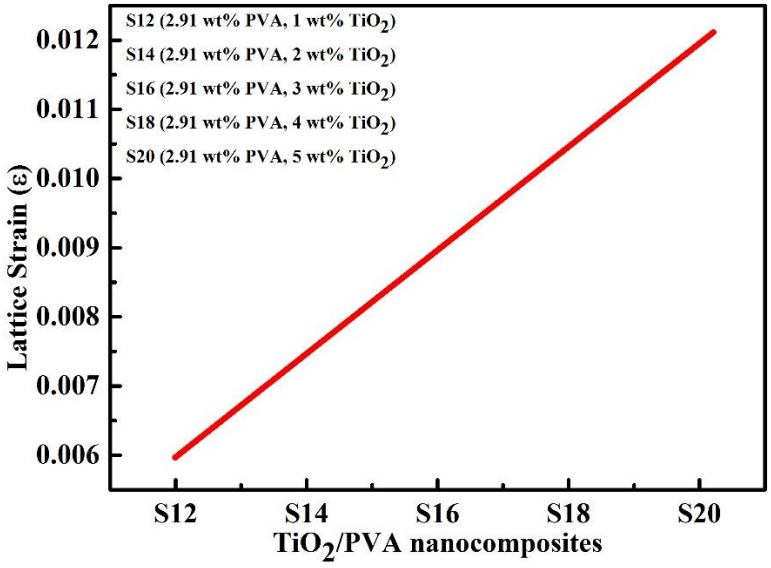

Figure 6.23: The relation between TiO_2 content with 2.91 wt% of PVA and lattice strain

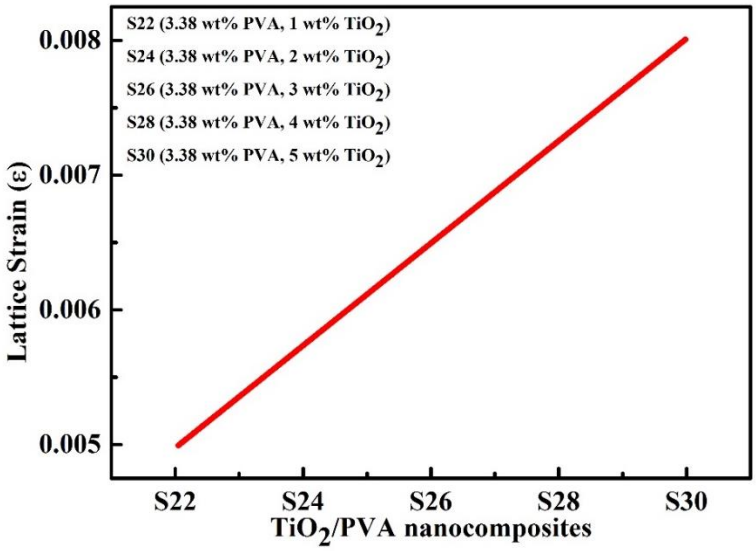

Figure 6.24: The relation between TiO_2 content with 3.38 wt% of PVA and lattice strain

The effect of different TiO_2 content with 2.91 wt% of PVA on dislocation density is shown in Fig. 6.25, and that with 3.38 wt% of PVA is shown in Fig. 6.26. It can be seen that dislocation density is increasing with increasing weight percent of TiO_2. The dislocation density was increased by 2.8×10^{15} for S20, and 1.1×10^{15} S30 sample in compare to S12, and S22, respectively. Thus, number of dislocations in unit volume are higher in TiO_2/PVA nanocomposites with 2.91 wt% of PVA than in 3.38 wt% of PVA.

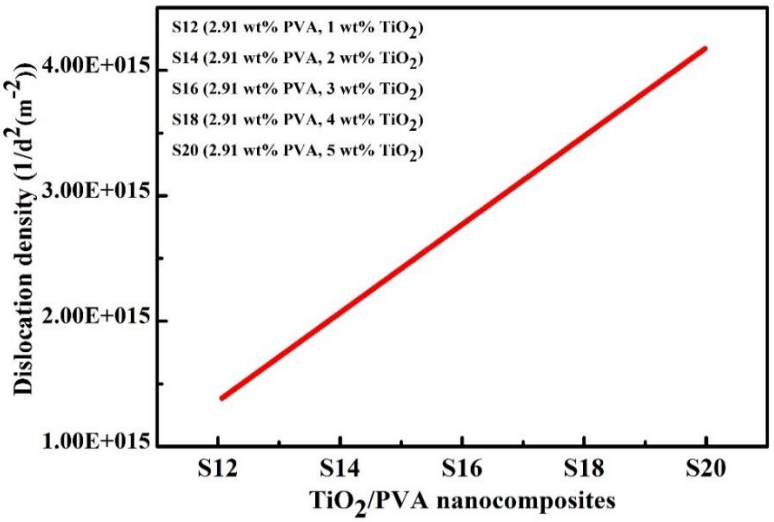

Figure 6.25: The relation between TiO_2 content with 2.91 wt% of PVA and dislocation density

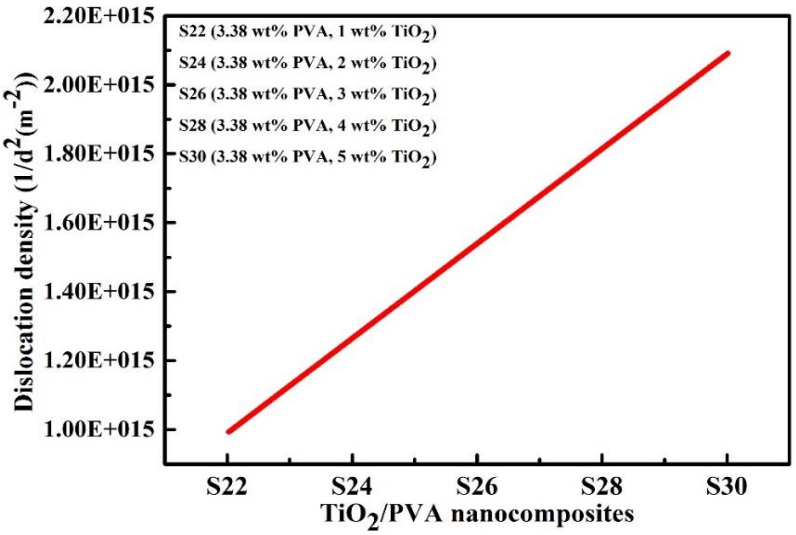

Figure 6.26: The relation between TiO_2 content with 3.38 wt% of PVA and dislocation density

The effect of different TiO_2 content with 2.91 wt% of PVA on crystallite size is shown in Fig. 6.27, and that with 3.38 wt% of PVA is shown in Fig. 6.28. It can be seen that crystallite size is decreasing with increasing weight percent of TiO_2. The crystallite size was decreased by 11.57 nm for S20, and 9.27 nm for S30 sample in compare to S12, and S22, respectively. Thus, crystallite size for TiO_2/PVA nanocomposites with 2.91 wt% of PVA is smaller than in TiO_2/PVA nanocomposites with 3.38 wt% of PVA. The reduction in crystallite size of TiO_2 nanoparticles is due to contraction along a-axis, b-axis, and c-axis of tetragonal lattice. This contraction resulted in overall reduction of unit cell volume.

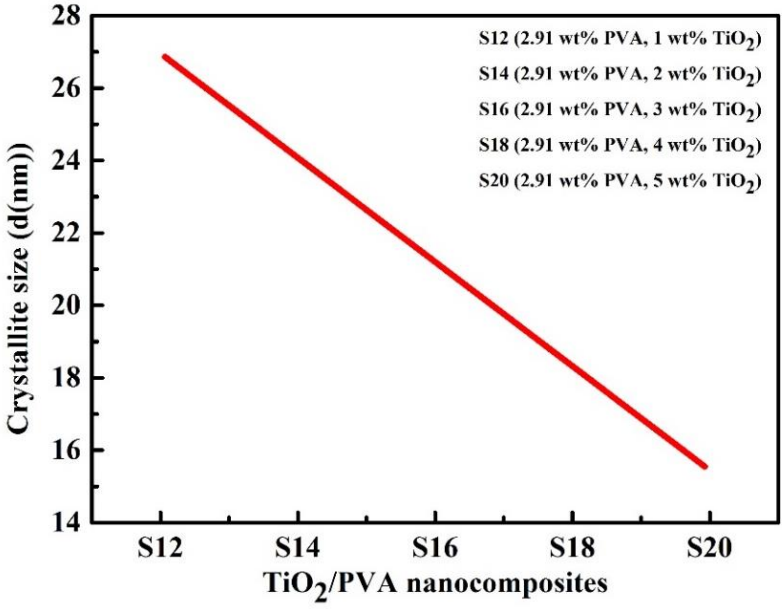

Figure 6.27: The relation between TiO_2 content with 2.91 wt% of PVA and crystallite size

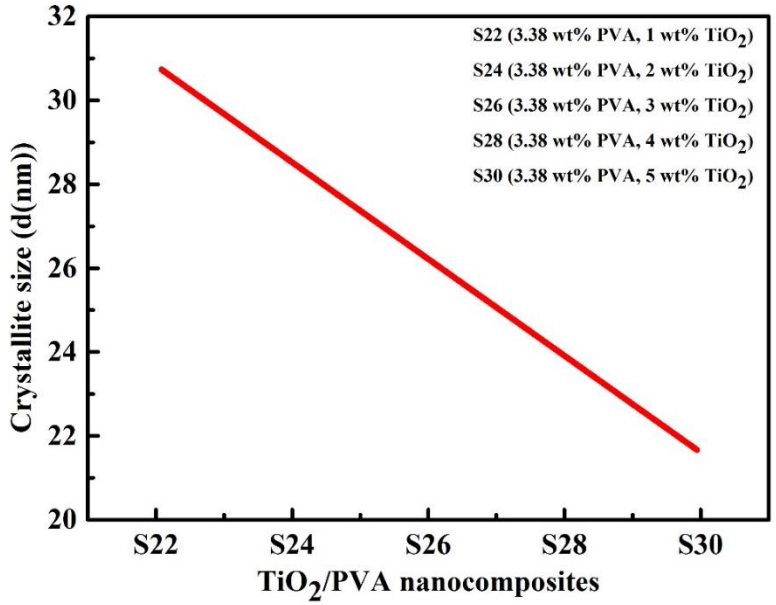

Figure 6.28: The relation between TiO_2 content with 3.38 wt% of PVA and crystallite size

From above discussions, it is concluded that crystallinity of TiO_2/PVA nanocomposites is increasing with increasing weight percent of TiO_2 nanoparticles with both variation of PVA (2.91, and 3.38 wt %). The improvement in crystallinity is due to Ti-O-O bond formation between TiO_2 nanoparticles and PVA which results in ordered structure. The lattice strain and dislocation density are increasing with

increasing weight percent of TiO_2 nanoparticles with both variation of PVA (2.91, and 3.38 wt%), but higher in TiO_2/PVA nanocomposites with 2.91 wt% of PVA than in 3.38 wt% of PVA. The displacements of atoms in TiO_2 nanoparticles was due to interaction with PVA matrix. Also, crystallite size of TiO_2 nanoparticles is decreasing with increasing weight percent of TiO_2 nanoparticles with both variation of PVA (2.91, and 3.38 wt%). The reduction in crystallite size with increasing weight percent of TiO_2 nanoparticles was higher for 2.91 wt% of PVA than in 3.38 wt% of PVA.

The reduction in crystallite size with increasing weight percent of TiO_2 nanoparticles indicates PVA has prevented aggregation of TiO_2 nanoparticles by bonding with TiO_2 nanoparticles and steric hindrance. Thus, prepared TiO_2/PVA nanocomposites are having smaller TiO_2 nanoparticles which will result in better thermal and mechanical properties.

6.4 Morphological Analysis

Surface morphology of prepared TiO_2/PVA nanocomposites was investigated by scanning electron microscopy (SEM). In this research work, S1 to S5 and S11 to S20 samples of TiO_2/PVA nanocomposites, were prepared by doping of different weight percent of TiO_2 nanoparticles in 2.91 wt% of PVA (P1). Whereas, S6 to S10 and S21 to S30 samples of TiO_2/PVA nanocomposites, were prepared by doping of different weight percent of TiO_2 nanoparticles in 3.38 wt% of PVA (P2). The SEM was performed for P1, P2, S1, S5, S6, S10, S12, S14, S16, S18, S20, S22, S24, S26, S28, S30 samples of TiO_2/PVA nanocomposites. Mapping analysis was performed for S14 and S22 samples of TiO_2/PVA nanocomposites.

The surface morphology study with EDAX of TiO_2/PVA nanocomposites is important to check incorporation of TiO_2 nanoparticles within PVA matrix and mapping analysis is significant to explore whether dispersion of TiO_2 nanoparticles within PVA matrix is homogenous or not.

SEM micrographs with EDAX for pure PVA (P1 and P2) and TiO_2/PVA nanocomposites (S1, S5, S6, S10, S12, S14, S16, S18, S20, S22, S24, S26, S28, and S30) are shown in Fig. 6.29. The observations of these micrographs are given below.

The EDAX confirms the presence of C, Ti and O atoms in all TiO_2/PVA nanocomposites and C and O atoms in Pure PVA (P1 and P2). Also, mapping analysis was possible only for S14 and S22 samples of TiO_2/PVA nanocomposites. For mapping analysis, high voltage is required; other samples started to degrade when high voltage was applied. The S14 and S22 samples of TiO_2/PVA nanocomposites did not degrade on applying high voltage because of high gold coating, as seen by EDAX analysis.

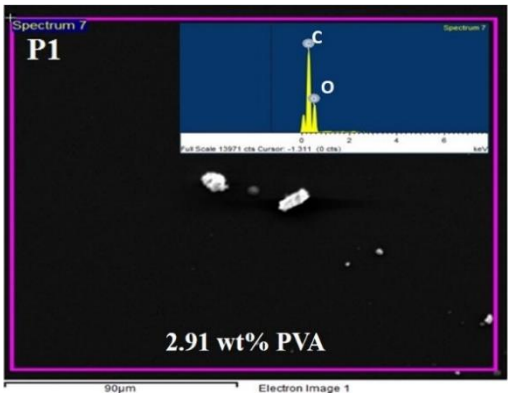

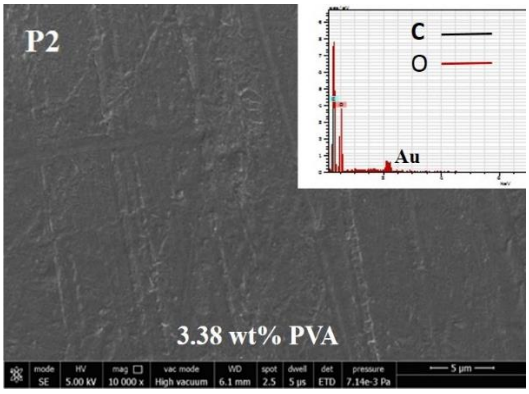

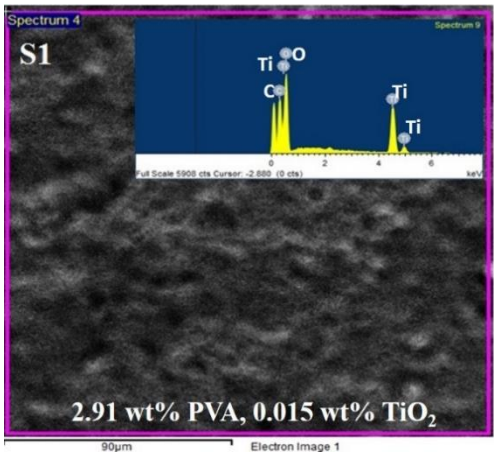

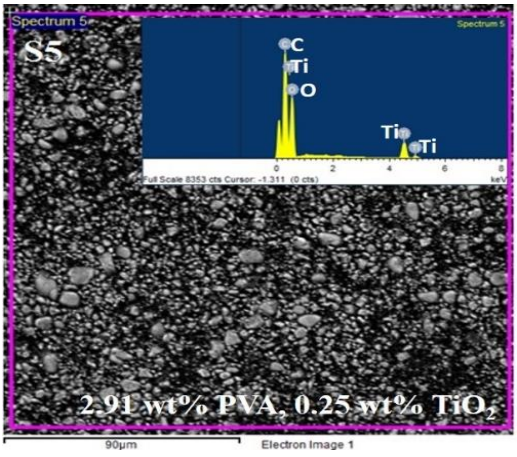

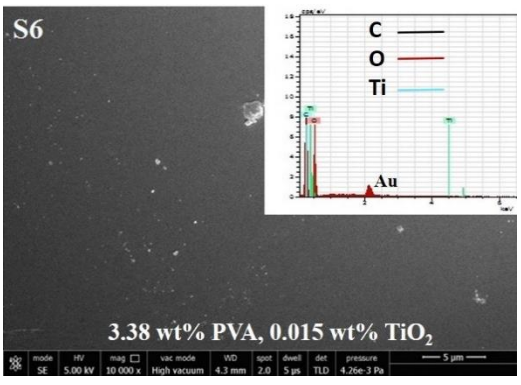

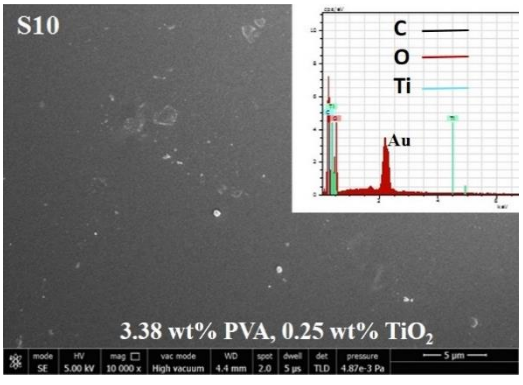

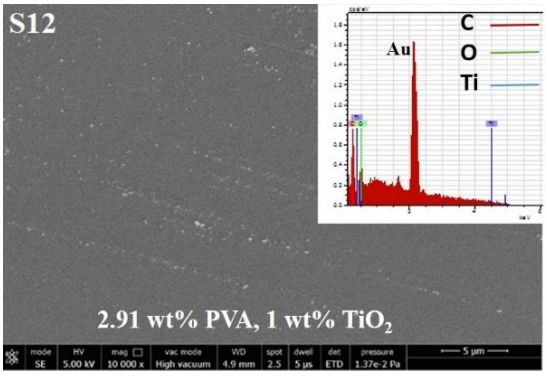
S12
C
O
Ti
Au
2.91 wt% PVA, 1 wt% TiO2

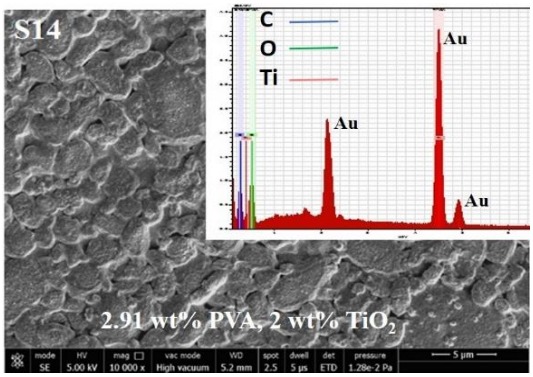
S14
C
O
Ti
Au
Au
Au
2.91 wt% PVA, 2 wt% TiO2

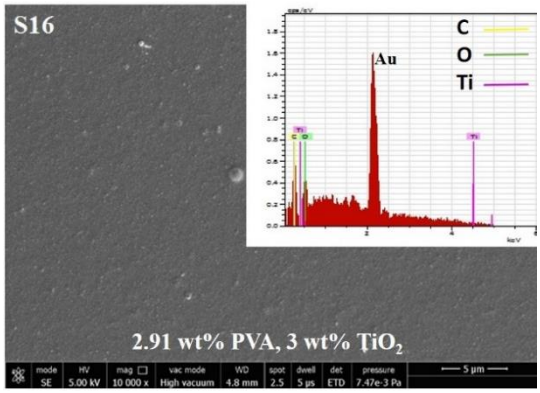
S16
C
O
Ti
Au
2.91 wt% PVA, 3 wt% TiO2

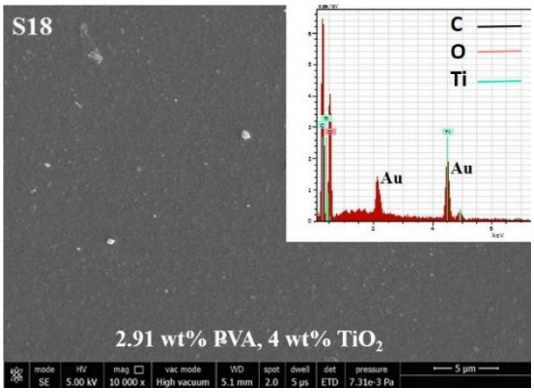
S18
C
O
Ti
Au
Au
2.91 wt% RVA, 4 wt% TiO2

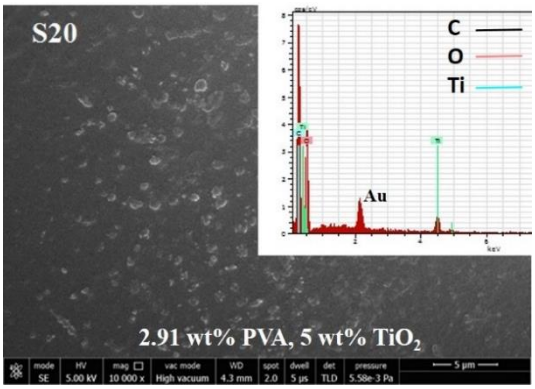
S20
C
O
Ti
Au
2.91 wt% PVA, 5 wt% TiO2

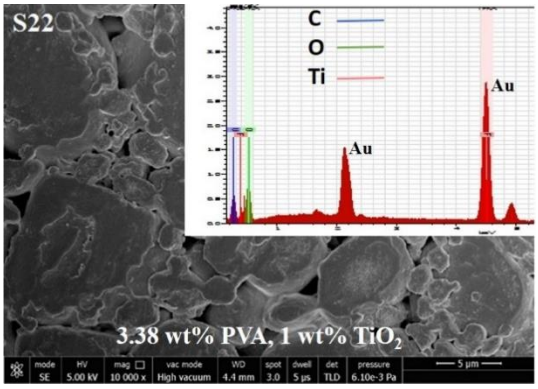
S22
C
O
Ti
Au
Au
3.38 wt% PVA, 1 wt% TiO2

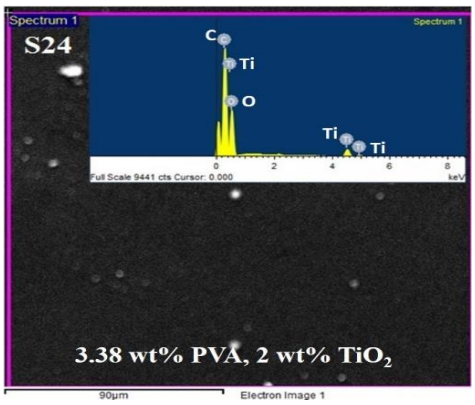
Spectrum 1
S24
C
Ti
O
Ti
Ti
3.38 wt% PVA, 2 wt% TiO2
90µm
Electron Image 1

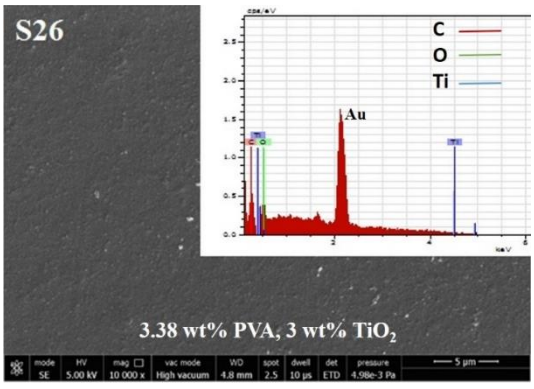
S26
C
O
Ti
Au
3.38 wt% PVA, 3 wt% TiO2

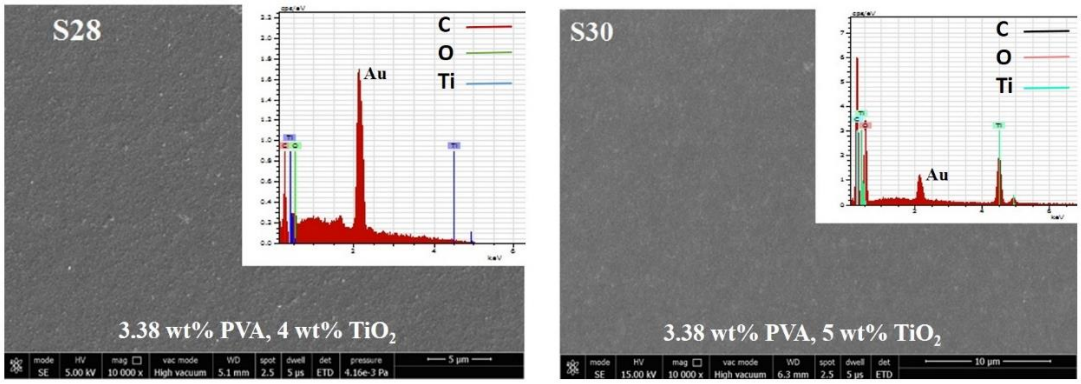

Figure 6.29: SEM image of pure PVA (P1 and P2) and TiO_2/PVA nanocomposites (S1, S5, S6, S10, S12, S14, S16, S18, S20, S22, S24, S26, S28, and S30)

The PVA chains are aligned parallel in PVA (P1 and P2), and all TiO_2/PVA nanocomposites (S1, S5, S6, S10, S12, S14, S16, S18, S20, S22, S24, S26, S28, and S30). It can be seen from SEM micrographs that TiO_2 nanoparticles were forming clusters when embedded in PVA matrix (Fig. 6.29). The white spots present in SEM micrographs are due to charging of particles when high voltage was applied. Comparison of SEM micrographs of pure PVA and TiO_2/PVA nanocomposites clearly indicates homogenous dispersion of TiO_2 nanoparticles.

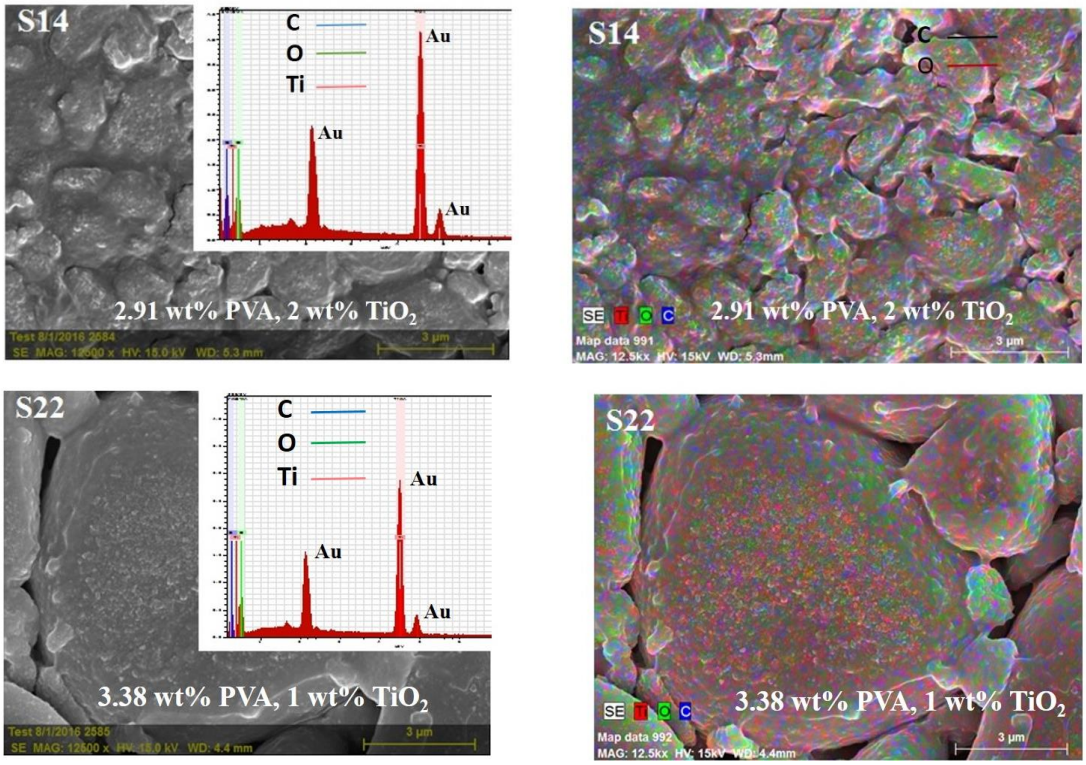

Figure 6.30: Mapping analysis of TiO_2/PVA nanocomposites (S14, S22)

The mapping analysis of TiO_2/PVA nanocomposites (S14, S22) is shown in Fig. 6.30. These images are showing homogenous presence of Ti, O, and C atoms in TiO_2/PVA nanocomposites. It was confirmed by mapping analysis (Fig. 6.30). From SEM analysis, Homogenous dispersion of TiO_2 nanoparticles within PVA matrix was seen which is necessary for good thermal and mechanical properties.

In summary, the blue shift in absorbance spectra of TiO_2/PVA nanocomposites with increasing concentration of TiO_2 nanoparticles was observed for both P1 (2.91 wt% PVA) and P2 (3.38 wt% PVA) which indicates reduction in aggregation of TiO_2 nanoparticles. The reduction in aggregation of TiO_2 nanoparticles resulted in smaller crystallite sizes of TiO_2 nanoparticles. The crystallite sizes of TiO_2 nanoparticles, determined by XRD graphs using Debye-Scherrer formula, are showing similar results to the UV-Vis. The smaller crystallite size of TiO_2 nanoparticles as calculated from UV-Vis and XRD is due to Ti-O-O bond formation between TiO_2 nanoparticles and PVA which was confirmed by FTIR. Surface morphology analysis of TiO_2/PVA nanocomposites is showing homogenous dispersion of TiO_2 nanoparticles within PVA matrix. The prevention of aggregation and homogenous dispersion of TiO_2 nanoparticles is necessary for good thermal and mechanical properties of TiO_2/PVA nanocomposites.

Chapter 7
RESULTS AND DISCUSSIONS-II
(Thermal analysis of TiO_2/PVA nanocomposites)

The prepared TiO_2/PVA nanocomposites are important for applications in anti-reflection coatings in solar cells, humidity sensing, gas sensing, and water purification. The device fabrication techniques for above applications require good thermal stability of TiO_2/PVA nanocomposites. Thus, it is important to study thermal behaviour of prepared TiO_2/PVA nanocomposites. Results and discussions regarding thermal behaviour of prepared TiO_2/PVA nanocomposites are discussed in this chapter.

This chapter is divided into two sections. Thermal transitions like glass transition temperature, and melting point are discussed with the help of differential scanning calorimetry (DSC) curves in first section. Thermal degradation behaviour of TiO_2/PVA nanocomposites is discussed by thermal gravimetric analysis (TGA) curves in second section.

7.1 Thermo-physical Analysis of TiO_2/PVA Nanocomposites

The effect of doping of TiO_2 nanoparticles on glass transition temperature of TiO_2/PVA nanocomposites was understood by differential scanning calorimetry (DSC). It is important to study the glass transition temperature Tg of TiO_2/PVA nanocomposites because properties of polymers abruptly changes after this point. Below glass transition temperature Tg, polymers are in rigid and glassy state whereas above glass transition temperature Tg, they are in flexible and rubbery state. The glass transition temperature Tg affects the end use of prepared TiO_2/PVA nanocomposites. The applications of TiO_2/PVA nanocomposites like anti-reflection coatings in solar cells, humidity sensing, gas sensing, and water purification, depends upon its glass transition temperature Tg. So, identifying the glass transition temperature Tg of TiO_2/PVA nanocomposites is important for above mentioned applications.

TiO_2/PVA nanocomposites designated (described in chapter 5) as S1 to S5 and S11 to S20 were prepared by taking different weight percent of TiO_2 nanoparticles with 2.91 wt% of PVA (P1). Whereas, TiO_2/PVA nanocomposites designated as S6 to S10 and S21 to S30 were prepared by taking different weight percent of TiO_2 nanoparticles with 3.38 wt% of PVA (P2). DSC experiment was performed for all samples of TiO_2/PVA nanocomposites to obtain thermal analysis curves. Thermal analysis curves of TiO_2/PVA nanocomposites in the temperature range 25-300°C are shown in Fig. 7.1 (P1, S1, S2, S3, S4, and S5), Fig. 7.2 (P2, S6, S7, S8, S9, and S10), Fig. 7.3 (S11, S12, S13, S14, S15, S16, S17, S18, S19, and S20), and Fig. 7.4 (S21, S22, S23, S24, S25, S26, S27, S28, S29, and S30).

From Fig. 7.1, Fig. 7.2, Fig. 7.3, and Fig. 7.4, it can be seen that both exothermic and endothermic peaks are present. Endothermic peaks correspond to glass transition region (Tg), and melting point region (Tm) whereas exothermic peaks correspond to crystallization region (Tc) of TiO_2/PVA nanocomposites [213-215].

The changes in sample weight or specific heat of the sample results in baseline shifts [213]. The change in specific heat of a sample happens when it is going through a transition like crystallization or melting and the weight of sample generally changes after decomposition.

The obtained thermal analysis curves for TiO_2/PVA nanocomposites are showing six base line shift regions which indicate different thermal transitions. These regions are related with, differences between heat capacity of TiO_2/PVA nanocomposites and reference material (below 70°C), Region I; evaporation of entrapped solvent (between 70-100°C) [216], Region II; glass transition temperature (between 100-145°C), Region III; crystallization temperature (rearrangement into ordered structure), Region IV; melting point temperature of PVA matrix (215-230 °C), Region V; and degradation temperature of PVA backbone (between 270-280°C), Region VI.

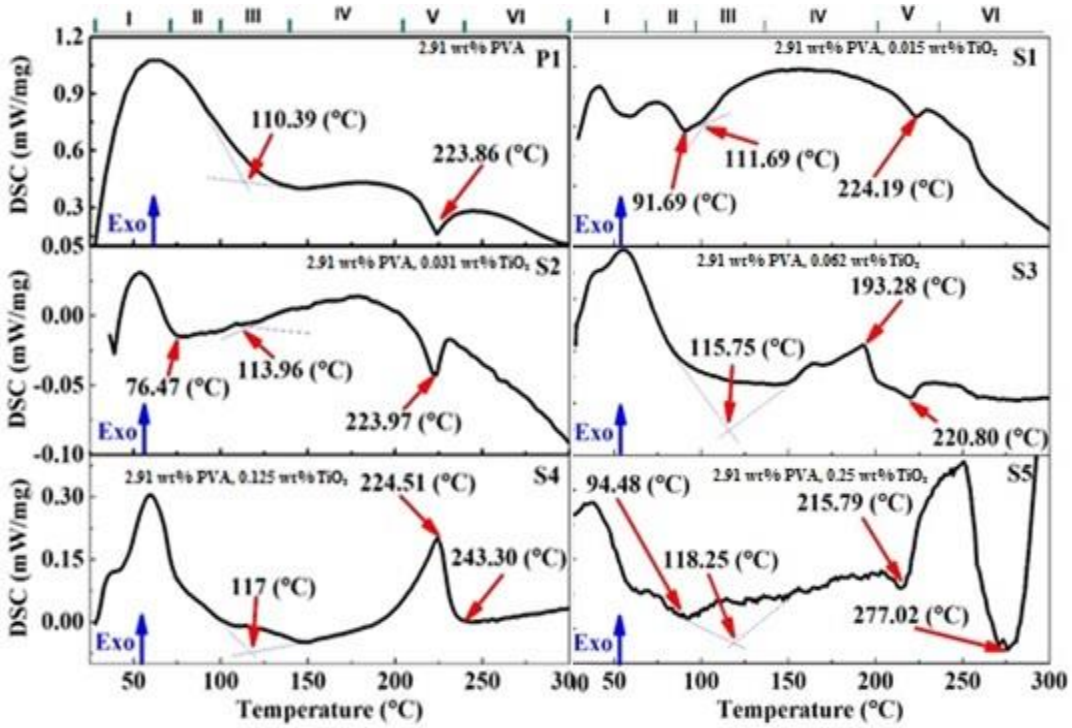

Figure 7.1: Thermograms of TiO_2/PVA nanocomposites (P1, S1, S2, S3, S4, and S5) with 2.91 wt% PVA

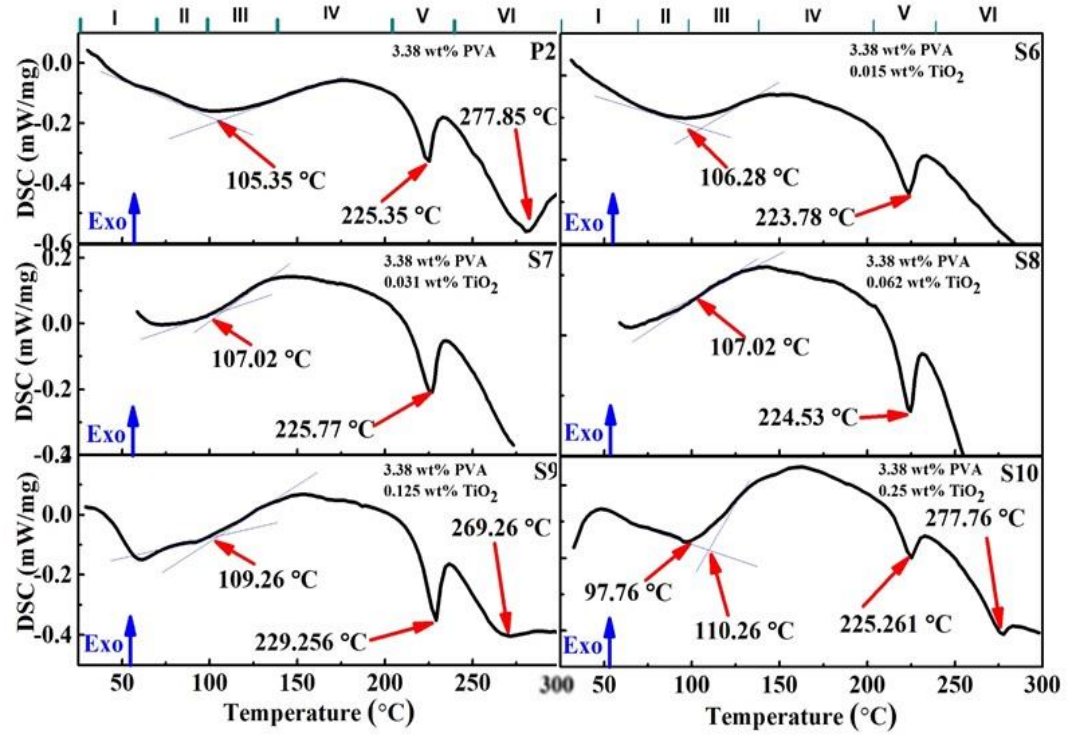

Figure 7.2: Thermograms of TiO_2/PVA nanocomposites (P2, S6, S7, S8, S9, and S10) with 3.38 wt% PVA

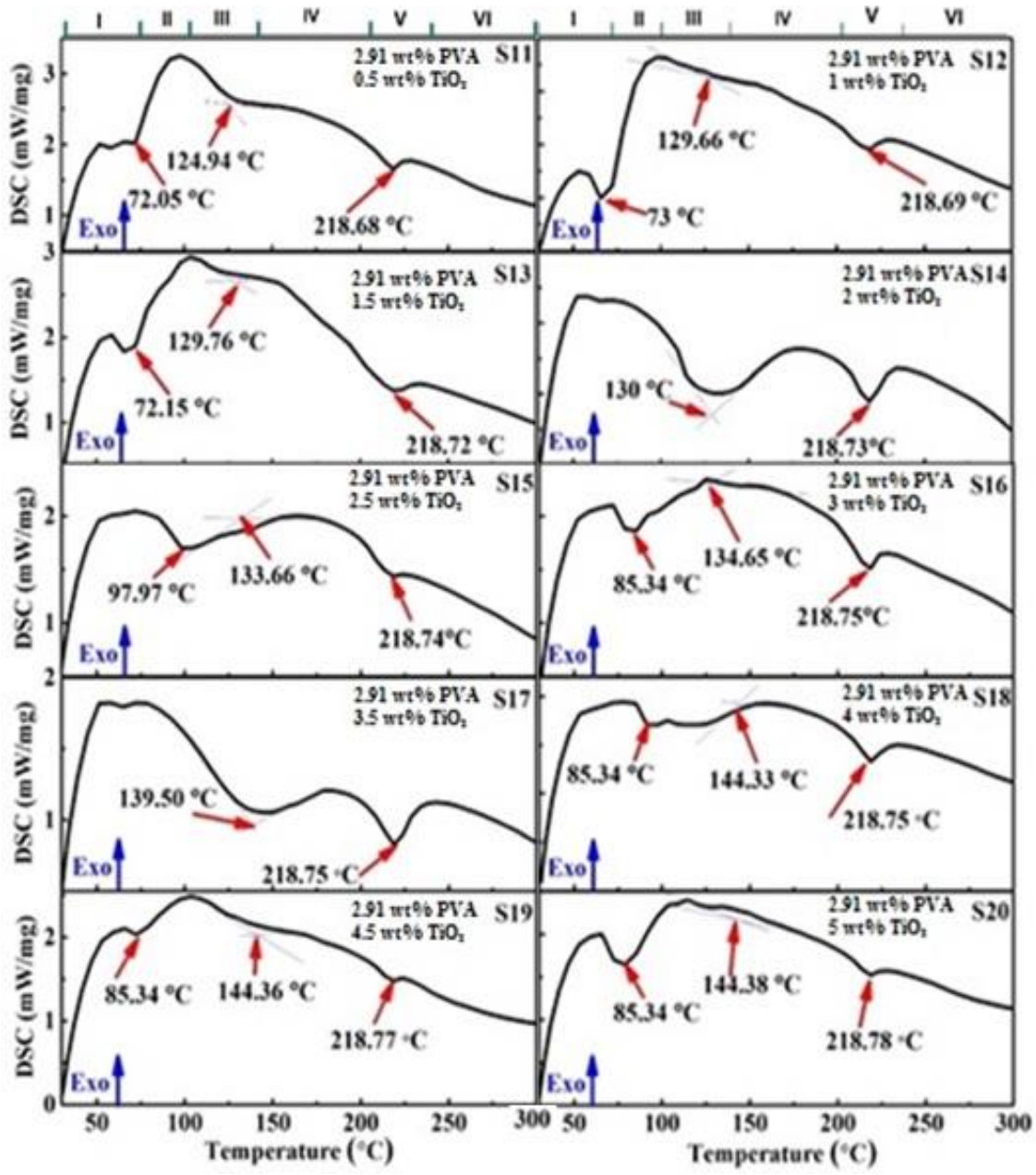

Figure 7.3: Thermograms of TiO_2/PVA nanocomposites (S11, S12, S13, S14, S15, S16, S17, S18, S19, and S20) with 2.91 wt% PVA

All six thermal transition regions were not observed in all samples, only glass transition temperature region and melting point temperature region were observed for all samples which are important for this study. The observations for TiO_2/PVA nanocomposites regarding four baseline shift regions of heat flow with respect to temperature are mentioned below.

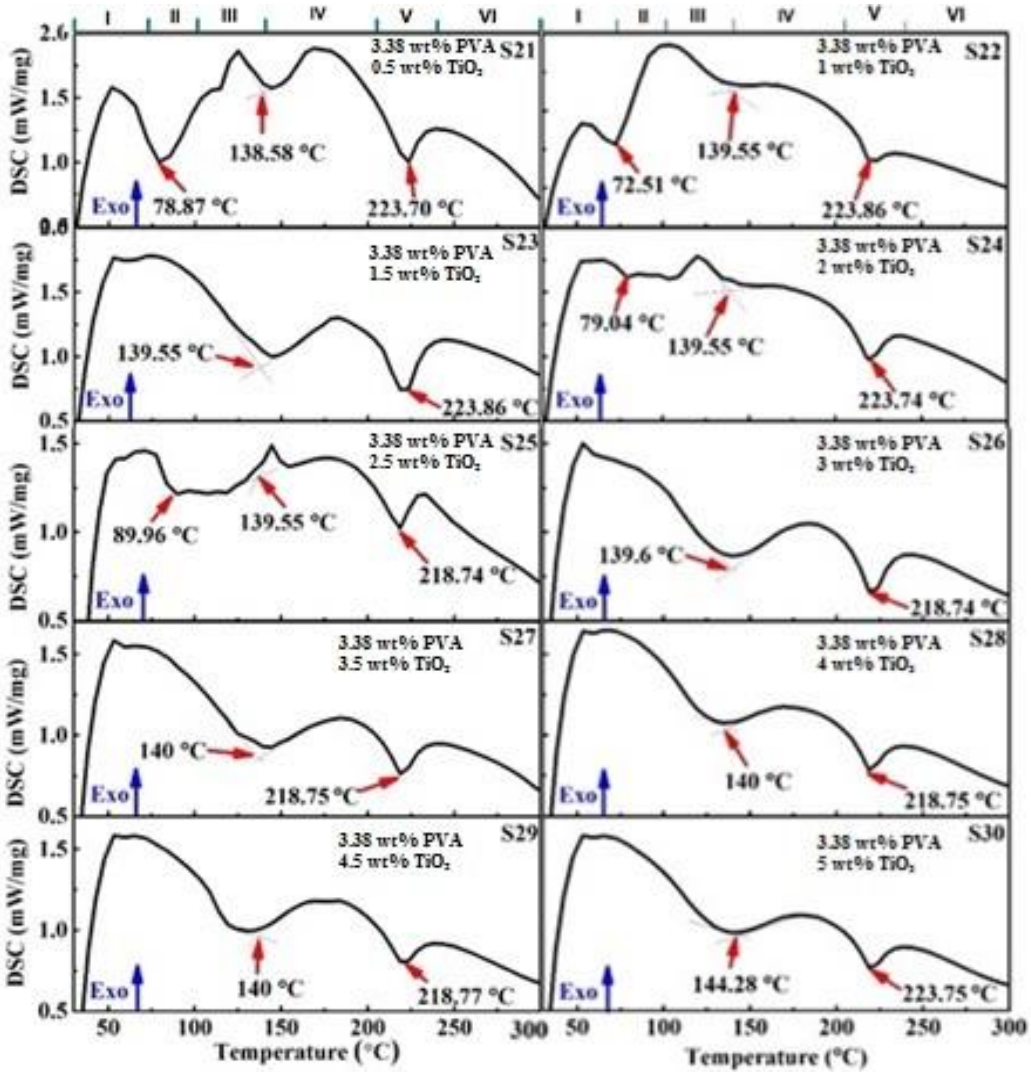

Figure 7.4: Thermograms of TiO_2/PVA nanocomposites (S21, S22, S23, S24, S25, S26, S27, S28, S29, and S30) with 3.38 wt% PVA

The glass transition temperature Tg for P1 (2.91 wt% of PVA) and P2 (3.38 wt% of PVA) were observed at 110.39°C, and 105.35°C, respectively. Whereas melting point temperature for P1 and P2 were observed at 223.86°C and 225.35°C, respectively. The degradation of PVA backbone was observed in P2 at 277.85°C.

The evaporation of solvent occurred in S1, S2, S5, S10, S11, S12, S13, S15, S16, S18, S19, S20, S21, S22, S24, and S25 samples of TiO_2/PVA nanocomposites at 91.69°C, 76.47°C, 94.48°C, 97.76°C, 72.95°C, 73°C, 72.15°C, 97.97°C, 85.34°C, 85.34°C, 85.34°C, 85.34°C, 78.87°C, 72.51°C, 79.04°C, and 89.96°C, respectively which is due to embedded moisture or solvent within sample during synthesis.

The glass transition temperatures Tg for S1, S2, S3, S4, S5, S6, S7, S8, S9, S10, S11, S12, S13, S14, S15, S16, S17, S18, S19, S20, S21, S22, S23, S24, S25,

S26, S27, S28, S29, and S30 samples of TiO_2/PVA nanocomposites were observed at 111.69°C, 113.96°C, 115.75°C, 117°C, 118.25°C, 106.28°C, 107.02°C, 107.02°C, 109.26°C, 110.26°C, 124.94°C, 129.66°C, 129.76°C, 130°C, 133.66°C, 134.65°C, 139.50°C, 144.33°C, 144.36°C, 144.38°C, 138.58°C, 139.55°C, 139.55°C, 139.55°C, 139.55°C, 139.6°C, 140°C, 140°C, 140°C, and 144.28°C, respectively. The glass transition temperature Tg was observed due to sudden increase in specific heat of sample upon heating and it leads to segmental motion of PVA chains. The kinetic energy for mobility of PVA chains was provided by heat. This transition is second order transition because no latent heat was involved. The segmental motion occurs only in amorphous domain of PVA matrix

The melting point temperature for S1, S2, S3, S4, S5, S6, S7, S8, S9, S10, S11, S12, S13, S14, S15, S16, S17, S18, S19, S20, S21, S22, S23, S24, S25, S26, S27, S28, S29, and S30 samples of TiO_2/PVA nanocomposites were observed at 224.19°C, 223.97°C, 220.8°C, 243.5°C, 215.79°C, 223.78°C, 225.77°C, 224.53°C, 229.26°C, 225.26°C, 218.68°C, 218.69°C, 218.72°C, 218.73°C, 218.74°C, 218.75°C, 218.75°C, 218.75°C, 218.77°C, 218.78°C, 223.7°C, 223.86°C, 223.86°C, 223.74°C, 218.74°C, 218.74°C, 218.75°C, 218.75°C, 218.77°C, and 223.75°C, respectively. The crystalline domains of PVA undergoes phase change at melting point temperature. At this point, ordered arrangement of PVA chains is destroyed and they start to move around freely within TiO_2/PVA nanocomposites. In this process, latent heat is involved, hence it is first order transition.

The degradation of PVA backbone was observed in P2, S5, S9, and S10 samples of TiO_2/PVA nanocomposites at 277.85°C, 277.02°C, 269.26°C, and 277.76°C, respectively. This happens as a result of cleavage of bonds in PVA backbone.

From above observations, it can be clearly seen that glass transition temperature Tg of TiO_2/PVA nanocomposites is increasing with increased TiO_2 content for TiO_2/PVA nanocomposites with both variations of PVA (P1 and P2). The maximum value of glass transition temperature Tg for TiO_2/PVA nanocomposites with P1 is 144.38°C (for S20 sample) and that for TiO_2/PVA nanocomposites with

P2 is 144.28°C (for S30 sample). The increase in glass transition temperature Tg can be explained by H-bonding formation between TiO_2 nanoparticles and PVA matrix, which results in development of rigidity in PVA chains and restrict their thermal actions [217]. Thus, it is expected that TiO_2 nanoparticles are dispersed homogeneously into PVA matrix and thermal motion of PVA segment is prevented by the interaction between TiO_2 nanoparticles and PVA. The homogenous dispersion of TiO_2 nanoparticles into PVA matrix was seen by mapping results of scanning electron microscopy.

Whereas, no significant change was observed in melting point temperature of PVA crystallites with doping of TiO_2 nanoparticles within TiO_2/PVA nanocomposites.

The observations of DSC curves for TiO_2/PVA nanocomposites from Fig. 7.1, Fig. 7.2, Fig. 7.3, and Fig. 7.4 are summarized in Table 7.1, Table 7.2, Table 7.3, and Table 7.4.

Table 7.1: Thermal analysis (DSC) data for TiO_2/PVA nanocomposites (P1, S1, S2, S3, S4, and S5) with 2.91 wt% PVA

Designation of sample	**Glass Transition Temperature (°C)**	**Melting Temperature (°C)**
P1	110.39	223.86
S1	111.69	224.19
S2	113.96	223.97
S3	115.75	220.8
S4	117	243.5
S5	118.25	215.79

Table 7.2: Thermal analysis (DSC) data for TiO_2/PVA nanocomposites (P2, S6, S7, S8, S9, and S10) with 3.38 wt% PVA

Designation of sample	**Glass Transition Temperature (°C)**	**Melting Temperature (°C)**
P2	105.35	225.35
S6	106.28	223.78
S7	107.02	225.77
S8	109.26	224.53
S9	110.26	229.26
S10	110.26	225.26

Table 7.3: Thermal analysis (DSC) data for TiO_2/PVA nanocomposites (S11, S12, S13, S14, S15, S16, S17, S18, S19, and S20) with 2.91 wt% PVA

Designation of sample	**Glass Transition Temperature (°C)**	**Melting Temperature (°C)**
S11	124.94	218.68
S12	129.66	218.69
S13	129.76	218.72
S14	130	218.73
S15	133.66	218.74
S16	134.65	218.75
S17	139.5	218.75
S18	144.33	218.75
S19	144.36	218.77
S20	144.38	218.78

Table 7.4: Thermal analysis (DSC) data for TiO_2/PVA nanocomposites S21, S22, S23, S24, S25, S26, S27, S28, S29, and S30 with 3.38 wt% PVA

Designation of sample	Glass Transition Temperature (°C)	Melting Temperature (°C)
S21	138.58	223.7
S22	139.55	223.86
S23	139.55	223.86
S24	139.55	223.74
S25	139.55	218.74
S26	139.6	218.74
S27	140	218.75
S28	140	218.75
S29	140	218.77
S30	144.28	223.75

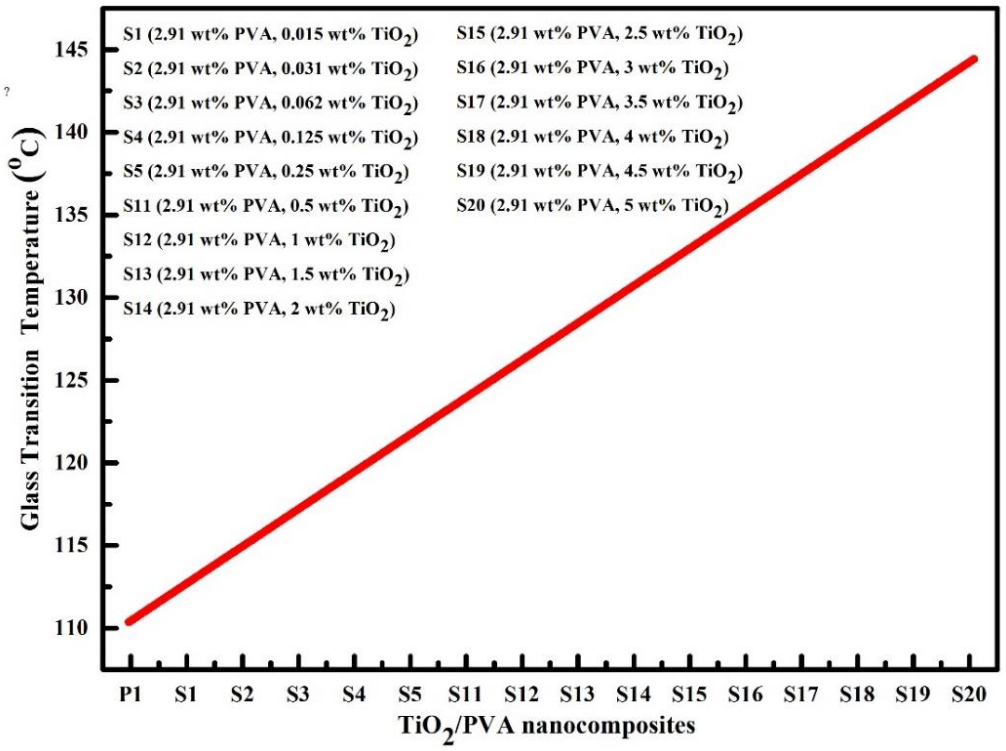

Figure 7.5: Effect of TiO_2 nanoparticles on glass transition temperature of TiO_2/PVA nanocomposites with 2.91 wt% PVA

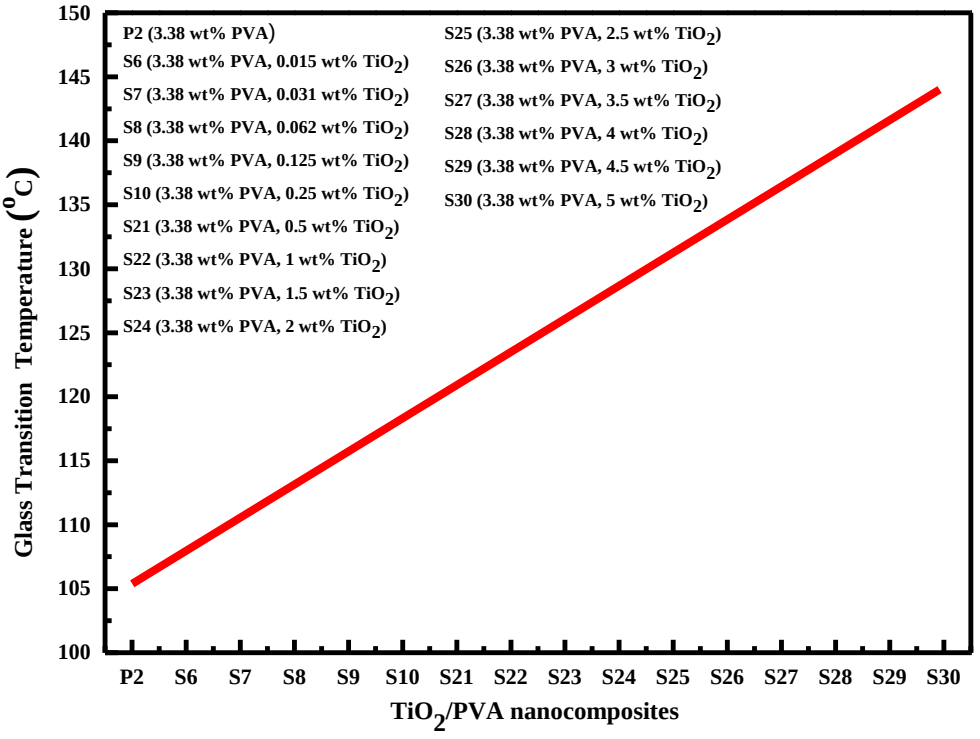

Figure 7.6: Effect of TiO_2 nanoparticles on glass transition temperature of TiO_2/PVA nanocomposites with 3.38 wt% PVA

The relationship between TiO_2 content and the glass transition temperature Tg for TiO_2/PVA nanocomposites with P1 (2.91 wt% PVA) is shown in Fig. 7.5 and with P2 (3.38 wt% PVA) is shown in Fig. 7.6. The increment in glass transition temperature Tg with increasing weight percent of TiO_2 can be seen from these graphs for TiO_2/PVA nanocomposites with both variations of PVA (P1 and P2). It is due to increased interaction between TiO_2 nanoparticles and PVA with increasing TiO_2 content.

The effect of lattice strain (calculated in Table 6.2) on glass transition temperature Tg for TiO_2/PVA nanocomposites with 2.91 wt% PVA and 3.38 wt% PVA are shown in Fig. 7.7, and Fig. 7.8, respectively. It can be seen from these graphs that glass transition temperature Tg is increasing with increasing lattice strain (ε) in both variations of PVA (2.91 wt% PVA and 3.38 wt% PVA). The lattice strain (ε) was developed in TiO_2 nanoparticles due to interaction with PVA. The reason behind development of lattice strain (ε) in tetragonal crystal structure of TiO_2 nanoparticles is contraction along a-axis, b-axis, and c-axis induced by PVA chains (described in chapter 6). The increased interaction of TiO_2 nanoparticles and PVA

with increased TiO_2 content, resulted in increased lattice strain (ε) which improved glass transition temperature Tg finally.

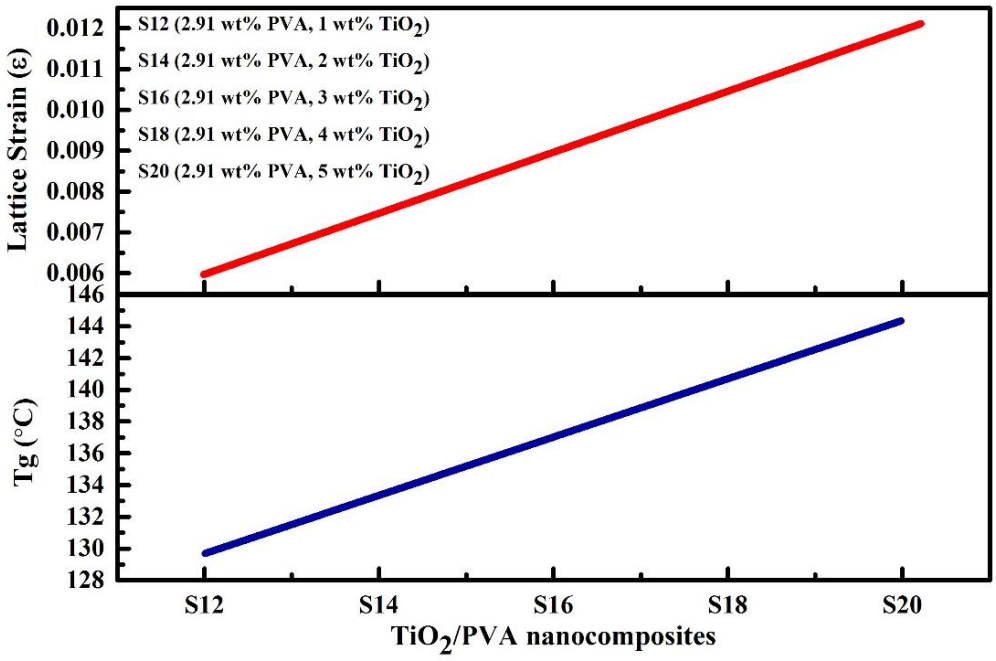

Figure 7.7: Effect of lattice strain on glass transition temperature of TiO_2/PVA nanocomposites with 2.91 wt% PVA

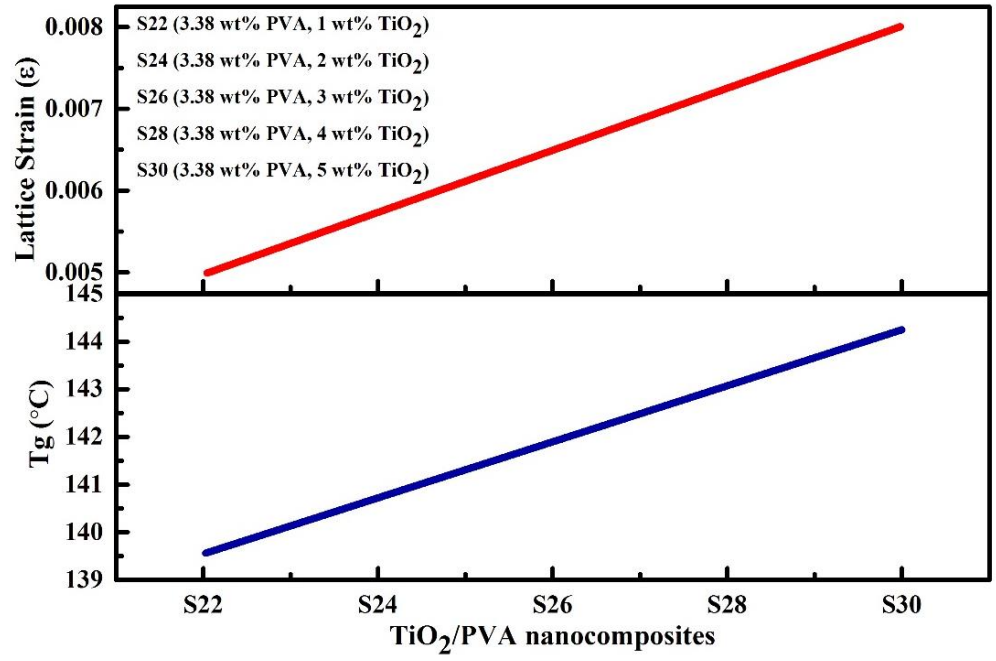

Figure 7.8: Effect of lattice strain on glass transition temperature of TiO_2/PVA nanocomposites with 3.38 wt% PVA

It is concluded from thermo-physical analysis of TiO_2/PVA nanocomposites that glass transition temperature of TiO_2/PVA nanocomposites is increasing with increasing TiO_2 content for both variations of PVA (P1 and P2). The value of glass transition temperature Tg was increased by 33.99°C from 110.39°C for S20 sample in compare to P1 and 38.93°C from 105.35°C for S30 sample in compare to P2. The increment in S30 is higher than in S20 due to presence of more hydroxyl groups in S30 which resulted in increased interaction between TiO_2 nanoparticles and PVA.

7.2 Thermal Degradation Behaviour of TiO_2/PVA Nanocomposites

The effect of TiO_2 nanoparticles on thermal degradation of TiO_2/PVA nanocomposites was understood by thermal gravimetric analysis (TGA) in terms of weight loss with respect to temperature. The TGA graphs reveals the evaporation of materials, decomposition of polymers, and the presence of fillers in TiO_2/PVA nanocomposites. Thus, TGA curves gives information about thermal stability of TiO_2/PVA nanocomposites as well as their composition. The temperature at which weight loss occurs is important to understand holding up of TiO_2/PVA nanocomposites under thermal conditions.

TiO_2/PVA nanocomposites designated as S1 to S5 and S11 to S20 were prepared by taking different weight percent of TiO_2 nanoparticles with 2.91 wt% of PVA (P1). Whereas, TiO_2/PVA nanocomposites designated as S6 to S10 and S21 to S30 were prepared by taking different weight percent of TiO_2 nanoparticles with 3.38 wt% of PVA (P2). TGA was performed for PVA (P1, P2), and TiO_2/PVA nanocomposites with 2.91 wt% PVA (S1, S5, S11, S12, S13, S14, S15, S16, S17, S18, S19, S20) and with 3.38 wt% PVA (S6, S10, S21, S22, S23, S24, S25, S26, S27, S28, S29, S30).

TGA curves of TiO_2/PVA nanocomposites in the temperature range 25-600°C are shown in Fig. 7.9 (P1, S1, S5, S6, and S10), Fig. 7.10 (P1, S11, S12, S13, S14, and S15), Fig. 7.11 (P1, S16, S17, S18, S19, and S20), Fig. 7.12 (P2, S21, S22, S23, S24, and S25), and Fig. 7.13 (P2, S26, S27, S28, S29, and S30).

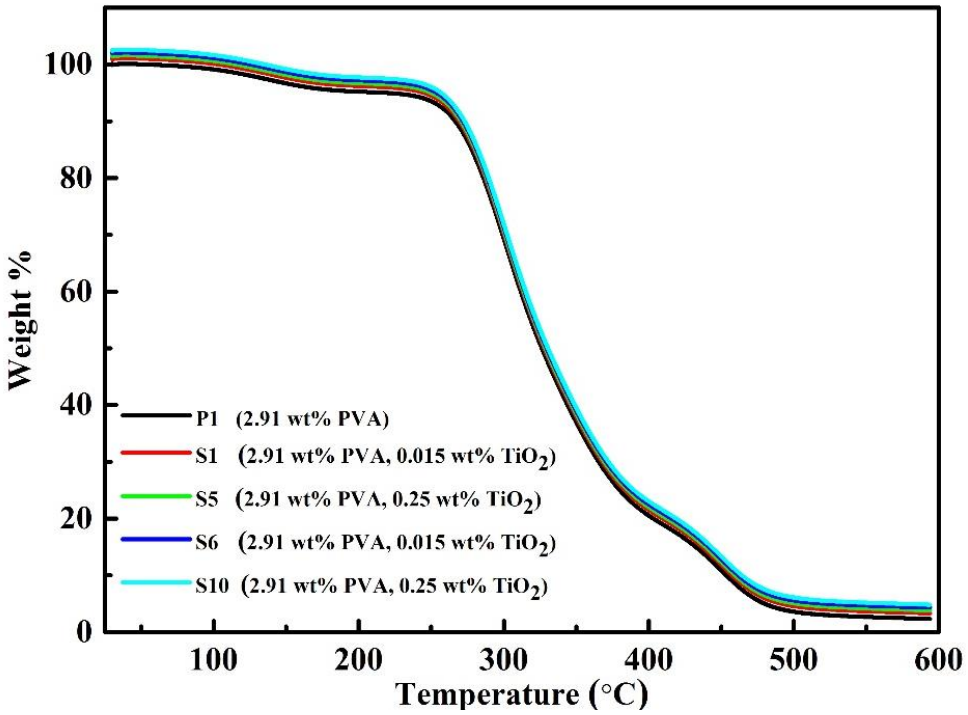

Figure 7.9: TGA curves of TiO_2/PVA nanocomposites with 2.91 wt% PVA (P1, S1, S5), and 3.38 wt% PVA (S6, S10)

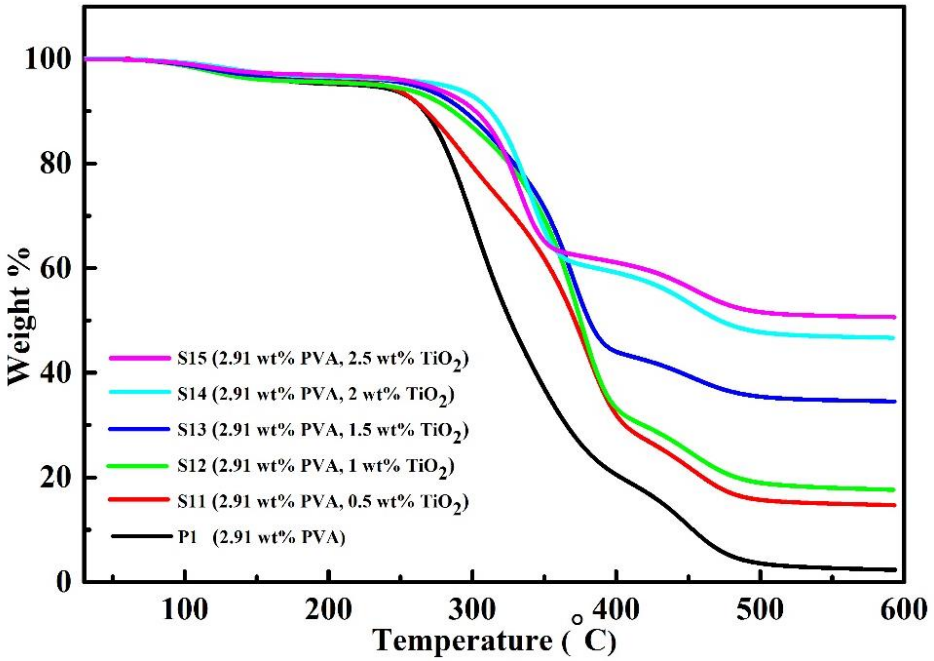

Figure 7.10: TGA curves of TiO_2/PVA nanocomposites (P1, S11, S12, S13, S14, and S15) with 2.91 wt% PVA

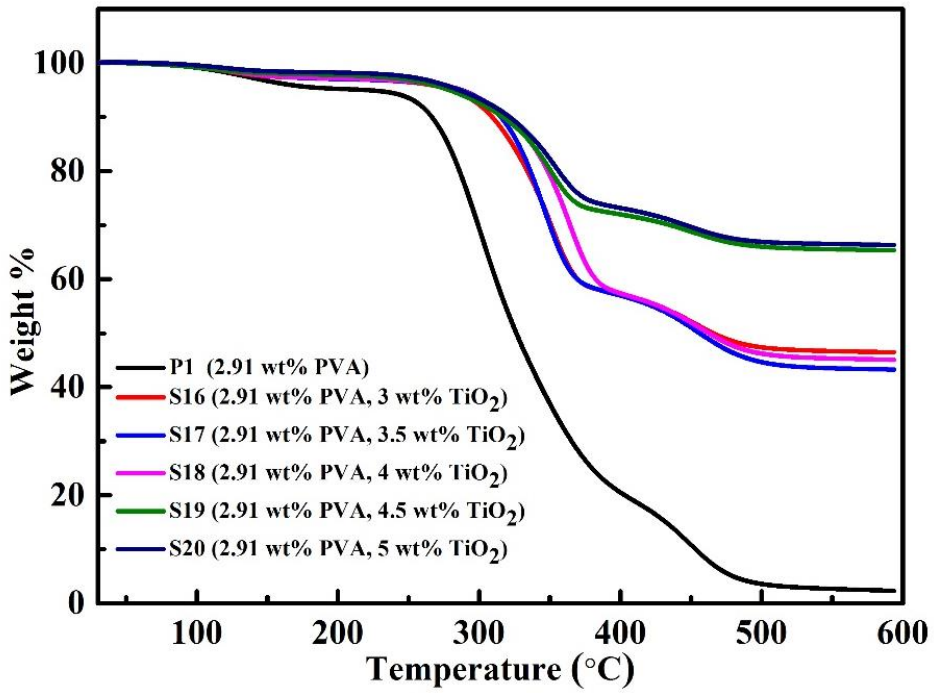

Figure 7.11: TGA curve of TiO_2/PVA nanocomposites (P1, S16, S17, S18, S19, and S20) with 2.91 wt% PVA

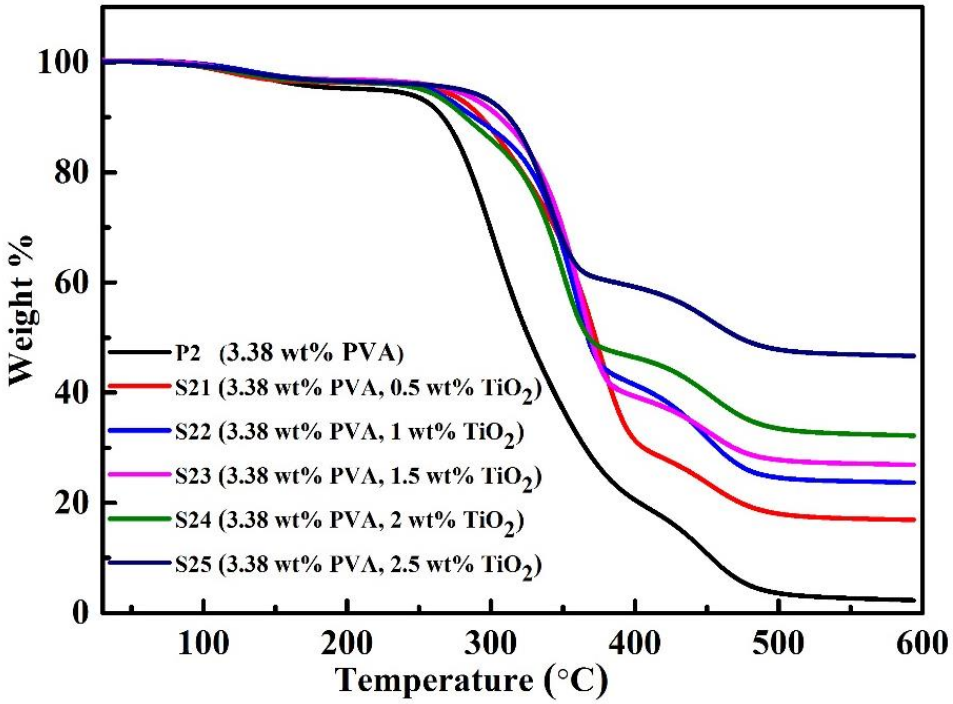

Figure 7.12: TGA curve of TiO_2/PVA nanocomposites (P2, S21, S22, S23, S24, and S25) with 3.38 wt% PVA

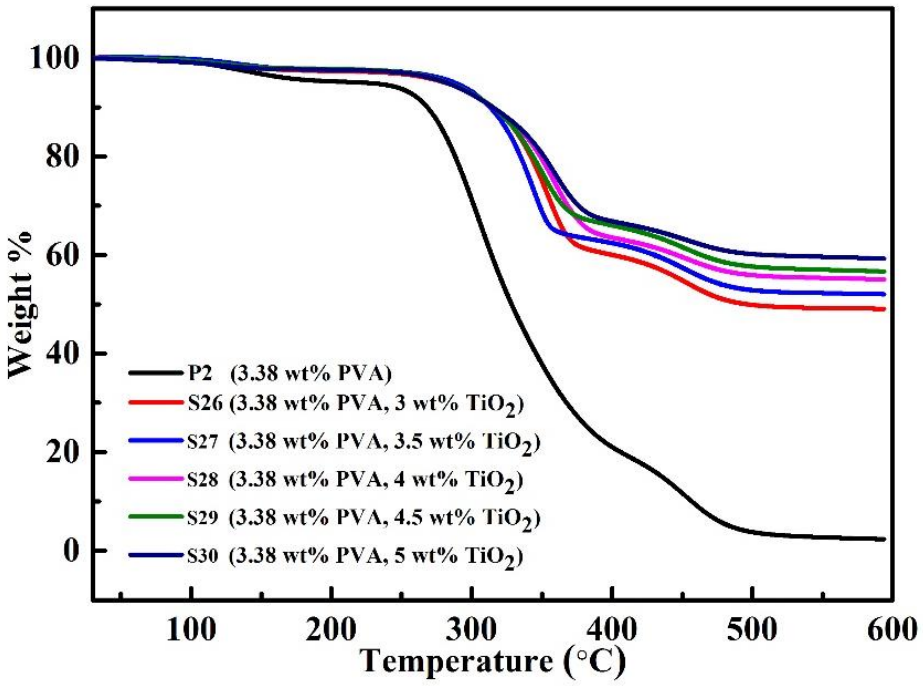

Figure 7.13: TGA curve of TiO_2/PVA nanocomposites (P2, S26, S27, S28, S29, and S30) with 3.38 wt% PVA

The obtained TGA curves (Fig. 7.9, Fig. 7.10, Fig. 7.11, Fig. 7.12, and Fig. 7.13) are showing weight loss in three stages for pure PVA and TiO_2/PVA nanocomposites as reported in literature [216-224]. In stage-I, weight loss take place between 100-150°C, which is due to evaporation of residual solvent, mainly water [216-225]. Stage-II weight loss around 200-380°C is due to elimination reactions of water [216] and stage-III weight loss region is at 380-500°C. It is linked with decomposition of polyene residues to yield carbon and hydrocarbons [216]. Hence, second and third stage are mainly involved in degradation of pure PVA and TiO_2/PVA nanocomposites. The observations of TiO_2//PVA nanocomposites regarding thermal degradation in second and third stage, and 50% weight loss temperature point are mentioned below.

For P1 (2.91 wt% PVA), and P2 (3.38 wt% PVA), degradation in second stage occurred at 71.91°C and 70.73°C, respectively. Whereas degradation in third stage occurred at 19.02°C and 20.19°C, respectively. Also, 50% weight loss occurred at 325.87°C and 328.94°C for P1 and P2 respectively.

The weight loss in second degradation stage for S1, S5, S6, S10, S11, S12, S13, S14, S15, S16, S17, S18, S19, S20, S21, S22, S23, S24, S25, S26, S27, S28, S29, and S30 samples of TiO_2/PVA nanocomposites occurred at 70.19%, 69.633%, 68.81%, 67.59%, 62.28%, 61.31%, 60.27%, 37.31%, 37.57%, 35.73%, 33.43%, 32.17%, 21.96%, 21.72%, 65.64%, 52.96%, 51.35%, 51.35%, 34.84%, 34.63%, 31.18%, 31.75%, 29.74%, and 27.99%, respectively.

The weight loss in third degradation stage for S1, S5, S6, S10, S11, S12, S13, S14, S15, S16, S17, S18, S19, S20, S21, S22, S23, S24, S25, S26, S27, S28, S29, and S30 samples of TiO_2/PVA nanocomposites occurred at 18.36%, 18.33%, 17.15%, 16.38%, 15.27%, 13.16%, 14.2%, 15.61%, 12.97%, 12.46%, 13.93%, 11.93%, 9.01%, 8.73%, 12.46%, 17.71%, 16.68%, 16.13%, 14.81%, 13.43%, 13.28%, 9.83%, 9.52%, and 8.67%, respectively.

The temperature at 50% weight loss for S1, S5, S6, S10, S11, S12, S13, S14, S15, S16, S17, S18, S21, S22, S23, S24, S25, and S26 samples of TiO_2/PVA nanocomposites was observed at 328.67°C, 328.67°C, 329.59°C, 331.39°C, 371.2°C, 374.73°C, 381.12°C, 470.44°C, 472.44°C, 473.96°C, 473.96°C, 473.96°C, 372.47°C, 367.41°C, 370.50°C, 367.41°C, 469.90°C, 482.10°C, respectively. Also, 50% weight loss did not occur for S19, S20, S27, S28, S29, and S30 samples of TiO_2/PVA nanocomposites even up to 600°C because interaction between TiO_2 nanoparticles and PVA improved thermal stability of TiO_2/PVA nanocomposites.

It can be inferred from above observations that thermal decomposition of TiO_2/PVA nanocomposites with P1 and P2 is decreasing with increased TiO_2 content due to interaction between TiO_2 and PVA. All three degradation stages are present in both PVA and TiO_2/PVA nanocomposites but degradation is shifted to higher temperature for TiO_2/PVA nanocomposites in compare to PVA.

The percentage weight loss in second and third stage, and temperature at 50% weight loss, for TiO_2/PVA nanocomposites are presented in Table 7.5, Table 7.6, and Table 7.7.

Table 7.5: Thermogravimetric analysis of TiO_2/PVA nanocomposites with 2.91 wt% PVA (P1, S1, S5) and 3.38 wt% PVA (P2, S6, S10)

Designation of sample	Decomposition Temperature Range (°C)	%Weight Loss	Temperature at which 50% weight loss occurred (°C)
P1	220.86-389.42	71.91	325.87
	389.42-496.22	19.02	
P2	220.41-385.66	70.73	328.94
	385.66-494.31	20.19	
S1	220.86-388.16	70.19	328.67
	388.16-489.61	18.36	
S5	220.86-387.26	69.63	328.67
	387.26-489.61	18.33	
S6	220.86-387.25	68.81	329.59
	387.25-489.61	17.15	
S10	220.86-387.25	67.59	331.39
	387.25-489.61	16.38	

Table 7.6: Thermogravimetric analysis of TiO_2/PVA nanocomposites (S11, S12, S13, S14, S15, S16, S17, S18, S19, and S20) with 2.91 wt% PVA

Designation of sample	Decomposition Temperature Range (°C)	%Weight Loss	Temperature at which 50% weight loss occurred (°C)
S11	248.18-400.55	62.28	371.2
	400.55-486.06	15.27	
S12	248.18-398.12	61.31	374.73
	398.12-493.53	13.16	
S13	248.54-398.60	60.27	381.12
	398.60-487.03	14.2	
S14	253.83-370.50	37.31	470.44
	370.50-493.31	15.61	
S15	253.83-383.69	37.57	472.44
	383.69-493.20	12.97	
S16	253.83-367.41	35.73	473.96
	367.41-487.15	12.46	
S17	251.23-359.94	33.43	473.96
	359.94-485.24	13.93	
S18	251.23-356.24	32.17	473.96
	356.24-492.63	11.93	
S19	253.83-365.43	21.96	50% weight loss didn't occur upto 600°C
	365.43-486.17	9.01	
S20	253.83-371.48	21.72	50% weight loss didn't occur upto 600°C
	371.48-491.23	8.73	

Table 7.7: Thermogravimetric analysis of TiO_2/PVA nanocomposites (S21, S22, S23, S24, S25, S26, S27, S28, S29, S30) with 3.38 wt% PVA

Designation of sample	Decomposition Temperature Range (°C)	%Weight Loss	Temperature at which 50% weight loss occurred (°C)
S21	243.72-402.93	65.64	372.47
	402.93-487.16	12.46	
S22	243.72-384.68	52.96	367.41
	384.68-484.08	17.71	
S23	243.72-376.54	51.35	370.50
	376.54-483.9	16.68	
S24	243.72-367.41	51.35	367.41
	367.41-496.29	16.13	
S25	243.72-357.30	34.84	469.90
	357.30-483.09	14.81	
S26	251.86-371.48	34.63	482.10
	371.48-490.24	13.43	
S27	251.86-356.31	31.18	50% weight loss didn't occur upto 600°C
	356.31-492.22	13.28	
S28	251.86-383.69	31.75	50% weight loss didn't occur upto 600°C
	383.69-497.27	9.83	
S29	251.86-374.57	29.74	50% weight loss didn't occur upto 600°C
	374.57-500.35	9.52	
S30	251.86-381.72	27.99	50% weight loss didn't occur upto 600°C
	381.72-490.22	8.67	

The mechanism of thermal degradation of PVA and TiO_2/PVA nanocomposites during second stage involves OH group elimination reactions and chain-scission reactions (see Scheme 7.1). OH group elimination reactions in PVA chains results in polyene generation. Haigang Yang et al. confirmed that conjugated structures and carbonyl groups are formed in this degradation step [225]. They also reported that the content of conjugated structure formation depends upon hydroxyl contents in PVA. More hydroxyl groups in PVA increased interaction with TiO_2 nanoparticles.

After second stage degradation process, PVA chain contains conjugated structure which is more stable. Thus, degradation in third stage occurred at slower

rate than in second stage and it involves chain-scission and Diels-Alder intramolecular and intermolecular cyclization [216, 222]. In this stage, polyene residues will yield carbon and hydrocarbons [223].

The degradation mechanism of PVA explained here is in coherence with the mechanism reported by other researchers [216, 220-222].

Thermal degradation mechanism of PVA was not affected by the presence of TiO_2 nanoparticles but overall thermal stability of PVA was improved (see Fig. 7.7, Fig. 7.8, Fig. 7.9, Fig. 7.10, and Fig. 7.11). The increase in thermal stability of PVA matrix by presence of TiO_2 nanoparticles was noted as increased temperatures of following degradation process: formation of polyenes ($\Delta T \approx 32.97^{\circ}C$ for S20 in compare to P1, and $\Delta T \approx 31.45^{\circ}C$ for S30 in compare to P2). Improved thermal stability of TiO_2/PVA nanocomposites can be explained by the reduced mobility of polymer chain within TiO_2/PVA nanocomposite. Due to reduced mobility of chain, collision frequency will be reduced and there will be suppression in chain transfer reaction. This kind of physical restriction affects the OH group elimination reactions and chain-scission reactions which occurs in second degradation stage. Subsequently, the degradation process will slow down and decomposition of nanocomposite will take place at higher temperature [219].

$$-CH_2-CH(OH)-CH_2-CH(OH)-CH_2-CH(OH)-CH_2- \xrightarrow{-H_2O} -CH_2-CH=CH-CH=CH-CH=CH-$$

(a)

$$-CH_2-CH(OH)-CH_2-CH(OH)-CH_2-CH(OH)-CH_2- \rightarrow -CH_2-CH(OH)-CH_2-C(O) + -CH_2-C(O)-CH_2-$$

(b)

Scheme 7.1: Degradation reactions of PVA under thermal treatment

Another theory for explaination of thermal degradation of TiO_2/PVA nanocomposites is barrier model which suggests that polymer-inorganic scorch is formed on the surface of melted polymer, resulting in reduction of mass and heat transfer [216, 226]. Jamil Ahmad et al. has suggested formation of strong interfacial bonds, like Ti-O-C between TiO_2 nanoparticles and PVA. It is formed by dehydration and condensation reactions. Resultant core shell microstructure is responsible for uniform dispersion of TiO_2 nanoparticles into PVA which is desired

for better thermal and mechanical properties. Also, OH group elimination and chain-scission reactions in PVA are decreased due to interaction between TiO_2 nanoparticles and PVA. These interactions increased energy barrier related with OH group elimination reactions. Thus, overall degradation of PVA is reduced.

The effect of TiO_2 content on thermal degradation in TiO_2/PVA nanocomposites are compared in Fig. 7.12, Fig. 7.13, and Fig. 7.14 in terms of percent weight loss in second and third degradation stage. It is clear from these graphs that increase in content of TiO_2 nanoparticles have reducing effect on percentage weight loss in second degradation stage of nanocomposite. An agreeable explanation for this is, OH groups which are responsible for water elimination reactions of PVA in second degradation stage; are not free now due to interaction with TiO_2 nanoparticles.

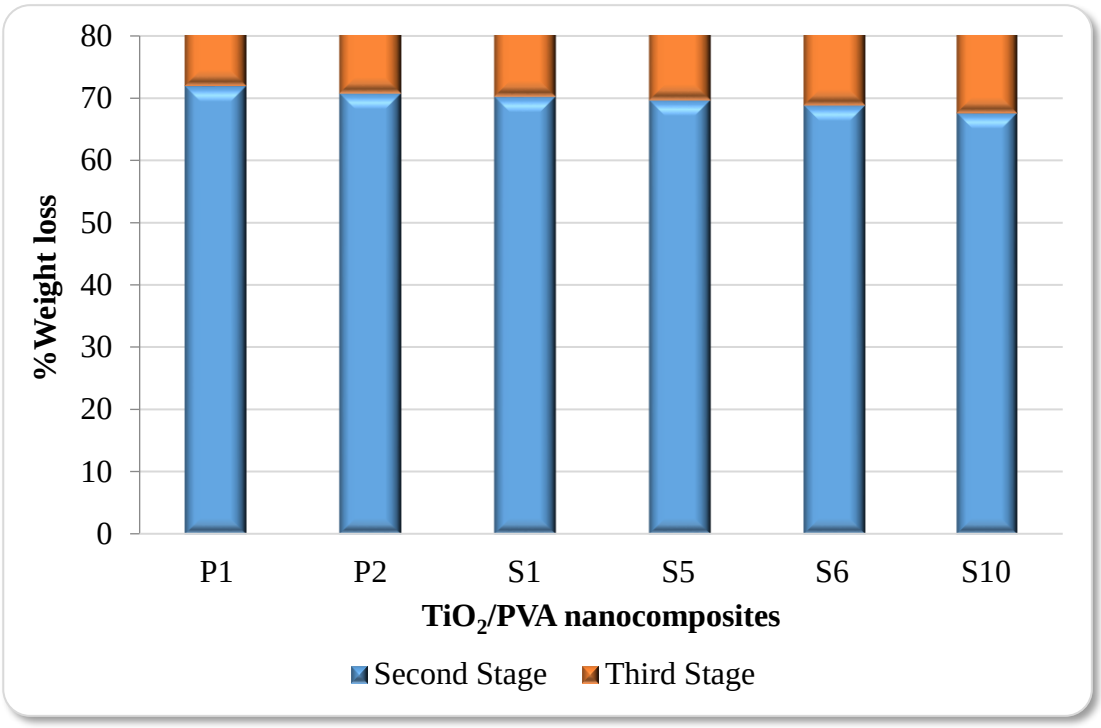

Figure 7.14: The effect of TiO_2 content on thermal degradation in TiO_2/PVA nanocomposites with 2.91 wt% PVA (P1, S1, S5) and 3.38 wt% PVA (P2, S6, S10)

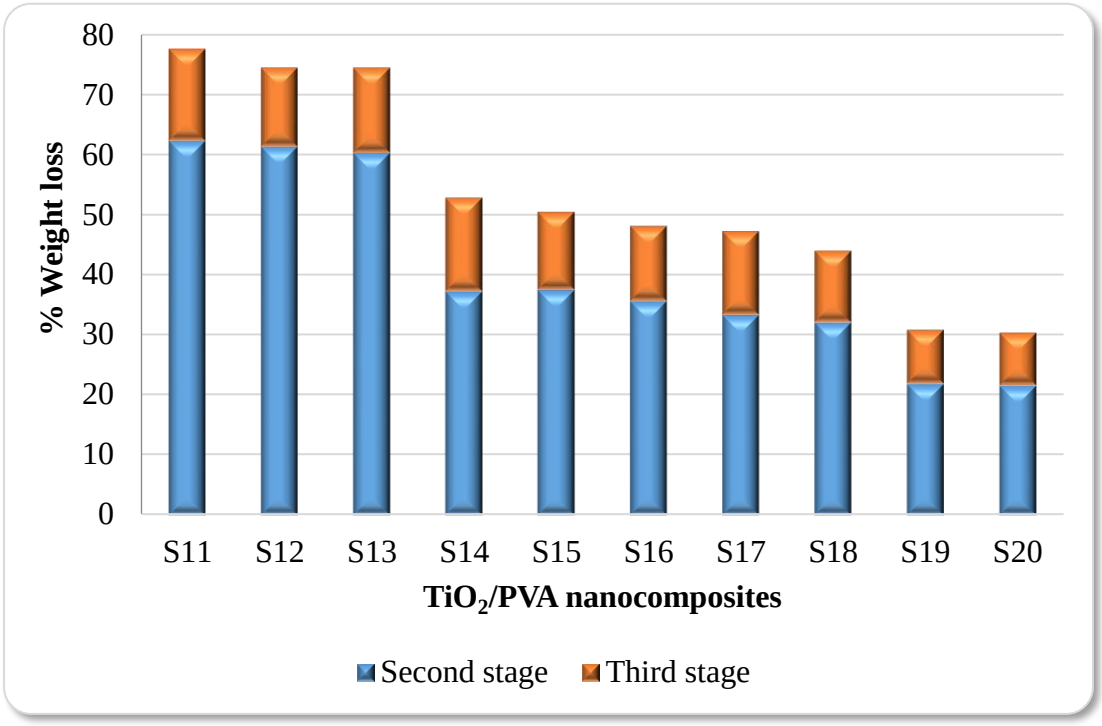

Figure 7.15: The effect of TiO_2 content on thermal degradation in TiO_2/PVA nanocomposites with 2.91 wt% PVA

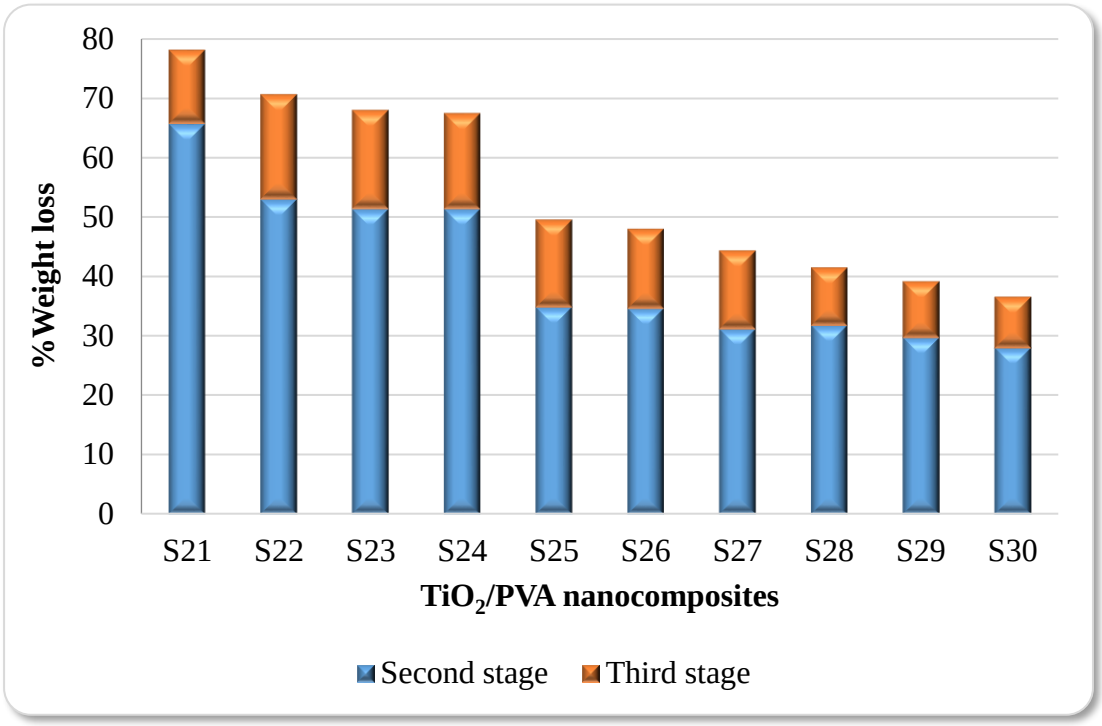

Figure 7.16: The effect of TiO_2 content on thermal degradation in TiO_2/PVA nanocomposites with 3.38 wt% PVA

It is inferred from TGA results that incorporation of TiO_2 nanoparticles within PVA matrix reduced thermal degradation of PVA for both variations of PVA (P1 and P2) within TiO_2/PVA nanocomposites. It is revealed that thermal degradation of TiO_2/PVA nanocomposites in second degradation stage was reduced with doping of TiO_2 nanoparticles. There is 50% less weight loss for S20 in compare to P1 and 42.74% less weight loss for S30 in compare to P2 in second degradation stage. Also, 50% weight loss did not occur for S19, S20, S27, S28, S29, and S30 samples even upto 600°C. Thus, it is concluded that overall thermal stability of TiO_2/PVA nanocomposites was improved which is important for applications in anti-reflection coatings in solar cells, humidity sensing, gas sensing, and water purification.

The discussions made in this chapter are summarized as follows: The results of thermal analysis curves for TiO_2/PVA nanocomposites with P1 and P2 are showing noticeable increase in glass transition temperature Tg with increased TiO_2 content. Also, the thermal degradation of TiO_2/PVA nanocomposites is reduced with increased TiO_2 content as realized by TGA results. The thermal stability of S20 (5 wt% TiO_2 with 2.91 wt% PVA) was maximum. The overall thermal stability of TiO_2/PVA nanocomposites was improved due to formation of Ti-O-O bond as seen by FTIR. This bond formation resulted in development of lattice strain in tetragonal lattice of TiO_2 nanoparticles as revealed by XRD. Improved thermal stability of TiO_2/PVA nanocomposites is important for applications in anti-reflection coatings in solar cells, gas sensing in industries, and humidity sensing because synthesis techniques of TiO_2/PVA nanocomposites for these applications requires thermally stable nanocomposite. The viscoelastic behaviour of prepared TiO_2/PVA nanocomposites is discussed in next chapter.

Chapter 8
RESULTS AND DISCUSSIONS-III
(Viscoelastic behaviour of TiO_2/PVA nanocomposites)

Viscoelasticity is the property of materials which shows both viscous and elastic characteristics when material is subjected to deformation. In, viscoelastic materials, elements with both viscous and elastic characteristics are present. The viscous behaviour of TiO_2/PVA nanocomposites is due to presence of amorphous region in PVA whereas elastic behaviour is due to presence of TiO_2 nanoparticles and crystalline region of PVA. The viscous behaviour results from movement of side chain and small groups within amorphous domain of PVA whereas the elastic behaviour results from bond stretching along crystallographic planes of TiO_2 nanoparticles and crystalline region of PVA. The crystallinity in TiO_2 nanoparticles is due to tetragonal crystal structure however, crystallinity in PVA is due to intermolecular and intramolecular hydrogen bonding.

It is important to study viscoelastic behaviour of TiO_2/PVA nanocomposites because mechanical performance of anti-reflection coatings, gas sensors, and humidity sensors made by using TiO_2/PVA nanocomposites depends on it. Also, success of fabrication processes for above applications at intermediate stage of fabrication depends on viscoelastic behaviour. The study of viscoelastic properties depends on variables like temperature and pressure with respect to time. Viscoelastic properties of polymers depend upon chemical composition, molecular weight and weight distribution, branching and crystallinity of polymer. It also depends upon addition of fillers in nanocomposite systems [227]. In this research work, TiO_2 nanoparticles are added in PVA matrix and effect of TiO_2 nanoparticles on viscoelastic properties of PVA is discussed in this chapter.

TiO_2/PVA nanocomposites designated (described in chapter 5) as S1 to S5 and S11 to S20 were prepared by taking different weight percent of TiO_2 nanoparticles with 2.91 wt% of PVA (P1) as shown in previous studies. Whereas, TiO_2/PVA nanocomposites designated as S6 to S10 and S21 to S30 were prepared by taking different weight percent of TiO_2 nanoparticles with 3.38 wt% of PVA (P2) as shown in previous studies. Viscoelastic behaviour of prepared TiO_2/PVA nanocomposites were studied by performing dynamic mechanical analysis (DMA) in tensile mode for all nanocomposites and tanδ versus temperature curves were obtained.

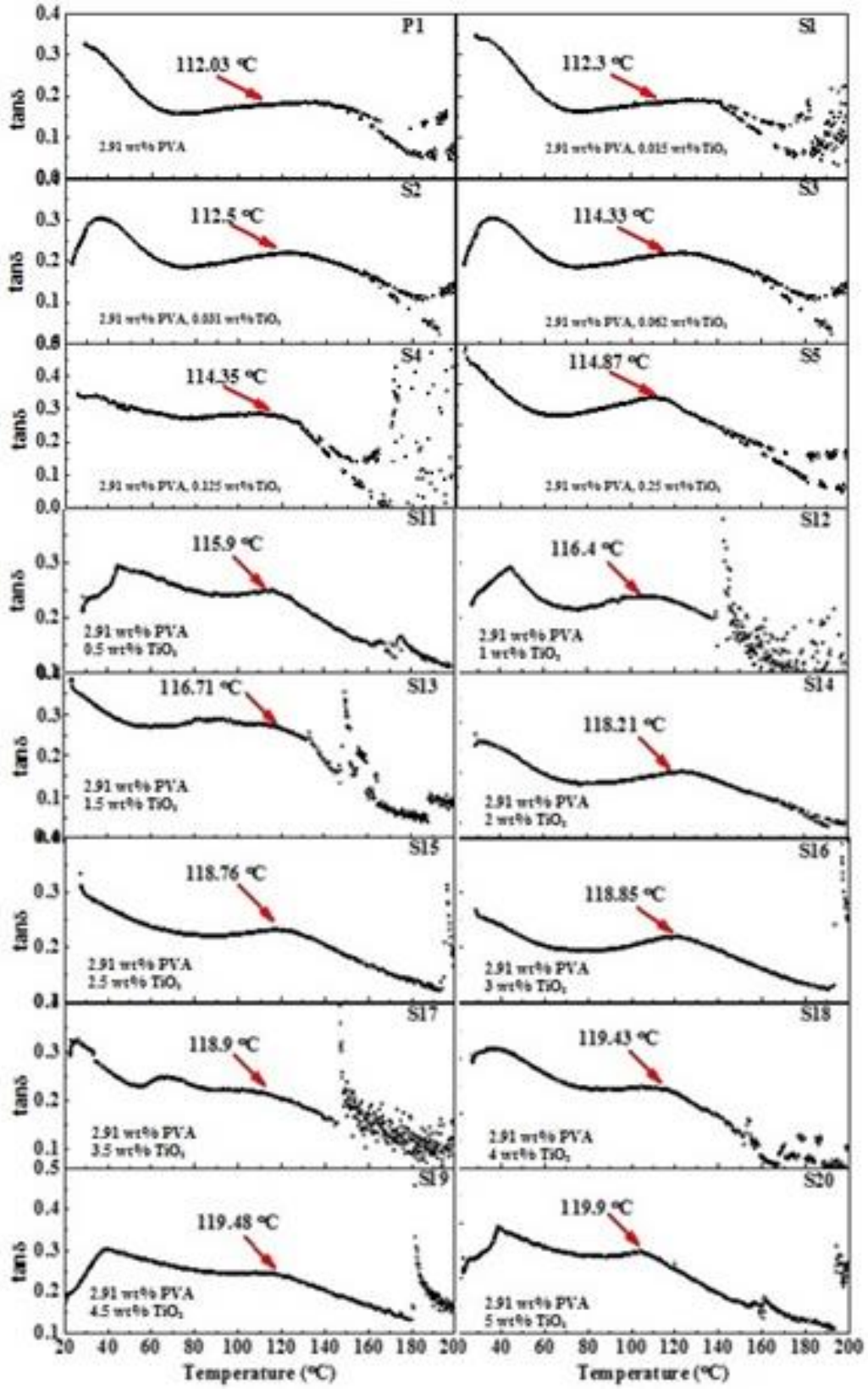

Figure 8.1: DMA curves of TiO_2/PVA nanocomposites (P1, S1, S2, S3, S4, S5, S11, S12, S13, S14, S15, S16, S17, S18, S19, and S20) with 2.91 wt% PVA

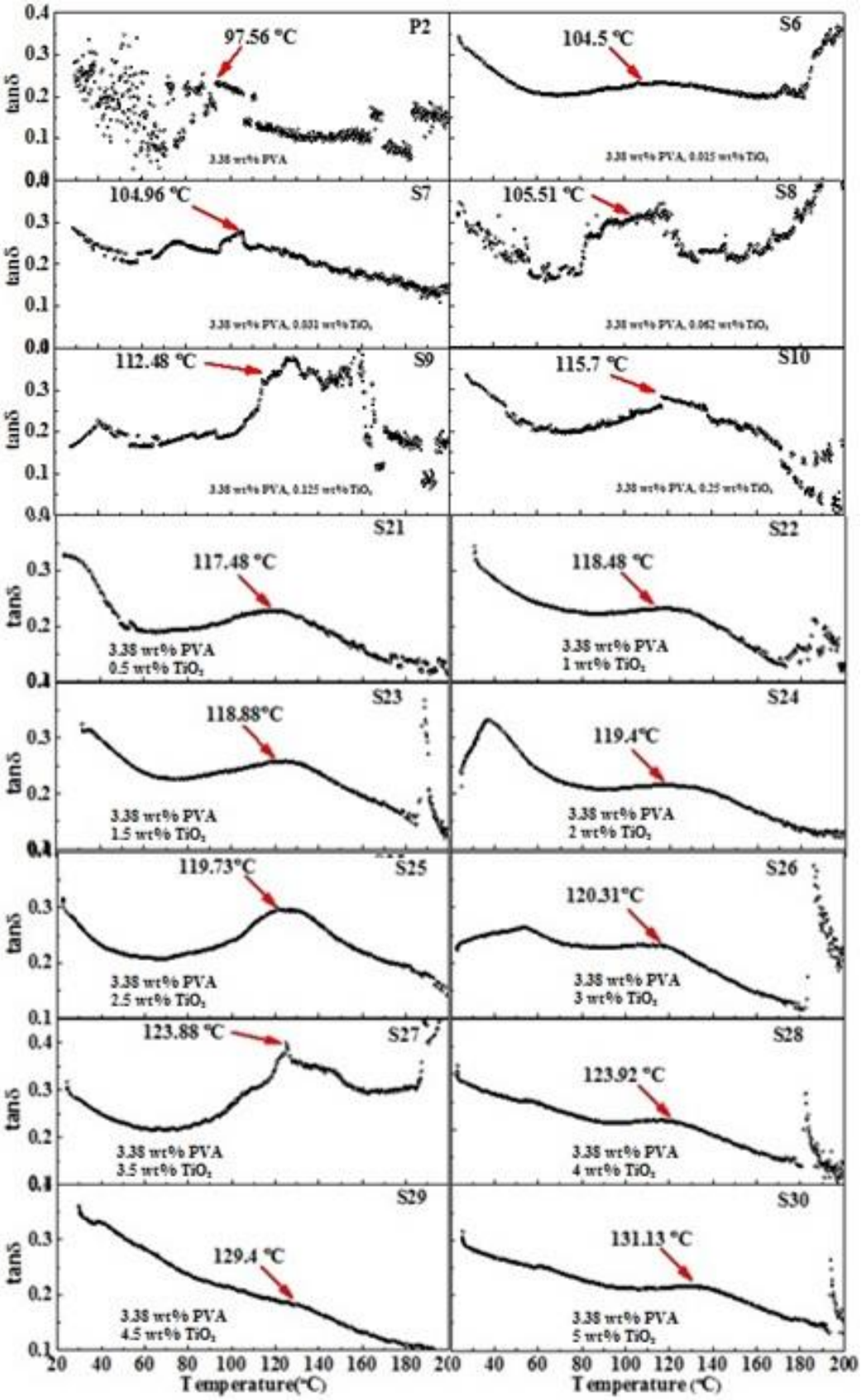

Figure 8.2: DMA curves of TiO_2/PVA nanocomposites (P2, S6, S7, S8, S9, S10, S21, S22, S23, S24, S25, S26, S27, S28, S29, and S30) with 3.38 wt% PVA

In tensile mode, a continuous tensile stress is applied during dynamic thermal cycling. These DMA thermograms were recorded by applying oscillating stress and resultant strain was measured as functions of both oscillatory frequency and temperature. The frequency and heating rate were kept as 1 Hz, and 3°C per minute, respectively.

Dynamic mechanical analysis (DMA) curves for TiO_2/PVA nanocomposites with 2.91 wt% and 3.38 wt% of PVA, over temperature range 20-200°C in tensile mode are shown in Figure 8.1 ((P1, S1, S2, S3, S4, S5, S11, S12, S13, S14, S15, S16, S17, S18, S19, and S20) and Figure 8.2 (P2, S6, S7, S8, S9, S10, S21, S22, S23, S24, S25, S26, S27, S28, S29, and S30), respectively. Transitions in TiO_2/PVA nanocomposites are shown as changes in tanδ versus temperature curve.

The observations for TiO_2/PVA nanocomposites regarding DMA are mentioned below.

For pure PVA (P1 and P2), broad peaks were observed at 112.03°C and 97.56°C respectively, which represents glass transition temperature and peaks at higher temperature are due to relaxation in PVA crystalline domains [228].

The glass transition temperatures Tg for S1, S2, S3, S4, S5, S6, S7, S8, S9, S10, S11, S12, S13, S14, S15, S16, S17, S18, S19, S20, S21, S22, S23, S24, S25, S26, S27, S28, S29, and S30 samples of TiO_2/PVA nanocomposites were observed at 112.3°C, 112.5°C, 114.33°C, 114.35°C, 114.87°C, 104.5°C, 104.96°C, 105.51°C, 112.48°C, 115.7°C, 115.9°C, 116.4°C, 116.71°C, 118.21°C, 118.76°C, 118.85°C, 118.9°C, 119.43°C, 119.48°C, 119.9°C, 117.48°C, 118.48°C, 118.88°C, 119.4°C, 119.73°C, 120.31°C, 123.88°C, 123.92°C, 129.4°C, and 131.13°C, respectively. For all TiO_2/PVA nanocomposites, glass transition temperature was observed as broad peak in temperature range 110°C-132°C, and the peak is shifting from 110°C to 132°C with increasing concentrations of TiO_2 nanoparticles. The value of glass transition temperature observed from DMA vary a bit than glass transition temperature observed from thermo-physical analysis by DSC due to the different measurement processes of DMA and DSC [229]. The value of tanδ is increasing with increasing weight percent of TiO_2 nanoparticles for S1, S2, S3, S4, S5, S6, S7, S8, S9, S10,

S11, S12, S13, S14, S15, S16, S17, S21, S22, S23, S24, S25, S26, S27 samples but it decreases for S18, S19, S20, S29 and S30 samples. It indicates that for dopings of TiO_2 nanoparticles higher than 3.5 wt%, PVA matrix is confined by TiO_2 nanoparticles because of improved interfacial reinforcement of TiO_2 nanoparticles into PVA matrix. Also, decreased tanδ indicated that TiO_2/PVA nanocomposites became more elastic, and they had more potential to store energy rather than dissipating it when subjected to deformation by applying load.

The observations of DMA curves (Fig. 8.1 and Fig. 8.2) are summarized in Table 8.1 and Table 8.2.

Table 8.1: Dynamic mechanical analysis (DMA) data for TiO_2/PVA nanocomposites (P1, S1, S2, S3, S4, S5, S11, S12, S13, S14, S15, S16, S17, S18, S19, and S20) with 2.91 wt% PVA

Designation of sample	**Glass Transition Temperature Tg (°C)**
P1	112.03
S1	112.30
S2	112.50
S3	114.33
S4	114.35
S5	114.87
S11	115.90
S12	116.40
S13	116.71
S14	118.21
S15	118.76
S16	118.85
S17	118.90
S18	119.43
S19	119.48
S20	119.90

The explanation of observed DMA results for TiO_2/PVA nanocomposites is given below. The value of tanδ peak (damping) obtained for TiO_2/PVA nanocomposites by DMA, indicated dissipation of energy due to internal friction and molecular motions within PVA [230]. The damping peak occurred in the glass transition region Tg where TiO_2/PVA nanocomposites changes from rigid to more elastic state and it is associated with the movement of small groups and chains of molecule within the structure of PVA, all of which were initially stationary [230]. In TiO_2/PVA nanocomposites, damping is affected through the incorporation of TiO_2 nanoparticles. The reason behind this is shear stress concentrations at the filler surface in association with additional viscoelastic energy dissipation in the PVA matrix [230].

Table 8.2: Dynamic mechanical analysis (DMA) data for TiO_2/PVA nanocomposites (P2, S6, S7, S8, S9, S10, S21, S22, S23, S24, S25, S26, S27, S28, S29, and S30) with 3.38 wt% PVA

Designation of sample	**Glass Transition Temperature (°C)**
P2	97.56
S6	104.50
S7	104.96
S8	105.51
S9	112.48
S10	115.70
S21	117.48
S22	118.48
S23	118.88
S24	119.40
S25	119.73
S26	120.31
S27	123.88
S28	123.92
S29	129.40
S30	131.13

The increased TiO_2 content in TiO_2/PVA nanocomposites resulted in increment in damping for S1 to S17 and S21 to S28 samples of TiO_2/PVA nanocomposites whereas decrement in damping for S18, S19, S20, S29 and S30 samples of TiO_2/PVA nanocomposites. The lowering of tanδ peak in S18 (4 wt% TiO_2 with 2.91 wt% PVA), S19 (4.5 wt% TiO_2 with 2.91 wt% PVA), S20 (5 wt% TiO_2 with 2.91 wt% PVA), S29 (4.5 wt% TiO_2 with 3.38 wt% PVA) and S30 (5 wt% TiO_2 with 2.91 wt% PVA) samples of TiO_2/PVA nanocomposites is result of increased TiO_2 content. It is attributed to confinement of PVA matrix by TiO_2 nanoparticles with increased TiO_2 content which indicated improvement in interfacial reinforcement in TiO_2/PVA nanocomposites [114, 231].

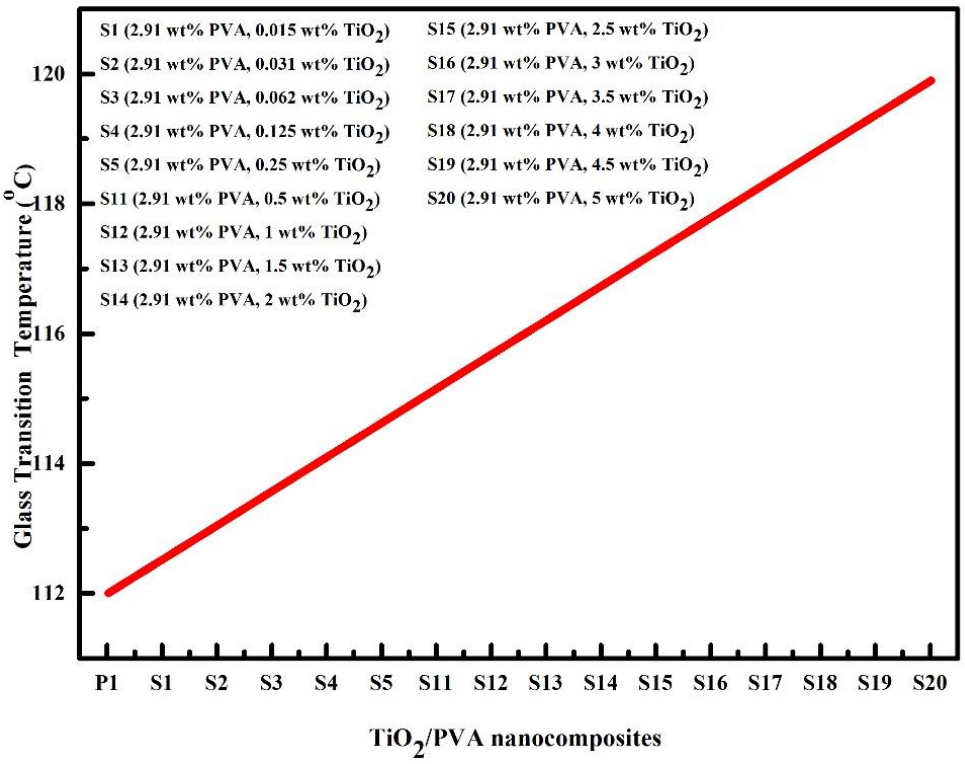

Figure 8.3: Effect of TiO_2 nanoparticles on glass transition temperature of TiO_2/PVA nanocomposites with 2.91 wt% PVA

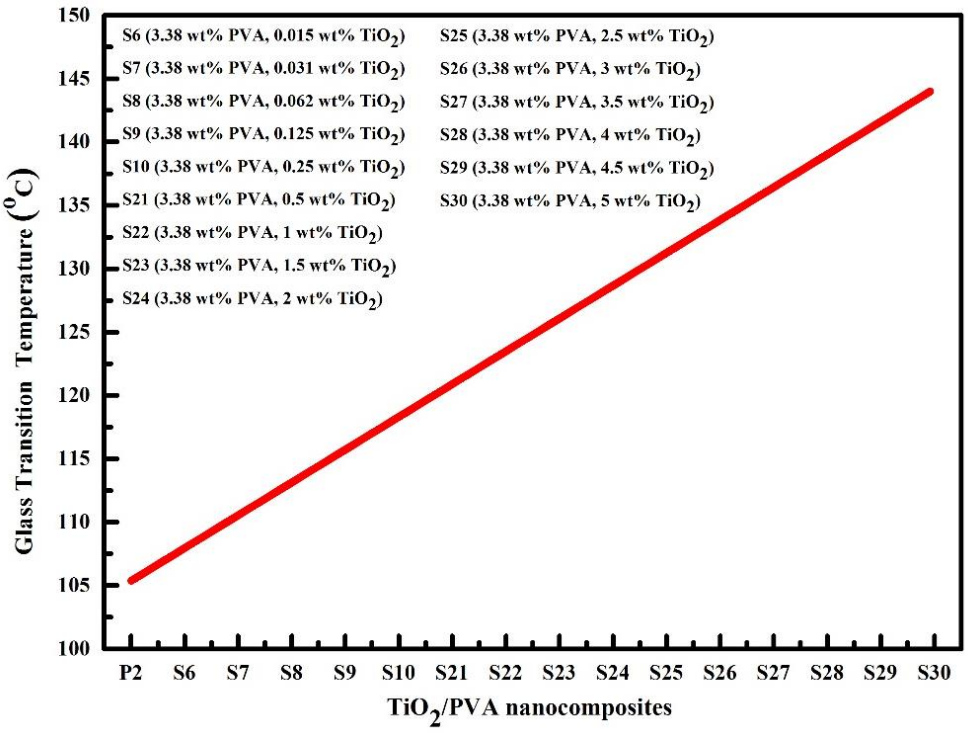

Figure 8.4: Effect of TiO_2 nanoparticles on glass transition temperature of TiO_2/PVA nanocomposites with 3.38 wt% PVA

The effect of TiO_2 nanoparticles on glass transition temperature of TiO_2/PVA nanocomposites with 2.91 wt% PVA and 3.38 wt% PVA are shown in Fig. 8.3 and Fig. 8.4, respectively. The increment in glass transition temperature Tg with increasing weight percent of TiO_2 is seen from these graphs for TiO_2/PVA nanocomposites with both variations of PVA (P1 and P2). It is due to increased interaction between TiO_2 nanoparticles and PVA with increasing TiO_2 content. The value of glass transition temperature Tg was increased by 7.87°C from 112.03°C for S20 sample in compare to P1 and 33.57°C from 97.56°C for S30 sample in compare to P2. The maximum value of glass transition temperature Tg was obtained as 131.13°C for S30 sample. The values of glass transition temperature Tg are much higher for TiO_2/PVA nanocomposites with P2 than P1 which is due to availability of more hydroxyl groups in P2 than P1 to interact with TiO_2 nanoparticles.

In summary, DMA results showed increased glass transition temperature of TiO_2/PVA nanocomposites with increasing weight percent of TiO_2. Also, elastic behaviour was dominating over viscous behaviour for TiO_2/PVA nanocomposites

with increasing weight percent of TiO_2 nanoparticles. The value of glass transition temperature Tg was improved by 7.87°C for S20 in compare to P1 and by 33.57°C for S30 in compare to P2. Damping was decreased for S18, S19, S20, S29, and S30 samples due to restriction in movement of PVA chains with increased concentration of TiO_2 nanoparticles. Thus, prepared TiO_2/PVA nanocomposites had increased capacity to absorb energy rather than dissipating it when load is applied. Improved mechanical strength of TiO_2/PVA nanocomposites is important for applications like anti-reflection coatings in solar cells, gas sensing in industries, and humidity sensing because fabrication techniques for these applications requires TiO_2/PVA nanocomposites with good mechanical performance.

Chapter 9

CONCLUSIONS & SUGGESTIONS FOR FUTURE WORK

This chapter concludes the research work of this thesis in first part and suggestions for future work are given in second part.

9.1 Conclusions

The significant conclusions of this research work are as follows:

(i) TiO_2 nanoparticles were synthesized by sol-gel method.

(ii) Formation of TiO_2 nanoparticles was confirmed by EDAX and FTIR. Blue shift of 0.3 eV in band gap of TiO_2 powder was observed due to quantum confinement effect. Anatase phase of TiO_2 was confirmed by XRD and SEM analysis confirmed the size of TiO_2 powder in nanometer range.

(iii) Pure PVA and TiO_2/PVA nanocomposites were developed by solvent casting method.

(iv) As mentioned in results and discussions section (chapter 6, 7, and 8) spectroscopic analysis, phase analysis, morphological study, thermal analysis and mechanical analysis for TiO_2/PVA nanocomposites were performed.

(v) TiO_2/PVA nanocomposites (S1 to S30) were showing $\pi \rightarrow \pi^*$ electronic transition in UV-Vis spectra whereas $n \rightarrow \pi^*$ electronic transition was seen for pure PVA (P1 and P2).

TiO_2/PVA nanocomposites showed absorption only for UV region and they were completely transparent for visible region.

The blue shift in absorbance spectra of TiO_2/PVA nanocomposites with increasing concentration of TiO_2 nanoparticles was observed for both variations of PVA, P1 (2.91 wt% PVA) and P2 (3.38 wt% PVA) which indicated reduction in aggregation of TiO_2 nanoparticles.

(vi) The broadening of transmittance peaks for O-H vibrations and C-H vibrations, and C=O stretching in TiO_2/PVA nanocomposites was observed in compared to PVA and formation of Ti-O-O bond between TiO_2 nanoparticles and PVA was seen by FTIR spectroscopy.

(vii) The phase analysis data by XRD confirmed that TiO_2 nanoparticles and PVA were in anatase, and orthorhombic phases, respectively. Latttice parameters, dislocation density and crystallite size were determined for TiO_2 nanoparticles within TiO_2/PVA nanocomposites.

The lattice strain (ε) and dislocation density were increasing with increasing weight percent of TiO_2. For S20 sample (5 wt% TiO_2 with 2.91 wt% PVA), lattice strain (ε) was increased by 0.006 in compare to S12 sample (1 wt% TiO_2 with 2.91 wt% PVA) and for S30 sample (5 wt% TiO_2 with 3.38 wt% PVA), it was increased by 0.003 in compare to S22 sample (1 wt% TiO_2 with 3.38 wt% PVA).

Also, dislocation density for S20 sample (5 wt% TiO_2 with 2.91 wt% PVA), was increased by 2.8×10^{15} m^{-2} in compare to S12 sample (1 wt% TiO_2 with 2.91 wt% PVA) and for S30 sample (5 wt% TiO_2 with 3.38 wt% PVA), it was increased by 1.1×10^{15} m^{-2} in compare to S22 sample (1 wt% TiO_2 with 3.38 wt% PVA).

Whereas, decrement in crystallite size was observed with increasing TiO_2 content. The value of crystallite size for S20 sample (5 wt% TiO_2 with 2.91 wt% PVA), was increased by 11.57 nm in compare to S12 sample (1 wt% TiO_2 with 2.91 wt% PVA) and that for S30 sample (5 wt% TiO_2 with 3.38 wt% PVA), was increased by 9.27 nm in compare to S22 sample (1 wt% TiO_2 with 3.38 wt% PVA).

(viii) Presence of Ti, O, and C atoms and homogenous dispersion of TiO_2 nanoparticles within TiO_2/PVA nanocomposites was observed by SEM micrographs with EDAX analysis and mapping analysis.

(ix) DSC results showed increase in glass transition temperature Tg for all TiO_2/PVA nanocomposites in compare with pure PVA.

The value of glass transition temperature Tg was improved by 33.99°C for S20 (5 wt% TiO_2 with 2.91 wt% PVA) in compare to P1 (2.91 wt% PVA) and by 38.93°C for S30 (5 wt% TiO_2 with 3.38 wt% PVA) in compare to P2 (3.38 wt% PVA) according to DSC results.

(x) Maximum thermal degradation of TiO_2/PVA nanocomposites occured in second degradation stage and it was reduced with increased doping of TiO_2 nanoparticles as seen by TGA results.

The weight loss for S20 (5 wt% TiO_2 with 2.91 wt% PVA) was 50% less in compare to P1 (2.91 wt% PVA) and for S30 (5 wt% TiO_2 with 3.38 wt% PVA), it was 42.74% less in compare to P2 (3.38 wt% PVA) in second degradation stage. Also, 50% weight loss did not occur for S19, S20, S27, S28, S29, and S30 samples even upto 600°C.

(xi) Increase in glass transition temperature Tg of TiO_2/PVA nanocomposites was observed with increasing weight percent of TiO_2 nanoparticles by DMA. Also, shifting from viscous to more elastic behaviour was seen with increasing content of TiO_2 nanoparticles.

a. The value of glass transition temperature Tg was improved by 7.87°C for S20 (5 wt% TiO_2 with 2.91 wt% PVA) in compare to P1 (2.91 wt% PVA) and by 33.57°C for S30 (5 wt% TiO_2 with 3.38 wt% PVA) in compare to P2 (3.38 wt% PVA) according to DMA results. The differences in glass transition temperature Tg obtained from results of DSC and DMA are due to their different operating principles.

b. The reduction in damping was seen for S18, S19, S20, S29, and S30 samples due to restriction in movement of PVA chains with increased TiO_2. Thus, prepared TiO_2/PVA nanocomposites are more resistant to applied load.

(xii) From above conclusions, best thermal and mechanical properties were observed for S30 sample (5 wt% TiO_2 with 3.38 wt% PVA) of TiO_2/PVA nanocomposites.

(xiii) On the basis of properties of prepared TiO_2/PVA nanocomposites, they can be used as UV filter, humidity sensing, gas sensing and anti-reflection coatings.

9.2 Suggestions for Future Work

(i) Tensile strength of these films can be investigated further.

(ii) Transmittance and refractive index studies of TiO_2/PVA nanocomposites can also be explored.

(iii) Transimission electron microscopy studies of TiO_2/PVA nanocomposites can give information about internal structure.

(iv) Testing of these films to be used as anti-reflection coatings.

Reference

1. Camargo, P. H. C., Satyanarayana, K. G., & Wypych, F. (2009). "Nanocomposites: synthesis, structure, properties and new application opportunities." Materials Research, 12(1), 1-39.
2. Roy, R., Roy, R. A., & Roy, D. M. (1986). "Alternative perspectives on "quasicrystallinity": non-uniformity and nanocomposites." Materials Letters, 4(8-9), 323-328.
3. ISO, TS. (2011). "80004-4 Nanotechnologies–Vocabulary–Part 4: Nanostructured Materials." ISO, Geneva.
4. Müller, K., Bugnicourt, E., Latorre, M., Jorda, M., EchegoyenSanz, Y., Lagaron, J. M., & Pérez, G. (2017). "Review on the processing and properties of polymer nanocomposites and nanocoatings and their applications in the packaging, automotive and solar energy fields." Nanomaterials, 7(4), 74.
5. Baksi, S., & Biswas, S. (2014). "Nanocomposites–An Overview." The Scitech Journal, 1(5), 22-30.
6. Okpala, C. C. (2013). "Nanocomposites–an overview." Int. J. Eng. Res. Dev., 8(11), 17-23.
7. Asmatulu, R., Khan, W. S., Reddy, R. J., & Ceylan, M. (2015). "Synthesis and analysis of injection molded nanocomposites of recycled high density polyethylene incorporated with graphene nanoflakes." Polymer Composites, 36(9), 1565-1573.
8. Khan, W. S., Hamadneh, N., & Khan, W. A. (2016). "Polymer nanocomposites–synthesis techniques, classification and properties." Science and applications of Tailored Nanostructures: One Central Press (OCP).
9. Parameswaranpillai, J., Hameed, N., Kurian, T., & Yu, Y. (2016). "Nanocomposite Materials: Synthesis, Properties and Applications." CRC Press.
10. Zoli, L.; Sciti, D. (2017). "Efficacy of a ZrB 2 –SiC matrix in protecting C fibres from oxidation in novel UHTCMC materials". Materials & Design. 113, 207–213.

11. Zoli, L., Vinci, A., Silvestroni, L., Sciti, D., Reece, M., & Grasso, S. (2017). "Rapid spark plasma sintering to produce dense UHTCs reinforced with undamaged carbon fibres." Materials & Design, 130, 1-7.
12. Peigney, A., Laurent, C., Flahaut, E., & Rousset, A. (2000). "Carbon nanotubes in novel ceramic matrix nanocomposites." Ceramics International, 26(6), 677-683.
13. Galizia, P., Failla, S., Zoli, L., &Sciti, D. (2018). "Tough salami-inspired Cf/ZrB2 UHTCMCs produced by electrophoretic deposition." Journal of the European Ceramic Society, 38(2), 403-409.
14. Vinci, A., Zoli, L., Sciti, D., Melandri, C., &Guicciardi, S. (2018). "Understanding the mechanical properties of novel UHTCMCs through random forest and regression tree analysis." Materials & Design, 145, 97-107.
15. Cooke, T. F. (1991). "Inorganic fibers—a literature review." Journal of the American Ceramic Society, 74(12), 2959-2978.
16. Kumagawa, K., Yamaoka, H., Shibuya, M., & Yamamura, T. (2009). "Fabrication and mechanical properties of new improved Si-M-C-(O) tyranno fiber." In 22nd Annual Conference on Composites, Advanced Ceramics, Materials, and Structures-A, 218, 65.
17. Naslain, R., Langlais, F., & Fedou, R. (1989). "The CVI-processing of ceramic matrix composites." Le Journal de Physique Colloques, 50(C5), C5-191.
18. Probst, K. J., Besmann, T. M., Stinton, D. P., Lowden, R. A., Anderson, T. J., & Starr, T. L. (1999). "Recent advances in forced-flow, thermal-gradient CVI for refractory composites." Surface and Coatings Technology, 120, 250-258.
19. Ziegler, G., Richter, I., & Suttor, D. (1999). "Fiber-reinforced composites with polymerderived matrix: processing, matrix formation and properties." Composites Part A: Applied Science and Manufacturing, 30(4), 411-417.
20. Kotani, M., Katoh Y., Kohyama A., & Narisawa M. (2003). "Fabrication and oxidation-resistance property of allylhydridopolycarbosilane-derived SiC/SiC composites." Journal of the Ceramic Society of Japan, 111(1293), 300-307.

21. Rocha, R. M., Cairo, C. A. A., & Graça, M. L. A. (2006). "Formation of carbon fiberreinforced ceramic matrix composites with polysiloxane/silicon derived matrix." Materials Science and Engineering: A, 437(2), 268-273.
22. Krenkel, W. (2009). "Cost effective processing of CMC composites by melt infiltration (LSI-process)." In Ceramic Engineering and Science Proceedings, 443-454.
23. Simon, R. A. (2005). "Progress in processing and performance of porous-matrix oxide/oxide composites." International Journal of Applied Ceramic Technology, 2(2), 141-149.
24. Pritzkow, W. E. C. (2001). ""Keramikblech" Properties and Applications." High Temperature Ceramic Matrix Composites, 681-685.
25. Stoll, E., Mahr, P., Krüger, H. G., Kern, H., & Boccaccini, A. R. (2006). "Progresses in the electrophoretic deposition technique to infiltrate oxide fibre mats for fabrication of ceramic matrix composites." In Key Engineering Materials, 314, 195-200.
26. Bao, Y., & Nicholson, P. S. (2007). "Constant current electrophoretic infiltration deposition of fiberreinforced ceramic composites." Journal of the American Ceramic Society, 90(4), 1063-1070.
27. Camargo, P. H. C., Satyanarayana, K. G., & Wypych, F. (2009). "Nanocomposites: synthesis, structure, properties and new application opportunities." Materials Research, 12(1), 1-39.
28. Callister, W. D., & Rethwisch, D. G. (2007). "Materials science and engineering: an introduction." 7, 665-715. New York: John wiley& sons, [Book].
29. Wu, Y., & Kim, G. Y. (2011). "Carbon nanotube reinforced aluminum composite fabricated by semi-solid powder processing." Journal of Materials Processing Technology, 211(8), 1341-1347.
30. Wu, Y., Kim, G. Y., Anderson, I. E., & Lograsso, T. A. (2010). "Fabrication of Al6061 composite with high SiC particle loading by semi-solid powder processing." Acta Materialia, 58(13), 4398-4405.
31. Wu, Y., & Kim, G. Y. (2015). "Compaction behavior of Al6061 and SiC binary powder mixture in the mushy state." Journal of Materials Processing Technology, 216, 484-491.

32. Aghdam, M. M., Morsali, S. R. (2014). "Residual Stresses in Composite Materials." Woodhead Publishing, 233–255.
33. Ahmad, Z., & Khan, S. (2015). "A review paper on tribological and mechanical properties of Aluminium metal matrix composites manufactured by different route." 53.
34. Tjong, S. C. (2007). "Novel nanoparticle-reinforced metal matrix composites with enhanced mechanical properties." Advanced engineering materials, 9(8), 639-652.
35. Ratti, A., Gough, R., Hoff, M., Keller, R., Kennedy, K., MacGill, R., & Yourd, R. (1999). "The SNS RFQ prototype module." In Particle Accelerator Conference, 2, 884-886.
36. Schadler, L. S., Brinson, L. C., & Sawyer, W. G. (2007). "Polymer nanocomposites: a small part of the story." Jom, 59(3), 53-60.
37. Thostenson, E. T., Li, C., & Chou, T. W. (2005). "Nanocomposites in context." Composites Science and Technology, 65(3-4), 491-516.
38. Winey, K. I., & Vaia, R. A. (2007). "Polymer nanocomposites." MRS bulletin, 32(4), 314-322.
39. Jordan, J., Jacob, K. I., Tannenbaum, R., Sharaf, M. A., & Jasiuk, I. (2005). "Experimental trends in polymer nanocomposites—a review." Materials science and engineering: A, 393(1-2), 1-11.
40. Jeon, I. Y., & Baek, J. B. (2010). "Nanocomposites derived from polymers and inorganic nanoparticles." Materials, 3(6), 3654-3674
41. Koo, J. H. (2006). "Polymer nanocomposites." McGraw-Hill Professional Pub., [Book].
42. Lampman, S. (2003). "Characterization and failure analysis of plastics." ASM International.
43. Yang, F., Ou, Y., & Yu, Z. (1998). "Polyamide 6/silica nanocomposites prepared by in situ polymerization." Journal of Applied Polymer Science, 69(2), 355-361.
44. Alexandre, M., & Dubois, P. (2000). "Polymer-layered silicate nanocomposites: preparation, properties and uses of a new class of materials." Materials Science and Engineering: R: Reports, 28(1-2), 1-63.

45. Jannapu Reddy, R. (2010). “Preparation, characterization and properties of injection molded graphenenanocomposites” [Doctoral dissertation, Wichita State University].

46. Peixoto, L. S., Silva, F. M., Niemeyer, M. A., Espinosa, G., Melo, P. A., Nele, M., & Pinto, J. C. (2006). “Synthesis of Poly (Vinyl Alcohol) and/or Poly (Vinyl Acetate) Particles with Spherical Morphology and Core-Shell Structure and its Use in Vascular Embolization.” In Macromolecular Symposia, 243(1), 190-199. Weinheim: WILEY-VCH Verlag.

47. Mark, H. F., Bikales, N. M., Overberger, C. G., Menges, G. (1989). “Vinyl Alcohol Polymers.” In Encyclopedia of Polymer Science and Engineering.

48. Hallensleben, M. L., Fuss, R., & Mummy, F. (2000). “Polyvinyl compounds, others.” Ullmann's Encyclopedia of Industrial Chemistry, 1-23.

49. Razzak, M. T., & Darwis, D. (2001). “Irradiation of polyvinyl alcohol and polyvinyl pyrrolidone blended hydrogel for wound dressing.” Radiation Physics and Chemistry, 62(1), 107-113.

50. DeMerlis, C. C., & Schoneker, D. R. (2003). “Review of the oral toxicity of polyvinyl alcohol (PVA).” Food and chemical Toxicology, 41(3), 319-326.

51. Liu, M., Guo, B., Du, M., & Jia, D. (2007). “Drying induced aggregation of halloysite nanotubes in polyvinyl alcohol/halloysite nanotubes solution and its effect on properties of composite film.” Applied Physics A, 88(2), 391-395.

52. Limpan, N., Prodpran, T., Benjakul, S., & Prasarpran, S. (2012). “Influences of degree of hydrolysis and molecular weight of poly (vinyl alcohol)(PVA) on properties of fish myofibrillar protein/PVA blend films.” Food hydrocolloids, 29(1), 226-233.

53. Maria, T. M., De Carvalho, R. A., Sobral, P. J., Habitante, A. M. B., & Solorza-Feria, J. (2008). “The effect of the degree of hydrolysis of the PVA and the plasticizer concentration on the color, opacity, and thermal and mechanical properties of films based on PVA and gelatin blends.” Journal of Food Engineering, 87(2), 191-199.

54. Qiu, K., & Netravali, A. N. (2013). “A composting study of membrane-like polyvinyl alcohol based resins and nanocomposites.” Journal of Polymers and the Environment, 21(3), 658-674.

55. Tang, Y., Zhou, D., & Zhang, J. (2013). "Novel polyvinyl alcohol/styrene butadiene rubber latex/carboxymethyl cellulose nanocomposites reinforced with modified halloysite nanotubes." Journal of Nanomaterials, 128.

56. Qiu, K., & Netravali, A. N. (2012). "Fabrication and characterization of biodegradable composites based on microfibrillated cellulose and polyvinyl alcohol." Composites Science and Technology, 72(13), 1588-1594.

57. Qiu, K., & Netravali, A. N. (2013). "Halloysite nanotube reinforced biodegradable nanocomposites using noncrosslinked and malonic acid crosslinked polyvinyl alcohol." Polymer Composites, 34(5), 799-809.

58. Cho, D., Netravali, A. N., & Joo, Y. L. (2012). "Mechanical properties and biodegradability of electrospun soy protein Isolate/PVA hybrid nanofibers." Polymer degradation and stability, 97(5), 747-754.

59. Luo, S., & Netravali, A. N. (2003). "A study of physical and mechanical properties of poly (hydroxybutyrate-co-hydroxyvalerate) during composting." Polymer degradation and stability, 80(1), 59-66.

60. Chiellini, E., Corti, A., D'Antone, S., & Solaro, R. (2003). "Biodegradation of poly (vinyl alcohol) based materials." Progress in Polymer science, 28(6), 963-1014.

61. Solaro, R., Corti, A., & Chiellini, E. (2000). "Biodegradation of poly (vinyl alcohol) with different molecular weights and degree of hydrolysis." Polymers for Advanced Technologies, 11(8-12), 873-878.

62. Vijayalakshmi, S. P., & Madras, G. (2006). "Effects of the pH, concentration, and solvents on the ultrasonic degradation of poly (vinyl alcohol)." Journal of applied polymer science, 100(6), 4888-4892.

63. Corti, A., Solaro, R., & Chiellini, E. (2002). "Biodegradation of poly (vinyl alcohol) in selected mixed microbial culture and relevant culture filtrate." Polymer Degradation and Stability, 75(3), 447-458.

64. Chiellini, E., Corti, A., &Solaro, R. (1999). "Biodegradation of poly (vinyl alcohol) based blown films under different environmental conditions." Polymer Degradation and Stability, 64(2), 305-312.

65. Jayasekara, R., Harding, I., Bowater, I., Christie, G. B., & Lonergan, G. T. (2003). "Biodegradation by composting of surface modified starch and PVA blended films." Journal of Polymers and the Environment, 11(2), 49-56.

66. Matsumura, S., & Tanaka, T. (1994). "Novel malonate-type copolymers containing vinyl alcohol blocks as biodegradable segments and their builder performance in detergent formulations." Journal of environmental polymer degradation, 2(2), 89-97.

67. Ashori, A., Raverty, W. D., & Harun, J. (2005). "Effect of chitosan addition on the surface properties of kenaf (Hibiscus cannabinus) paper." Fibers and Polymers, 6(2), 174-179.

68. Zainuddin; Hill, D.J.; Le, T.T. "An ESR study on -irradiated poly (vinyl alcohol)." Rad. Phys. Chem. 2001, 62, 283–291.

69. Pal, K., Banthia, A. K., &Majumdar, D. K. (2007). "Preparation and characterization of polyvinyl alcohol-gelatin hydrogel membranes for biomedical applications." Aaps Pharmscitech, 8(1), E142-E146.

70. Horii, F., Hu, S., Ito, T., Odani, H., Kitamaru, R., Matsuzawa, S., & Yamaura, K. (1992). "Cross polarization/magic angle spinning 13C nmr study of solid structure and hydrogen bonding of poly (vinyl alcohol) films with different tacticities. Polymer, 33(11), 2299-2306.

71. Albdiry, M. T., & Yousif, B. F. (2013). "Morphological structures and tribologicalperformance of unsaturated polyester based untreated/silane-treated halloysite nanotubes." Materials & Design, 48, 68-76.

72. Anderson, M. A., Gieselmann, M. J., & Xu, Q. (1988). "Titania and alumina ceramic membranes." Journal of Membrane Science, 39(3), 243-258.

73. Penn, R. L., & Banfield, J. F. (1999). "Morphology development and crystal growth in nanocrystalline aggregates under hydrothermal conditions: Insights from titania." Geochimica et cosmochimica acta, 63(10), 1549-1557.

74. Barbe, C. J., Arendse, F., Comte, P., Jirousek, M., Lenzmann, F., Shklover, V., & Grätzel, M. (1997). "Nanocrystalline titanium oxide electrodes for photovoltaic applications." Journal of the American Ceramic Society, 80(12), 3157-3171.

75. Zaban, A., Aruna, S. T., Tirosh, S., Gregg, B. A., & Mastai, Y. (2000). "The effect of the preparation condition of TiO_2 colloids on their surface structures." The Journal of Physical Chemistry B, 104(17), 4130-4133.

76. Zhang, Z., Wang, C. C., Zakaria, R., & Ying, J. Y. (1998). "Role of particle size in nanocrystalline TiO_2-based photocatalysts." The Journal of Physical Chemistry B, 102(52), 10871-10878.

77. Oskam, G., Nellore, A., Penn, R. L., & Searson, P. C. (2003). "The growth kinetics of TiO_2 nanoparticles from titanium (IV) alkoxide at high water/ titanium ratio." The Journal of Physical Chemistry B, 107(8), 1734-1738.

78. Banfield, J. (1998). "Thermodynamic analysis of phase stability of nanocrystalline titania." Journal of Materials Chemistry, 8(9), 2073-2076.

79. Zhang, H., & Banfield, J. F. (2000). "Understanding polymorphic phase transformation behavior during growth of nanocrystalline aggregates: insights from TiO_2." The Journal of Physical Chemistry B, 104(15), 3481-3487.

80. Navrotsky, A. (2003). "Energetics of nanoparticle oxides: interplay between surface energy and polymorphism." Geochemical Transactions, 4(1), 34.

81. Naicker, P. K., Cummings, P. T., Zhang, H., & Banfield, J. F. (2005). "Characterization of titanium dioxide nanoparticles using molecular dynamics simulations." The Journal of Physical Chemistry B, 109(32), 15243-15249.

82. Zhu, T., & Gao, S. P. (2014). "The stability, electronic structure, and optical property of TiO_2 polymorphs." The Journal of Physical Chemistry C, 118(21), 11385-11396.

83. Chen X., Mao S. S., (2007). "Titanium Dioxide Nanomaterials: Synthesis, Properties, Modifications, and Applications." Chem. Rev., 107, 2891-2959.

84. Varghese, O. K., Gong, D., Paulose, M., Ong, K. G., Dickey, E. C., & Grimes, C. A. (2003). "Extreme changes in the electrical resistance of titania nanotubes with hydrogen exposure." Advanced Materials, 15(7-8), 624-627.

85. Wen, B., Liu, C., & Liu, Y. (2005). "Depositional characteristics of metal coating on single-crystal TiO_2 nanowires." The Journal of Physical Chemistry B, 109(25), 12372-12375.

86. Wu, J. M., & Qi, B. (2007). "Low-temperature growth of a nitrogen-doped titania nanoflower film and its ability to assist photodegradation of rhodamine B in water." The Journal of Physical Chemistry C, 111(2), 666-673.

87. Yi, G. R., Moon, J. H., & Yang, S. M. (2001). "Ordered macroporous particles by colloidal templating." Chemistry of materials, 13(8), 2613-2618.

88. Andersson, M., Österlund, L., Ljungström, S., & Palmqvist, A. (2002). "Preparation of nanosize anatase and rutile TiO_2 by hydrothermal treatment of microemulsions and their activity for photocatalytic wet oxidation of phenol." The Journal of Physical Chemistry B, 106(41), 10674-10679

89. Wahi, R. K., Liu, Y., Falkner, J. C., & Colvin, V. L. (2006). "Solvothermal synthesis and characterization of anatase TiO_2 nanocrystals with ultrahigh surface area." Journal of colloid and interface science, 302(2), 530-536.

90. Bazargan, M. H., Byranvand, M. M., & Kharat, A. N. (2012). "Preparation and characterization of low temperature sintering nanocrystalline TiO_2 prepared via the solgel method using titanium (IV) butoxide applicable to flexible dye sensitized solar cells." International Journal of Materials Research, 103(3), 347-351.

91. Ryu, W. H., Park, C. J., & Kwon, H. S. (2008). "Surface Morphology and Growth of Anodic Titania Nanotubes Films: Photoelectrochemical Water Splitting Studies" J. Nano., 8, 1–4.

92. Shinde, P. S., & Bhosale, C. H. (2008). "Properties of chemical vapour deposited nanocrystalline TiO_2 thin films and their use in dye-sensitized solar cells." Journal of Analytical and Applied Pyrolysis, 82(1), 83-88.

93. Tan, W., Chen, J., Zhou, X., Zhang, J., Lin, Y., Li, X., & Xiao, X. (2009). "Preparation of nanocrystalline TiO_2 thin film at low temperature and its application in dye-sensitized solar cell." Journal of Solid State Electrochemistry, 13(5), 651-656.

94. Arami, H., Mazloumi, M., Khalifehzadeh, R., & Sadrnezhaad, S. K. (2007). "Sonochemical preparation of TiO_2 nanoparticles." Materials Letters, 61(23-24), 4559-4561.

95. Corradi, A. B., Bondioli, F., Focher, B., Ferrari, A. M., Grippo, C., Mariani, E., & Villa, C. (2005). "Conventional and Microwave-Hydrothermal Synthesis of TiO_2 Nanopowders." Journal of the American Ceramic Society, 88(9), 2639-2641.

96. Del Ángel-Sanchez, K., Vázquez-Cuchillo, O., Aguilar-Elguezabal, A., Cruz-López, A., & Herrera-Gómez, A. (2013). "Photocatalytic degradation of 2, 4-dichlorophenoxyacetic acid under visible light: Effect of synthesis route." Materials chemistry and Physics, 139(2-3), 423-430.

97. Albano, C., Sarmiento, Y., & González, G. (2012). "Synthesis and Characterization of Nanostructures: $MWCNT_f/TiO_2$ and $MWCNT_f/ TiO_2/$ HAp." In Macromolecular Symposia, 321(1), 76-79. Weinheim: WILEY-VCH Verlag.

98. Vijayalakshmi, R., & Rajendran, V. (2012). "Synthesis and characterization of nano-TiO_2 via different methods." Archives of Applied Science Research, 4(2), 1183-1190.

99. Haupert, F., & Wetzel, B. (2005). "Polymer Composites: From Nano- to Macro-Scale." Springer Science & Business Media, 45 [Book].

100. Aslam, M., Kalyar, M. A., & Raza, Z. A. (2018). "Polyvinyl alcohol: a review of research status and use of polyvinyl alcohol based nanocomposites." Polymer Engineering & Science, 2119-2132.

101. Yang, C. C. (2007). "Synthesis and characterization of the cross-linked PVA/TiO_2 composite polymer membrane for alkaline DMFC." Journal of Membrane Science, 288(12), 51-60.

102. Lee, J., Hong, J., Park, D. W., & Shim, S. E. (2010). "Microencapsulation and characterization of poly (vinyl alcohol)-coated titanium dioxide particles for electrophoretic display." Optical Materials, 32(4), 530-534.

103. Mallakpour, S., & Barati, A. (2011). "Efficient preparation of hybrid nanocomposite coatings based on poly (vinyl alcohol) and silane coupling agent modified TiO_2 nanoparticles." Progress in Organic Coatings, 71(4), 391-398.

104. Maurya, A., & Chauhan, P. (2012). "Synthesis and characterization of sol–gel derived PVA-titanium dioxide (TiO_2) nanocomposite." Polymer bulletin, 68(4), 961-972.

105. Mallakpour, S., Zhiani, M., Barati, A., & Rostami, H. (2013). "Improving the direct methanol fuel cell performance with poly (vinyl alcohol)/titanium dioxide nanocomposites as a novel electrolyte additive." international journal of hydrogen energy, 38(28), 12418-12426.

106. Mansour, A. F., Mansour, S. F., & Abdo, M. A. (2015). "Improvement structural and optical properties of ZnO/PVA nanocomposites." IOSR Journal of Applied Physics, 7(2), 60-69.

107. Abdullah, A. H., Ismail, Z., Abidin, A. S. Z., Ismail, F. S., & Yusoh, K. (2018). "PVA/Graphene Nanocomposite: Morphology and its Thermal Properties." In IOP Conference Series: Materials Science and Engineering, 319, (1), 012011). IOP Publishing.

108. Karthikeyan, B., Anija, M., & Philip, R. (2006). "In situ synthesis and nonlinear optical properties of Au: Ag nanocomposite polymer films." Applied physics letters, 88(5), 053104.

109. Upadhyay, V. S., Dubey, S. K., Singh, A., & Tripathi, S. (2014). "Structural, optical and morphological properties of PVA/Fe_2O_3 nanocomposite thin films." IJCPS, 3, 43.

110. Peng, Z., Kong, L. X., & Li, S. D. (2005). "Thermal properties and morphology of a poly (vinyl alcohol)/silica nanocomposite prepared with a self assembled monolayer technique. Journal of applied polymer science," 96(4), 1436-1442.

111. Wang, H., Fang, P., Chen, Z., & Wang, S. (2007). "Synthesis and characterization of CdS/PVA nanocomposite films." Applied Surface Science, 253(20), 8495-8499.

112. Cheng, H. K. F., Sahoo, N. G., Tan, Y. P., Pan, Y., Bao, H., Li, L., & Zhao, J. et al. (2012). "Poly (vinyl alcohol) nanocomposites filled with poly (vinyl alcohol)-grafted graphene oxide." ACS applied materials & interfaces, 4(5), 2387-2394.

113. Mallakpour, S., & Dinari, M. (2013). "Enhancement in thermal properties of poly (vinyl alcohol) nanocomposites reinforced with Al_2O_3 nanoparticles." Journal of Reinforced Plastics and Composites, 32(4), 217-224

114. Park, J. S., Park, J. W., & Ruckenstein, E. (2001). "Thermal and dynamic mechanical analysis of PVA/MC blend hydrogels." Polymer, 42(9), 4271-4280.

115. Mitra, S., Saha, D. R., Banerjee, S., & Chakravorty, D. (2013). "Viscoelastic properties of graphene/PVA nanocomposite." AIP Conference Proceedings, 1536(1), 83-84).

116. Agrawal, S. L., & Rai, N. (2015). "DMA and conductivity studies in PVA: NH_4SCN: DMSO: MWNT nanocomposite polymer dried gel electrolytes." Journal of Nanomaterials, 16(1), 90.

117. Khatua, C., Chinya, I., Saha, D., Das, S., Sen, R., & Dhar, A. (2015). "Modified clad optical fibre coated with PVA/TiO_2 nano composite for humidity sensing application." International Journal on Smart Sensing & Intelligent Systems, 8(3).

118. Hamming, L. M., Qiao, R., Messersmith, P. B., & Brinson, L. C. (2009). "Effects of dispersion and interfacial modification on the macroscale properties of TiO_2 polymer– matrix nanocomposites." Composites science and technology, 69(11-12), 1880-1886.

119. Qiao, Q., Xie, Y., & McLeskey, Jr, J. T. (2008). "Organic/inorganic polymer solar cells using a buffer layer from all-water-solution processing." The Journal of Physical Chemistry C, 112(26), 9912-9916.

120. Dridi, C., Barlier, V., Chaabane, H., Davenas, J., & Ouada, H. B. (2008). "Investigation of exciton photodissociation, charge transport and photovoltaic response of poly (N-vinyl carbazole): TiO_2 nanocomposites for solar cell applications." Nanotechnology, 19(37), 375201.

121. Yang, C. C., Chiu, S. J., Lee, K. T., Chien, W. C., Lin, C. T., & Huang, C. A. (2008). "Study of poly (vinyl alcohol)/titanium oxide composite polymer membranes and their application on alkaline direct alcohol fuel cell." Journal of Power Sources, 184(1), 44-51.

122. Abbaraju, R. R., Dasgupta, N., & Virkar, A. V. (2008). "Composite Nafion Membranes Containing Nanosize TiO_2/SnO_2 for Proton Exchange Membrane Fuel Cells." Journal of the Electrochemical Society, 155(12), B1307-B1313.

123. Ahn, J. H., Wang, G. X., Liu, H. K., & Dou, S. X. (2003). "Nanoparticle-dispersed PEO polymer electrolytes for Li batteries." Journal of power sources, 119, 422-426.

124. Şahin, A., & Ar, I. (2014). "Synthesis and characterization of polyvinyl alcohol based and titaniumdioxide doped nanocomposite membrane." Journal of Thermal Science & Technology, 34(1).

125. Ahmad, J., Deshmukh, K., Habib, M., & Hägg, M. B. (2014). "Influence of TiO_2 nanoparticles on the morphological, thermal and solution properties of PVA/TiO_2 nanocomposite membranes." Arabian Journal for Science and Engineering, 39(10), 6805-6814.

126. Lewis, S., Haynes, V., Wheeler-Jones, R., Sly, J., Perks, R. M., & Piccirillo, L. (2010). "Surface characterization of poly (methylmethacrylate) based nanocomposite thin films containing Al_2O_3 and TiO_2 nanoparticles. Thin solid films, 518(10), 2683-2687.

127. Matilainen, A., & Sillanpää, M. (2010). "Removal of natural organic matter from drinking water by advanced oxidation processes." Chemosphere, 80(4), 351-365.

128. Hjalmars, A. (2014). "Biofouling on plate heat exchangers and the impact of advanced oxidizing technology and ultrasound." [Master's thesis]

129. Liu, X., Chen, Q., Lv, L., Feng, X., & Meng, X. (2015). "Preparation of transparent PVA/TiO_2 nanocomposite films with enhanced visible-light photocatalytic activity." Catalysis Communications, 58, 30-33.

130. Tanahashi, M. (2010). "Development of Fabrication Methods of Filler/ Polymer Nanocomposites: With Focus on Simple Melt-Compounding-Based Approach without Surface Modification of Nanofillers." Materials, 3(3), 1593-1619.

131. Khan, W. S., Hamadneh, N., & Khan, W. A. (2016). "Polymer nanocomposites–synthesis techniques, classification and properties." Science and applications of Tailored Nanostructures: One Central Press (OCP), 50-67.

132. Kamigaito, O. (1991). "What can be improved by nanometer composites?." Journal of the Japan Society of Powder and Powder Metallurgy, 38(3), 315-321.

133. Hamming, L. M., Qiao, R., Messersmith, P. B., & Brinson, L. C. (2009). Effects of dispersion and interfacial modification on the macroscale properties of TiO_2 polymer–matrix nanocomposites. Composites science and technology, 69(11-12), 1880-1886.

134. Greenland, D. J. (1963). "Adsorption of polyvinyl alcohols by montmorillonite." Journal of Colloid Science, 18(7), 647-664.

135. Francis, C. W. (1973). “Adsorption of polyvinylpyrrolidone on reference clay minerals.” Soil Science, 115(1), 40-54.

136. Zhao X, Urano K, Ogasawara S. (1989). “Adsorption of polyethylene glycol from aqueous solutions on monmorillonite clays.” Colloid and Polymer Science, 267(10), 899-906.

137. Vaia, R. A., & Giannelis, E. P. (1997). “Polymer melt intercalation in organically-modified layered silicates: model predictions and experiment.” Macromolecules, 30(25), 8000-8009.

138. Gilman, J. W. (1999). “Flammability and thermal stability studies of polymer layered-silicate (clay) nanocomposites.” Applied clay science, 15(1-2), 31-49.

139. Evora, V. M., & Shukla, A. (2003). “Fabrication, characterization, and dynamic behavior of polyester/TiO_2 nanocomposites.” Materials Science and Engineering: A, 361(1-2), 358-366.

140. Di Lorenzo, M. L., Errico, M. E., & Avella, M. (2002). “Thermal and morphological characterization of poly (ethylene terephthalate)/calcium carbonate nanocomposites.” Journal of materials science, 37(11), 2351-2358.

141. Silva, B. L., Nack, F. C., Lepienski, C. M., Coelho, L. A. F., & Becker, D. (2014). “Influence of intercalation methods in properties of clay and carbon nanotube and high density polyethylene nanocomposites.” Materials Research, 17(6), 1628-1636.

142. Namazi, H., Mosadegh, M., & Dadkhah, A. (2009). “New intercalated layer silicate nanocomposites based on synthesized starch-g-PCL prepared via solution intercalation and in situ polymerization methods: As a comparative study.” Carbohydrate polymers, 75(4), 665-669.

143. Bhiwankar, N. N., & Weiss, R. A. (2006). “Melt intercalation/exfoliation of polystyrene–sodium-montmorillonite nanocomposites using sulfonated polystyrene ionomer compatibilizers.” Polymer, 47(19), 6684-6691.

144. Hallensleben, M. L., Fuss, R., & Mummy, F. (2000). “Polyvinyl compounds, others.” Ullmann's Encyclopedia of Industrial Chemistry, 1-23.

145. Lindeemann, M., K. (1971). “Thermodynamic properties of polymers" Encyclopedia of Polymer Science and Technology, 14, 165-207, John Wiley and Sons.

146. Haweel, C. K., & Ammar, S. H. (2008). "Preparation of polyvinyl alcohol from local raw material." Iraqi Journal of Chemical and Petroleum Engineering, 9(1), 15-21.

147. Kalaitzidou, K., Fukushima, H., & Drzal, L. T. (2007). "A new compounding method for exfoliated graphite–polypropylene nanocomposites with enhanced flexural properties and lower percolation threshold." Composites Science and Technology, 67(10), 2045-2051.

148. Jankong, S., & Srikulkit, K. (2008). "Preparation of polypropylene/ hydrophobic silica nanocomposites." J. Met. Mater. Miner, 18(2), 43-146.

149. Chae, D. W. Kim, B. C. (2005). "Characterization on polystyrene/zinc oxide nanocomposites prepared from solution mixing." Polym. Adv. Technol., 16, 846–850.

150. Carotenuto, G., Her, Y. S., & Matijević, E. (1996). "Preparation and characterization of nanocomposite thin films for optical devices." Industrial & engineering chemistry research, 35(9), 2929-2932.

151. Andrews, R., Jaques, D., Quian, D., & Rantell, T. (2002). "Multiwall carbon nanotubes: Synthesis and application." Acc. Chem. Res., 35, 1008–1017.

152. Preghenella, M., Pegoretti, A., & Migliaresi, C. (2005). "Thermo-mechanical characterization of fumed silica-epoxy nanocomposites." Polymer Journal, 46, 12065–12072.

153. Agarwal, U. S., Nisal, A., & Joseph, R. (2007). "PET-SWNT nanocomposites through ultrasound assisted dissolution-evaporation." European Polymer Journal, 43(6), 2279-2285.

154. Manas-Zloczower, I., Nir, A., & Tadmor, Z. (1982). "Dispersive mixing in internal mixers—a theoretical model based on agglomerate rupture." Rubber Chemistry and Technology, 55(5), 1250-1285.

155. Shiga, S., & Furuta, M. (1985). "Processability of EPR in an internal mixter (II)―Morphological changes of carbon black agglomerates during mixing." Rubber chemistry and technology, 58(1), 1-22.

156. Palmgren, H. (1975). "Processing conditions in the batch-operated internal mixer." Rubber chemistry and technology, 48(3), 462-494.

157. Ess, J. W., & Hornsby, P. R. (1987). "Twin-screw extrusion compounding of mineral filled thermoplastics: Dispersive mixing effects." Plastics and rubber processing and applications, 8(3), 147-156.

158. Tanahashi, M., Watanabe, Y., Lee, J. C., Takeda, K., & Fujisawa, T. (2009). "Melt flow and mechanical properties of silica/perfluoropolymer nanocomposites fabricated by direct melt-compounding without surface modification on nano-silica." Journal of nanoscience and nanotechnology, 9(1), 539-549.

159. https://www.tollcoating.com/using-polymer-solution-casting-to-deliver - high-quality-films/

160. Duda, J., L. (1985). "Molecular diffusion in polymeric systems." Pure & Appl. Chem. 57, 1681-1690.

161. Vrentas, J., S., Liu, H., T., & Duda, J., L. (1980). "Comparison of theory and experiments for diffusion in dilute polymer solutions." J. Polymer Sci., 18, 1633-1641.

162. Vrentas, J., S., & Duda, J., L. (1976). "Diffusion in dilute polystyrene solutions." J. Poly. Sci., 14, 101.

163. Vrentas, J., S., & Duda, J., L. (1979). "Molecular diffusion in polymer solutions." AIChE J., 25, 1-24.

164. Huggins, M., L. (1964). "A revised theory of high polymer solutions." J. Am. Chem. Soc., 86(17), 3535–3540.

165. Danner, R., P., High, M., S. (1993). "Handbook of polymer solution thermodynamics." American Institute of Chemical Engineers, New York, [Book].

166. Eagland, D. et al. (1986). "The degree of dispersion of poly (vinyl alcohol) in water/n-propanol solutions." European Polymer Journal, 22, 351–356.

167. Fried, J., R. (2003). "Polymer science and technology, 2nd edition." Pearson Education, [Book].

168. Teraoka, I. (2002). "Polymer solutions: an introduction to physical properties." Polytechnic University, Brooklyn, New York, [Book].

169. Demir, G. M., Karaküçük, A., Değim, Z., Bektaş, D., Çoban, Ö., Gülpınar, E., & Torunoğlu, S. T. (2014). "Stirring Speed Effects on Physical Characteristics of Theophylline Microsphere." In Proceedings of the 5th International Conference on Nanotechnology: Fundamentals and Applications.

170. Barclay, L. M. (1976). "Formation and structure of PVC particles." Applied Macromolecular Chemistry and Physics, 52(1), 1-20.

171. Lewis, M. H., & Johnson, G. R. (1981). "Agitation scale-up effects during VCM suspension polymerization." Journal of Vinyl Technology, 3(2), 102-106.

172. Marinho, R., Horiuchi, L., & Pires, C. A. (2018). "Effect of stirring speed on conversion and time to particle stabilization of poly (vinyl chloride) produced by suspension polymerization process at the beginning of reaction." Brazilian Journal of Chemical Engineering, 35(2), 631-640.

173. Sato, K., Li, J. G., Kamiya, H., & Ishigaki, T. (2008). "Ultrasonic dispersion of TiO_2 nanoparticles in aqueous suspension." Journal of the American Ceramic Society, 91(8), 2481-2487.

174. Taurozzi, J. S., Hackley, V. A., & Wiesner, M. R. (2011). "Ultrasonic dispersion of nanoparticles for environmental, health and safety assessment–issues and recommendations." Nanotoxicology, 5(4), 711-729.

175. Nia, M., H., et al. (2015). "Stabilizing and dispersing methods of TiO2 nanoparticles in biological studies", Journal of Paramedical Sciences, 6(2) ISSN 2008-4978.

176. Kusters, K. A., Pratsinis, S. E., Thoma, S. G., & Smith, D. M. (1994). "Energy—size reduction laws for ultrasonic fragmentation." Powder technology, 80(3), 253-263.

177. Thoma, S. G., Ciftcioglu, M., & Smith, D. M. (1991). "Determination of agglomerate strength distributions Part 3. Application to titania processing." Powder Technology, 68(1), 71-78.

178. Jiang, J., Oberdörster, G., & Biswas, P. (2009). "Characterization of size, surface charge, and agglomeration state of nanoparticle dispersions for toxicological studies." Journal of Nanoparticle Research, 11(1), 77-89.

179. Hayakawa, O., Nakahira, K., Naito, M., & Tsubaki, J. (1998). "Experimental analysis of sample preparation conditions for particle size measurement." Powder technology, 100(1), 61-68.

180. Mahbubul, I. M., Chong, T. H., Khaleduzzaman, S. S., Shahrul, I. M., Saidur, R., Long, B. D., & Amalina, M. A. (2014). "Effect of ultrasonication duration on colloidal structure and viscosity of alumina–water nanofluid." Industrial & Engineering Chemistry Research, 53(16), 6677-6684.

181. Baveye, P., & Laba, M. (2008). "Aggregation and toxicology of titanium dioxide nanoparticles." Environmental Health Perspectives, 116(4), A152-A152.

182. Derjaguin, B. et al. (1941). "Theory of the stability of strongly charged lyophobic sols and the adhesion of strongly charged particles in solutions of electrolytes." Acta Physicochim USSR, 14, 633-62.

183. Widegren, J., & Bergström, L. (2002). "Electrostatic stabilization of ultrafine titania in ethanol." Journal of the American Ceramic Society, 85(3), 523-528.

184. Mates, T. E., & Ring, T. A. (1987). "Steric stability of alkoxy-precipitated TiO_2 in alcohol solutions." Colloids and Surfaces, 24(4), 299-313.

185. Wassell, D. T. H., Hall, R. C., & Embery, G. (1995). "Adsorption of bovine serum albumin onto hydroxyapatite." Biomaterials, 16(9), 697-702.

186. Deiss, J., Anizan, P., Hadigui, S., Wecker, C. (1996). "Steric stability of TiO_2 nanoparticles in aqueous dispersions." Colloids Surf A Physicochem Eng Asp. 106(1), 59-62.

187. Yamaguchi, S., Kobayashi, H., Narita, T., Kanehira, K., Sonezaki, S., Kubota, Y., & Iwasaki, Y. (2010). "Novel photodynamic therapy using water-dispersed TiO_2–polyethylene glycol compound: evaluation of antitumor effect on glioma cells and spheroids in vitro." Photochemistry and photobiology, 86(4), 964-971.

188. Kanehira, K., Banzai, T., Ogino, C., Shimizu, N., Kubota, Y., & Sonezaki, S. (2008). "Properties of TiO_2–polyacrylic acid dispersions with potential for molecular recognition." Colloids and Surfaces B: Biointerfaces, 64(1), 10-15.

189. Zhang, H., Shi, R., Xie, A., Li, J., Chen, L., Chen, P., & Shen, Y. (2013). "Novel TiO_2/PEGDA hybrid hydrogel prepared in situ on tumor cells for effective photodynamic therapy." ACS applied materials & interfaces, 5(23), 12317-12322.

190. http://shodhganga.inflibnet.ac.in/bitstream/10603/4748/14/14_chapter%204.pdf

191. Devi, R., S., Venckatesh, R., and Sivaraj, R., (2014). "Synthesis of titanium dioxide nanoparticles by sol-gel technique," International Journal of Innovative Research in Science, Engineering and Technology, 3(8).

192. Thangavelu, K., Annamalai, R., & Arulnandhi, D. (2013). "Preparation and characterization of nanosized TiO_2 powder by sol-gel precipitation route." International Journal of Emerging Technology and Advanced Engineering, 3(1), 636-639.

193. Tumuluri, A., Naidu, K. L., & Raju, K. J. (2014). "Band gap determination using Tauc's plot for $LiNbO_3$ thin films." Int. J. Chem. Tech. Res, 6(6), 3353-3356.

194. Garcia-Vaquero, M., Rajauria, G., O'Doherty, J. V., & Sweeney, T. (2017). "Polysaccharides from macroalgae: Recent advances, innovative technologies and challenges in extraction and purification." Food Research International, 99, 1011-1020.

195. https://www.hielscher.com/probe-type-sonication-vs-ultrasonic-bath-an-efficiency-comparison.htm

196. Taurozzi, J. S., Hackley, V. A., & Wiesner, M. R. (2011). "Ultrasonic dispersion of nanoparticles for environmental, health and safety assessment–issues and recommendations." Nanotoxicology, 5(4), 711-729.

197. Gharoy Ahangar, E., Abbaspour-Fard, M. H., Shahtahmassebi, N., Khojastehpour, M., & Maddahi, P. (2015). "Preparation and characterization of PVA/ZnO nanocomposite." Journal of food processing and preservation, 39(6), 1442-1451.

198. Gautam, A., & Ram, S. (2010). "Preparation and thermomechanical properties of Ag-PVA nanocomposite films." Materials Chemistry and Physics, 119(1-2), 266-271.

199. Siemann, U. (2005). "Solvent cast technology–a versatile tool for thin film production." Scattering methods and the properties of polymer materials, 1-14, Springer, Berlin, Heidelberg.

200. McCormick, C. L. (1991). "Structural design of water-soluble copolymers." ACS Symposium Series, 467, 2.

201. Coats, A. W., & Redfern, J. P. (1963). "Thermogravimetric analysis. A review." Analyst, 88(1053), 906-924.

202. Spectronic, T. (2012). "Basic UV-Vis theory, concepts and applications." Thermo Spectronic, 1-28.

203. Shah, R., S., Shah, R., R., Pawar, R., B., Gayakar, P., P., (2015). "UV-Visible spectroscopy- a review", International journal of institutional pharmacy and life sciences, (ISSN): 2249-6807.

204. Haiss, W., Thanh, N. T., Aveyard, J., & Fernig, D. G. (2007). "Determination of size and concentration of gold nanoparticles from UV− Vis spectra." Analytical chemistry, 79(11), 4215-4221.

205. Shehap, A. M., & Akil, D. S. (2016). "Structural and optical properties of TiO_2 nanoparticles/PVA for different composites thin films." International Journal of Nanoelectronics & Materials, 9(1).

206. Sugumaran, S., & Bellan, C. S. (2014). "Transparent nano composite PVA–TiO_2 and PMMA–TiO_2 thin films: Optical and dielectric properties." Optik-International Journal for Light and Electron Optics, 125(18), 5128-5133.

207. Macyk, W., Szaciłowski, K., Stochel, G., Buchalska, M., Kuncewicz, J., & Łabuz, P. (2010). "Titanium (IV) complexes as direct TiO_2 photosensitizers." Coordination Chemistry Reviews, 254(21-22), 2687-2701.

208. Šajinović, D., Šaponjić, Z. V., Cvjetićanin, N., Marinović-Cincović, M., & Nedeljković, J. M. (2000). "Synthesis and characterization of CdS quantum dots–polystyrene composite." Chemical Physics Letters, 329(1-2), 168-172.

209. Zhang, L. S., Wu, W. Z., & Wang, J. L. (2007). "Immobilization of activated sludge using improved polyvinyl alcohol (PVA) gel." Journal of environmental sciences, 19(11), 1293-1297.

210. Abdelaziz, M., & Ghannam, M. M. (2010). "Influence of titanium chloride addition on the optical and dielectric properties of PVA films." Physica B: Condensed Matter, 405(3), 958-964.

211. Ravi, M., Bhavani, S., Kumar, K. K., & Rao, V. N. (2013). "Investigations on electrical properties of PVP: KIO_4 polymer electrolyte films." Solid State Sciences, 19, 85-93.

212. Hodge, R. M., Edward, G. H., & Simon, G. P. (1996). "Water absorption and states of water in semicrystalline poly (vinyl alcohol) films." Polymer, 37(8), 1371-1376.

213. Thomas, L. C. (2010). "Interpreting unexpected events and transitions in DSC results." Technical publication TA-039, TA Instruments.

214. Lu, H., Xu, X., Li, X., & Zhang, Z. (2006). "Morphology, crystallization and dynamic mechanical properties of PA66/nano-SiO_2 composites." Bulletin of Materials Science, 29(5), 485-490.

215. Kasper, M. (2004). "GWH Höhne, WF Hemminger, H.-J. Flammersheim: Differential scanning calorimetry." Analytical and Bioanalytical Chemistry, 380(3), 366-367.

216. Radoičić, M. B., Šaponjić, Z. V., Marinović-Cincović, M. T., Ahrenkiel, S. P., Bibić, N. M., & Nedeljković, J. M. (2012). "The influence of shaped TiO_2 nanofillers on thermal properties of polyvinyl alcohol." Journal of the Serbian Chemical Society, 77(5), 699-714.

217. Ahmad, J., Deshmukh, K., Habib, M., & Hägg, M. B. (2014). "Influence of TiO_2 nanoparticles on the morphological, thermal and solution properties of PVA/TiO_2 nanocomposite membranes." Arabian Journal for Science and Engineering, 39(10), 6805-6814.

218. Kaler, V., Pandel, U., & Duchaniya, R. K. (2018). "Development of TiO_2/PVA nanocomposites for application in solar cells." Materials Today: Proceedings, 5(2), 6279-6287.

219. Yang, H., Xu, S., Jiang, L., & Dan, Y. (2012). "Thermal decomposition behavior of poly (vinyl alcohol) with different hydroxyl content." Journal of Macromolecular Science, Part B, 51(3), 464-480.

220. Peng, Z., & Kong, L. X. (2007). "A thermal degradation mechanism of polyvinyl alcohol/silica nanocomposites." Polymer Degradation and Stability, 92(6), 1061-1071.

221. Fernández, M. D., & Fernández, M. J. (2008). "Thermal degradation of copolymers from vinyl acetate and vinyl alcohol." Journal of Thermal Analysis and Calorimetry, 92(3), 829-837.

222. Peng, Z., & Kong, L. X. (2007). "A thermal degradation mechanism of polyvinyl alcohol/silica nanocomposites." Polymer Degradation and Stability, 92(6), 1061-1071.

223. Mallakpour, S., & Barati, A. (2011). "Efficient preparation of hybrid nanocomposite coatings based on poly (vinyl alcohol) and silane coupling agent modified TiO_2 nanoparticles." Progress in Organic Coatings, 71(4), 391-398.

224. Yang, C. C. (2007). "Synthesis and characterization of the cross-linked PVA/ TiO_2 composite polymer membrane for alkaline DMFC." Journal of Membrane Science, 288(1-2), 51-60.

225. Yang, H., Xu, S., Jiang, L., & Dan, Y. (2012). "Thermal decomposition behavior of poly (vinyl alcohol) with different hydroxyl content." Journal of Macromolecular Science, Part B, 51(3), 464-480.

226. Krklješ, A. N., Marinović-Cincović, M. T., Kačarević-Popović, Z. M., & Nedeljković, J. M. (2007). "Dynamic thermogravimetric degradation of gamma radiolytically synthesized Ag–PVA nanocomposites." Thermochimica Acta, 460(1-2), 28-34.

227. Ferry, J. D., & Ferry, J. D. (1980). "Viscoelastic properties of polymers." John Wiley & Sons.Jones [Book].

228. Jones, D. S. (1999). "Dynamic mechanical analysis of polymeric systems of pharmaceutical and biomedical significance." International journal of pharmaceutics, 179(2), 167-178.

229. Shaffer, M. S., & Windle, A. H. (1999). "Fabrication and characterization of carbon nanotube/poly (vinyl alcohol) composites. Advanced materials, 11(11), 937-941.

230. "Dynamic Mechanical Analysis (DMA): A Beginner's guide", (2013). Perkin Elmer, 1-23.

231. Sung, Y. T., Kum, C. K., Lee, H. S., Byon, N. S., Yoon, H. G., & Kim, W. N. (2005). "Dynamic mechanical and morphological properties of polycarbonate/multi-walled carbon nanotube composites." Polymer, 46(15), 5656-5661.

Publications

(i) Vandana Kaler, R. K. Duchaniya, and U. Pandel, " **Development of TiO_2/PVA nanocomposites for application in solar cells**" 7th International Conference on Materials Processing and Characterization at GRIET, Hyderabad, India, from 17-03-2017 to 19-03-2017. Published by Materials Today: Proceedings.

(ii) Vandana Kaler, R. K. Duchaniya, and U. Pandel, "**Synthesis of nano-titanium dioxide by sol-gel route"** International Conference on Emerging Technologies: Micro to Nano 2015 by American Institute of Physics at Jaipur, from 24-10-2015 to 25-10-2015.

Citation: AIP Conference Proceedings 1724, 020127 (2016); doi: 10.1063/1.4945247

View online: http://dx.doi.org/10.1063/1.4945247

Published by the AIP Publishing

International Conference Proceedings

(i) Rajendra Kumar Duchaniya, Vandana Kaler, and U. Pandel "**Viscoelastic behaviour of TiO_2/PVA nanocomposites**" World congress on Material Science and Technology (EuroSciCon), Paris, France on 04-06-2019 to 06-06-2019.

(ii) Vandana Kaler, R. K. Duchaniya, and U. Pandel "**Thermogravimetric analysis of TiO_2/PVA nanocomposites**" International Conference on recent trends in Science, Engineering and Management (ICRTSEM-2018, Jaipur) on 23-09-2018.

(iii) Vandana Kaler, R. K. Duchaniya, and U. Pandel "**Thermal and Mechanical analysis of TiO_2/PVA nanocomposites"** ICAMT 2017, Pattaya, Thailand, 22-12-2017 to 23-12-2017.